A biophysical cortical column model for optical signal analysis

Sandrine Chemla

▶ To cite this version:

Sandrine Chemla. A biophysical cortical column model for optical signal analysis. Neurons and Cognition [q-bio.NC]. INRIA Sophia-Antipolis, 2010. English. NNT : . tel-00459780

HAL Id: tel-00459780

https://theses.hal.science/tel-00459780

Submitted on 25 Feb 2010

PhD THESIS

prepared at

INRIA Sophia Antipolis

and presented at the

University of Nice-Sophia Antipolis

Graduate School of Information and Communication Sciences

A dissertation submitted in partial fulfillment
of the requirements for the degree of

DOCTOR OF SCIENCE

Specialized in Control, Signal and Image Processing
In the field of Computational Neuroscience

A biophysical cortical column model for optical signal analysis

Sandrine CHEMLA

Advisor	Thierry Viéville	INRIA Sophia Antipolis, France
Co-Advisor	Frédéric Chavane	INCM, CNRS Marseille, France
Reviewers	Alain Destexhe	Laboratoire UNIC, CNRS Gif-sur-Yvette, France
	Paul Salin	Université Claude-Bernard Lyon1 CNRS, France
Examiners	Rachid Deriche	INRIA Sophia Antipolis, France
	Lionel Nowak	Université Toulouse CNRS, France
	Olivier Faugeras	INRIA Sophia-Antipolis, France
	Dirk Jancke	Ruhr-University Bochum, Germany

UNIVERSITÉ NICE-SOPHIA ANTIPOLIS - UFR Sciences

École Doctorale STIC
(Sciences et Technologies de l'Information et de la Communication)

THÈSE

pour obtenir le titre de

DOCTEUR EN SCIENCES

de l'UNIVERSITÉ de Nice-Sophia Antipolis

Discipline: Automatique, Traitement du Signal et des Images

Application: Neurosciences computationnelles

présentée et soutenue par

Sandrine CHEMLA

Un modèle biophysique de colonne corticale pour l'analyse du signal d'imagerie optique

Thèse dirigée par Frédéric CHAVANE et Thierry VIEVILLE

Soutenue le 18 février 2010

Composition du jury:

Rapporteurs	Alain Destexhe	Laboratoire UNIC, CNRS Gif-sur-Yvette, France
	Paul Salin	Université Claude-Bernard Lyon1 CNRS, France
Examinateurs	Rachid Deriche	INRIA Sophia Antipolis, France
	Lionel Nowak	Université Toulouse CNRS, France
	Olivier Faugeras	INRIA Sophia-Antipolis, France
	Dirk Jancke	Ruhr-University Bochum, Germany

A Lihana, future chercheuse.

Abstract

Voltage-sensitive dye imaging (VSDI) is a powerful modern neuroimaging technique whose application is expanding worldwide because it offers the possibility to monitor the neuronal activation of a large population with high spatial and temporal resolution. In this thesis, we investigate the biological sources of the voltage-sensitive dye signal (VSD signal), since this question remains unresolved in the literature.

What does the voltage-sensitive dye imaging signal measures? This question is difficult to resolve at the physiological level as the signal is multi-component: The dye reflects the dynamics of the membrane potential of all membranes in the neuronal tissue, including all layers of the circuitry, all cell types (excitatory, inhibitory, glial) and all neuronal compartments (somas, axons, dendrites). To answer this question, we propose to use a biophysical cortical column model, at a mesoscopic scale, taking into account biological and electrical neural parameters of the laminar cortical structure. The model is based on a cortical microcircuit, whose synaptic connections are made between six specific populations of neurons, excitatory and inhibitory neurons in three main layers. Each neuron is represented by a reduced compartmental description with conductance-based Hodgkin-Huxley neuron model. The model is fed by a thalamic input with increasing activity, background activity and lateral connections. Isolated neurons and network behavior have been adjusted to fit data published in the literature. The so-calibrated model offers the possibility to compute the VSD signal with a linear formula. We validated the model by comparing the simulated and the measured VSD signal.

Thanks to the compartmental construction of this model, we confirm and quantify the fact that the VSD signal is the result of an average from multiple components, with excitatory dendritic activity of superficial layers as the main contribution. It also suggests that inhibitory cells, spiking activity and deep layers are contributing differentially to the signal dependently on time and response strength. We conclude that the VSD signal has a dynamic multi-component origin and propose a new framework for interpreting VSD data.

Résumé

L'imagerie optique extrinsèque basée sur l'utilisation de colorants sensibles aux potentiels (VSD) est actuellement la seule technique de neuroimagerie offrant la possibilité d'observer l'activité d'une large population de neurones avec une forte résolution spatiale et temporelle. Dans cette thèse, notre but est d'étudier les origines biologiques du signal d'imagerie optique (signal VSD), étant donné que cette question reste sans réponse claire dans la littérature.

Identifier l'origine du signal VSD est difficile au niveau physiologique car les molécules de colorant reflètent la dynamique du potentiel de membrane de toutes les membranes du tissu cortical, incluant toutes les couches corticales, tous les types de cellules (excitatrices, inhibitrices, gliales) et tous les compartiments neuronaux (somas, axons, dendrites). Pour répondre à cette question, nous proposons dans cette thèse d'utiliser un modèle biophysique de colonne corticale, à une echelle mésoscopique, prenant en compte les paramètres neuronaux biologiques connus de la structure corticale. Le modèle est basé sur un microcircuit cortical à six populations de neurones interconnectés: une population excitatrice et une population inhibitrice dans chacune des trois principales couches du cortex. Chaque neurone est représenté par une structure morphologique réduite à compartiments avec une dynamique de type Hodgkin-Huxley. Le modèle est alimenté par une activité spontanée, des connexions latérales et une entrée thalamique d'intensité croissante. Les neurones isolés et le comportement en réseau ont été ajustés pour correspondre à des données publiées dans la litterature. Le modèle ainsi ajusté offre la possibilité de calculer le signal VSD avec une formule linéaire. Nous avons validé le modèle en comparant le signal VSD simulé et le signal VSD mesuré expérimentalement.

Grâce à la construction compartimentale de ce modèle, nous confirmons et quantifions le fait que le signal VSD est le résultat d'une moyenne de plusieurs composantes, avec comme contribution majeure, l'activité dendritique des neurones excitateurs des couches superficielles du cortex. Le modèle suggère également que les neurones inhibiteurs, l'activité supraliminaire et les couches profondes participent également au signal, et ce de manière dépendante du temps et de la force de la réponse. Nous arrivons à la conclusion que le signal VSD possède une origine multicomposante dynamique et proposons un nouveau formalisme pour l'interpréter.

Acknowledgments

This thesis started at INRIA Sophia-Antipolis in the Odyssée Lab (now NeuroMath-Comp project), then continued at INCM in the DyVA team. This work was also partially supported by the European FACETS integrated project (IST-15879).

This thesis would definitely not have been possible without the subtle pressure of my first supervisor Thierry Viéville. I remember that one day when I said: "No, thank you but I am sure, I don't want to do a PhD thesis", and his answer was: "Ok, fine...anyway you should apply for a grant (for fun)". Well done Thierry and thank you for having been such a great supervisor!

Conversely, my second supervisor Frédéric Chavane had no other choice than to hire me, since I came into his office and asked to work in his Lab (thanks to my grant, thus thanks to Thierry...remember?). I would like to thank him for giving me this opportunity, as well as his passion for Biology and Neuroscience. Even though, sometimes I had doubts about the real impact of our work, I knew that the question was important to him and it was enough for me to go on. I would also like to thank him for the hard work of correction he did for me during the writing of this manuscript and for the two days off he forced me to take for Christmas. Thank you Fredo for your unfailing energy, you can be so persuasive!

I am very grateful to Alain Destexhe and Paul Salin for having accepted to review my manuscript, and to Olivier Faugeras, Lionel Nowak, Rachid Deriche and Dirk Jancke for having kindly accepted to examine this thesis. Although stressful, it is a real honor for me to present this work in front of you.

I am also very grateful to Ted Carnevale, Michael Hines and Padraig Gleeson for their help with the simulation softwares.

I would like to thank all the Odyssée, NeuroMathComp and DyVA members for all manner of support that they gave me during these three years and few months. A big

x

Contents

List of Figures

List of Tables

Context and motivations

CONTEXT AND MOTIVATIONS

How does the brain works? For ages, philosophers and scientists are motivated by this question. Today, thanks to our good knowledge of its architecture and the associated functions, we have made explicit to which extent the underlying circuitry, composed of billions of neurons that communicate between each other, makes the brain the most complex system in the body.

Modern neuroimaging and computational neuroscience are two recent neuroscience disciplines that are very important to understand brain mechanism. New imaging techniques, such as functional magnetic resonance imaging (fMRI) or optical imaging (OI), allowed researchers to observe the brain (of human or animal) in activity, at the level of large populations of neurons. However, these amazing techniques are based on complex observation of the system, that is not yet fully understood.

In this thesis, we present the voltage-sensitive dye imaging (VSDI) method. The possibility offered for *in vivo* (and *in vitro*) brain imaging is unprecedented in terms of spatial and temporal resolution. This technique is based on the use of a dye that binds to membranes and acts as a local probe indicating the level of depolarization by an emission of fluorescent photons. Therefore, the voltage-sensitive dye signal (VSD signal) originates from a large amount of intermingled neuronal and glial membranes components. Combined intracellular recording with VSDI has demonstrated the linear correspondence between VSD signal and membrane potential of individual neuron, but so far no studies have focused on what exactly the VSD signal actually measures when applied to a cortical population *in vivo*. We believe that it is of tremendous importance to understand what is the origin of this signal in order to exploit and interpret it.

Here we propose a solution to study the origin of the VSD signal. Experimental approaches for such purposes are not really feasible because the available methodologies do not offer the possibility to inspect simultaneously all the components that may contribute to the signal. Therefore, to solve this issue, we propose that computational models based on biological properties of the brain can help. They provide important tools for understanding all this complexity. Indeed, building a computational model can help to better understand phenomena by making simplifications of the biological reality and being explicit. Each parameter of the model is under control and can be tested separately, which is impossible for the real system. Another advantage of building models is the possibility to make predictions in order to develop targeted experiments. However, modeling the brain or even a brain sub-system is a real challenge, since simple models are unlikely to be useful to encounter for the complexity of such a system while accurate

ones will certainly be too complicated to interpret.

We thus developed, for that purpose, what we think to be the most simple realistic biophysical model, whose neuronal behavior properly fits the literature. The model is also reproducing the global dynamics of experimental VSD signals (e.g. VSDI experiments done on monkeys at the DyVA Lab.), allowing us to perform a detailed quantitative analysis of the VSD signal sources.

DETAILED ORGANIZATION

This thesis is organized in four parts, as follows:

PartI - Introduction

The first part deals with brain structures, an overview of how to understand, observe and model them. At different scales, two main units of the brain, the neuron and the cortical column, provide two natural ways to model this complex system.
Chapter 1 presents the biological structure of a neuron and its electrophysiology, followed by a characterization of neurons in the visual cortex: the contrast response function (CRF). **Chapter 2** deals with cortical columns. In the literature, this concept appears to be confusing since the name "cortical column" has been used in so many ways. We try here to clarify the concept as understood today. Observing those brain structures have always been a challenge for neuroscientists. Today, they dispose of a battery of techniques to measure brain activity directly or indirectly at different scales. All these techniques are reviewed in **Chapter 3**, with an emphasis on techniques that allow to visualize columns. Finally, we go from the observation to the modelization of those brain structures in **Chapter 4**, by reviewing neuron and cortical column models. Indeed, from artificial models to biological ones, neuron models have been used either to reproduce the computational effectiveness of the brain (artificial neural networks (ANN)) or to accurately describe and predict biological processes (biological neural networks (BNN)). Here, we emphasize the famous model of Hodgkin and Huxley, since this is the one we will use in our cortical column modelization.

PartII - VSDI: Review and Models

The second part focuses on the VSDI technique. We explain its principle for non-expert readers and list the main possibilities offered by this method for brain imaging in **Chapter 5**. What does the VSD signal measures? This question is difficult to solve at the

physiological level since the signal is multi-component: The dye reflects the dynamics of the membrane potential of all membranes in the neuronal tissue, including all layers of the circuitry, all cell types (excitatory, inhibitory, glial) and all neuronal compartments (somas, axons, dendrites). This is why we performed a detailed analysis of the method limitations. It raises many questions concerning the VSD signal origin. In order to answer them, modeling seems to be an appropriate solution. It was therefore important to see what has been already done in the literature in this context. Models that try to reproduce and analyse the VSDI measures are reported in **Chapter 6**.

PartIII - A biophysical cortical column model to study the multi-component origin of the VSD signal

The third part of this thesis is dedicated to the proposed biophysical model. Since none of the previous models was specific enough to answer our questions, we propose a biophysical cortical column model taking into account biological and electrical neural parameters of the laminar cortical structure. The model is based on a cortical microcircuit, whose synaptic connections are made between six specific populations of neurons, excitatory and inhibitory neurons in three main layers. Each neuron is represented by a reduced compartmental description based on the conductance-based Hodgkin-Huxley neuron model. The model is fed by a thalamic input with increasing activity, background activity and lateral connections. Thanks to its compartmental construction, this model offers the possibility to compute the VSD signal with a linear formula and can quantitatively predict the different contributions of the VSD signal. We validated the model by comparing the simulated and the measured VSD signal. The model specifications, its behavior and the explicit computation of the VSD signal can be found in **Chapter 7**, while the quantitative analysis, relative to the VSD contributions, is reported in **Chapter 8**.

PartIV - Discussion

In the last part of this thesis, we discuss the main achievements of this work (**Chapter 9**). In particular, we review the advantages and weaknesses of the model and propose several improvements for the future. A general conclusion about this thesis is finally reported.

Contexte et motivations (en français)

CONTEXTE ET MOTIVATIONS

Comment le cerveau fonctionne t-il ? Depuis des années, philosophes et scientifiques sont fascinés par cette question. Aujourd'hui, grâce à notre bonne connaissance de l'architecture du cerveau et des fonctions associées, nous avons rendu explicite le circuit neuronal sous-jacent, composé de milliers de neurones qui communiquent entre eux, et qui fait du cerveau le système le plus complexe du corps.

La neuroimagerie moderne et les neurosciences computationnelles sont deux disciplines récentes en neuroscience très importantes pour comprendre les mecanismes du cerveau. De nouvelles techniques d'imagerie telles que l'imagerie par résonance magnétique fonctionnelle (IRMf) ou encore l'imagerie optique (IO), ont permis aux chercheurs d'observer le cerveau (humain ou animal) en activité, à l'échelle de grandes populations de neurones. Cependant, ces techniques révolutionnaires sont basées sur des observations complexes et souvent indirectes du système qui ne sont pas encore complètement comprises.

Dans cette thèse, nous présentons la méthode d'imagerie optique basée sur les colorants sensibles au potentiel de membrane (VSDI). Cette technique offre la possibilité d'observer le cerveau aussi bien *in vitro* que *in vivo*, avec une résolution spatiale et temporelle sans précédent. Elle consiste à utiliser un colorant qui s'ancre dans les membranes plasmiques des cellules corticales et agit comme une sonde locale, indiquant le niveau de dépolarisation des cellules par une émission de photons fluorescents. De ce fait, le signal d'imagerie optique basée sur les colorants sensibles au potentiel (signal VSD) provient d'un grand nombre de composants neuronaux et gliaux entremêlés. Des enregistrements intracellulaires combinés au VSDI ont démontré la relation linéaire entre le signal VSD et le potentiel de membrane d'un neurone individuel, mais jusqu'à présent, aucune étude ne s'est vraiment concentrée sur l'origine exacte du signal VSD d'une population neuronale enregistrée *in vivo*. Nous croyons que l'étude des sources du signal VSD est capitale pour pouvoir mieux exploiter et interpréter ce signal.

Dans cette thèse, nous proposons une solution pour étudier l'origine du signal VSD. Les approches expérimentales ne sont pas réellement faisables car les méthodologies disponibles n'offrent pas la possibilité d'inspecter simultanément tous les composants susceptibles de contribuer au signal. C'est pourquoi nous proposons la construction d'un modèle computationnel basé sur des propriètés biologiques du cerveau. Ces modèles fournissent des outils importants pour mieux apprehender toute cette complexité. En effet, un tel modèle peut aider à mieux comprendre certains phénomènes en simplifiant la réalité biologique et en nous forçant à etre explicite. Chaque paramètre du modèle

est contrôlable et peut être testé séparemment, ce qui est impossible dans le cas du système réel. Un autre avantage des modèles est la possibilité de faire des prédictions dans le but de développer des expériences dédiées. Cependant, modéliser le cerveau ou un sous-sytème cérébral est un vrai défi étant donné que les modèles trop simples sont problablement inutiles face à la complexité d'un tel système, tandis que les modèles très précis seront certainement trop difficiles à interpréter.

Dans ce but, nous avons donc développé ce que nous pensons être le plus simple des modèles biophysiques réalistes, dont le comportement neuronal correspond parfaitement à la littérature. Le modèle reproduit également la dynamique globale des signaux expérimentaux en VSDI (e.g. expériences VSDI faites sur le singe au laboratoire DyVA, Marseille), nous permettant de conduire une analyse quantitative détaillée des sources du signal VSD.

Organisation détaillée

Cette thèse est organisée en quatre parties:

PartI - Introduction

La première partie porte sur les structures du cerveau: comment les comprendre, les observer et les modéliser. A différentes échelles, deux unités principales du cerveau, le neurone et la colonne corticale, offrent deux approches naturelles pour modéliser ce sytème complexe.

Le **chapitre 1** présente la structure biologique d'un neurone et son électrophysiologie, suivi d'une caractérisation des neurones dans le cortex visuel: la fonction de réponse au contraste. Le **chapitre 2** traite des colonnes corticales. Dans la littérature, ce concept apparaît assez confus du fait de l'utilisation du même terme "colonne corticale" pour plusieurs définitions. Nous essayons ici de clarifier le concept avec les informations dont nous disposons aujourd'hui. L'observation de ces deux structures, i.e. neurone et colonne corticale, a toujours été un défi pour les neuroscientifiques. Aujourd'hui, ils disposent d'une serie de techniques pour mesurer directement ou indirectement l'activité cérébrale à différentes échelles. Toutes ces techniques sont passées en revue dans le **chapitre 3**, avec un accent sur les techniques qui permettent de visualiser les colonnes corticales. Enfin, dans le **chapitre 4**, nous passons de l'observation à la modélisation de ces structures du cerveau en examinant les modèles de neurones et de colonnes corticales. Les modèles de neurones, qu'ils soient artificiels ou biologiques, ont été utilisés pour reproduire l'efficacité computationnelle du cerveau (réseaux de neurones artificiels) ou pour décrire et prédire précisément certains processus biologiques (réseaux de neurones bi-

ologiques). Dans cette partie, nous mettons l'accent sur le célèbre modèle d'Hogkin et Huxley, car nous l'utiliserons dans notre modèle de colonne corticale par la suite.

PartII - VSDI: Revue et Modèles

La seconde partie porte sur la technique VSDI. Dans le **chapitre 5**, nous expliquons son principe et dressons la liste des possibilités majeures offertes par cette méthode pour imager le cerveau. Identifier l'origine du signal VSD est difficile au niveau physiologique car les molécules de colorant reflètent la dynamique du potentiel de membrane de toutes les membranes du tissu cortical, incluant toutes les couches corticales, tous les types de cellules (excitatrices, inhibitrices, gliales) et tous les compartiments neuronaux (somas, axons, dendrites). C'est pourquoi, dans ce chapitre, nous faisons également une analyse détaillée des limitations de la méthode, qui soulève alors plusieurs questions concernant l'origine du signal VSD. Pour répondre à ces questions, la modélisation se présente comme une solution adaptée. Il est alors essentiel de faire la revue des modèles du signal VSD déjà existants dans la littérature. Ces modèles sont reportés dans le **chapitre 6**.

PartIII - Un modèle biophysique de colonne corticale pour l'analyse du signal d'imagerie optique

La troisième partie est dédiée au modèle biophysique proposé. Etant donné qu'aucun des précédents modèles n'est suffisamment spécifique pour répondre aux questions posées, nous proposons un modèle de colonne corticale biophysique, prenant en compte les paramètres neuronaux biologiques connus de la structure corticale. Le modèle est basé sur un microcircuit cortical à six populations de neurones interconnectés: une population excitatrice et une population inhibitrice dans chacune des trois principales couches du cortex. Chaque neurone est représenté par une structure morphologique réduite à compartiments avec une dynamique de type Hodgkin-Huxley. Le modèle est alimenté par une activité spontanée, des connexions latérales et une entrée thalamique d'intensité croissante. Grâce à sa constructure compartimentale, ce modèle offre la possibilité de calculer le signal VSD avec une formule linéaire et de prédire quantitativement les différentes contributions du signal VSD. Nous avons validé le modèle en comparant le signal VSD simulé au signal VSD mesuré expérimentalement. Les spécifications du modèle, son comportement et le calcul explicite du signal VSD sont traités dans le **chapitre 7**, tandis que l'analyse quantitative relative aux contributions du signal est reportée dans le **chapitre 8**.

PartIV - Discussion

Dans la dernière partie, nous discutons des principaux résultats présentés dans cette thèse (**Chapitre 9**). En particulier, nous passons en revue les avantages et inconvénients du modèle et nous proposons plusieurs améliorations possibles pour le futur. Enfin, nous concluons de manière très générale sur les aspects traités dans cette thèse.

Part I

Introduction

THE NEURON

OVERWIEW

In this chapter, we briefly review some fundamental concepts in Neuroscience. We start with the structure and the physiology of a general biological neuron (Section 1.1) and move quickly towards the properties of neurons in the primary visual cortex (Section 1.2).

This chapter is not meant to be a "state-of-the-art" of the neuron, it is rather a prerequisite to introduce the basic concepts used in the following parts, which deal with neuronal activities imaging and neuronal activities modelling. It is especially useful since this thesis is at the interface between neuroscience and computer science.

In order to understand in depth each of the following concepts, we propose two text book references: Kandel et al. (2000); Purve et al. (2004).

Contents

1.1   FUNDAMENTALS

The vertebrate nervous system is divided into two main components: the central nervous system (CNS) and the peripheral nervous system. The CNS contains the brain and the spinal cord. The brain is a very complex system and we start grossly describing the main subdivisions of its anatomy. The brain consists of two cerebral hemispheres, composed of many millions of neural fibers (white matter) and covered by a thin layer of nerve cells (gray matter) called the cerebral cortex or neocortex. The corpus callosum, a collection of fibers, forms a bridge between the left and right hemisphere. The thalamus, a large mass of gray matter, relays to the cerebral cortex or the spinal cord information received from diverse brain regions and sensory organs. The cerebellum, little brain at the bottom of the brain, is a reflex center of equilibration, mainly responsible of balance and muscle coordination. The hypothalamus regulates many of the body's functions (temperature, heart-rate, etc.) through the control of involuntary movements and the secretion of hormones. The brainstem (comprising the midbrain, pons, and medulla), lower extension of the brain, is the pathway for all fiber tracts passing up and down from peripheral nerves and spinal cord to the highest parts of the brain and controls vital functions of the body (breathing, digestion, etc.), as well as posture and movements (walking, reaching, etc.). The cerebral cortex is divided into four anatomically distinct lobes: frontal, parietal, temporal and occipital, that have specialized functions. Further information on the functional organization of the brain will be given in Chapter 2, dealing with cortical columns.

There are a hundred billion neurons times fifty thousand synaptic connections, each synapse being a complex neurotransmitter relay with a huge amount of information bits. Interactions with the external world is definitely possible thanks to his level of complexity. Indeed, the mammalian nervous system is packed of neurons and each neuron has a job: To process information with other neurons by making connections, integrating and sending signals. The nervous system has actually two classes of cells: Neurons and glial cells. Neurons are specialized for information processing over long distances whereas glial cells, at first glance, do not participate directly in synaptic interactions and electrical signaling but provide support and nutrition for neurons.

1.1.1   Glial cells

Glial cells (the name of these cells derives from the Greek for glue) are known as the "supporting cells" of the CNS and are estimated to outnumber neurons by as much as 50 to 1. Despite their large numbers, glial cells occupy only about half the volume of the brain, because they do not branch as extensively as neurons do. Their main functions

are to surround neurons and hold them in place, to supply them nutrients and oxygen, to insulate one neuron from another, and to destroy pathogens and remove dead neurons. There are four major types of glial cells in the CNS: astrocytes, oligodendrocytes, microglial cells and one major type in the peripheral nervous system: the schwann cells, as illustrated in Figure 1.1. Astrocytes, named for their starlike shape, are the most abundant. They hold neurons together, anchor them to blood vessels thereby forming the bloodbrain barrier, regulate their micro-environment and regulate transport of nutrients and wastes to and from them. Oligodendrocytes produce the myelin sheath in the CNS, which insulates and protects axons of neurons, helping them to conduct impulses faster. Microglia cells are phagocytes that defend against pathogens (e.g. infection, injury or disease). Finally, schwann cells has the same role than the oligodendrocytes, i.e. producing the myelin sheath, but in the peripheral nervous system.

Glial cells have long been thought to be not directly involved in information processing because they do not initiate or conduct action potentials (Kandel et al., 2000). However, recent *in vivo* studies have shown increasing evidence for an active role of astrocytes in brain function. For example, astrocytes can respond to a number of chemical agents (i.e. neurotransmitters), as neurons do. They release neurotransmitters and other neuroactive substances, called gliotransmitters, that modulate neuronal excitability and synaptic transmission (Schummers et al., 2008). This new vision of glial cells as active elements of synapses is also supported by the study of Perea and Araque (2009), who besides showed that astrocytes play an important role in regulating synaptic plasticity. Moreover, Schummers et al. (2008) discovered that astrocytes respond to visual stimuli along with their neighboring neurons in the visual cortex (Kelly and Van Essen, 1974). This raises the possibility that astrocytic networks engage in information processing but with very different temporal and spatial characteristics from neuronal signaling (see Chapter 5). The role of glial cells in information processing remains thus unresolved but glia became to get more attention in the last decade, partly thanks to novel imaging techniques allowing to image both neurons and glial cells in response to sensory stimuli (e.g. 2-photon microscopy, see Chapter 3).

1.1.2 Neuron structure

Neurons are the main signaling units of the nervous system (Figure 1.2). The unicity of this cell comes from the two major structures (also called *processes*) spreading out the cell body: the dendritic tree and the axon, which roughly correspond to the input and the output functions respectively; the integration function being done by the soma. The dendritic tree is a branched structure that forms the main inputs receiver of a neuron, while the axon represents its output transmitter. Generally, the axon is covered by an insulating sheath called myelin and separated by some relay station (nodes of Ranvier),
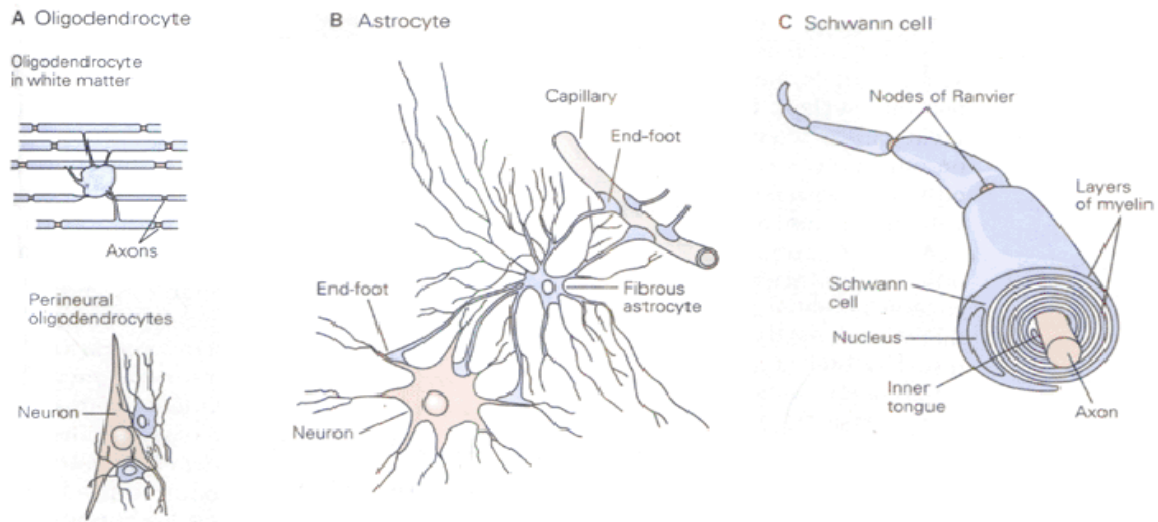
Figure 1.1: The three main types of glial cells in the nervous system. Modified from Kandel et al. (2000).

allowing neurons to send signals faster over very long distances in the cortex (i.e. the saltatory conduction). Myelin is a major component of the white matter of the brain, as opposed to the gray matter of neocortex, which has a high concentration of cell bodies and dendrites. This axon myelination increases the propagation speed of the signal with a linear dependence on axonal diameter (a myelinated 20-μm vertebrate axon can reach over 100 m/s (Arbib, 2002)). Then, as the axon itself branches out, the pulse is transmitted to several thousand target neurons, through chemical and electrical junctions called synapses (see Section 1.1.4 for details on the synaptic transmission).

The neuron is recovered by a phospholipid bilayer, i.e. the membrane, which forms a separation between the extracellular space around the neuron and its intracellular fluid. The membrane is mostly impermeable to many proteins, molecules and ions and only selectively permeable to a few ions, through specialized proteins called channels. This separation of various ions across this membrane creates the potentials that form the basis of the electrophysiology of the neuron, as detailed in the next section.

1.1.3   Neuron electrophysiology

The neuron is an electrophysiological entity that can be understood using the principles of electricity and diffusion.

Ion channels

Incoming signals come into the neuron primarily through *channels* located in synapses, allowing ions to move across the neuron membrane. Ion channels are pore-forming mem-
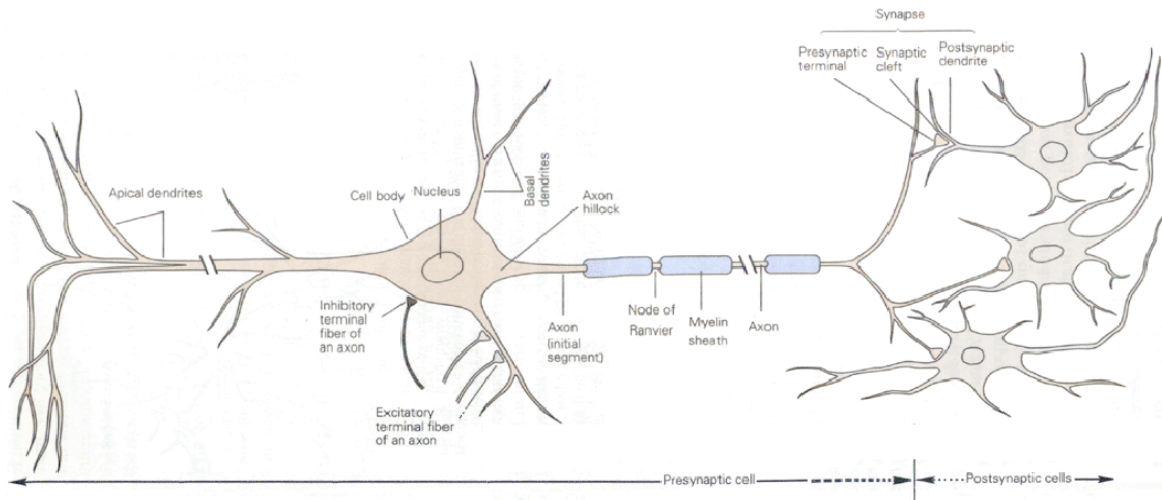
Figure 1.2: Structure of a neuron and signaling process. Modified from Kandel et al. (2000).

brane proteins that span the cell membrane to allow a highly selective ionic pathway into the cell. Some channels are always open (i.e. non-gated open channels) and some others can change from a closed to an open state (Opie, 2004), governed by one or several *gates*. For example, two main gated-channels will be discussed in the next paragraphs: *Voltage-gated ion channels* and *Ligand-gated channel*. Voltage-gated ion channels (this type of ion channel underlies the nerve impulse mechanism, as explained later), thus change state (open/close) in response to changes in membrane potential, while ligand-gated channels open when a specific neurotransmitter binds to it.

The most relevant ions for neural processing are sodium (Na^+), potassium (K^+), chloride (Cl^-) and calcium (Ca^{++}). Na^+ and Cl^- are higher concentrated outside the cell, while K^+ and large negatively charged protein molecules (noted A^- for anions) are in higher concentration inside the cell (see Fig. 1.3). Furthermore, there are more A^- molecules inside the cell than K^+ ions. At rest, i.e. when no inputs are coming into the neuron, the inside of the cell is therefore more negative than the outside and the membrane potential is called *resting potential*. This will change with the arrival of the action potential (see Section 1.1.5).

The equilibrium potentials

As these ions are unequally distributed across the membrane, their movements generate electrical currents and electrical potentials following the Ohm's law (Equation 1.1).

$$I = G\,V \tag{1.1}$$

where I is the electrical current, V is the electrical potential and G is the conductance, i.e. the inverse of resistance, which represents how easily ions can move across the membrane. I is then called the transmembrane current and V the transmembrane potential.

In addition to electrical potentials, ions also move because their concentrations are different inside and outside of the neuron. They diffuse down their concentration gradient following the Fick's law (Equation 1.2):

$$I = -D\,C \tag{1.2}$$

where I is the movement of ions (i.e. diffusion current), D is the diffusion coefficient and C is the concentration potential. Note that the ionic concentrations of sodium and potassium are produced and maintained by an active system of membrane pumps, i.e. the sodium-potassium pump. This mechanism uses ATP (i.e. adenosine triphosphate) as energy to create an imbalance in the concentrations of the sodium and potassium ions outside and inside the neuron. This Na/K pump thus maintain the resting potential at a typical value of -70 mV (Hodgkin and Huxley, 1952d). Chloride ions diffuse passively across the membrane.

Electrical and diffusion forces can balance each other, the ion then being "in equilibrium". The membrane potential needed to counteract the diffusion force is called the equilibrium potential or the reversal potential, and the previous Ohm's law can thus be written as follows (Equation 1.3), now referring to the diffusion corrected version of the Ohm's law:

$$I_{ion} = G_{ion}\,(V - E_{ion}) \tag{1.3}$$

where E_{ion} is the equilibrium potential of the given ion. The equilibrium potential for any ion can be calculated using the Nernst equation (Hille, 1992):

$$E_{ion} = \frac{RT}{zF}\,ln\,\frac{[Ion]_e}{[Ion]_i} \tag{1.4}$$

where R is the universal gas constant ($R = 8.31 J.mol^{-1}.K^{-1}$), T is the absolute temperature, F is the Faraday's constant ($F = 96500 C.mol^{-1}$), z is the valence of the ion (number of electrons), $[Ion]_e$ and $[Ion]_i$ are the ion concentrations in the extracellular and in the intracellular space respectively.

For example, the reversal potential of Na^+, which are concentrated outside the neuron, is positive with a typical value of around 60 mV, whereas those of K^+, which are concentrated inside the neuron, is negative around -90 mV (see Figure 1.3).

When considering that the membrane is actually permeable to several other ions, more exact values are given by the Goldman-Hodgkin-Katz equation (Equation 1.5), which is a generalization of the Nernst equation to all the monovalent positive and neg-
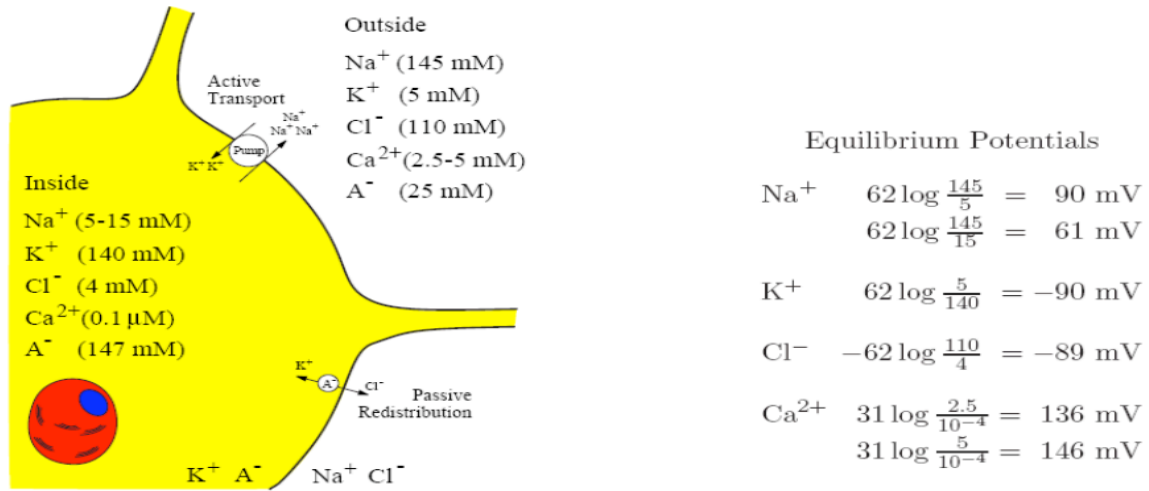
Figure 1.3: The electrophysiology of the neuron: Major ion concentrations and equilibrium potentials. From Izhikevich (2006).

ative ionic species:

$$E_m = \frac{RT}{F} ln(\frac{\sum P_{ion^+} [ion^+]_e + \sum P_{ion^-} [ion^-]_i}{\sum P_{ion^+} [ion^+]_i + \sum P_{ion^-} [ion^-]_e}) \qquad (1.5)$$

where E_m is the membrane potential, P_{ion} is the permeability for that ion, $[ion]_e$ and $[ion]_i$ are respectively the extracellular and intracellular concentrations of that ion.

In summary, ions flow through the neuron membrane under the forces of electric and chemical concentration gradients.

1.1.4 Synaptic transmission

As said earlier, the synapse is the communication junction between two neurons, and more precisely between the axon of the presynaptic neuron (before the synapse) and the processes (e.g. dendrites, soma, axon) of the postsynaptic neuron (after the synapse). The contacts of the axon to target other neurons are mainly either located on the dendritic tree (excitatory connections) or directly on the soma (inhibitory connections more generally), and are known as axodendritic or axosomatic synapses respectively. More precisely, excitatory synapses mostly occur on spines (see section 1.1.6 for a definition) and dendrites, while inhibitory synapses are more concentrated near the soma. Most synapses are chemical contacts, that is, the arrival of a nerve impulse at the presynaptic terminal of the synapse produces an influx of Ca^{++} ions through voltage-gated calcium channels which induces the exocytosis of neurotransmitters (stored in the synaptic vesicles), then fusing with the presynaptic membrane and releasing their contents into the synaptic cleft, i.e. the very narrow region between the axon terminal of the presynaptic

neuron and the dendrite of the target neuron. Neurotransmitters then diffuse across the gap and activate receptors that are located in the postsynaptic membrane. It results in the opening of certain ion channels, thus in a change in membrane conductance associated with a ionic flux, therefore a postsynaptic current (PSC), following Equation 1.3. Depending of the type of ion channels opened by the released neurotransmitter, the PSC could be either excitatory (EPSC) or inhibitory (IPSC), thus causes the membrane potential to respectively depolarize, i.e. getting closer to the spike threshold, or hyperpolarize, i.e. getting further to the spike threshold. A membrane depolarization is also called an excitatory postsynaptic potential (EPSP) and is the result of an excitatory synapse, while an inhibitory synapse will cause an inhibitory postsynaptic potential (IPSP), which is classically a membrane hyperpolarization. Shunting effect of inhibitory synapses will be approached later.

Excitatory and inhibitory neurotransmitters

Among the large number of neurotransmitters released by neurons, the most prevalent in the nervous system are amino acids (i.e. molecules containing both amine and carboxyl functional groups): glutamic acid ($glutamate$) and γ-aminobutyric acid ($GABA$). Fewer synapses, but not less functionally important, use monoamines neurotransmitters like $epinephrine$ (i.e. $adrenaline$), $serotonin$ or $dopamine$. The latter plays a very important role in the reward system, involved for example in drugs addiction. Acetylcholine was the first identified neurotransmitter, as being released from motor nerves at the neuromuscular junction. The list of neurotransmitters is long, hence we will only emphasize $glutamate$ and $GABA$ because they respectively represent the most abundant excitatory and inhibitory neurotransmitters in the mammalian central nervous system (Connors and Gutnick, 1990). The major role of an excitatory (resp. inhibitory) neurotransmitter is to increase (resp. decrease) the neuron excitability. In fact, the nature of a neurotransmitter is linked to the type of receptor it activates. Thus, we must say that specific receptors of $glutamate$ are exclusively excitatory, while specific receptors of $GABA$ are exclusively inhibitory. The two main $glutamate$ receptors are $NMDA$ (N-methyl-D-aspartic acid) and $AMPA$ (α-amino-3-hydroxy-5-methyl-4-isoxazolepropionic acid), while the main $GABA$ receptors are $GABA_A$ and $GABA_B$. Receptors are often coupled to ion channels (i.e. ionotropic receptors), being then only permeable to certain ions. $AMPA$ receptors are permeable to Na^+ and Ca^{2+} ions, $NMDA$ receptors to Ca^{++} ions, and $GABA$ receptors to Cl^- and K^+ ions.

Excitatory synapses

As explained above, the excitation process in the neocortex is mediated by the release of glutamate from the axon terminals of the cells into the synaptic cleft, which will ac-

tivate two classes of receptors: $AMPA$ and $NMDA$. The strength of synaptic excitation depends on many things, such as the amount of neurotransmitter released, the number of receptors on the membrane, the conductance of the ion channels gated by these receptors. Several experimental studies, *in vitro* on slices of visual (Mason et al., 1991) or sensorimotor (Thomson and West, 1993; Thomson et al., 1993) cortex, allowed to characterize EPSPs between pairs of intracellularly recorded pyramidal cells, and between pyramidal and inhibitory neurons, within cortical columns. $AMPA$ EPSPs amplitude ranges from about 0.5 to 3 mV and their duration ranges from about 15 to 60 msec (Fig. 1.4, top left).

Moreover, we can differentiate fast and slow excitatory transmissions. Indeed, ion channels controlled by $AMPA$ receptors are characterized by a fast response ($\tau_{rise} < 0.1$ ms) to presynaptic spikes and a quickly decaying postsynaptic current ($\tau_{decay} = 1.5$ ms), while ion channels controlled by $NMDA$ receptor are significantly slower ($\tau_{rise} = 3$ ms and $\tau_{decay} = 40$ ms, see Fig. 1.4, top left). The rapid time course of $AMPA$ responses is thought to be due to a combination of rapid clearance of neurotransmitter and rapid channel closure (Hestrin, 1992). $NMDA$ receptors have additional interesting properties that are due to a voltage-dependent blocking by magnesium ions (Hille, 1992), generating a negative I/V slope up to -40mV (Fig. 1.4, bottom left). Contrary to $AMPA$, $NMDA$ EPSPs will increase in amplitude when the neuron is depolarized.
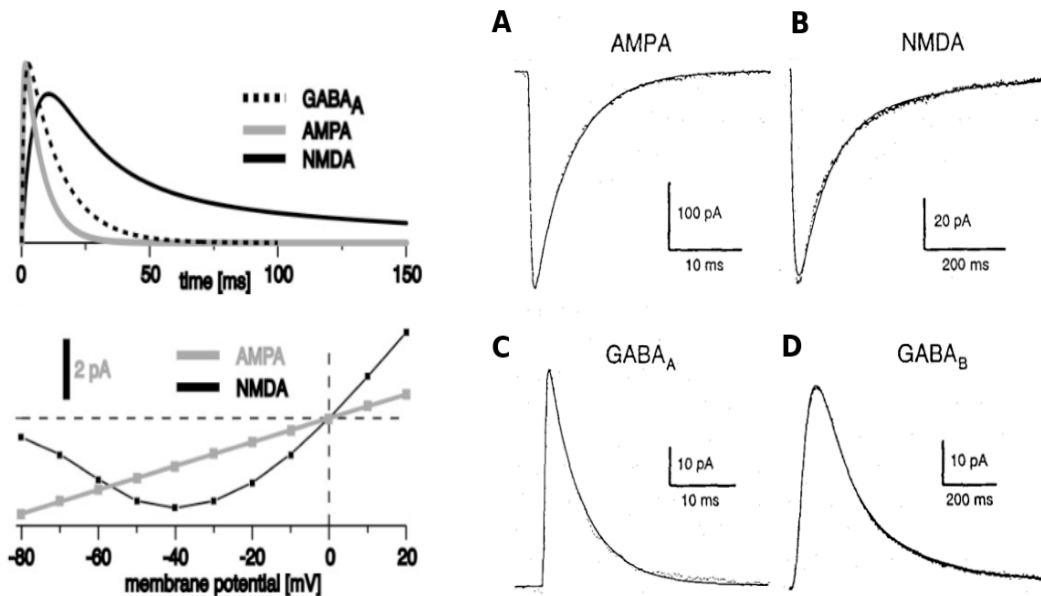
Figure 1.4: *Left:* $AMPA$, $NMDA$ and $GABA_A$ responses. From Gauck and Jaeger (2003). *Right:* Postsynaptic currents obtained from whole-cell recordings, fitting by detailed kinetic models (see Chapter 4): (A) AMPA-mediated currents (B) NMDA-mediated currents (C) $GABA_A$-mediated currents (D) $GABA_B$-mediated currents. From Destexhe et al. (1998).

Inhibitory synapses

Similarly to excitation, the inhibition process is mainly caused by the binding of $GABA$ neurotransmitter to its specific receptors. This binding causes the opening of ion channels to allow the flow of either chloride ions into the cell or potassium ions out of the cell. It results in a negative change in the transmembrane potential, usually causing an hyperpolarization. Quantitatively, the number of GABAergic synapses in the mammalian cerebral cortex is about 17% (Halasy and Somogyi, 1993). There are three different types of $GABA$ receptor, i.e. $GABA_A$, $GABA_B$ and $GABA_C$, but for our modeling considerations, we will only discuss about $GABA_A$ and $GABA_B$, and in the following parts we will globally refer to $GABA$ as $GABA_A$ channels which are all permeable to Cl^-. As illustrated in Figure 1.4C, $GABA_A$ receptors have relatively fast kinetics compared to $GABA_B$ receptors (Fig. 1.4D), which are much slower and involve second messengers (i.e. metabotropic receptor) (Destexhe et al., 1998). Note that there is a large diversity of GABAergic synapses in the neocortex with highly specific temporal dynamics (Gupta et al., 2000).

As opposed to $GABA_B$, which activate K^+ channels, bringing the neuron closer to the potassium reversal potassium thus hyperpolarizing it, activation of the $GABA_A$ receptors on the postsynaptic membrane does not only result in a net IPSP. The direction of the chloride flow will determine the action of $GABA$. Indeed, another inhibitory effect called *shunting inhibition* appears when the membrane potential is very close to the synaptic reversal potential of the Cl^- ions. Due to the lack of electrochemical gradient for these ions, there will be almost no movement of ions and thus no current. However, $GABA$ receptor activation will lead to a significant decrease in the membrane resistance of the cell, thus an increase in membrane conductance. The high concentration of $GABA$, mostly at the soma where $GABA$ receptors are more concentrated, will reduce or "shunt" the postsynaptic excitatory depolarization expression of the EPSC (Fig. 1.5) (Borg-Graham et al., 1998).
Recently, Destexhe et al. (2003), using intracellular recordings *in vivo*, showed that neocortical neurons are in a "high-conductance" state, resulting in a pure shunting effect of inhibition.

Synaptic integration

Actually, neurons in the mammalian CNS receive thousands of excitatory and inhibitory synaptic inputs broadly distributed on their dendritic trees. The classical way to understand dendritic integration is to consider that dendrites passively conduct and spatially and temporally summate the net current resulting from EPSCs and IPSCs converging to the axon initial segment, where it would trigger or not an action potential (see next section). This simple view also assumes that the conveyed signal always flows in the

same direction, from the dendrites and soma towards the axon.

Depending on the intrinsic properties of the dendrites, e.g. membrane resistance and capacitance, length, postsynaptic signals can be deformed. To be added to this passive filtering, complex active phenomena, i.e. active conductances, may non-linearly increase or attenuate the synaptic events integration, as well as shunting inhibition which will act nonlinearly by causing an increase in membrane conductance, thus "shunting" the excitatory response (see the two different sketches in Figure 1.5).
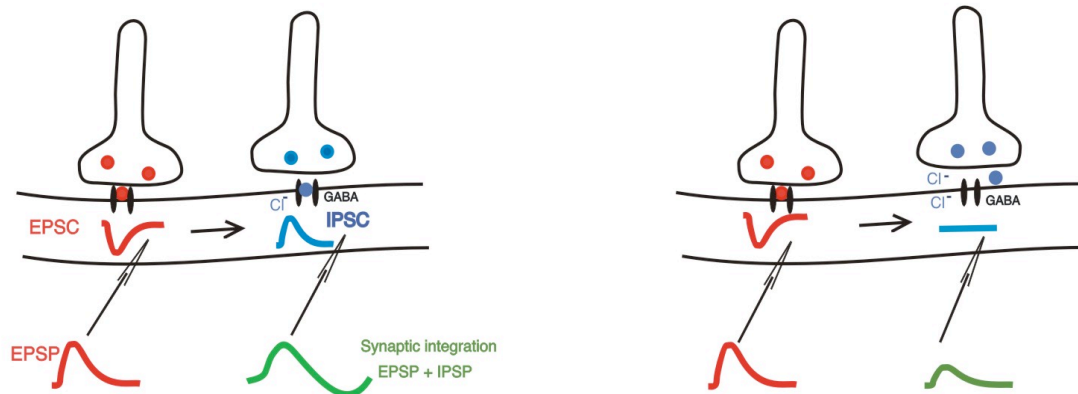
Figure 1.5: Hyperpolarizing and shunting inhibition. *A:* Once $GABA$ receptors are activated, Cl^- ions move through the membrane and enter the cell, resulting in an IPSC. The membrane is thus hyperpolarized. Depolarizing and hyperpolarizing waves are spatially and temporally summated. *B:* In most situations, due to the lack of electrochemical gradient for Cl^- ions, these latter do not actually move, resulting in a null current. However, activation of $GABA$ receptors induces a local decrease in membrane resistance, leading to the "shunt" of the depolarizing wave.

Thanks to novel techniques (e.g. two-photon imaging, see Denk et al. (1994) and Chapter 3), several studies have provided clear evidence, under *in vivo* conditions, for active conductances in dendrites (Markram et al., 1995; Eilers and Konnerth, 1997; Svoboda et al., 1997). Electrophysiological and imaging experiments revealed the presence of sodium and calcium voltage-gated channels on apical dendrites of cortical pyramidal neurons (Huguenard et al., 1989; Stuart and Sakmann, 1994; Markram et al., 1995; Magee and Johnston, 1995). These channels allow to propagate and even amplify depolarizing signals. Their summation are thus facilitated (Nettleton and Spain, 2000) leading to retrograde propagation of action potentials initialized at the soma (Stuart et al., 1997). Moreover, these active channels on dendrites play a role in the restoration of dendritic democracy, i.e. distal synapses have the same efficacy than proximal ones (Hausser, 2001).

Dynamic synapses

Synaptic transmission is history-dependent, meaning that a postsynaptic response depends on the history of previous activations of the synapse (Markram et al., 1998a), thus of the history of presynaptic activity (Thomson and Deuchars, 1994; Fuhrmann et al., 2002). More precisely, depending on the frequency of presynaptic spike trains or similarly their interspike interval (ISI), one can distinguish *depressing synapses* and *facilitating synapses*. See Tsodyks et al. (1998); Abbott and Regehr (2004) for more details on these mechanisms and more generally for a review on synaptic computation.

1.1.5   Description of the action potential

If the neuron membrane is sufficiently depolarized to push the membrane potential over the firing threshold for the neuron (typically -55 mV), then the neuron fires, i.e. delivers an action potential or spike. The first published intracellular action potential, dated from 1939 (Hodgkin and Huxley, 1939). It was obtained by English electrophysiologists Alan Hodgkin and Andrew Huxley from the squid giant axon. Hodgkin and Huxley (HH) were pioneers in understanding the dynamics of single nerve ((Hodgkin et al., 1952; Hodgkin and Huxley, 1952b,a,c,e)). More precisely, in these series of experiments, they succeeded to measure the currents and the conductances of the two major ionic components of the squid axon membrane, Na^+ and K^+. The techniques of space clamping (i.e. removing space variations from membrane measurements by holding transmembrane voltage constant over the full axon lenght) and voltage clamping (i.e. maintaining the transmembrane voltage at a fixed value), developed by Cole (1949), were fundamental for their experiments (see also Scott (2002) for a summary on these two techniques). It allows them to quantitatively measure these ionic currents, showing that they were strongly dependent of membrane voltage and to precisely describe the laws which govern movements of ions across the membrane during a general action potential event. Today we know that this voltage-dependence is directly linked to the biophysical properties of the membrane channels that control the flow of ions across the membrane (see the previous section). However, in 1952, Hodgkin and Huxley did not know about these ion-selective membrane channels. Though this anachronism, for our convenience here, we will use the modern concept to describe easily the action potential event.

The action potential is a result of ion flow through voltage-gated ion channels. Functionally, the voltage-gated sodium channel has two gates that can close its pore. The gate on the outside of the membrane is called the *activation* gate and the gate on the inside of the membrane is called the *inactivation* gate. The voltage-gated potassium channel has only one gate. The action potential can be divided into six phases (see Figure 1.6, the two gates of voltage-gated sodium channel are not explicitly represented):
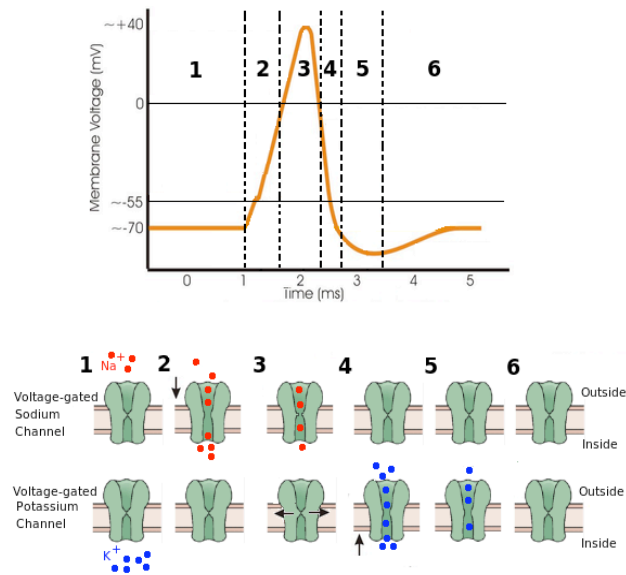
Figure 1.6: Schematic of an action potential. It can be divided into six major phases: (1) Resting phase, (2) Rising phase, (3) Overshoot phase, (4) Falling phase, (5) Undershoot phase and (6) Recovery phase. A schematic of the voltage-gated channels mechanism is also represented.

1. The initial steady state or resting phase: The neuron is at rest. Its resting potential is about -70 mV. Sodium channels have the activation gate closed and the inactivation gate open. Potassium channels are closed.

2. The rising phase: When the neuron threshold is reached, the increasing positive shift in membrane potential is driven by the opening of progressively more and more voltage-gated sodium channels, through their activation gates and the entry of Na^+ ions (red dots) into the neuron. This inward sodium current depolarizes the membrane voltage, inducing in return a dynamical closing of the inactivation gate of sodium channels. Note that the inactivation gate closes slowly compared to the rapidity of channel opening.

3. The overshoot phase: The membrane potential is now at its most positive state, i.e. it has overshot $0mV$. At this positive potential two processes are occuring simultaneously. First, the inactivation gate of sodium channels has closed, and as a result, sodium conductance have started to decline. Next, potassium channels begin to open, driving the membrane potential back toward the equilibrium potential for K^+. These voltage-gated potassium channels differ from leak potassium channels in that they are normally closed at the resting potential but open in response to depolarization (thus the term voltage-gated).

4. The falling phase: The action potential is now in its repolarizing phase, i.e. the

membrane potential is rapidly returning to the resting potential. During the falling phase, activation of voltage-gated potassium channels is maximal (huge influx of K^+ ions), while sodium channels are closed (no further Na^+ enters).

5. The after-hyperpolarization (AHP) phase: The undershoot occurs because most voltage-gated potassium channels are still open, such that the total potassium conductance of the neuron is greater than when the membrane is at its resting steady state.

6. The recovery phase: The membrane potential returns to the original steady-state resting potential. This occurs as the potassium channels close, Na^+ and K^+ ions are respectively moved out and into the neuron as initially. During this time called the absolute refractory period, the neuron can not spike again. This refractory period arises primarily because of the voltage-dependent inactivation of sodium channels, which "locks" the channel closed for milliseconds. As the sodium channels begin to activate again, the neuron is enable to fire an action potential, but it is has a much higher threshold. This is the relative refractory period (absolute plus relative refractory period last about 5 ms).

Though this complex shape, at the mesoscopic scale, the action potential is an all-or-nothing event, which means that once generated, its amplitude and its duration are independent of the amount of the level of activation that produced it. Instead, the intensity of the stimulus can be encoded by the frequency of action potentials, i.e. the firing rate. This principle of nerve impulse conduction was actually first proposed by the English electrophysiologist Edgar Douglas Adrian in 1914 (Adrian, 1914). Hodgkin and Huxley have then theoretically integrated their experimental discovery into the famous mathematical HH model whose equations are detailed in Chapter 4, Section 4.1.

1.1.6 Neurons Classifications

Though its general structure presented in Section 1.1.2, there are more than 10,000 different types of neurons in the brain. In the mammalian cortex, neurons come in many different shapes and sizes. There are thus several ways to classify them. In this manuscript, we are only interested in the excitatory-inhibitory diversity among cortical neurons and our classification is mainly based on morphological and electrophysiological features.

It is indeed important, for our biophysical modelization purpose, to take into account the main difference in morphology of the different populations of neurons (since the optical signal is proportional to the membrane area of cells, see Chapter 5), and to be able to reproduce the signaling pattern of each of them. The electrophysiological classification

was defined by experimental observations of the firing patterns of neurons in response to current injection of various amplitudes (McCormick et al., 1985; Izhikevich, 2003; Contreras and Palmer, 2003; Nowak et al., 2003). There are at least four fundamental classes of firing patterns observed in the mammalian neocortex (see Figure 1.7): Regular spiking (RS), intrinsically bursting (IB), chattering (CHT), fast spiking (FS). These patterns mainly result from different ion channel composition (Bargas and Galarraga, 1998). Furthermore, this classification is also interesting because there is a general correspondence with the neurotransmitter released by the cell (DeFelipe, 1993), thus the excitatory or inhibitory character of the cell. For example, FS cells are GABAergic inhibitory cells, whereas RS cells are glutamatergic excitatory cells. In this thesis, we are mainly interested in two of them, i.e. RS and FS cells, because they constitute the great majority of respectively excitatory and inhibitory cells in the neocortex.

Excitatory neurons

80% of cortical cells are excitatory. Among them, two main classes are distinguishable (Peters and Jones, 1984; Somogyi, 1989; White, 1989):

- Pyramidal cells constitute the majority of cortical neurons (about 60%) and are mainly located in layers II/III and V/VI (see Chapter 2, Section 2.1.1). Their name comes from their pyramidal-shaped somata and their main morphological characteristics come from their so-called apical dendrite and basal dendrites. The apical dendrites vertically traverses through layers, while basal dendrites mainly remain within the layer of the somata. Moreover, there are small pyramidal cells and large pyramidal cells, according to their size. Their somas average from 10 to 100 μm in diameter. Electrophysiologically, they mostly belong to the RS-type class: The neuron produces adapting spike trains. For example, Contreras and Palmer (2003) showed that RS cell of cat primary visual cortex, responded to a depolarizing pulse with an accommodating train of single spikes of 1 ms duration at threshold. The adaptation mechanism is due to the slow activation of Ca^{2+}-dependent K^+ channels (Sanchez-Vives et al., 2000a). Few pyramidal cells also exhibit IB or CHT behaviors (see Fig. 1.7).

- Spiny Stellate cells constitute about 20% of cortical neurons and are almost exclusively located in layer IV. They are morphologically characterized by their stellate appearance (spherical somata) and multiple short spiny dendrites remaining within a layer and column. Spines are small membranous protuberances found on dendrites. They are preferential sites of neuronal integration (Yuste and Denk, 1995) (see also Holmes (1990); Yuste and Majewska (1991) to learn more about the
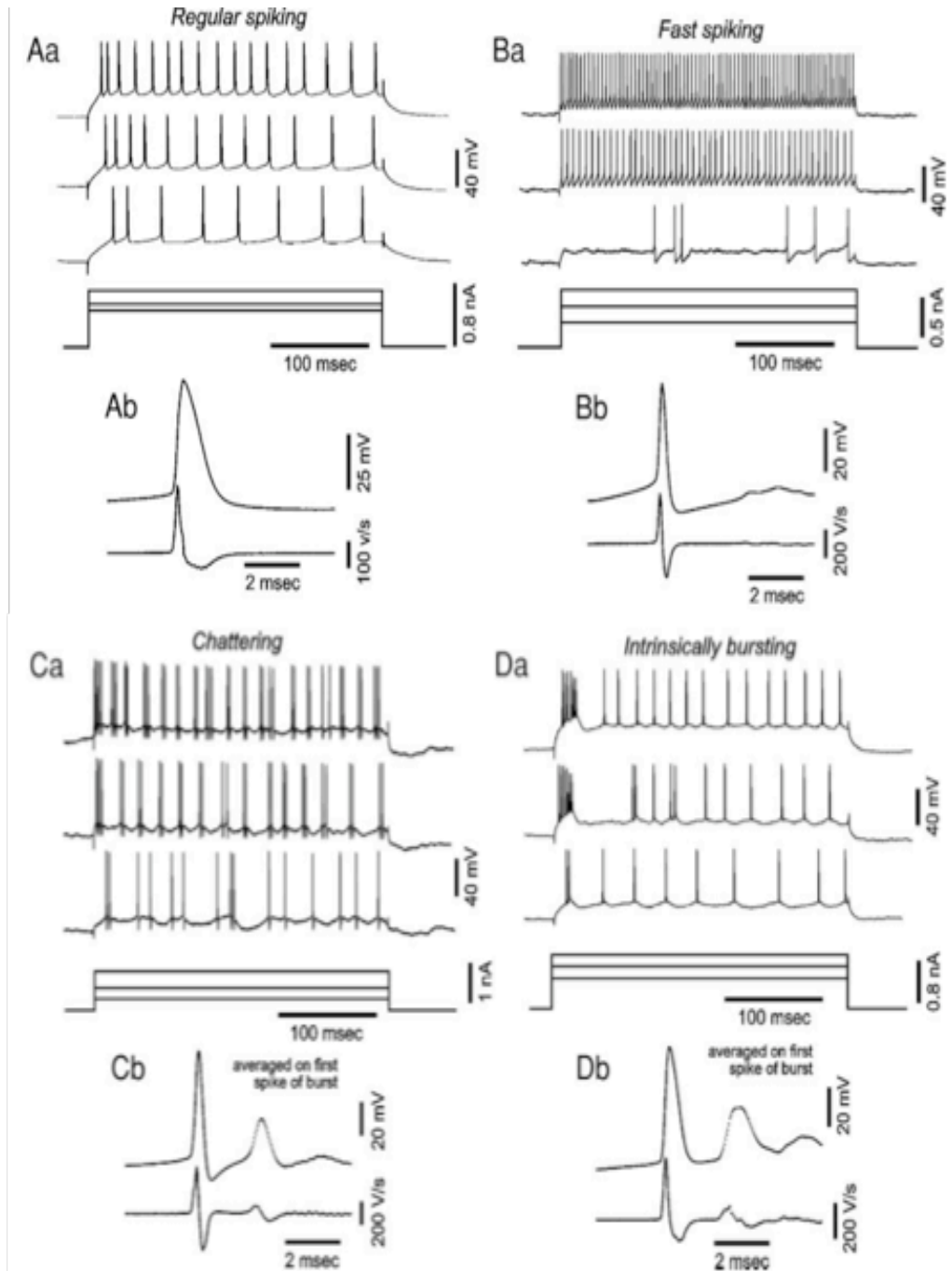
Figure 1.7: Four fundamental classes of firing patterns of cat primary visual neurons in response to pulses of depolarizing current pulses of various amplitudes. From Nowak et al. (2003).

function of dendritic spines). Electrophysiologically, they also belong to the RS-type class. Some spiny stellate cells display IB firing pattern.

Inhibitory neurons

20% of cortical cells are inhibitory. They are much more heterogeneous and present a much larger repertoire of firing patterns than excitatory cells (see Toledo-Rodriguez et al. (2003) for a review of all inhibitory neuron types in the neocortex). Here, for modeling convenience, we will only consider, as initially by Connors and Gutnick (1990), one main morphological inhibitory neuron found in all cortical layers, known as smooth or sparsely spiny neurons and one single inhibitory discharge behavior, known as FS. As their name indicates, smooth stellate cells are morphologically distinguishable from excitatory neurons by their lack of spines on dendrites. As shown in Contreras and Palmer (2003) or Nowak et al. (2003), FS cells fired, at very high frequency with little or no adaptation, very sharp spikes (0.6 ms duration at threshold) with pronounced fast afterhyperpolarizing potentials (AHPs).

1.2 NEURON'S PROPERTIES IN THE VISUAL CORTEX ———

1.2.1 Overview of visual processing

Receptive field definition

"A given optic nerve fiber responds to light only if a particular region of the retina receives illumination. This region is termed the receptive field of that fiber" (Hartline, 1940).
The receptive field (RF) is defined as the region of the retina or its equivalence in visual space, within which a stimulus evokes a change in the discharge of a neuron. Therefore, it characterizes the transformation between the visual image and neuronal activity.

Receptive fields in the retina

Visual processing begins in the retina, i.e. the receptive surface inside the back of the eye. Light enters the eye, passes through the layers of cells in the retina before reaching the photoreceptors (cone cells for daylight vision and rod cells for twilight vision) which are located at the back of the retina. Light activates the photoreceptors, which modulate the activity of bipolar cells. As a first approximation, bipolar cells, in turn, connect with ganglion cells located at the front of the retina. The axons of these output cells form the optic nerve, which carries information to the brain (Fig. 1.8,1). Two other types
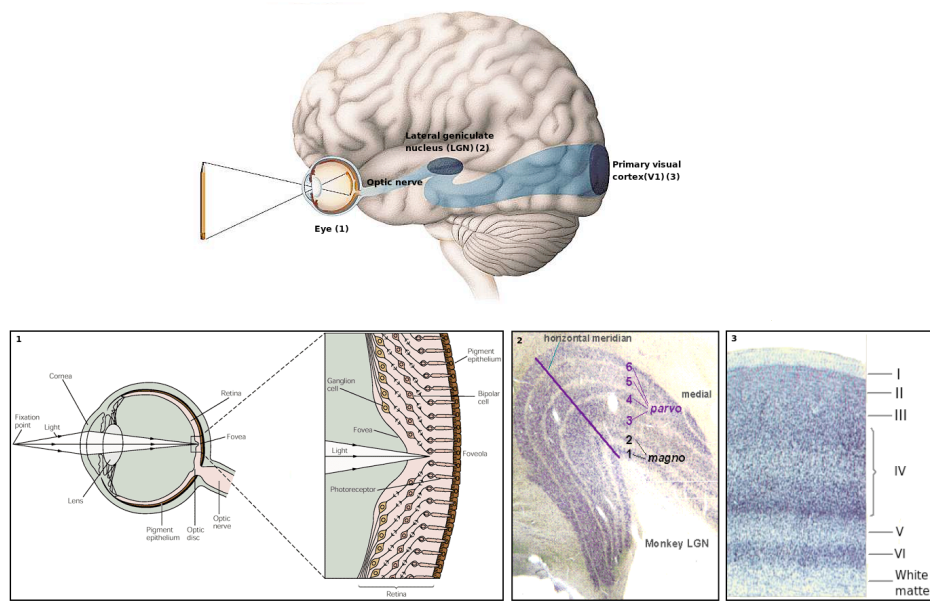
Figure 1.8: The visual pathway: from the retina to the primary visual cortex. (1) Retinal network. Adapted from Kandel et al. (2000). (2) Thalamic network:. In primates, the LGN contains six layers of cells. Layers 1 and 2 comprise the magnocellular layers, layers 3 through 6 comprise the parvocellular layers. (3) Primary visual cortex network

of neurons, horizontal cells and amacrine cells, are primarily responsible for lateral interactions within the retina (see Wohrer (2008) for an extensive introduction about the retina).

The RF of retinal ganglion cells have a roughly concentric spatial organization with a central area and an antagonist surround (Kuffler, 1953). Two functional types of cells can be distinguished depending on this spatial organization and the cell's response to luminance changes: ON-center/OFF-surround and OFF-center/ON-surround neurons. Figure 1.9 shows the cartoon of the response of either one type or the other to a spot of light. The first ones is activated by a spot of light in the center of their RF (row 3), while displayed merely no activity when the spot of light is presented in its surround region (row 2). A maximal response cell is achieved when the entire center of the RF is illuminated (row 4). Likewise, if we illuminate only the surround (with a ring of light), the ganglion cell is maximally inhibited (row 5). It corresponds to a property of summation within the subregions of the RF. A simultaneous stimulation of the center and surround region leads to the response's decrease (row 6), thus confirming the existence of an antagonism between the center and the surround regions (Enroth-Cugell and Robson, 1966). The same behavior is observed for an off-center ganglion cell by switching center and surround. This organization makes the ganglion cells sensitive to local differences

in the level of illumination across the receptive field, i.e. when the light intensities in the center and surround are quite different, thus sensitive to luminance contrast rather than the absolute intensity.
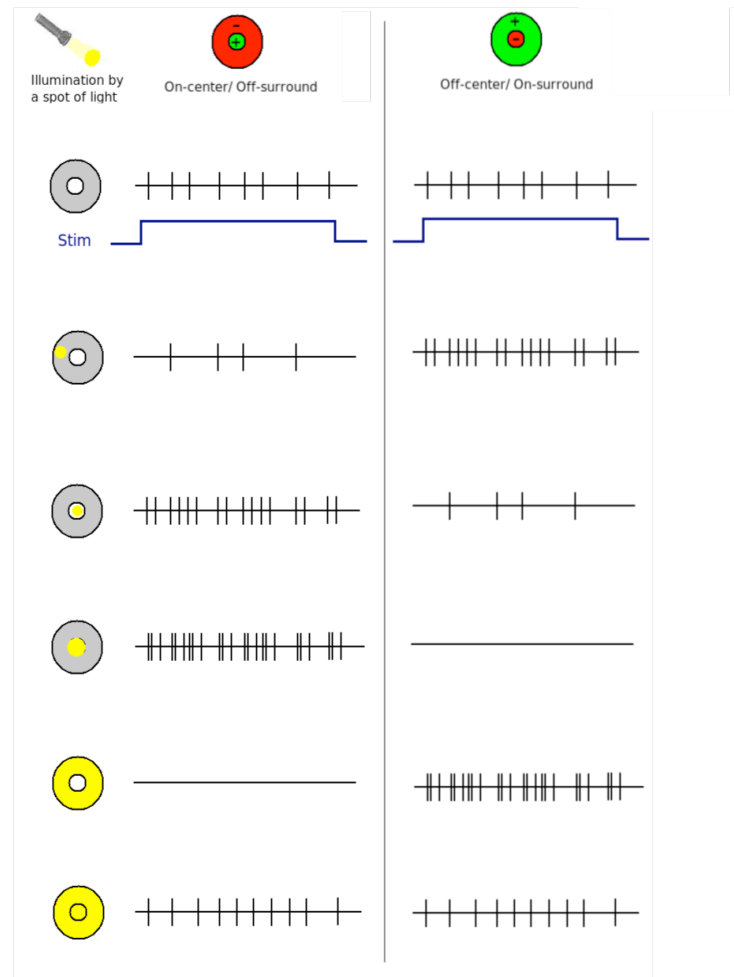
Figure 1.9: Schematic of the receptive field properties of a ganglion cell. Ganglion cells have circular receptive fields divided into two subregions: a central area and a surrounding ring. ON-center cells (left) are excited when the center is illuminated by a spot of light and inhibited when stimulated in the surround, whereas off-center cells (right) are excited when the surround is illuminated and inhibited when stimulated in the center.

Ganglion cells can also be divided into two functional classes according to their size: M cells and P cells (respectively for *magni* and *parvi*), thus providing the magno- and parvocellular pathways. The magnocellular pathway carries information from the large retinal ganglion cells to the large cells in the LGN and from there to the primary visual

cortex (V1) (Fig. 1.8, 2-3). This M-pathway carries all transient, motion related and low contrast black-and-white visual information and is responsive to low spatial frequencies and high temporal frequencies. The parvocellular pathway from the small retinal ganglion cells is color sensitive, has lower contrast sensitivity and is responsive to higher spatial frequencies and lower temporal frequencies.

From the retina to the visual cortex

The magno- and parvocellular pathways remains segregated in the lateral geniculate nucleus (LGN), providing the magno- and parvocellular layers, respectively forming by projection of the above M and P ganglion cells (Fig. 1.8, 2). More information about the LGN anatomy can be found in the review of Sherman and Guillery (1996). Note that in these layers, the RFs of thalamic neurons have the same concentric center-surround organization (Fig. 1.10A) as the retinal ganglion cells that feed into them (Hubel and Wiesel, 1959). However, their sensitivity to stimulus features, e.g. color contrast, luminance contrast, spatial and temporal frequency, are quite different (see Subsection 1.2.2). The pathways segregation continues in layer IV of V1, which consists of six layers of cells (see Fig. 1.8, 3 and Chapter 2 for an overview of the cortical structure).

Unlike subcortical cells with concentric spatial organization, cortical cells have elongated RFs with adjacent ON and OFF antagonist subregions (Fig. 1.10B,C), presumably resulting of the convergence of several concentric RFs of thalamic cells (Hubel and Wiesel, 1962; Chapman et al., 1991; De Valois et al., 2000; Alonso et al., 2001). This spatial organization thus gives to cortical cells a sensitivity to elongated stimuli, therefore to their orientation. Those neurons, contrary to retinal or thalamic ones, respond best to oriented bars of light than to spots of light. In fact, RFs of cortical cells present a large variability in their ON/OFF organization (Hubel and Wiesel, 1962). By using extracellular recordings of single cells in the visual cortex of anesthetized cats and simple set of geometric test stimuli, Hubel and Wiesel (1962) mainly classified them into two groups: *simple* and *complex*. They proposed the following definition: A simple cell is defined as a cell whose the RF verifies the four following criteria:

1. It has spatially distinct excitatory (ON) and inhibitory (OFF) subregions.

2. Evoked responses by stimuli restricted to either one subregion or the other are spatially and linearly summed.

3. It has antagonist excitatory and inhibitory subregions.

4. From the arrangement of its two subregions, one can predict the responses to any shape of stimulus, stationary or moving.

A complex cell is then defined as a cell whose RF failed in verifying at least one of these criteria. In other terms, RFs are complex when evoked responses could not be predicted from the spatial organization of excitatory and inhibitory subregions, since they do not present clear subdivisions (Fig. 1.10C). Complex cells non-linearly sum light-evoked responses from different parts of their RFs. Therefore, unlike simple cells, an oriented stimulus is effective wherever it is placed in the field. Many complex cells are also direction-selective in the sense that they respond better to one direction of movement than to the diametrically opposite direction.
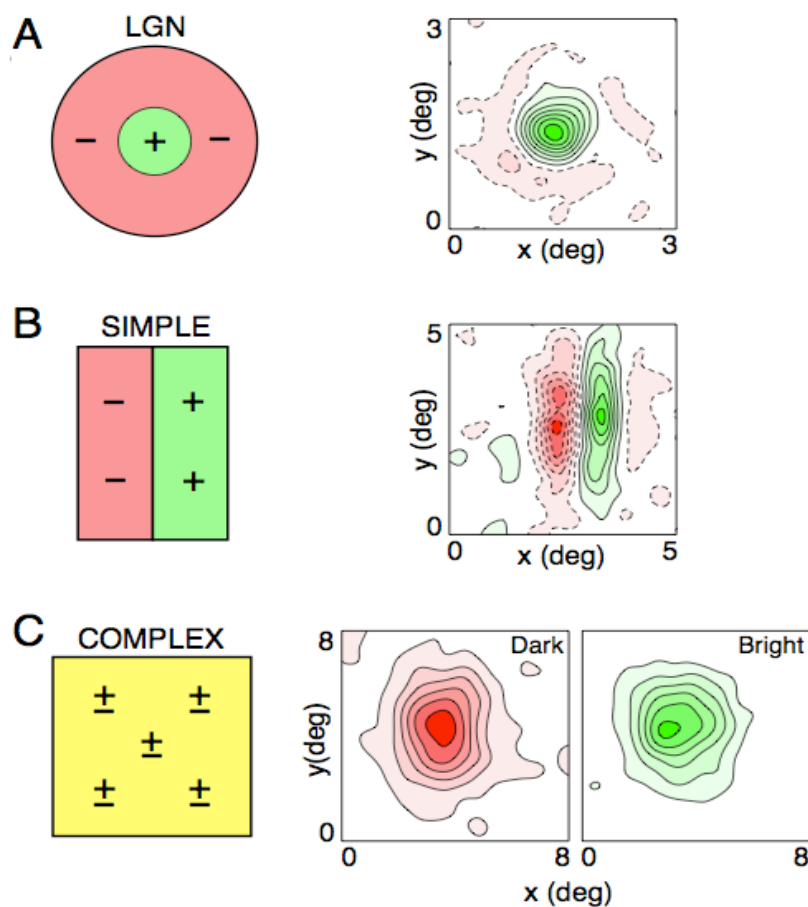
Figure 1.10: Spatial arrangement of receptive fields of cat LGN and V1 cells. Schematic (left) and two-dimensional spatial (x-y) (right) RF profiles *A:* ON-center LGN neuron. The RF has a central ON region, surrounded by an antagonist OFF region *B:* V1 simple cell RF exhibits an alternating arrangement of elongated excitatory and inhibitory subregions that are responsive to either bright (green, +) or dark (red, -) stimuli. *C:* V1 complex cell RF do not present net subdivision between excitatory and inhibitory subregions. This cells thus responds to both bright and dark stimuli at each position. From DeAngelis et al. (1995).

An other criterion, in correlation with the original definition of Hubel and Wiesel (1962), has been used to differentiate simple and complex cells, based on the linearity of their responses to drifting sinusoidal grating stimuli (see Figure 1.11, Contreras and Palmer (2003)). Cells are classified as simple if the modulation of their spike trains at the temporal frequency of the sinusoidal grating (fundamental frequency: F1 component) equals or exceeds the average increase in firing rate (DC component). Otherwise cells are classified as complex (Movshon et al., 1978b,a; Skottun et al., 1991). Complex cells usually respond with an elevation of the mean DC value without modulation, i.e. independently of the stimulus frequency. Some complex cells, however, oscillate at twice the frequency of the stimulus (half-wave rectifying) (Malonek and Spitzer, 1989; Movshon et al., 1978a).
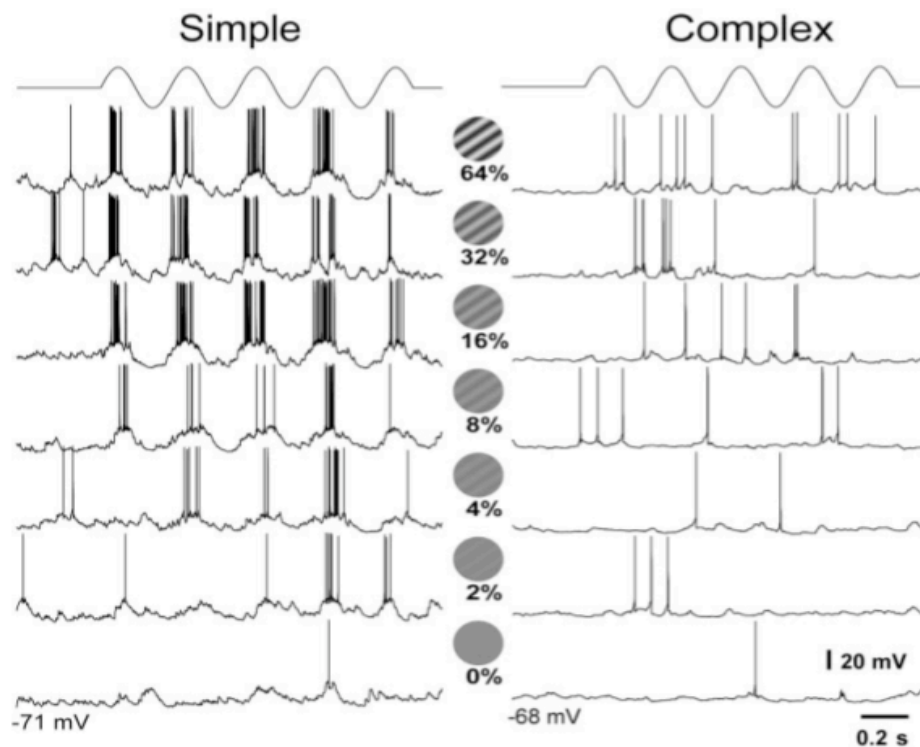
Figure 1.11: Responses of simple and complex cells to drifting sinusoidal gratings of increasing contrast. Grating was confined to the RF of the cell. From Contreras and Palmer (2003).

Neurons in the primary visual cortex can actually be selective along many stimulus dimensions, such as spatial position, phase, temporal and spatial frequency, orientation, direction of movement, binocular disparity. As shown in Figure 1.11, the stimulus contrast differentially modulates the functional selectivity of single cells. Additionally, it has also been shown to modulate functional connectivity in visual cortex (Nauhaus et al.,

2009), thus also affecting the global network level. The control of the contrast response function is a fundamental first input normalization step where non-linear mechanisms allow to reveal weak input or contain too strong input. We therefore decided to focus our modeling study to the cortical integration and control of the response to increasing level of contrast.

1.2.2 Representation of image contrast along the visual pathway

The spatiotemporal distribution of local luminance contrasts is the basic information that needs to be represented by the visual system to represent objects. In fact, the visibility of every image can be directly related to its contrast, which delineates what is visible to us and is the basis of all subsequent analysis performed on the visual input. We are thus interested in the contrast-response function (CRF) of neurons, i.e. how neurons respond to variation in the stimulus contrast, at the two different processing stages after the retina, i.e the thalamus and the primary visual cortex, previously described.

Classically, the contrast is the relationship between the local luminance of a brighter area of interest and that of an adjacent darker area. Mathematical, there are, however, various definitions of contrast:

- Simple Contrast, is often used in photography to specify the difference between bright and dark parts of the picture:

$$C_{simple} = \frac{L_{max}}{L_{min}} \tag{1.6}$$

  where L_{max} and L_{min} are the maximum and minimum luminances respectively.

- Weber Contrast, largely used in the context of lighting, measures the difference between the two luminances divided by the lower one:

$$C_{weber} = \frac{L_{max} - L_{min}}{L_{min}} \tag{1.7}$$

- Michelson Contrast, measures the relation between the spread and the sum of the two luminances, i.e. the standard deviation of intensity relative to the mean. This definition is typically used in signal processing theory, to determine the quality of a signal relative to its noise level:

$$C_{michelson} = \frac{L_{max} - L_{min}}{L_{max} + L_{min}} \tag{1.8}$$

From now, the term "contrast" will refer to the Michelson Contrast definition.

Contrast-response functions in the LGN

The LGN is typically organized into six main layers, with magno- and parvocellular sub-divisions. One criterion to dissociate this two layers is their response sensitivity to stimulus contrast. Typically, M-cells are characterized by transient discharge patterns and high gain (i.e. respond better to a low-contrast stimulus), while P-cells are characterized by sustained discharge patterns and low gain (Shapley et al., 1981; Sclar et al., 1990). This difference in contrast sensitivity between M- and P-cells has been demonstrated to be due to differences in sensitivity of different ganglion cells in the retina (Kaplan and Shapley, 1986). Figure 1.12 shows examples of contrast-response functions obtained from isolated neurons in the M and P layers of the macaque monkey (Sclar et al., 1990).
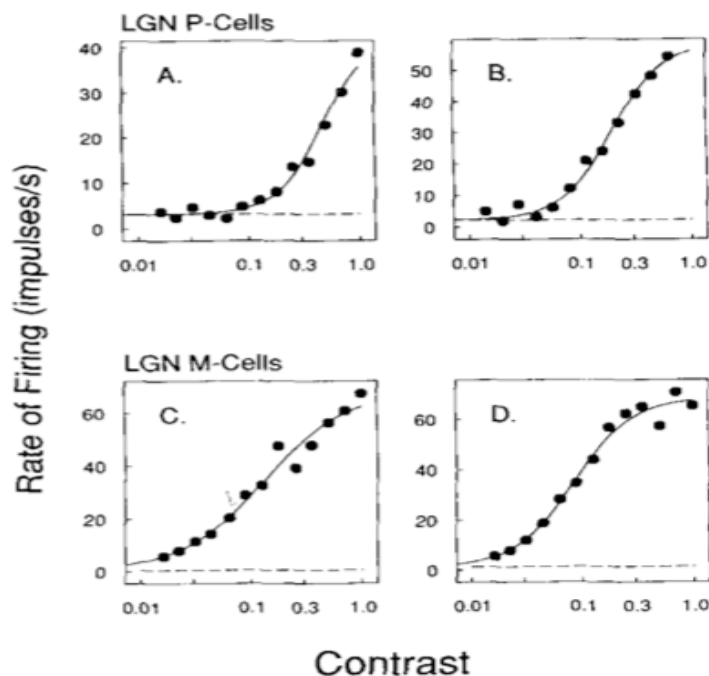
Figure 1.12:   Contrast-response functions obtained from neurons in the parvocellular layers (A, B) and magnocellular layers (C, D) of the macaque monkey's LGN. From Sclar et al. (1990).

The authors characterized contrast responses of LGN neurons by the Naka-Rushton function of the form:

$$R(C) = R_{max} \cdot \frac{C^n}{C_{50}^n + C^n} \tag{1.9}$$

where R denotes the response of the cell and C the contrast levels. This function has three parameters: R_{max}, the maximum value of the response, i.e. the response rate at which the cell saturates, C_{50} the semisaturation contrast, i.e. the contrast at which the response has reached a half of R_{max} and n the exponent, i.e. the slope of the linear part

of the response. The contrast response function can thus be characterized by those three parameters. This function has previously been shown to provide a good fit to contrast response functions from visual cortex in the cat and monkey (Albrecht and Hamilton, 1982, see next paragraph).

These results are in accordance with other studies also reported on monkey LGN neurons Derrington and Lennie (1984); Levitt et al. (2001): Parvocellular responses were nearly linear over the range of contrasts used, while magnocellular responses often showed a nonlinear saturation at higher contrasts.

Recent studies and models allowed a more precise description. The CRF of LGN neurons was assume to follow the Naka-Rushton function (see Eq. 1.9) with n = 1 (Bonin et al., 2005; Li et al., 2006; Priebe and Ferster, 2006). This assumption implies an approximately linear response at low contrasts and a nonlinear response at high contrasts, consistent with earlier results (n = 1.6 and 1.2 for respectively P and M cells in Sclar et al. (1990)). However, Duong and Freeman (2007) measurements in cat's LGN clearly showed a nonlinearity also at low contrasts (see Figure 1.13). LGN cells thus increase their responses with stimulus contrast following a Naka-Rushton function with n > 1. This function is expansive at low-contrasts levels and compressive at high contrasts with an inflection point at

$$C_i = C_{50}^n \left(\frac{n-1}{n+1}\right)^{\frac{1}{2}} \tag{1.10}$$

Although this thalamic nonlinearity at low contrasts has been largely ignored in models of early visual processing, it could be of importance in explaining basic properties of cortical neurons. Note that this study was done in cat's LGN whereas previous ones were done on monkeys. Caution should therefore be taken when trying to generalize all the data.

Contrast-response functions in V1

In the 70s, the CRF of V1 neurons to drifting sinusoidal grating stimuli was generally considered as a monotonic function of contrast (Cooper and Robson, 1968; Maffei and Fiorentini, 1973; Ikeda and M.J., 1974; Movshon and Tolhurst, 1975). However, trying to provide a more detailed description of the CRF, these authors came to conflicting results. They generally reported the existence of a distinct contrast threshold. However, Cooper and Robson (1968); Movshon and Tolhurst (1975) observed a linear increase after threshold and saturation for the highest contrast, whereas Maffei and Fiorentini (1973); Ikeda and M.J. (1974) found a logarithmic relationship with contrast.

A general characterization of the CRF of V1 neurons came with Dean (1981) and Albrecht and Hamilton (1982). The latter measured the responses of large number of neurons recorded from the primary visual cortex of cats and monkeys as a function
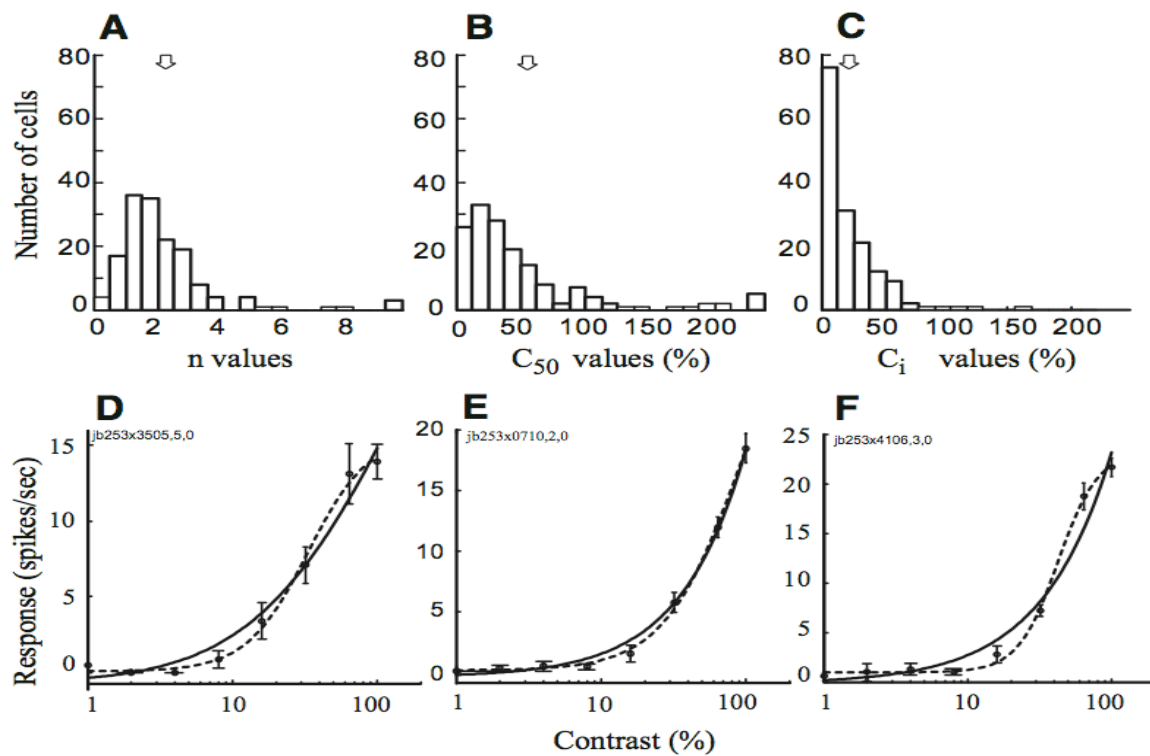
Figure 1.13: Contrast response function in the LGN of cat. *A, B, C:* Histograms giving best Naka-Rusthon fit values for respectively n, C_{50} and C_i, as computed using eqs. 1.9 and 1.10. The mean values for each distribution is indicated by arrows on top. *D, E, F:* CRFs of three representative LGN neurons. Solid and dashed lines denote, respectively, the best-fit Naka-Rushton functions, and the condition in which the numerator exponent is set to 1. From Duong and Freeman (2007).

of luminance contrast of visual stimuli. Although they found large variations in the response shapes from cell to cell (Fig. 1.14), they were able to give a general description of the CRF of V1 neurons: V1 neurons increase their firing rate as the contrast of the stimulus increases with a sigmoidal shape. More precisely, neurons respond weakly at low contrasts, then their responses increase roughly linearly over different limited range of contrast, before showing a gradual compression and they finally saturate at high contrasts. This description mathematically fits with an hyperbolic ratio function.
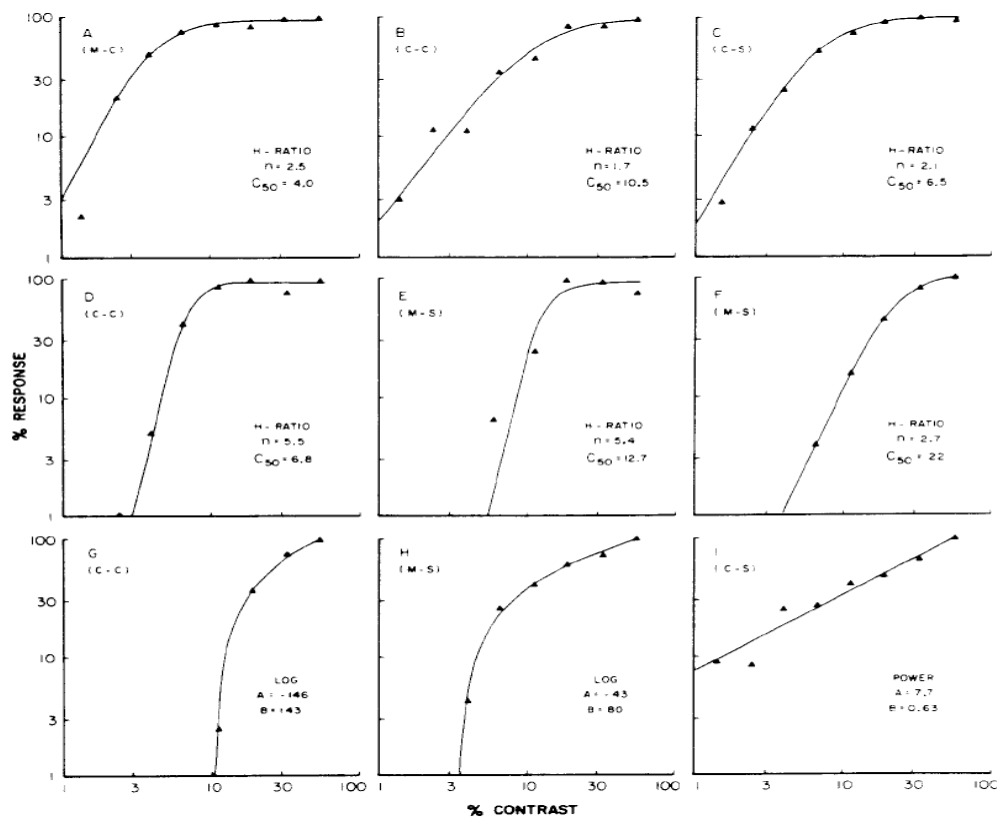
Figure 1.14: Examples of contrast response functions of nine V1 neurons, showing the large variability of CRT shape. Each response is fitted by a mathematical function (linear, logarithmic, power or hyperbolic ratio function). The hyperbolic ratio function appears to best fit the majority of responses. From Albrecht and Hamilton (1982).

The basic properties of the CRF of visual cells (the common used stimuli was drifting sine gratings) have then been intensively studied thanks to the work of many research groups, (e.g. Sclar and Freeman, 1982; Li and Creutzfeldt, 1984; Albrecht and Geisler, 1991; Sclar et al., 1990; Bonds, 1991; Geisler et al., 1991; Geisler and Albrecht, 1992; DeAngelis et al., 1993; Carandini and Heeger, 1994; Albrecht, 1995; Carandini et al., 1997, 2002; Contreras and Palmer, 2003), clarifying definitively minds: Response amplitude and phase of V1 neurons depend non-linearly on contrast. As the contrast

increases, the amplitudes saturate (sometimes even supersaturate) and the phases advance. Moreover, the temporal frequency of the stimulus plays an important role on the CRF. When increasing the temporal frequency, the responses saturated at higher contrast and the total phase advance decreases. Conversely, there are invariances of the contrast responses when changing orientations or spatial frequencies of the grating stimulus.

Contrast-response relationships obtained from V1 neurons are different to those of LGN neurons. V1 neurons saturate for lower contrast more than thalamic neurons and have smaller dynamic range, i.e. increase linearly their response for a smaller range of contrasts.

How do neuron responses saturate at high stimulus contrast? Robson (1966) and Bonds (1989) suggested that striate cells mutually inhibit one another, effectively normalizing their responses with respect to stimulus contrast. Carandini and Heeger (1994); Carandini et al. (1997) also attributed the compressive nonlinearity at high contrasts (i.e. saturation) to a divisive normalization mechanism. Additionally, the saturation might be due to contrast-gain control (i.e. contrast adaptation, see next paragraph) mechanism (Geisler and Albrecht, 1992). More recently, Carandini et al. (2002) suggested that gain control operates through synaptic depression at thalamocortical synapse. This could then explain why responses of neurons in V1 saturate at high contrast, whereas responses of thalamic neurons increase with stimulus contrast over a larger range of contrasts. Regarding the power-law expansive nonlinearity at low contrasts, the explanation is trickier. Duong and Freeman (2007) proposed a probable origin at previous stages and more likely in the retina.

The stimulus contrast, as increasing input, is thus a fundamental functional parameter for our direct cortical column model of optical imaging signal (see Part III), because it differentially affects neuronal responses and therefore allows us to inspect the columnar VSDI activation for different regimes. We decided to fit data from Contreras and Palmer (2003) because it reports CRFs of cat's striate cells, both for spikes and membrane depolarization, of the two main electrophysiological classes of excitatory and inhibitory neurons, i.e. RS and FS cells (see Section 1.1.6). The authors found that both the spike rate and the membrane potential responses are best described by the hyperbolic ratio (Fig. 1.15), whose parameters are very similar. In addition, they showed that RS and FS cells have similar CRFs in membrane depolarization while CRFs in firing rates strongly differ: FS neurons show much higher firing rates than RS neurons.
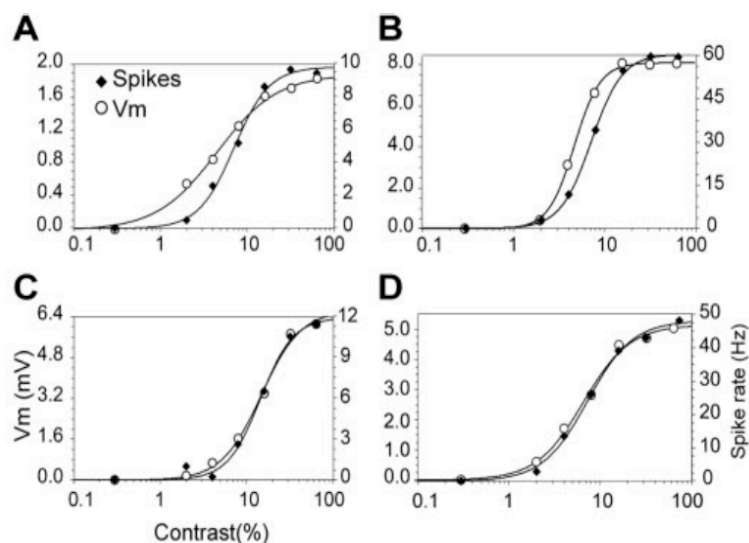
Figure 1.15: Example of contrast response functions of cat V1 neurons. *A:* Simple RS cells. *B:* Simple FS cells. *C:* Complex RS cells. *D:* Complex FS cells. From Contreras and Palmer (2003).

Contrast adaptation

Maintaining the best sensitivity to contrast in the environment is a major task for the visual system. The latter naturally adapts to light and contrast (Blakemore and Campbell, 1969), thanks to mechanisms of light adaptation and gain control which begins in the retina (Shapley and Victor, 1978). The purpose of these non-linear mechanisms is to keep the retinal response approximately the same when the level of illumination changes. More precisely, there are two ways for neurons to adapt and prevent response saturation at high contrast: By reducing the gain or by hyperpolarizing the membrane (Sanchez-Vives et al., 2000a,b; Demb, 2008). Both mechanisms actually co-occur (Baccus and Meister, 2002).

Moreover, unlike lights adaptation, which occurs entirely in the retina (Shapley and Enroth-Cugell, 1984), contrast gain control occurs in the retina (Shapley and Victor, 1978; Chander and Chichilnisky, 2001; Baccus and Meister, 2002; Zaghloul et al., 2005), possibly in the thalamus (Ohzawa et al., 1985; Shou et al., 1996) and in the cortex (Dean, 1983; Albrecht et al., 1984; Ohzawa et al., 1985; Kaplan et al., 1987; Sclar, 1987; Sclar et al., 1890, 1990; Cheng et al., 1995; Sanchez-Vives et al., 2000a,b).

As the LGN is the direct recipient of retinal outputs, and that neurons in the retina show contrast adaptation, it is natural to think that LGN neurons will also show contrast adaptation. Several studies, however, reported that neurons in the LGN, as opposition to those in the retina or in V1, do not show contrast adaptation in cat (Maffei et al.,

1973; Ohzawa et al., 1982; Bonds, 1991; Ahmed et al., 1997; Mante et al., 2005) and monkey (Derrington and Lennie, 1984; Sclar et al., 1890). For example, Ohzawa et al. (1982) have recorded single neurons from cats visual cortex, in response to drifting sinusoidal gratings of different contrasts (see Figure 1.16). Solid lines represent contrast-response functions when the neurons were adapted to different levels of contrast, while dotted line represent contrast response functions when all contrasts are randomly presented. Both simple and complex cells show contrast adaptation (see respectively a and b panels in Fig. 1.16). LGN afferents also recorded in V1 (Fig. 1.16d), suggest no adaptation at this stage. Actually, contrast adaptation have been observed in the LGN, but they are weak compared with those in primary visual cortex (Ohzawa et al., 1985; Shou et al., 1996; Sanchez-Vives et al., 2000b; Duong and Freeman, 2007). Moreover, contrast adaptation has been reported for M-cells in the monkey LGN (Solomon et al., 2004).

In the cortex, contrast gain control allows to keep the orientation tuning invariant across contrast (Sclar and Freeman, 1982; Somers et al., 1995; Ben-Yishai et al., 1995; Nowak and Barone, 2009).
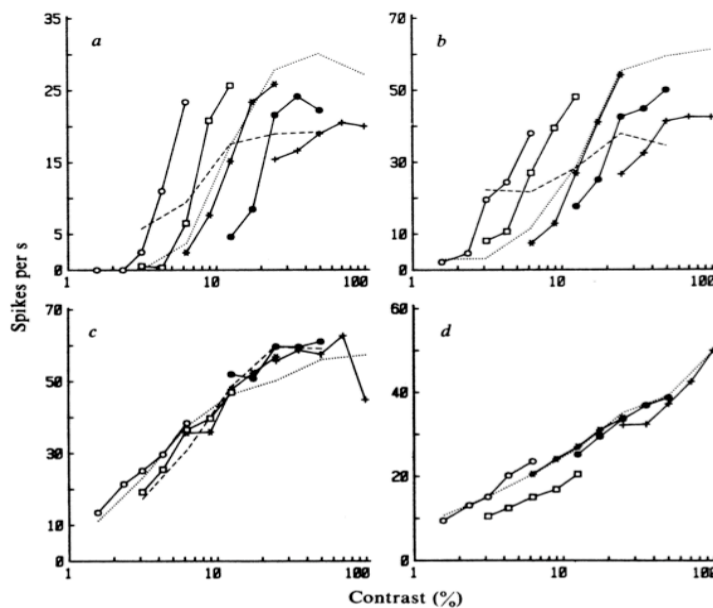
Figure 1.16: *a:* CRF of a simple cell when adapted to different levels of contrast (3.1, 6.3, 12.5, 25, 50%). Dotted line represent contrast response functions when all contrasts (from 1.56 to 100%) are randomly presented. *b:* CRF of a complex cell when adapted to different levels of contrast. *c:* CRF of another complex cell which did not show contrast adaptation. *d:* LGN fibres do not show contrast gain control mechanism. From Ohzawa et al. (1982).

Conclusion

The representation of image contrast is thus subjected to a strong transformation as it goes through the visual pathway. The majority of LGN neurons gradually change their responses with contrast, providing information about contrast over a relatively large range, even though M-cells exhibit saturation at high contrasts. As one moves to V1, CRFs become progressively steeper and more readily saturated at high contrasts, thus reducing the range over which neurons are contrast sensitive. Contrast adaptation then provides a way to overcome this limitation by shifting the operating range of a neuron towards the new average level of contrast (see Figure 1.17 for an illustration).
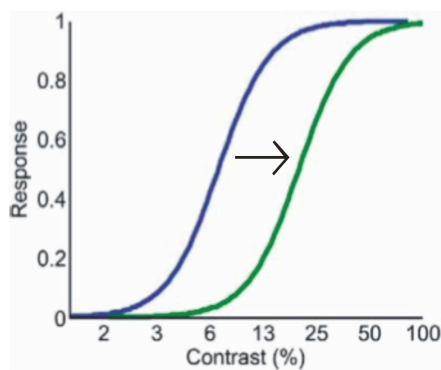
Figure 1.17: Mechanism of contrast adaptation in the visual cortex. Classical CRFs of V1 neurons, before (blue curve) and after (green curve) prolonged exposure to high contrasts. Adapted from Boynton (2005).

THE CORTICAL COLUMN

OVERWIEW

In the previous chapter, we have reviewed some fundamentals about the individual neuron and some specific properties of visual neurons. Brain functions mostly emerge from the coordinated activity of many neurons, so we are now going to discuss about cortical circuits. We consider here, the columnar functional organization of the mammalian cortex, giving us a functional scale to study populations of neurons. This chapter aims at better understanding the cortical columns concept, still quite confusing term being extensively used in the literature at different scales.

Contents

2.1 AN OVERVIEW OF CORTICAL STRUCTURE

From Chapter 1, we know that the cerebral cortex is the outer part of the cerebral hemispheres. It is not much thicker than 2 to 4 mm, but consists into four main lobes, each subserving a more of less distinct function and named according to the cranial bone which recovers them. Very briefly, the frontal lobe deals with higher level cognitive functions like reasoning and judgment. It is also involved in the control of voluntary motor action. The parietal lobe is immediately posterior to the frontal lobe (separated by the central sulcus) and is involved in multi-sensory integration from somesthetic, auditory and visual adjacent areas. The temporal lobe is ventral to the frontal and the parietal lobe (separated by the lateral sulcus) and is mainly dedicated in auditory processing (primary auditory cortex), but also in processing of semantics in both speech and vision and spatial memory (hippocampus). Finally, the occipital lobe is specialized for visual processing. The primary visual cortex is situated on the edge of the calcarine sulcus, located in the medial surface of the occipital lobe. Based on cytoarchitectural distinctions, the cortical lobes were further subdivided into processing areas by Brodmann, as shown in Figure 2.1. Indeed, the cerebral cortex has an horizontal laminar structure, as revealed by different staining methods (Golgi, Nissl and Weigert's coloration), and shows a differential cytoarchitectonic arrangement, i.e different areas are identified by differences in cell size, packing density and laminar arrangement. Despite its apparent functional organization into specialized areas, the cortex has a more general columnar/laminar structure shared by almost all the different cortical areas. This chapter focuses on the primary visual cortex with some generalizations to other cortical areas when needed to emphasize certain points.

In this thesis, we are more particularly interested in the primary visual cortex because the cortical column model proposed in Part III has been built based on biological data from rat, cat and monkey primary visual cortex, in order to reproduce visual experiments in optical imaging. However, this general structure could allow us to generalize the basic results of our model to other cortical areas (see Discussion in Part IV).

2.1.1   A common laminar organization

As shown in Figure 2.1, the structure of the cortex is not even over its surface, but laminar. It is mostly made up of six cellular layers, labelled I to VI. In Figure 2.2, Felleman and Van Essen (1991) depicted a very general laminar scheme of feedforward, lateral and feedback cortico-cortical connectivity in the cortex. Typically, layer IV receives feedforward input from the thalamus, but also from lower cortical areas. Output to subcortical motor structures (basal ganglia, brainstem and spinal cord) issues from layer V (not mentioned on the figure). Lateral projections mainly originate in superficial layers
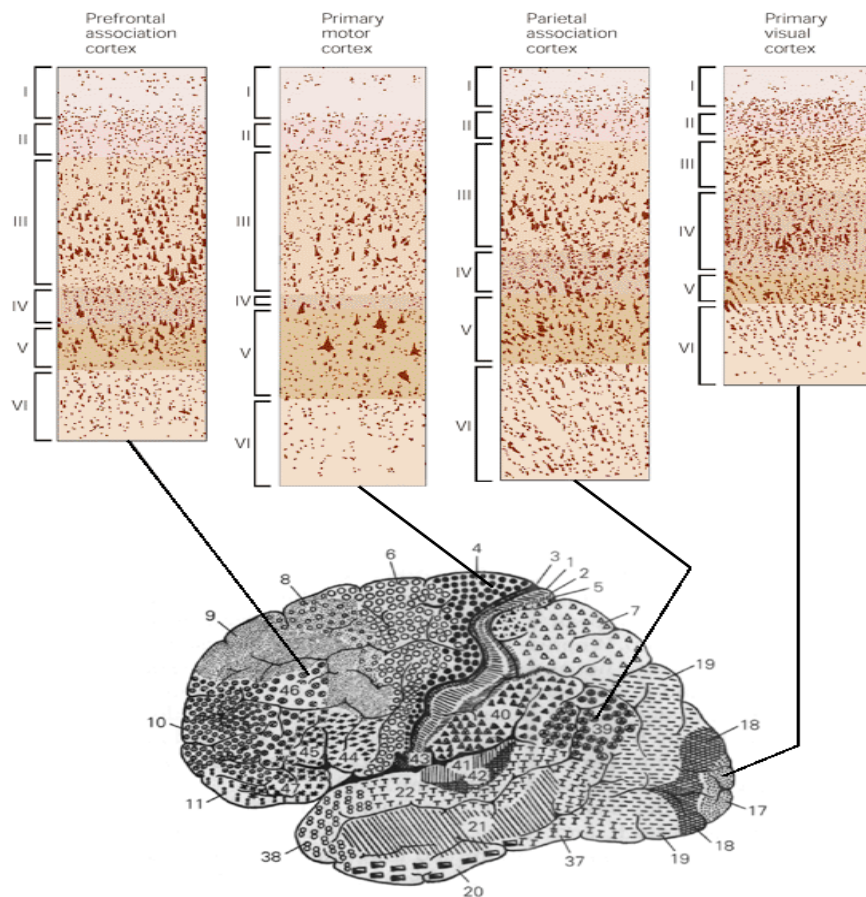
Figure 2.1: Brodmann areas and cortical layers cytoarchitecture. In 1909, the German neuroanatomist Korbinian Brodmann divided the human cerebral cortex into 52 discrete areas based on cytoarchitectural visible differences in the structure of the cortical layers. From Kandel et al. (2000).

II/III and lower layers V/VI and stay mostly within their layer. Feedback connections terminate predominantly outside of layer IV and originate mainly from cells in deep layers. Regarding the layer VI, it is the next principal target of thalamic inputs and it also projects back to the thalamus. Thus, this layering of neurons defines the input-output relationships between neurons (intra- and extra-cortical) (Callaway, 2004; Douglas and Martin, 2004).
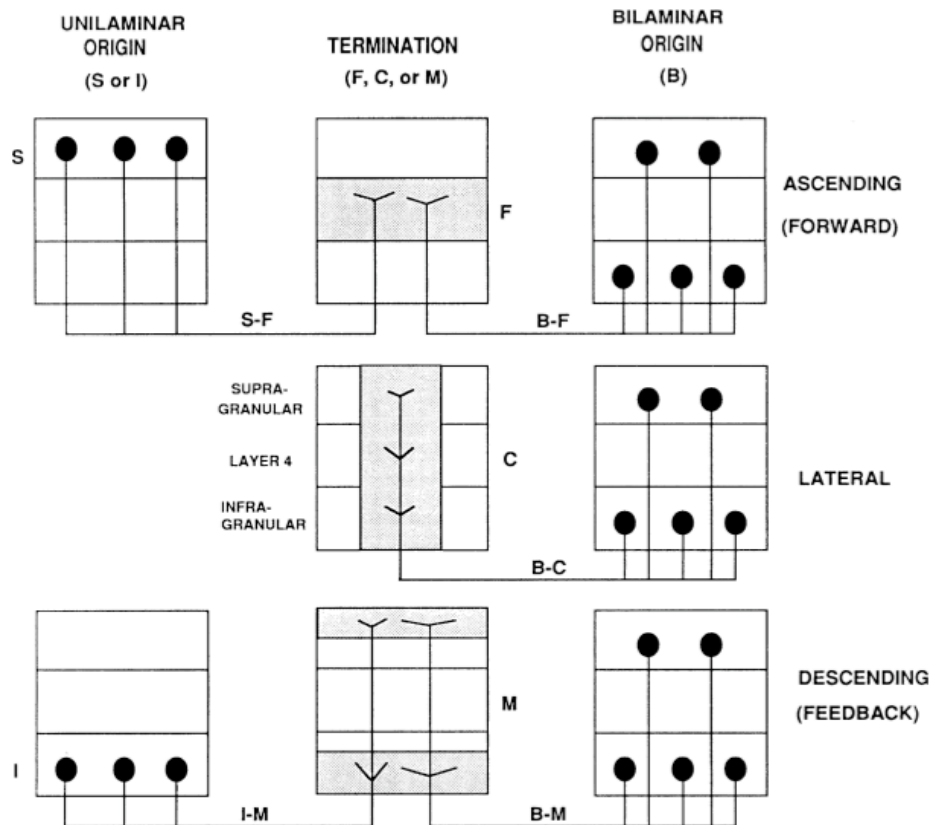
Figure 2.2: A very general scheme of feedforward, lateral and feedback cortico-cortical connections in the cortex. See text for details. From Felleman and Van Essen (1991).

There are two main classes of neurons in this laminar structure, as explained in the preceding chapter: Excitatory neurons that release the excitatoy neurotransmitter glutamate and that represent 80 % of the total cells, and inhibitory neurons that release the inhibitory neurotransmitter GABA and that represent the remaining 20 % (see Section 1.1.6). More precisely, we have also seen that there are many types of neurons with different shapes and sizes. The distribution of these neurons along the laminar structure is visible thanks to staining techniques like Golgi-impregnation or horseradish peroxidase labeling (Fig. 2.3, see Chapter 3 for details on the staining methods), and can be briefly summarized as follows: Only few unclassified inhibitory neurons are found in

layer I. Layer II contains small pyramidal cells and some inhibitory neurons, mainly cells called basket cells and double-bouquet cells. Layer III contains a mix of almost all cell types found in the neocortex, with a majority of small pyramidal cells. The major exception are spiny stellate cells, exclusively located in layer IV. It also contains a variety of inhibitory cells. Layer V is mainly composed of large pyramidal cells with a smaller population of inhibitory cells: non-spiny bipolar cells and chandelier cells. Finally, most of the cells in layer VI are large pyramidal cells. Inhibitory cells, called Martinotti cells are also found in this output layer. See Salin and Bullier (1995) for a complete review of the different neuronal types per layer.
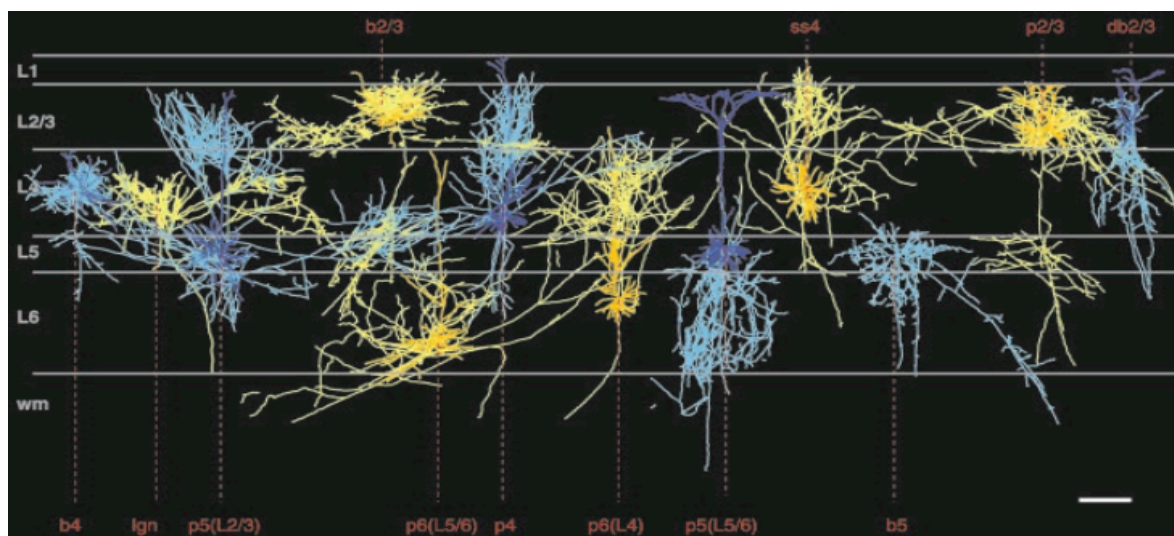
Figure 2.3: Reconstructed neurons found in the cat primary visual cortex, using horseradish peroxidase labeling. p2/3, b2/3, db2/3, ss4, b4, p4, p5(L2/3), p5(L5/6), b5, p6(L4), p6(L5/6) designed respectively pyramidal, basket and double bouquet cells in layer II/III, spiny stellate, basket and pyramidal cells in layer IV, pyramidal cells in layer V with axon in layer II/III or in layer V/VI, basket cell in layer V and pyramidal cells in layer VI with axon in layer IV or in layer V/VI. Axons are shown in bright colors (blue or yellow), while dendrites are shown in dark colors (blue or yellow). From Binzegger et al. (2004).

Note that pyramidal cells are also called *projection neurons* because they can project information over long distances, while spiny stellate cells and the majority of inhibitory cells (e.g. smooth stellate cells, see Subsection 1.1.6 in Chapter 1) are also called *interneurons* because they only convey information into local circuits, i.e. in the same stage of information processing.

2.1.2 A common columnar organization

Since the 1950s, thanks to the work of Mountcastle (Mountcastle, 1957), we know that the cerebral cortex has also a columnar organization. Indeed, using a microelectrode in cat primary somatosensory cortex, he found that neurons responding to the same stimu-

lation, i.e. sharing common receptive field properties (see Section 1.2 in Chapter 1), were arranged vertically into columns, crossing the six layers of the cortical tissue. In 1960s and 1970s, Hubel and Wiesel followed Mountcastle's discoveries by showing that ocular dominance and orientations are organized in a columnar manner in cat and monkey visual cortex (Hubel and Wiesel, 1962, 1965, 1977). A generalization to any functional parameter α is shown in Figure 2.4. By inserting an electrode perpendicularly oriented to the surface of the primary visual cortex, all encountered neurons (from 1 to N) will display very similar tuning curves. On the contrary, when inserted parallel to the cortical surface, neurons will gradually change their tuning curve, as a function of α.

The individual cortical column was then considered to be the elementary unit of organization in the cerebral cortex. Besides, the columnar organization were found in almost all areas in the neocortex of many mammals. Note that other names are also employed: *Barrels* for entities in the somatosensory cortex of rat, *bands* for ocular dominance regions in V1, *blobs* for cytochrome oxidase (CO) patches of V1 neurons involved in color processing and that selectively project to *stripes*, color-sensitive zones of V2. All those names are often related to the form of the considered area.
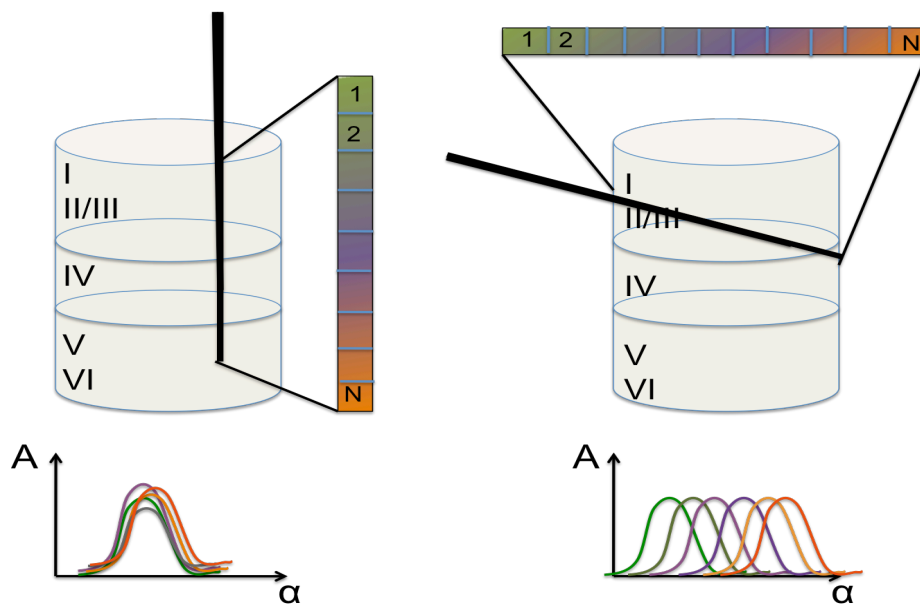
Figure 2.4: Generalization of the cortical columns discovery. See text for details.

2.2 THE CORTICAL COLUMN: FROM ANATOMY TO FUNCTION

Today, the notion of cortical column becomes a large controversy since the original con-

cept, i.e. a discrete structure spanning the cellular layers of the cortex, which contains cells responsive to only a single modality, is expanding, year after year, discovery after discovery, to embrace a variety of different structures, principles and names. A 'column' now refers to cells in any vertical cluster that share the same tuning for any given receptive field attribute (see Horton and Adams, 2005, for a detailed review on the cortical column concept). The term "cortical column" is thus used in the literature in so many way that it is first very confusing. There are minicolumns, microcolumns, hypercolumns, macrocolumns, orientation columns, ocular dominance bands, barrels, blobs, stripes and the list is not exhaustive. All these terms refer to anatomic or functional structures at several different scales, in different cortical systems of different mammals.

2.2.1 Minicolumns

The concept of minicolumn is actually simple and based on anatomical features. Minicolumns, sometimes also called microcolumns, are narrow vertical chains of neurons, barely more than one cell diameter wide, i.e. 20 up to 50 μm, which are formed during brain development, due to radial migration of neurons (Rakic, 1995; Mountcastle, 1957; Rakic, 2003). These anatomical columns consists of about a hundred neurons that throw their axons and dendrites vertically from the cortex surface to the white matter (Fig. 2.5) (Buxhoeveden and Casanova, 2002). Notice that in monkeys these minicolumns are 31 μm diameter, but in cats, there are about twice that diameter (Peters and Yilmaz, 1993).
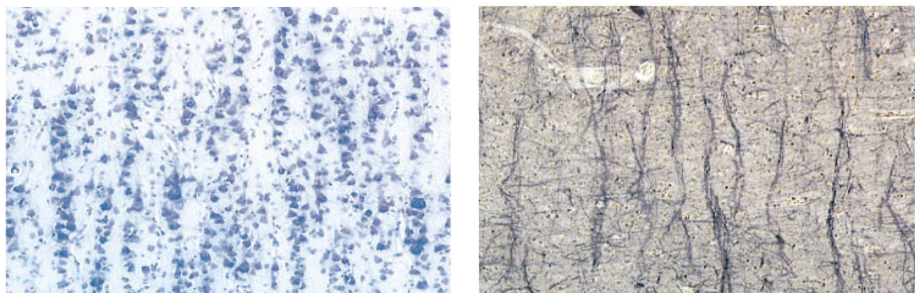
Figure 2.5: The anatomical minicolumn. *Left:* Nissl-stained tissue reveals vertically aligned cells, suggesting the existence of minicolumns in the developing cortex. *Right:* Myelinated fibre bundles in the same region of human cortex. The correlation between myelin bundles and cell soma aggregates is clear. From Buxhoeveden and Casanova (2002).

At this spatial scale, individual minicolumns have no reason to be considered as functional entities (Hubel and Wiesel, 1974; Swindale, 1990), and classical electrophysiological techniques limit the research. New optical imaging techniques, such as two-photons imaging, may soon elucidate whether the minicolumn has any functional properties.

2.2.2 Macrocolumns

The minicolumn is thus a well-defined structure. However, this anatomical column differs from that originally found by Mountcastle, especially regarding the diameter of the column. Indeed, when moving the electrode perpendicularly and obliquely to the cortex surface, he found that neurons inside columns of 300 to 500 μm of diameter displayed similar activities, which is much larger that the diameter of the above minicolumn. Mountcastle thus solved this ambiguity by defining "his column" as many minicolumns bound together by short-range horizontal connections (Mountcastle, 1997). This larger structure, regarding its spatial scale, has been redefined by Buxhoeveden and Casanova (2002) as a *macrocolumn*, a continuum of many minicolumns from 0.4 to 1 mm. It is, however, a very controversial theory. Section 2.3 may help to clear the question.

At the spatial scale of the macrocolumn, functional properties of macrocolumns have been intensively investigated, especially in the visual cortex (LeVay and Nelson, 1991), as briefly reviewed now.

Indeed, a cortical column can also be defined on the basis of functional features, e.g. columns of cortical cells all responding to the same stimulus property. Besides, columns, barrels, blobs, and stripes have all been called *cortical modules*, as any repeated functional clusters in different areas of the brain. Here, we briefly describe the ocular dominance and the orientation columns in order to provide an example of columnar arrangement in the primary visual cortex (V1).

2.2.3 Ocular-dominance columns

In the monkey visual cortex as many other species, thalamic input fibres from left and right eyes terminate in layer IVC in different regions (Fig. 2.6A), i.e. ocular dominance stripes (Hubel and Wiesel, 1969; LeVay et al., 1985). Ocular dominance thus showed well-defined monocular domains, with alternating right and left eye. However, outside of layer IV, the majority of neurons receive a mixture of inputs from layer IV neurons with selectivity to left and/or right eyes (see layers 2/3 in Fig. 2.6A). This convergence of inputs provides two functional receptive fields, one from left and the other from right eye, leading to the emergence of binocular disparity.

The variation in neurons response properties between two neighboring columns is very sharp. In this sense, ocular dominance columns defined discrete entities, since they are clearly separated with discrete boundaries.

2.2.4 Orientation columns

Visual cortical cells are also sensitive to orientation, meaning that they will selectively respond to stimuli, e.g. bars, edges, at particular orientations. Hubel and Wiesel (1962)

showed that orientation preference of neurons remains constant in vertical electrode penetrations through the entire thickness of the cortex, while gradually changes when moving the electrode obliquely. It thus led to orientation columns (Fig. 2.6B). Actually, orientation columns are arranged radially into pinwhell-like structures (see Fig. 2.6B, inset) and orientation preference changes in a continuous fashion, rotating around pinwheel center singularities.
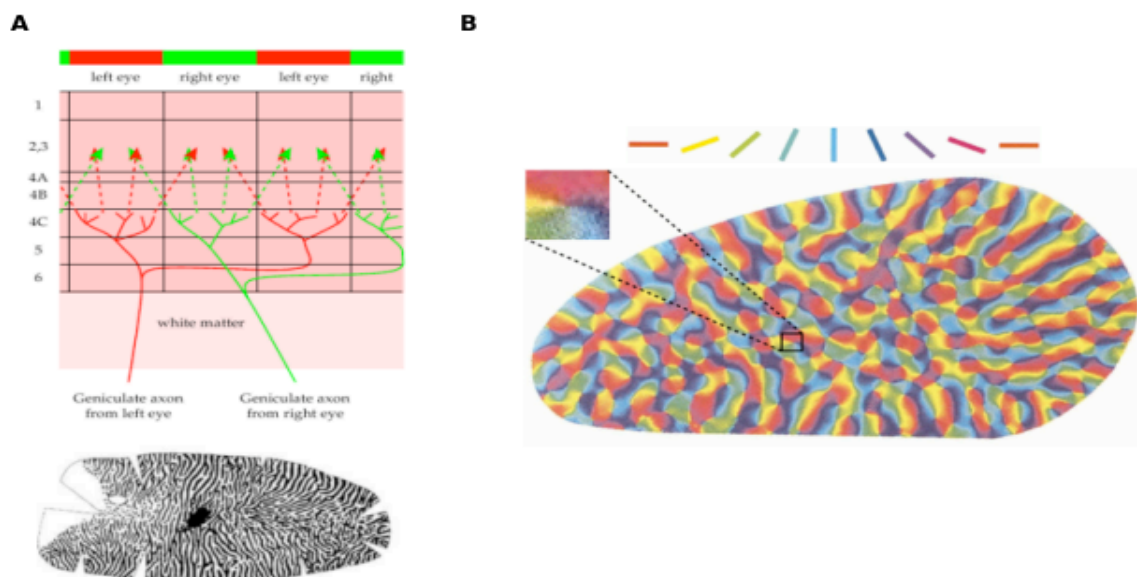
Figure 2.6: Ocular dominance and orientation columns in V1. **A**: *(Left)* Anatomical basis of ocular dominance columns in monkey primary visual cortex. *(Right)* Reconstruction of ocular dominance columns supplied by the left (black) and right eye (white). **B:** Neurons in V1 have also orientation preference,as shown by this orientation preference map. Each color represents the orientation for which the presented stimulus is the most effective to activate neurons in a given area. A pinwheel arrangement, i.e. when all orientations at a particular receptive field position are represented, is enlarged.

In comparison with ocular dominance discrete entities, continuous orientation columns have gradual boundaries, though pinwheel centers are discontinuous (Bonhoeffer and Grinvald, 1991; Blasdel, 1992; Crair et al., 1997). In this sense, a column can also be a structure without distinct and rigid borders. Those functional columns are much larger than minicolumns. They can have a width of about 200 to 400μm, centered on pinwheel center. However, these values should be taken with caution, since they are widely dependent on the area, the animal and the recording conditions.

2.2.5   Hypercolumns

Following this observation that orientation columns did not show discrete boundaries, Hubel and Wiesel defined a hypercolumn as the structure which contains representations of all orientations for both eyes (Hubel and Wiesel, 1977). The idea is that a hypercolumn regroups all the cells, hence columns, coding for a given position in the retina for a full functional set of orientations and ocular dominance. However, as orientation columns do not have fixed boundary, neither do hypercolumns. Bosking et al. (2002) inspected for a possible delineation by measuring the minimum cortical area for which all orientations are evenly represented. Regions representing 4x4° of visual space are necessary.

The primary visual cortex of many mammals species is thus arranged with several superimposed functional maps that represent the visuotopic position, orientation, ocular dominance, and several others properties not reviewed here, like spatial frequency, spatial disparity or movement direction, of visual stimuli (Hubel and Wiesel, 1963; Blasdel and Salama, 1986; Bonhoeffer and Grinvald, 1991; Hubener et al., 1997).

Through these above definitions of columns, we learnt that the columnar organization of the brain is based on anatomical and functional aspects, which are intricately linked. Neurons that share similar functional properties are close-by densely connected providing a strong cooperative effect (Shaw et al., 1982; Bullock, 1979). This vertical recurrent network helps emerging properties to stabilize. It should be noted that these small recurrent networks interact with each other by horizontal connections (Katz and Callaway, 1992), as detailed in the next section.

2.3   CORTICAL COLUMN CIRCUITRY

The columnar organization of the cortex presents a common recurrent circuitry. Indeed there are many vertical intrinsic connections linking neurons within the same column but in different layers, and horizontal connections linking different columns. Intra-columnar connections are also referred to local connections, in opposition to inter-columnar horizontal connections which can be short, middle and long-range horizontal connections.

2.3.1   Vertical intra-columnar connections

The cortical circuit of primary sensory areas has been largely studied over years. Anatomical investigations (Gilbert, 1983; Gilbert and Wiesel, 1983; Callaway, 1998) led to a detailed picture of a local recurrent intracortical network which can be considered as

the common pattern of intra-columnar connections (Fig. 2.7A) (Callaway, 1998; Hellwig, 2000; Stepanyants et al., 2002): Thalamic afferents to the cortex terminates mainly on stellate neurons in layer IV. These neurons in turn project their axons vertically toward the surface of the cortex to contact dendrites of pyramidal cells, whose somas lie in layer II/III or V. Pyramidal neurons then send axonal projections vertically to deeper layers and to other cortical or subcortical areas. This common pattern in fact corresponds to the main feedforward circuitry which is exclusively excitatory (Wells, 2005). There is also a local feedback excitatory pathway which mainly consists in dense projections from deep layers (V, VI) to superficial ones (II/II and IV respectively) (see Salin and Bullier, 1995; Nowak et al., 1997, for reviews on corticocortical connections in the visual system). However, anatomical techniques do not measure the effective functional connectivity strenght. It is therefore important to note that electrophysiological studies (Douglas et al., 1989; Douglas and Martin, 1990, 1991) (Fig. 2.7B) and pharmacological inactivation techniques (Bolz et al., 1989) (Fig. 2.7C) thus confirmed this general scheme and allowed to determine the role of such cortical circuits: Neurons are fed by the feedforward thalamic drive and their responses are shaped by this local recurrent network. As shown in Figure 2.7B, the performance of the microcircuit also depends on the existence of feedback and feedforward inhibition (Douglas and Martin, 1991).

More recently, neuronal circuits of the entire neocortex have been studied by Thomson and collaborators (Thomson and Deuchars, 1997; Thomson and Morris, 2002; Thomson and Bannister, 2003). It appears that this recurrent circuit pattern is also clearly emerging.

Despite this common pattern of vertical organization, local connectivity in the cortex is complicated by the large number of neuronal types (implying also the different types of synapses). Note also that the local inhibitory circuitry is much more complex than the excitatory one since there are many more types of inhibitory neurons. For further descriptions of inhibitory local circuits, see also Lund (1988); Lund and Wu (1997) and Lund and Yoshioka (1991).

Several groups, thanks to connectivity rules (e.g. Peters's rule) and efficient anatomo-functional techniques (e.g. multiple intracellular recordings, dye-filling), have been able to reconstruct very precisely cortical microcircuits by laminar-specific connection probabilities and connection strengths between all cortical neurons (Kisvarday et al., 1986; Markram et al., 1997; Gupta et al., 2000; Thomson and Bannister, 2003; Binzegger et al., 2004; Stepanyants et al., 2008). Figure 2.8A shows reconstructed neurons [1] and diagram of connectivity between neurons in layers III to IV from Thomson and colleagues work. Reciprocal connections between excitatory and inhibitory neurons within each layers are added to the previous feedforward and feeback recurrent excitatory connections

---

[1] Using biocytin during intracellular recordings in cat visual cortex
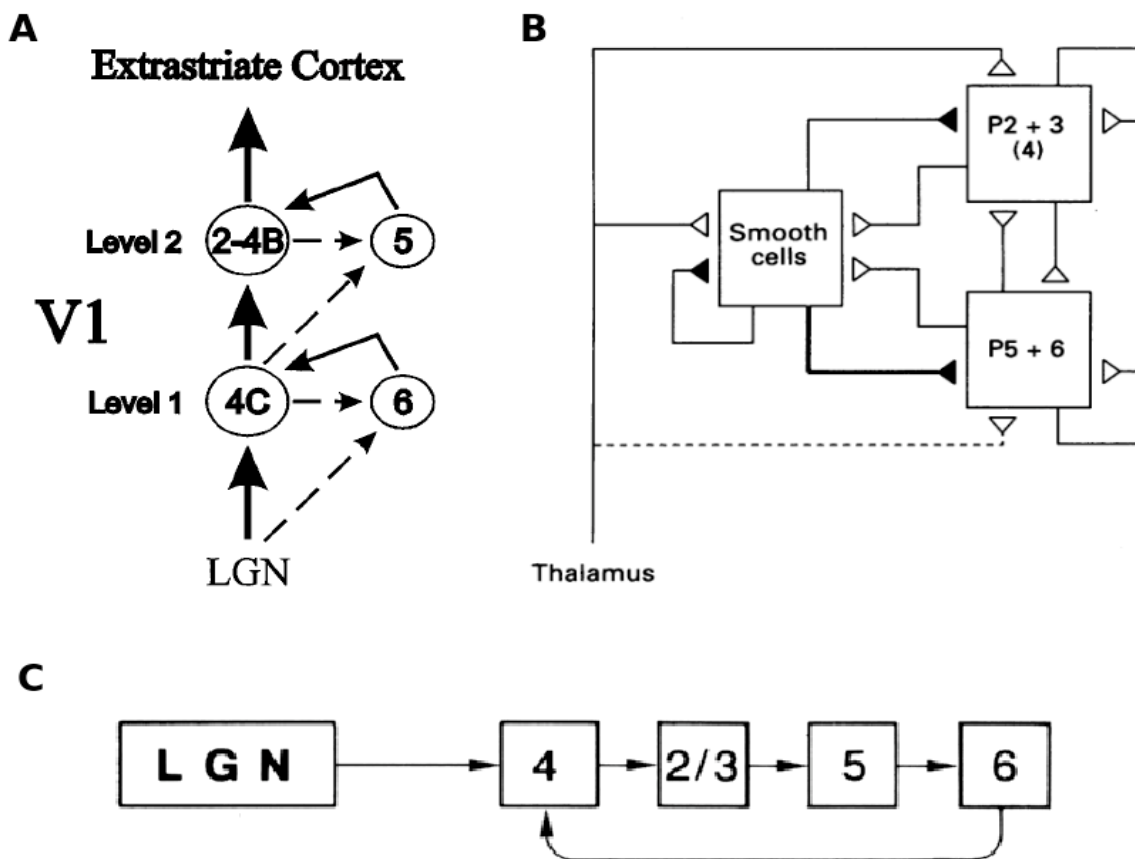
Figure 2.7: Cortical column circuitry patterns. See text for details. *A:* From Callaway (1998). *B:* From Douglas and Martin (1991). *C:* From Bolz et al. (1989).

(Fig. 2.8B). Even more recently, Binzegger et al. (2004) made three-dimensional recon-
structions [2] of the main types of neurons, including thalamic afferents, found in the cat
primary visual cortex (Fig. 2.3), in order to evaluate the laminar pattern of synaptic
connections formed by these neurons. Figure 2.9 gives those numbers.
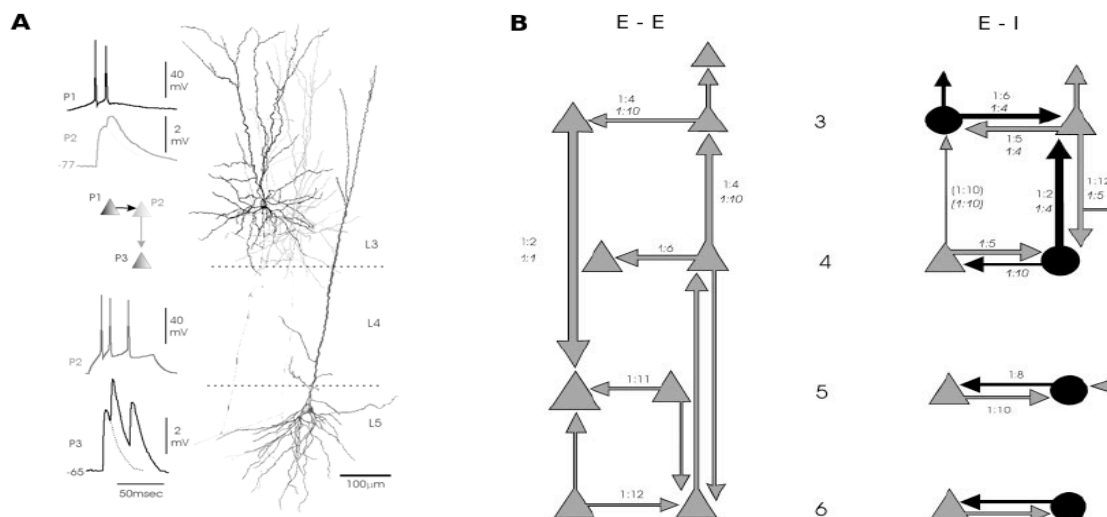
Figure 2.8: *A:* Reconstruction of layer III and layer V pyramidal neurons and the connections
between them. From Thomson et al. (2002). *B:* Diagram of connectivity between neurons in lay-
ers III to VI of the neocortex (Pyramidal and spiny stellate cells are represented by triangles and
inhibitory interneurons by circles). Ratios indicate the probability of recording a connection of
that type, while arrows size indicates the relative probabilities of connections. *Left:* Connections
between excitatory neurons. *Right:* Connections between excitatory and inhibitory neurons.
Adapted from Thomson and Bannister (2003).

This study thus provides us the quantitative description (i.e. the proportion of synapses
made between populations of neurons) of structural organization of local cortical cir-
cuits, required for our future cortical column modelization (see Part III). Note that in
their recent paper, Stepanyants et al. (2008) suggested that the characteristic geome-
try of specific types of neurons could confer a large degree of invariance in connectivity
across brain regions and species. This observation tends again to generalize our model.

2.3.2   Horizontal inter-columnar connections

Considering the previous concept of hypercolumns, the cerebral cortex has thus a modu-
lar structure consisting of repeating sets of functional columns. However, many anatom-
ical studies in cat and monkey visual cortex (Gilbert and Wiesel, 1979; Rockland and
Lund, 1982; Martin and Whitteridge, 1984) demonstrated that neighboring columns
are extensively connected by horizontal connections, i.e. cells communicate within a
layer. These horizontal inter-columnar connections are classically segregated into short-

---

[2]Using horseradish peroxidase labelling during intracellular recordings *in vivo*
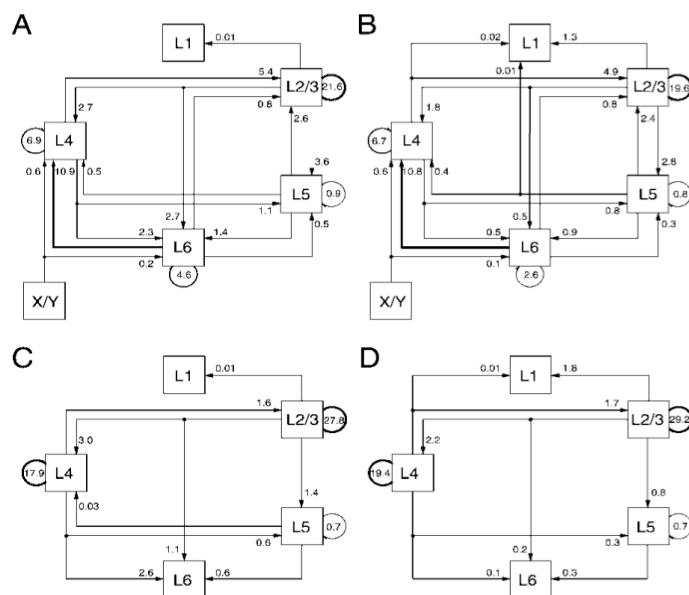
Figure 2.9: Laminar pattern of synaptic connections in the cat primary visual cortex. Each number indicates the proportion of synapses involved in *A:* Excitatory-excitatory connections *B:* Excitatory-inhbitory connections *C:* Inhibitory-excitatory connections *D:* Inhibitory-inhibitory connections. From Binzegger et al. (2004).

and long-range connections. In the visual cortex, a functional distinction could be that two neighboring columns of different orientations within a hypercolumn are connected by short-range lateral connections, while two columns belonging to two distinct hyper-columns are connected by long-range lateral connections.

In a general manner, over a spatial scale of about 800 μm, neighboring columns exhibit strong physiological short-range connections (excitatory and inhibitory) with each other, independently of any visual feature selectivity, and connection strength (or synaptic weight) decrease with cortical distance Das and Gilbert (1999). This is in accordance with what recently obtained Buzas et al. (2006) in cat primary visual cortex using biocytin labeling technique combined with optical imaging. Lateral excitatory connections mainly arise from excitatory neurons (pyramidal and spiny stellate cells) and mostly contact dendrites of target neurons [3]. The global distribution of excitatory synaptic boutons with respect to lateral distances from the injection site (see Fig. 2.11)A, left), revealed dense local connections with exponential decline of bouton density with radial distance from the injection site, surrounded by patches of long-range connections. This distribution can be reasonably predicted by a Gaussian distribution centered on the site of injection, as illustrated in Figure 2.11)A, right. The extent of short-range excitatory

---

[3]There was no evidence for preferential neuronal connectivity (McGuire et al., 1991), the ratio E:I = 80:20 being kept for the connections. However, as excitatory cells represent 80 % of all cortical cells, lateral excitatory connections mostly connect other excitatory neurons.

projections is thus about 1000 μm, while long-range projections can extent to about 3000 μm, which confirms results of earlier studies (Ts'o et al., 1986; LeVay, 1988; Gilbert and Wiesel, 1989; Kisvarday et al., 1997; Das and Gilbert, 1999).

Most of long-range intra-cortical connections are made by the axon collaterals of pyramidal neurons in superficial layers, parallel to the cortical surface (Douglas and Martin, 2004). These lateral connections are patchy and regular, and hought to be linked to the regularity of functional domains (e.g. neurons with similar orientation are connected together) (Mitchison and Crick, 1982; Gilbert and Wiesel, 1983; Xing and Gerstein, 1996; Shouval et al., 2000; Ernst et al., 2001). Indeed, a comparison between functional maps and horizontal network anatomy in the cat seemed to corroborate this correspondence between anatomy and function (Gilbert and Wiesel, 1989). The clearest relationship between anatomical connectivity and functional domains concerns excitatory long-range lateral connections and orientation columns. Several studies in different mammals (cats, ferrets, monkeys) have shown long-distance clustered horizontal connections that preferentially link columns with similar orientation preference (Gilbert and Wiesel, 1983; Ts'o et al., 1986; Gilbert and Wiesel, 1989; Malach et al., 1993; Kisvarday et al., 1997; Bosking et al., 1997). Long-range connections and ocular dominance columns has also been linked in monkey primary visual cortex, as well as lateral interactions between blob cells both within a single blob and between two different blobs (Ts'o and Gilbert, 1988). This relationship became recently even clearer thanks to optical imaging techniques (Bosking et al., 1997; Buzas et al., 2006), as illustrated in Figure 2.10. Optical imaging methods are reviewed in Chapter 3.

Inhibitory connections have a much more restricted lateral extent. Only few specific types (e.g. large basket cells) provide long-range axon collaterals extending up to 2 mm (Somogyi et al., 1983; Kisvarday et al., 1997; Buzas et al., 2001), while the majority of inhibitory cells have local axon collaterals (LeVay, 1988; Kisvarday et al., 1994; Matsubara, 1988; Buzas et al., 2001), thus contained within single vertical columns (Somogyi et al., 1983; DeFelipe and Jones, 1985). Buzas et al. (2001) have recently studied in details local and long-range connections of basket cells, then providing, like excitatory neurons, the global distribution of inhibitory synaptic boutons with respect to lateral distances from the parent somata (Fig 2.11B). The spread of lateral inhibitory projections is between 500 μm to 1500 μm and is consistent with previous studies in cat visual cortex (Kisvarday et al., 1997), but also in rat visual cortex (McDonald and Burkhalter, 1993) and monkey visual cortex (Kritzer et al., 1992).

The classical values of propagation speed for horizontal unmyelinated connectivity has been estimated to be about 0.1 m/s (Komatsu et al., 1988; Hirsch and Gilbert, 1991; Grinvald et al., 1994; Kisvarday et al., 1997; Nowak and Bullier, 1998a; Bringuier et al.,
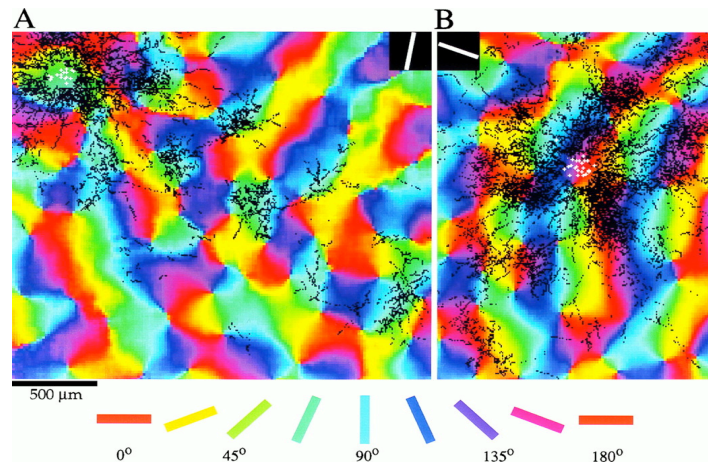
Figure 2.10: The patchy nature of horizontal connections in layer II/III of the tree shrew visual cortex. Axonal bouton distribution (black dots) after biocytin injection in layer II/III. *A:* Pyramidal neurons (white crosses) of the injected site have a preferred orientation of 80 degree. *B:* The injected site has an orientation preference of 160 degree. For both case, except for the region immediately adjacent to the injection sites, the labeled boutons are clustered in regions that have orientation preferences similar to that of the injection site, i.e. orientation columns are connected by long-range horizontal connections. From Bosking et al. (1997).

1999; Roland et al., 2006; Benucci et al., 2007; Xu et al., 2007; Ahmed et al., 2008). Following data of Buzas et al. (2001, 2006), temporal latencies of excitatory lateral connections can therefore reach 30 ms, while those of inhibitory lateral connections are about 10 ms. Note that pyramidal cells in layers II/III can also make white matter projections, i.e. cortico-cortical or inter-cortical connections, to connect even more distant columns of neurons (Gilbert and Wiesel, 1989), with even longer temporal latencies. Their functional properties are most likely quite heterogeneous compared to neurons involved in intra-cortical connections (Douglas and Martin, 2004).

It is however difficult to dissociate synapses made by local neurons from those made by long-distant neurons. Stepanyants et al. (2009) have recently done this quantitative analysis in the cat primary visual cortex, revealing surprisingly that excitatory connectivity is highly nonlocal ("74% of excitatory synapses near the axis of a 1,000 μm diameter cortical column come from neurons located outside the column"). Following these results, hypercolumns may be thus more strongly interconnected with one another by long-range lateral connections than columns within the same hypercolumn by short-range lateral connections, that contradicts the previous studies of Das and Gilbert (1999) and Buzas et al. (2006).
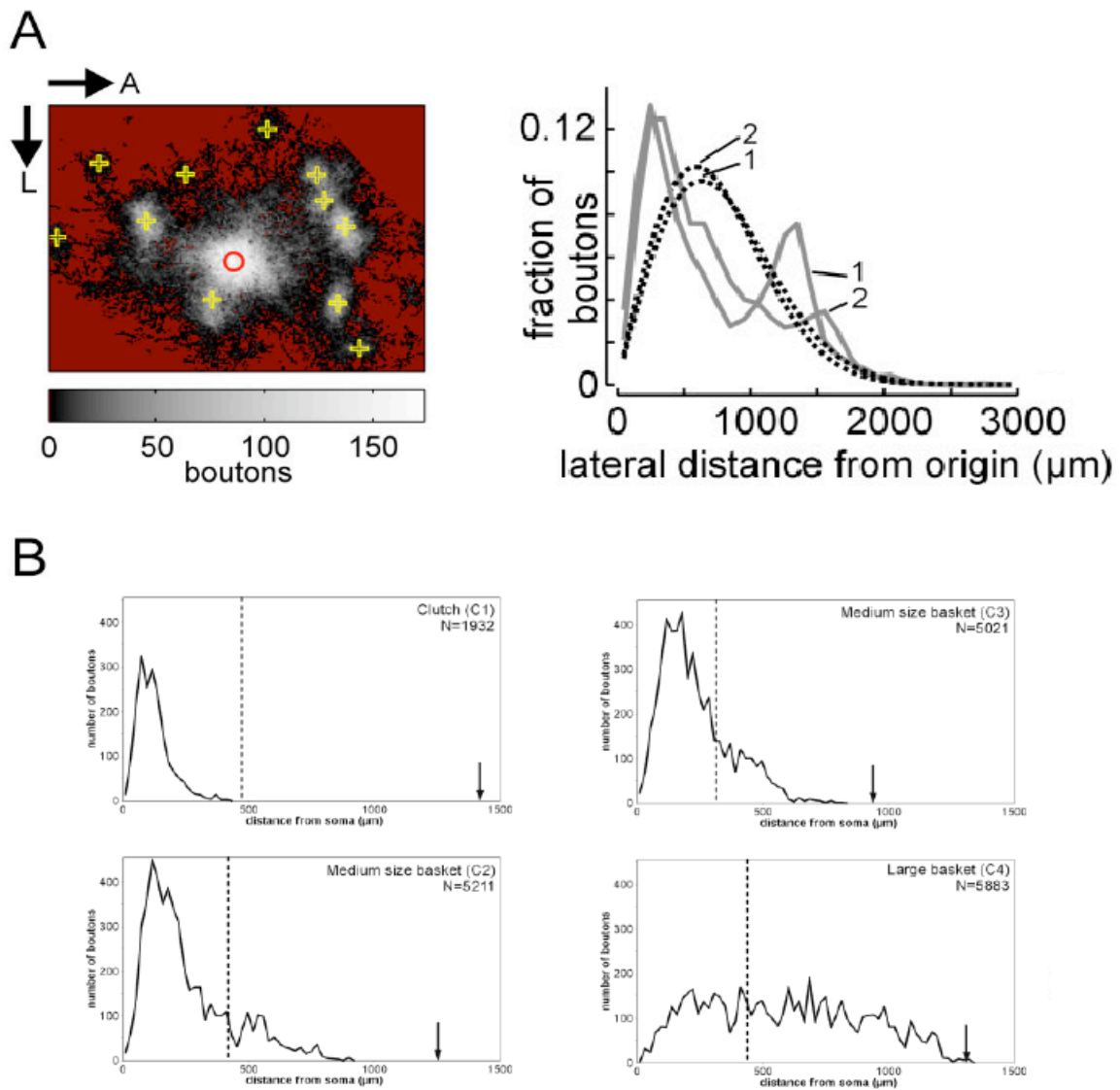
Figure 2.11: Excitatory lateral connections. *A: Left:* Bouton density map of an excitatory population of neurons, reconstructed using biocytin extracellular injection. *Right:* Spatial distribution of excitatory boutons found at the population level as a function of cortical distance from the injection site, compared to Rayleigh distributions (dashed black lines). From Buzas et al. (2006). *B:* Spatial distribution of inhibitory boutons found at the population level as a function of cortical lateral distances from the soma. Four different types of inhibitory neurons are presented. The border between local and long-range connections is indicated by dashed vertical lines. From Buzas et al. (2001).

2.4 POSSIBLE ENLIGHTENMENT OF THE CONFUSING CONCEPT OF CORTICAL COLUMN

We propose to clarify this columnar concept as follows: Each definition of cortical column depends on its type (anatomical or functional) and its spatial scale, as detailed in Table 2.1. A minicolumn or a microcolumn is an anatomical column of about one hundred neurons, since its spatial scale is about 40 μm. A macrocolumn is an anatomo-functional column, but at a larger scale, from 0.4 to 1 mm. Orientation and ocular dominance columns, as well as barrels, blobs or stripes are classified as functional columns whose the spatial scale is between 200 and 400 μm, containing several minicolumns. An hypercolumn, then represents a larger fonctional unit containing a full set of values for any given functional parameter. Its spatial scale can be up to 750 μm and contains about 10^4 neurons.

Type	Anatomical	Anatomo-functional	Functional	
Name	Microcolumn Minicolumn	Macrocolumn	Ocular dominance, Orientation, Blobs, Barrels, Stripes	Hypercolumn
Spatial scale (μm)	40	400-1000	200-400	600-1500
Number of neurons [4]	80-100	10,000-60,000	2500-10,000	20,000-140,000

Table 2.1: The different types of cortical columns.

Using this reformulation, the column denomination into mini-, micro-, macro-, hypercolumn, is not useful anymore. All these cortical columns thus share one common thing: A vertical organization.

Since the original use of electrode penetrations, a number of techniques have been employed for the experimental determination and the observation of cortical columns. These include methods based on axonal transport of substances such as horseradish peroxidase; on the differential consumption of radioactive 2-deoxyglucose by neurons; on optical imaging techniques, where cortical activity is converted to a visual signal by changes in reflectance or by voltage-sensitive dyes; and most recently on fMRI. We are going to give an introduction to these different techniques that allow columns observation in the next chapter.

---

[4]These values have been calculated from typical composition of monkey cortical tissues (Abeles, 1991), assuming the cortical thickness to be 2 mm and the neuronal density to be 40000 per cubic millimeter.

OBSERVING CORTICAL COLUMNS

OVERWIEW

Studying brain cognitive functions has always been a central question, from phrenologists in the early nineteenth century who believed that the personality traits of a person can be derived from the shape of its skull, to neuroscientists who used recent functional imaging techniques to take pictures and movies of the working brain. To this purpose, neuroscientists have developed several techniques for studying brain function. More precisely, thanks to large advances in the neuroimaging methods, brain structures, e.g. neuronal cells or cortical columns previously described, can be observed using several methodologies.

We have seen in the preceding chapters that the brain processes information at different spatial and temporal scales. More precisely, neurons with common functional properties tend to be clustered into sub-millimeter-scale columns. This chapter aims at reviewing the techniques allowing to observe the brain from microscopic (neuron) to mesoscopic scales (cortical column) scales.

Contents

3.1 DESCRIBING THE CORTICAL COLUMN ⸻

As explained in Chapter 1, cortical neurons can be classified morphologically into several categories, regarding mainly the morphology of their cell body and dendritic tree. This categorization was initially done by using staining methods, i.e. tissues or cells, are incubated with a staining solution for very long time, which highlight different aspects of the cell morphology.

3.1.1 Staining methods

The Golgi silver impregnation method is based in the formation of opaque intracellular deposits of silver chromate obtained by the reaction between potassium dichromate and silver nitrate (black reaction). This staining impregnates a limited number of neurons at random [1], and permitted for the first time a clear visualization of a nerve cell body with all its processes in its entirety (Fig. 3.1, left).

Nissl granules (or Nissl substance) found within the cell body cytoplasm, are composed of rRNA and nucleoproteins. The Nissl staining uses dyes that are absorbed by these macromolecules and allows for the visualization of all the cells nuclei in the brain, among which neurons and glia cells (Fig. 3.1, middle). Nerve cells staining is darker than that of glia cells, allowing to differentiate them. In contrast, Nissl stain is poor in labeling neuronal processes, i.e. dendrites and axons.

The Weigert stain is specific for the fatty materials that make up the myelin sheath, thus allowing to visualize myelinated axons (Fig. 3.1, right). Figure 3.1 shows cortical slices stained respectively by these three methods, emphasizing both the laminar and the columnar organization of the cortex.
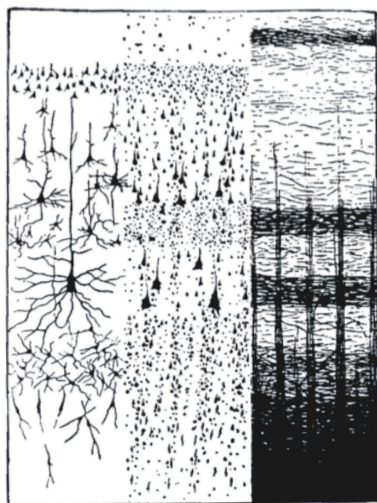
Figure 3.1: Golgi, Nissl and Weigert staining methods. See text for details. From Abeles (1991).

---

[1]The reasons are still mysterious.

Anatomical investigations of the neocortex reveal its columnar organization. However, more sensitive anatomical tracing methods were necessary to reveal connectivity and highlight a dense inter-columnar microcircuit of local and long-range connections (see Chapter 2). Indeed a large number of histological markers were developed over the years in order to trace mono- or polysynaptic, for specific antero- or retro-grade, connections.

Biocytin (biotinoyl-L-lysin) is a classical neuroanatomical tract-tracer that is taken up by neurons and rapidly transported down to axons mainly in anterograde direction. It is thus commonly used to map brain connectivity. Intracellular biocytin filling in slices of neocortex have been extensively used for anatomical three-dimensional computer reconstructions of specific neurons and connections (e.g. Kisvarday and Eysel, 1993; Kisvarday et al., 1994, 1997; Tamas et al., 1997; Markram et al., 1998a; Gupta et al., 2000, for studying GABAergic synapses organization). Figure 3.2, left shows for example a reconstruction of GABAergic connections between two interneurons.
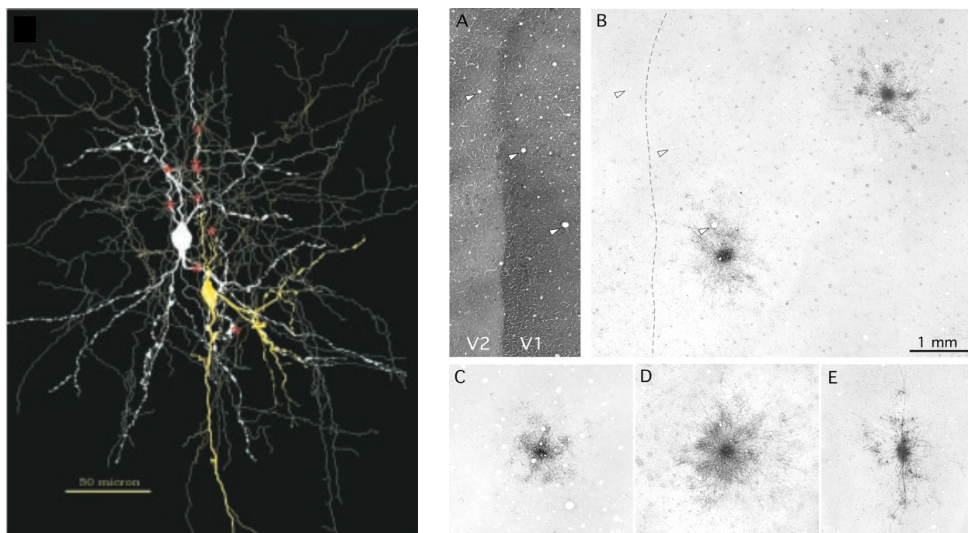
Figure 3.2: Biocytin intracellular and extracellular injections possibilities. *Left:* Reconstruction of GABAergic synaptic connections between two interneurons (presynaptic in yellow and postsynapic in white). Putative synapses are marked in red. From Gupta et al. (2000). *Right:* Biocytin labeling of axonal projections in monkey primary visual cortex. *A:* Cytochrome oxidase-stained section of flattened cortex showing V1-V1 border in layer 4. Three blood vessels found in the layer 3 section shown in B are marked by white arrows. *B,C,D,E:* Five examples of biocytin staining from different squirrel monkeys, illustrating the range of patchy distributions, from nearly circular to highly elongated. From Sincich and Blasdel (2001).

It is also possible to label an entire population of neurons using extracellular biocytin injections, as shown by Buzas et al. (2001, 2006) in Figure 2.11, Section 2.3. Similarly, Sincich and Blasdel (2001) have investigated monkey primary visual cortex, revealing a

highly stereotyped projection pattern of axons emanating from the injection site (Fig. 3.2, right).

3.1.2 Autoradiography

The 2-desoxyglucose method was developed by Louis Sokoloff at the National Institutes of Health, Bethesda, and allows post-mortem visualization of active brain areas, or even single cells, with a very low time resolution (minutes or hours) (Kennedy et al., 1975). The radioactive 2-deoxyglucose is taken up by active neurons via the glucose transporter, yet non metabolized. Radioactivity thus accumulates in active cells. To study the functional activation of a cerebral tissue, a stimulation is presented for a long time. The animal is then sacrificed, the brain perfused and mounted on a plate and the focus of activity are finally detected by autoradiography, hence locating cells activated by the stimulation.

One of the famous application of 2-DG is the retinotopic experience done by Tootell et al. (1982) in macaque striate cortex and illustrated in Figure 3.3, left. In this study, the 2-DG clearly revealed the precise retinotopic organization of the full primary visual cortex. Similarly, as explained in Chapter 2, Hubel and Wiesel revealed ocular dominance and orientation columns in cat and monkey visual cortex (Hubel et al., 1978). This discovery was done by using electrophysiology and post-mortem 2-DG autoradiography (see Figure 3.3, right).
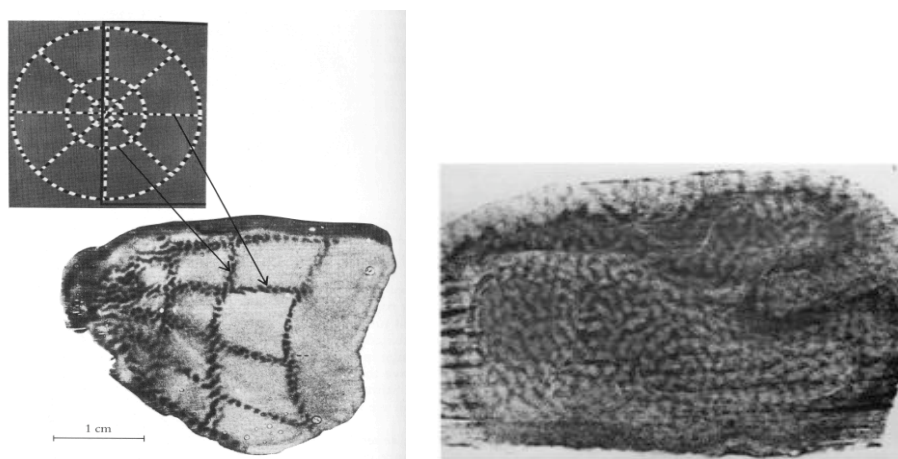
Figure 3.3: *Left:* Deoxyglucose analysis of retinotopic organization in primate striate cortex. From Tootell et al. (1982). *Right:* 2-deoxyglucose method reveals the columnar organization of the primary visual cortex. From Hubel et al. (1978).

As a post-mortem technique, the 2-DG method has been widely used for examining metabolic activity in the brain, in a variety of experimental studies, and on different animal species (Lancet et al., 1982; Friedman et al., 1989; Stewart et al., 2004). However,

in vivo imaging is not possible and only the map corresponding to one stimulus can be obtained.

3.2   INTERACTING WITH THE COLUMNAR STRUCTURE

3.2.1   Electrical stimulation

Electrical stimulation involves the use of metal or glass electrodes to trigger action potentials in individual neurons or groups of neurons. This technique is used to study neuronal mechanisms, such as synaptic transmission. An example of such experiment done by Bolz et al. (1992) is shown in Figure 3.4, eliciting synaptic transmission between thalamic and cortical neurons. Here, we mention only the specific case of recording the effect of stimulation with intracellular recordings. For extracellular stimulation coupled with intracellular recordings, see also Douglas and Martin (1991); Ferster and Lindstrom (1983, 1985a,b). Extracellular stimulation has been also coupled with many other recording techniques among which voltage-sensitive dye imaging (see Fig. 3.15).
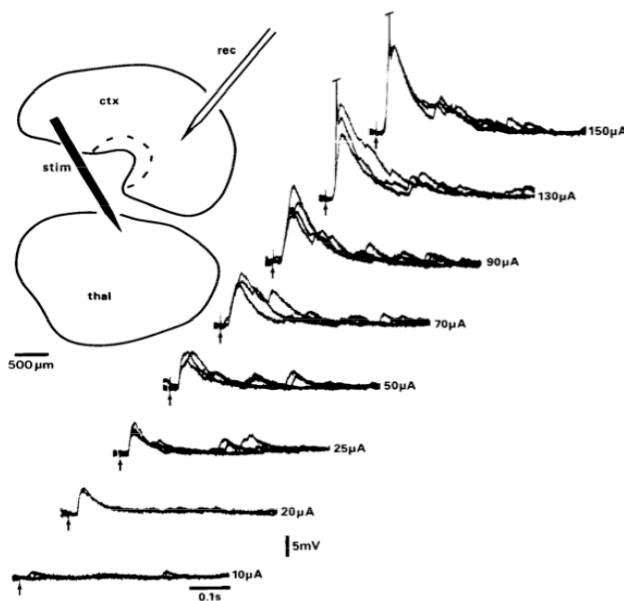
Figure 3.4: *In vitro* intracellular recordings from a cortical neuron after electrical stimulations of different intensities in the thalamus. From Bolz et al. (1992).

However, extracellular stimulation is problematic in that it mostly recruits axons and not cell bodies (Nowak and Bullier, 1998a,b), therefore in anterograde, but also retrograde directions, as well as fibers en passant. It is thus not simple to interpret. An

alternative, though much more demanding technique, consists in activation through intracellular depolarization of membrane potential: Only the recorded neuron will be activated and post-synaptic activation will reveal unambiguously contacts from the recorded neuron. As already explained in Chapter 2, Thomson and co-workers but also Markram and co-workers have extensively used dual/triple intracellular recordings in rat and cat neocortex slices to demonstrate excitatory and inhibitory connections between the different types of neurons in different layers accounting for a detailed view of the cortical column circuitry (Thomson et al., 1993; Thomson and West, 1993; Thomson and Deuchars, 1994, 1997; Gupta et al., 2000; Thomson et al., 2002; Thomson and Morris, 2002; Thomson and Bannister, 2003; Markram et al., 2004; Watts and Thomson, 2005; Thomson and Lamy, 2007).

3.2.2 Drug manipulation

We have learn in Chapter 1 that neurons, at the synapse level, have receptors that are sensitive to particular neurotransmitters (NTs), such as glutamate or GABA. In a general manner, the main principle of drug manipulations is to use these neurotransmitters artificially to study and observe their effects.

An example of drug manipulation, which is of interest here to interact with the column and study its function, came from the 70s with the use of bicuculline (i.e. alkaloid bicuculline) to selectively and reversely inactivate a cortical region. Bicuculline has been discovered as a specific antagonist of GABA receptors (Sillito, 1975b). Using bicuculline application to block GABA-mediated inhibitory action, Sillito (1975a) examined the contribution of inhibitory mechanisms to the receptive field properties of neurons in the striate cortex of the cat, and established the importance of GABAergic inhibitory processes for orientation tuning and direction selectivity (Sillito, 1977, 1979; Tsumoto et al., 1979; Sillito et al., 1980). Bicuculline was thus an efficient method for analyzing the role of local circuits, e.g. columnar micro-circuit, in shaping RF functional properties.

GABA neurotransmitter itself has been used to locally inactivate cells and study the activity of its neighbors (Crook and Eysel, 1992; Crook et al., 1996, 1998, 2002). These authors thus provided anatomical evidence for the presence of an inhibitory pathway, responsible for several receptive field properties, including orientation/directions selectivity (Fig. 3.5).

3.2.3 Optogenetics

A step further, in order to visualize and stimulate the nervous system, is the optogenetic tool: associating optical and genetic tools. Several of these methods use genetics
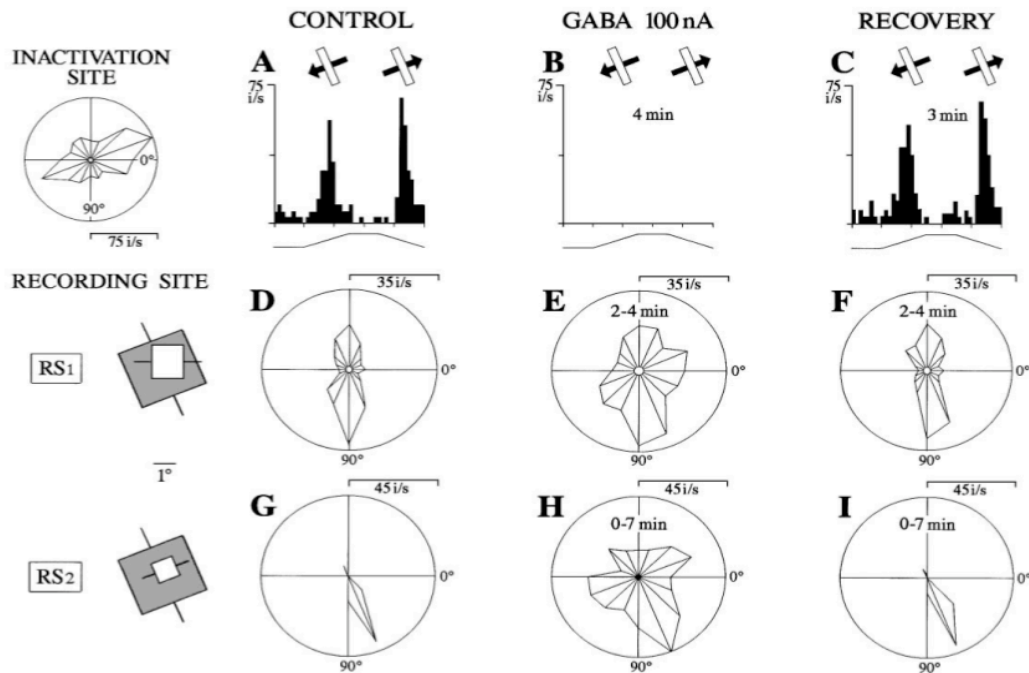
Figure 3.5: GABA inactivation of specific cells (IS = inactivation site) caused reversible broadening of orientation tuning in a nearby cells at two recording site (RS1 and RS2). Adapted from Crook et al. (1998).

manipulations to give a light sensibility on specific groups of neurons, allowing to control their neuronal activity with pulses of light. The central principle lies in the use of rhodopsin, a light-sensitive protein found in rod photoreceptor cells of the retina (photopsin is found in cone cells), that initiates an electrical signal when stimulated by photons. Two rhodopsins with intrinsic ion conductances have been identified recently in a green algae called Chlamydomonas reinhardtii (Nagel et al., 2002). They were named "channelrhodopsins" ChR1 and ChR2. Both were expressed in Xenopus laevis (i.e. south african clawed frog) oocytes, and their properties were studied by voltage clamp techniques. ChR1 is specific for H+, whereas ChR2 conducts Na+, K+, Ca2+, and guanidinium. They can be viewed as some "switches", since their ion flux regulating activity can be controlled externally by light. The idea is thus to genetically express these channels in specific cellular types that will be specifically activated by light (Boyden et al., 2005).

As an example, Deisseroth and collegues thus took benefits of those photosensitive proteins to interrogate the functions of specific cell populations within columnar circuits of living animals, in order to better understand the contribution of defined cell types to behavior (Schneider et al., 2008; Sohal et al., 2009; Cardin et al., 2009). This technique thus provides new insights into the role of particular neuron types in intact neural cir-

cuits. This ability to control and manipulate neuronal activity within an intact brain is of key importance for mapping functional connectivity and for dissecting the neural circuitry underlying behaviors. It could then be of interest for dissecting the neural microcircuit of the cortical column.

3.3 OBSERVING THE COLUMN RESOURCES

3.3.1 Functional magnetic resonance imaging

Magnetic resonance imaging

The phenomenon of nuclear magnetic resonance (NMR) was discovered in 1938 by Isidore Isaac Rabi. NMR is a spectroscopic technique, i.e. the study of the interaction of electromagnetic radiation with matter. It relies on the magnetic properties of atomic nuclei. NMR can be applied to different nuclei, the simplest being the hydrogen nucleus (a simple proton). Atomic nuclei which have a non-zero *nuclear spin* behave like magnetic dipoles. When placed in a strong magnetic field, the magnetic moments of these nuclei line up with and precess around the field's direction, thus creating a macroscopic magnetization. The rate of precession is given by the so-called Larmor relationship $f = \gamma\, Bo/2\pi$, where f is the resonance frequency in Hz, γ is a constant called the gyromagnetic ratio, and Bo is the magnetic field. The principal isotope of hydrogen relevant to most imaging studies has spin $I = \frac{1}{2}$. It has two allowed states with orientations parallel (lower energy) and antiparallel (higher energy) to the main magnetic field. NMR refers to the frequency-specific excitation produced by transitions between these two different energy states (Logothetis, 2003).

Magnetic resonance imaging (MRI) uses NMR phenomenon (the magnetic field is typically within the range of 1.5 to 4.0 Tesla) to create images of biological tissue with a high spatial resolution. More precisely, MRI works because our body is largely composed of water molecules, each containing two hydrogen atoms or protons. When these protons are placed inside a strong homogeneous magnetic field, their magnetic moments will line up with the direction of the magnetic field. Then if they receive radio waves (brief radiofrequency pulse) at the appropriate frequency, this will cause the protons to change the orientation of their spins as they absorb energy. These realignment changes create a radiowave signal which can be detected by the MRI scanner. In order to see where this signal is coming from, a magnetic field gradient, i.e. that makes a field stronger in one place and weaker in another place, is used on top of the homogenous field to encode

space. MRI thus produces images of biological tissues with high concentration of water molecule, e.g. white and gray matter, therefore displaying a high spatial precision (down to the millimeter). For details, see Callaghan (1991); de Graaf (1998); Stark and Bradley (1999).

Functional MRI

The basis of functional MRI is that neural activity (e.g. action potential generation, synaptic integration) engenders metabolic demands (i.e. glucose and oxygen). Classical fMRI researches make use of a technique discovered in the early 1900s, the BOLD (Blood Oxygenation Level Dependent) contrast (see Ogawa et al., 1990; Belliveau et al., 1991; Turner et al., 1991; Tank et al., 1992): Local changes in neural activity causes local changes in blood oxygenation and blood flow (hemodynamic response) (Roy and Sherrington, 1890). Since local neural activation increases local blood flow more than the local oxygen metabolism rate, less oxygen is removed from the blood and the venous blood oxygenation increases. It results in an increase in the concentration of oxygenated hemoglobin (HbO_2) and a decrease in the concentration of deoxygenated hemoglobin (Hbr) present in the blood. An early initial increase in Hbr has also been reported, most likely resulting from a highly localized increase in cerebral metabolic rate of oxygen, prior to the larger Hbr decrease. This phenomenon is commonly referred as the "initial dip", because it induces an early negative deflection of the BOLD signal. Although very local, the initial dip has a much smaller amplitude and duration than the later positive BOLD response and thus suffers under low signal to noise ratio. Its usefulness for fMRI mapping remains therefore limited. The MRI signal is sensitive to this change because HbO_2 and Hbr have different magnetic properties. Hbr is paramagnetic, while HbO_2 is not, thus only Hbr is visible in NMR, so a decrease in its concentration results in a stronger MRI signal. The BOLD signal can be used as an index of brain activity composed of several variables, some of which being not still completely understood.

fMRI presents as main advantages to be non-invasive and to have a high spatial resolution (mm). However, the BOLD signal depends on blood volume and oxygenation which changes relatively slowly, fMRI has a low temporal resolution (seconds). Furthermore, the BOLD signal is only an indirect measure of neural activity and how electrical activity is coupled to such metabolic responses remains unresolved.

fMRI allowed to accurately study the retinotopic organization of human primary visual cortex (Belliveau et al., 1991; Ogawa et al., 1992; DeYoe et al., 1994; Engel et al., 1997; Tootell et al., 1998; Warnking et al., 2002), as well as confirm other known anatomically distinct processing areas, as for example in the motor cortex (Kim et al., 1993a,b). We are thus wondering if fMRI has a sufficient spatial resolution to map submillimeter

functional structures, like cortical columns. Duong et al. (2000) and Kim et al. (2000) showed that the early-negative BOLD changes, in response to the first two seconds following visual stimulation, elicite patchy patterns consistent with columnar organization, as illustrated in Figure 3.6. However, this result is controversial Grinvald et al. (2000).
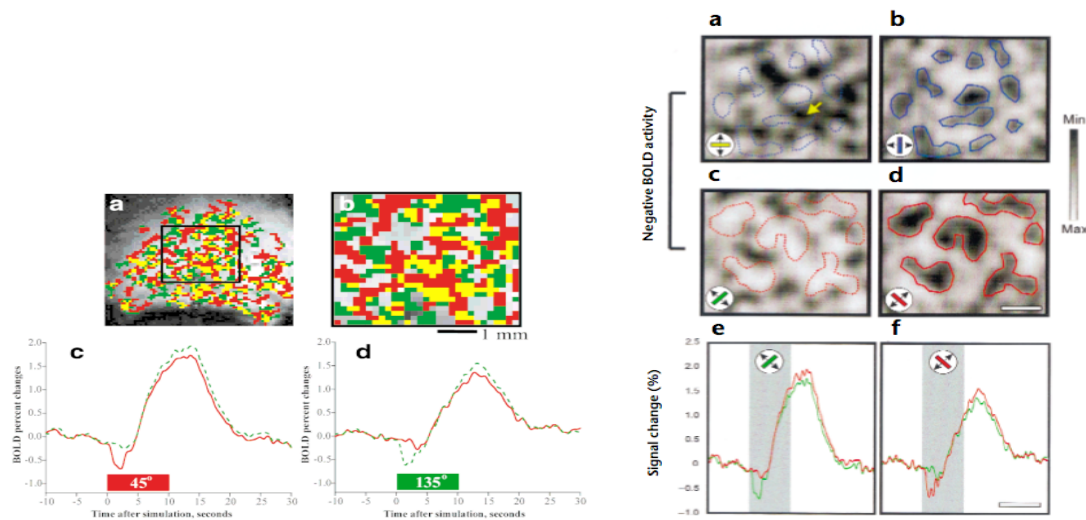
Figure 3.6: The early negative bold technique could map human functional columns. Only the early-negative response within 2 sec of the stimulus onset can achieve columnar resolution. By using the first 2 sec of the early-negative BOLD response, columns of about 500 μm size separated by about 1.3 mm can be resolved. The MR-derived orientation columns obtained using two orthogonal stimuli are complementary. From Duong et al. (2000) and Kim et al. (2000).

Recent advance in fMRI have led to enhanced sensitivity and spatial accuracy of the measured signals, and Kim and Fukuda (2008) showed that high-resolution fMRI (cerebral blood volume measurement instead of the BOLD technique) provides a technique to non-invasively and repeatedly map functional cortical columns in the visual cortex. A comparison with orientation maps obtained using optical imaging of intrinsic signals (see next paragraph) on the same animal validated their results (Fig. 3.7).

3.3.2 Optical imaging of intrinsic signal

Optical imaging of intrinsic signals (OIS) has been developed by Grinvald and others (Grinvald et al., 1986; Blasdel and Salama, 1986). The source of the intrinsic signals include reflectance changes from several optically active processes, which correlate indirectly with neuronal activity (see Vanzetta and Grinvald (2008) for a recent review on the subject). In particular, the changes in back reflected light depend on the distinctive absorption spectra of oxy- and desoxyhemoglobin and their concentration

Figure 3.7:   fMRI reveals functional cortical columns. Comparison between high-resolution fMRI (A) and optical imaging of intrinsic signals (B) on the same animal shows a good match between the two modalities. From Kim and Fukuda (2008).
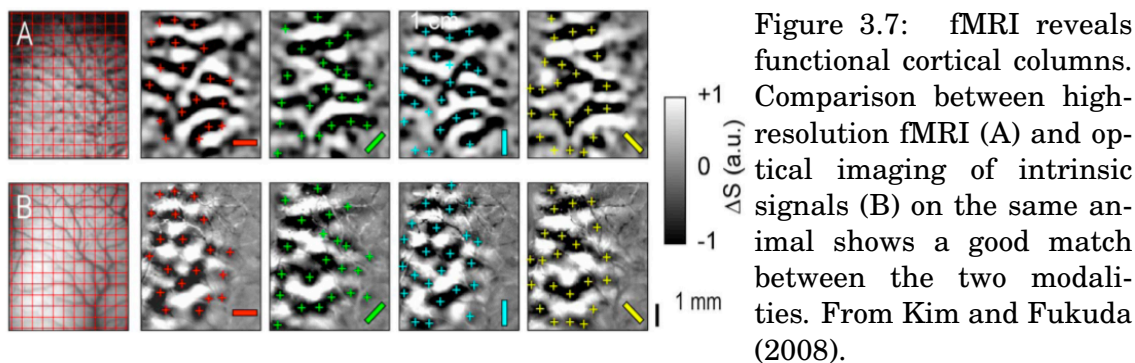
changes. As those vary in time, they can be selectively monitored using different illumination, eventually multiple, wavelenghs. At isosbestic wavelengths, Hbr and HbO_2 absorb equally, therefore allowing to measure blood volume (Hb total), whereas all the other wavelengths are oximetric and the intrinsic signal is thus multicomponent. When illuminating the cortex, through an optical chamber and artificial dura (see Bonhoeffer and Grinvald (1996) for details on the technique methodology), with light at the appropriate wavelength, it is then possible to measure blood volume or blood oxygenation dynamics in the superficial layers of the cortex and thus distinguish active cortical regions. Actually, intrinsic signals measured at specific wavelengths and times have been associated with the so-called *initial dip* in BOLD fMRI studies, corresponding to a short latency decrease in blood oxygenation, hence to an increase in Hbr concentration just after stimulus onset (Hu et al., 1997; Kim et al., 2000). Compared to fMRI, this technique offers a better spatial resolution (i.e. subcolumnar resolution) with a higher signal to noise ratio.

OIS allows to obtain high-resolution functional maps from a relatively large area (Fig. 3.8, left), as retinotopic map from Tootell et al. (1982) previously showed using 2-DG. In addition, the cortical responses to many different stimuli can be studied in the same area of cortex during the same experiment, which is not possible using such metabolic labeling techniques. For example, the overall pattern of orientation columns can be visualized by optical imaging methods on several animal preparations (Blasdel and Salama, 1986; Grinvald et al., 1986; Ts'o et al., 1990; Bonhoeffer and Grinvald, 1991; Weliky et al., 1995; Bosking et al., 1997) and chronically on the same area, as illustrated in Figure 3.8, right. Using OIS in cat primary visual cortex, Hubener et al. (1997) investigated the spatial relationship between these maps (orientation, ocular dominance and spatial frequency), as shown in Figure 3.9.

Although optical imaging based on intrinsic signals offers a very high spatial resolution, needed for accurately visualizing the columnar organization of the cortex, its temporal resolution is too low and the origin of the signal only indirectly linked to neuronal activity to study the dynamics of cortical processing.
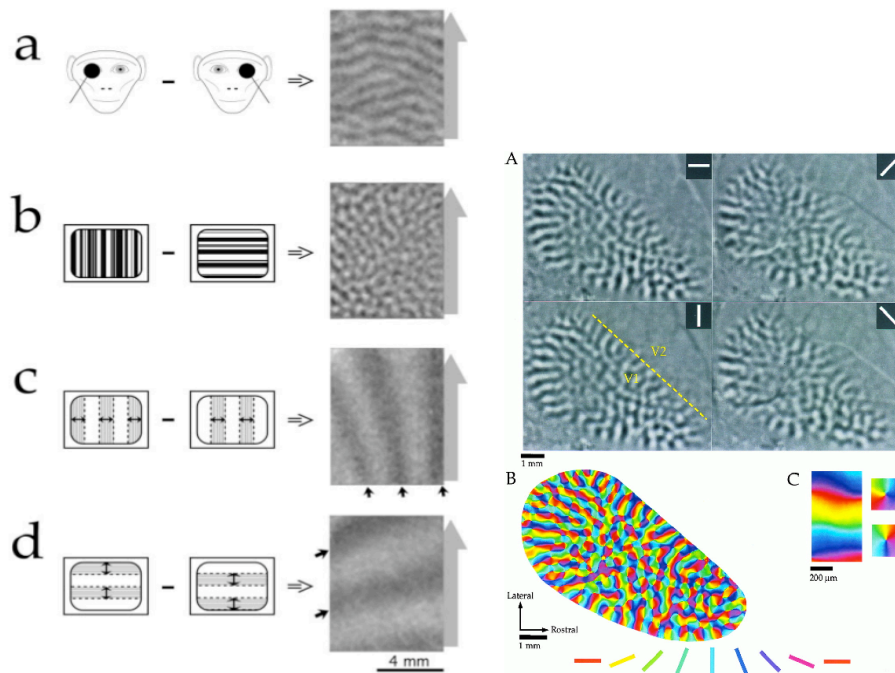
Figure 3.8: Functional maps revealed by optical imaging of intrinsic signals. *Left:* Ocular dominance (a), orientation (b) and retinotopic (c, d) maps recorded in monkey visual cortex. From Blasdel and Campbell (2001). *Right:* Orientation maps recorded in the tree shrew primary visual cortex. From Bosking et al. (1997).
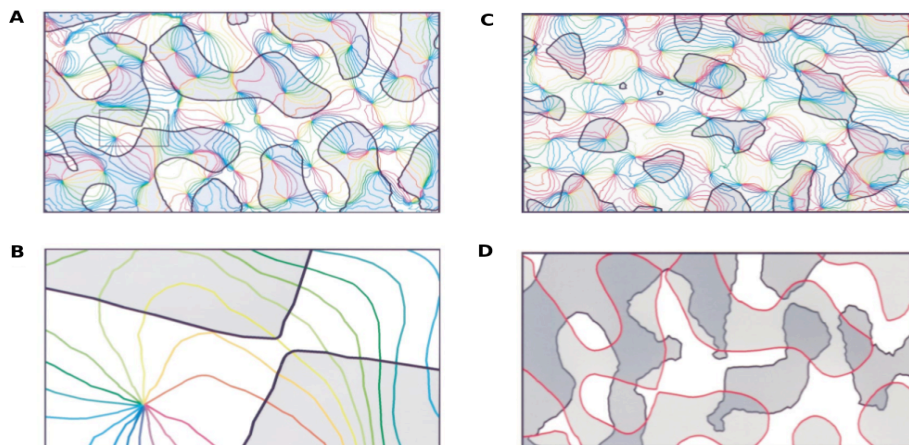
Figure 3.9: Spatial relationship between functional maps in V1. *A:* Ocular dominance (black contours delineate contralateral (gray areas) and ipsilateral eye dominance) and orientation (colored lines) maps. *B:* Enlarged detail from A (small rectangle), showing perpendicular intersections between the two functional maps. *C:* Spatial frequency (black contours separate low (gray areas) and high spatial frequencies) and orientation (colored lines) maps. *D:* Spatial frequency (dark gray with black contours) and ocular dominance (light gray with red contours) maps. From Hubener et al. (1997).

3.4 Observing the column in action

3.4.1 Electrophysiology

In 1848, Du Bois-Raymond demonstrated action potentials in nerves and less than 30 years later in 1875, Richard Caton described the electrical activity of the brain (of rabbits) and its link with brain function: "The electrical currents of the grey matter appear to have a relation to its function" (Caton, 1785). In 1929, Hans Berger (Berger, 1929) was the first to develop a recording system adapted to humans (i.e. without opening the skull), allowing to highlight electrical waves: The human electroencephalogram.

Electrophysiology provides the most direct measurement of neuronal activity. Classical electrophysiology techniques involve placing electrodes into various preparations of biological tissue. We have seen in the precedent chapters that electrophysiology was used both to understand the mechanisms underlying the generation of action potentials (i.e. spikes) in neurons and to discover the columnar organization of the brain. However, the electrophysiology techniques were different in each case. Hodgkin and Huxley experiments (Hodgkin and Huxley, 1939) involved **intracellular recordings** from the squid giant axon, which means that they inserted sharp microelectrode inside the axon and they measured the membrane potential (Fig. 3.10).

Figure 3.10:   The first published action potential (right) was obtained in 1939 by Hodgkin and Huxley from the squid giant axon (left), using glass capillary electrodes filled with sea water.   From Hodgkin and Huxley (1939).

In comparison, Mountcastle and Hubel and Wiesel used **extracellular recordings** from single neurons (**single-unit recording (SUA)**) respectively in the primary somatosensory cortex and in the primary visual cortex of anesthetized cats and monkeys, to measure action potentials from single cells. These electrophysiological studies were at the origin of the discovery of cortical columns in primary sensory areas. They were able to show that neurons in these areas, which respond to the same stimulation, were arranged vertically into columns (Mountcastle, 1957; Powell and Mountcastle, 1959a,b). If the electrode impedence is higher, then the electrode might record the activity generated by several neurons (**multi-unit activity (MUA)**). This technique was used for

example by DeAngelis et al. (1999) to study the micro-organization of columns by record-
ing neuronal pairs from the same electrode and compare the value of several particular
RF parameters for couples of nearby neurons, as illustrated in Figure 3.11. They found
strong clusters for RF preferred orientation (Fig. 3.11A), width (Fig. 3.11C) and preferred
spatial frequency (Fig. 3.11F). In addition, RF response latency (Fig. 3.11B), duration
(Fig. 3.11D) and preferred temporal frequency (Fig. 3.11F) exhibit significant clustering.
This method is interesting to depict the functional parameters that are predominantly
represented at the (micro)columnar level.
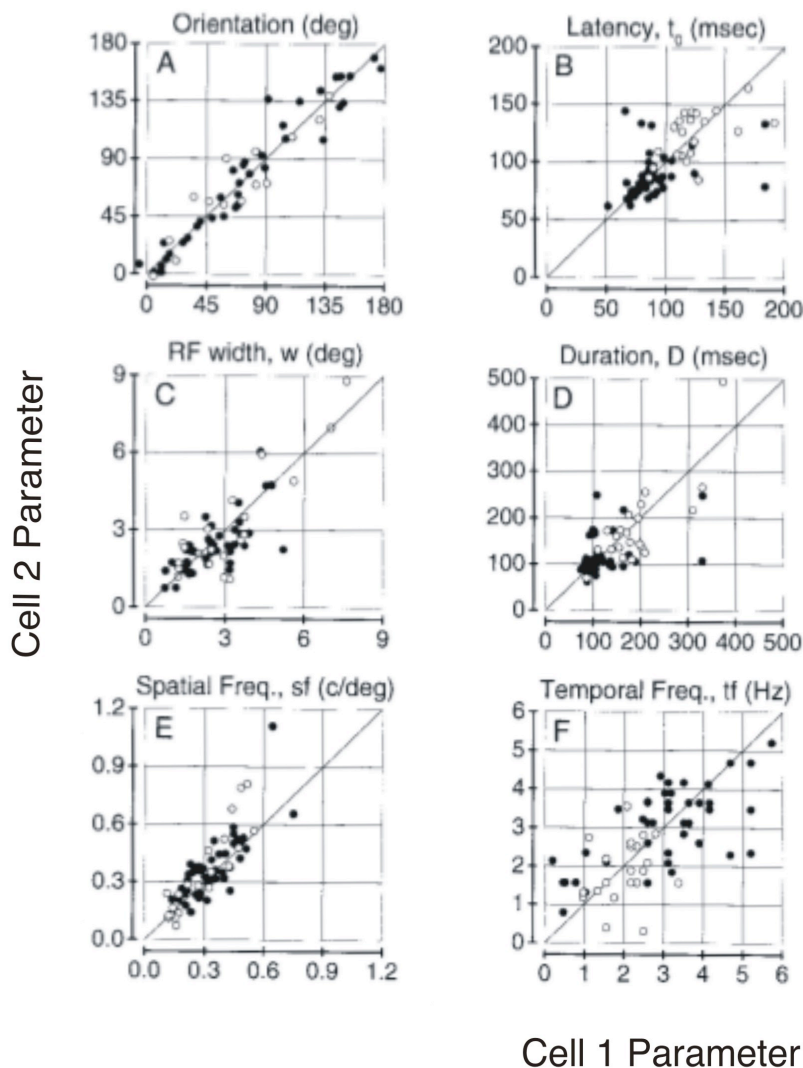
Figure 3.11: Extracellular multi-unit recordings revealing pairwise correlations in var-
ious RF parameters. Adapted from DeAngelis et al. (1999).

Among electrophysiological signals recorded with extracellular electrode, **local field**

potential (LFP) is another main class. In contrast to unit activity, which represents the
"spiking" of single or multiple neurons recorded near the electrode tip, the LFP reflects
slow modulation of the extracellular medium depolarization, with neurons closer to the
electrode tip making the greatest contribution. LFPs of multiple locations can be used
to identify the source of neuronal activity (**current source density (CSD)**). CSD is an
interesting method for dissecting the laminar origin of the cortical input integration.
See (Mitzdorf, 1985) for a detailed review on the subject.

Electrophysiology thus allows to directly record electrical activity within a cortical
column. However, we can easily imagine the amount of time needed to record a sufficient
number of neurons, using single or even multi-unit recordings, to obtain a partial picture
of the columnar arrangement, not to mention the well described sampling problem of
such techniques.

3.4.2   Two-photon imaging

Two-photon imaging actually refers to two-photon excitation (2PE) laser scanning fluo-
rescence microscopy. Fluorescence microscopy involves the labeling of a biological spec-
imen with a fluorescent molecule called a fluorophore and to excite it with light of a
specific wavelength. 2PE is then based on the idea that two photons of low energy (i.e.
1/2 energy necessary to excite the fluorophore) can excite the fluorophore only at the
point where they meet, resulting in the emission of fluorescent photons from only one
given and exact position in the neuronal tissue. Invented 20 years ago by Denk and
colleagues, 2PE laser scanning microscopy is based on the sequential two-photon exci-
tation of multiple locations in order to reveal spatial information usually along one to
two dimensions (Denk et al., 1990). The principle of this technique is illustrated in Fig-
ure 3.12. In opposition to classical and confocal imaging techniques, two-photon imaging
allows to excite through a laser only in the focus of the laser beam, thereby eliminating
excitation of out-of-focus fluorophore and providing an excellent spatial resolution.

Over the last years, two-photon imaging has became very popular in studying indi-
vidual neurons (or even synapses) or neuronal populations (Denk and Svoboda, 1997; So
et al., 2000; Zipfel et al., 2003; Helmchen and Denk, 2002, 2005). This effervescence is
due to the fact that two-photon imaging dramatically improves the detection of signal
photons per excitation event, thus minimizing photobleaching and phototoxicity, which
are the main limitations of fluorescence microscopy techniques. More importantly, it
allows to record many (> 100) neurons at the same time. Two-photon imaging thus pro-
vides a technique at the column's scale with unprecedent spatial resolution.
For example, Ohki et al. (2005, 2006) recently used 2PE microscopy with calcium sensi-
tive dyes to reveal the columnar organization of the visual cortex at single cell resolu-
tion (Fig. 3.13). They were able to clearly detect neurons with orientation and direction
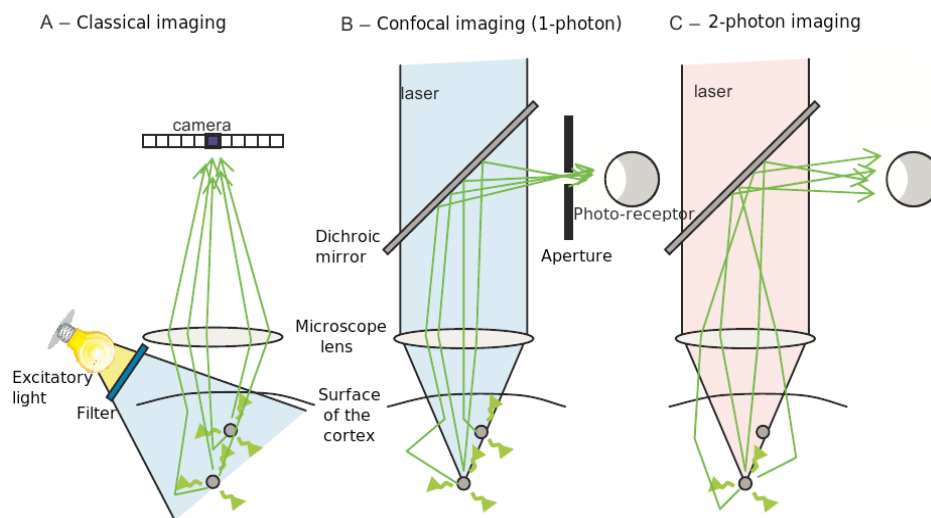
Figure 3.12: Fluorescence excitation in classical, 1-photon and 2-photon imaging. *A:* In classical imaging, the light source excites all the region stained by the fluorescent marker. As a result, fluorescent signals from several locations are mixed in a same image pixel recorded by the camera. *B:* On the contrary, the principle of confocal microscopy is to excite through a laser only one point at the time. The maximum of fluorescent light emitted by this point is collected thanks to a photoreceptor and an oscillating mirrors device allows to scan, point by point, an entire brain region with the laser beam. However, even if the maximal intensity is reached at the laser focus, the latter excites an entire cone and the aperture device required to filter the out-of-focus fluorescence does not guarantee a good spatial resolution. *C:* In 2-photon imaging, only the molecules located in the focus of the laser beam are excited, thus providing tridimensional images with an excellent spatial resolution. Figure courtesy of Thomas Deneux.

selectivity and to demonstrate that even neurons in the pinwheel centers are highly organized and orientation selective.
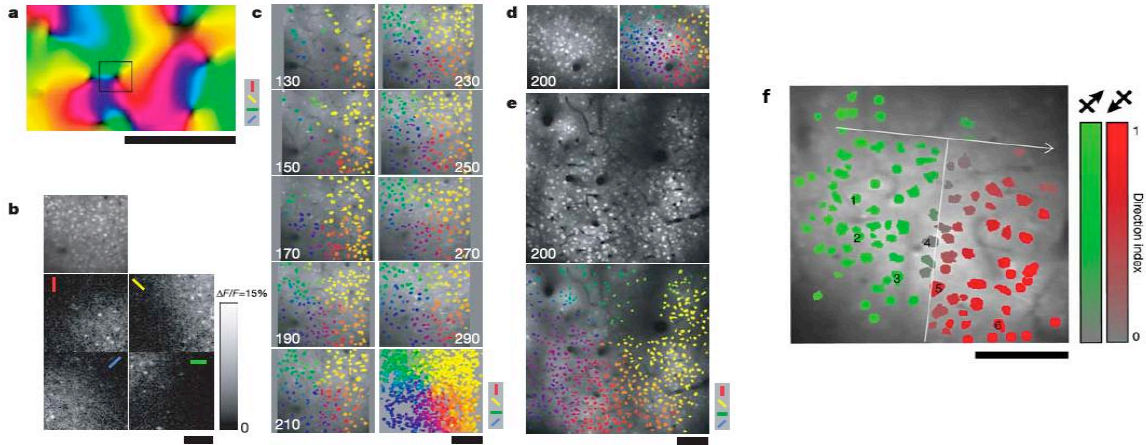
Figure 3.13: Two-photon microscopy (2PM) with calcium sensitive dyes allows to image functional columns at single cell resolution. Color indicates direction preference (grey cells respond to both directions). From Ohki et al. (2005).

Even more recently, Schummers et al. (2008) investigated glial cells responses using 2PM. They revealed that glial cells, like neurons, respond to visual stimuli (Fig. 3.14) but with a much slower time scale (Fig. 3.14B). These authors also revealed that glial cells are orientation selective and spatially organized in a columnar fashion such as neuronal cells (Fig. 3.14C).
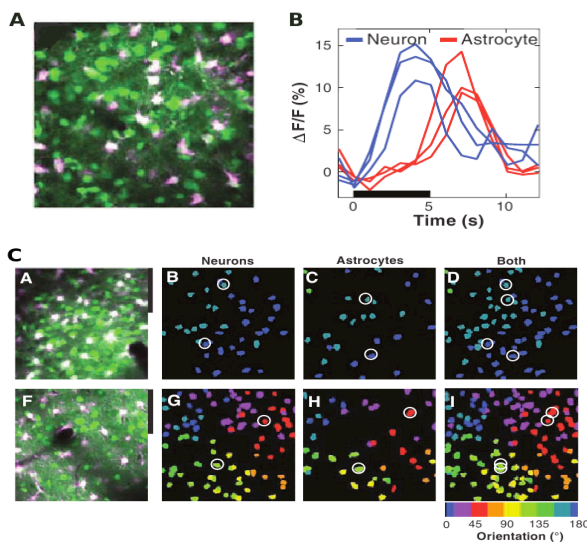
Figure 3.14:   *A, B:* Two-photon microscopy allows to compare neuronal (green fluorescence) and glial (red fluorescence) responses to visual stimuli. *C:* Two-photon microscopy reveals the orientation selectivity of astrocytes. From Schummers et al. (2008).

However, even for studies of neuronal activities, two-photon imaging is mostly based on the used of calcic fluorescent probe and the slow time course of intracellular calcium signals triggered by action potentials limits the temporal resolution of two-photon imag-

ing. It thus remains an expensive challenge for this imaging technique to achieve *in vivo* measurements of large-scale population activity with high temporal accuracy (Frostig, 2009).

3.4.3   Voltage-sensitive dye imaging

Voltage-sensitive dye imaging, as its name says, is based on the use of a dye that binds to cell's membranes and acts as a local probe indicating the level of depolarization by an emission of fluorescent photons. With a high spatial and a high temporal resolution, VSDI allows a direct recording of cortical activity within a large neuronal population (> 10 mm). A complete review of the technique is reported in Chapter 5.

Using VSDI *in vitro*, Petersen and Sakmann (2001) revealed the functional columnar architecture of rat somatosensory barrel cortex. Electrical stimulation of a single barrel in layer 4 evokes a cortical response initially restricted to the simulated barrel. Then the activity spread in a columnar manner into layer 2/3; the horizontal extent being always limited by the barrel-column width (Fig. 3.15).
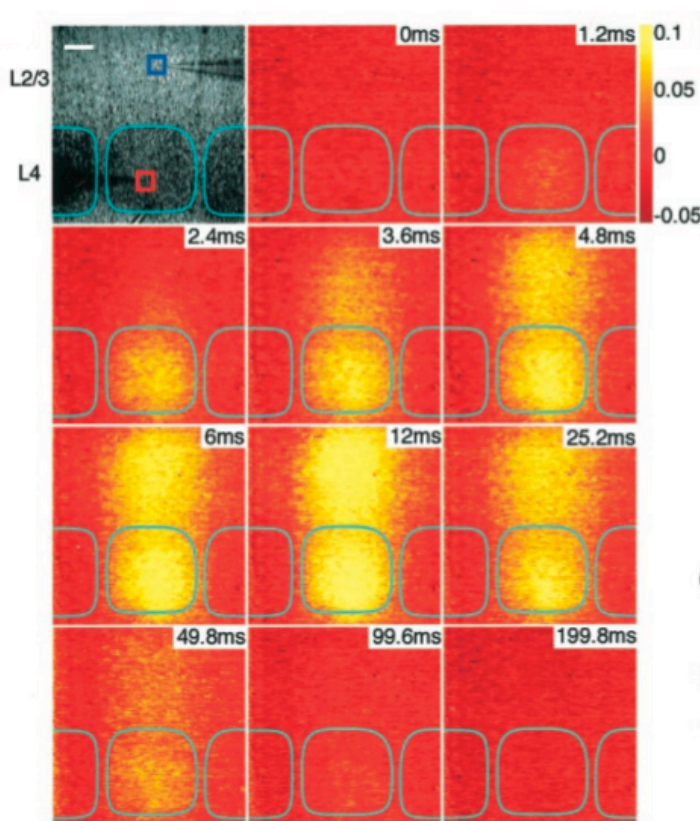
Figure 3.15:   *In vitro* voltage-sensitive dye recording revealed the columnar organization of the rat somatosensory barrel cortex.   Blue squares delineate the barrels.   The layer 4 barrel receives an extracellular stimulation at time 0 ms and spread gradually from layer 4 to layer 2/3 in a strict columnar manner. From Petersen and Sakmann (2001).

Complementary, *in vivo* VSDI measurements confirm these columnar confinement for the earliest detectable response in layer 2/3 to a single whisker deflection (Petersen et al., 2003, Fig. 3.16, 10 ms). However, depending on the strength of the stimulation,

the delayed response then propagates laterally to neighboring columns (Fig. 3.16, 20 ms), and can rapidly reach the entire barrel cortex (Fig. 3.16, 50 ms).
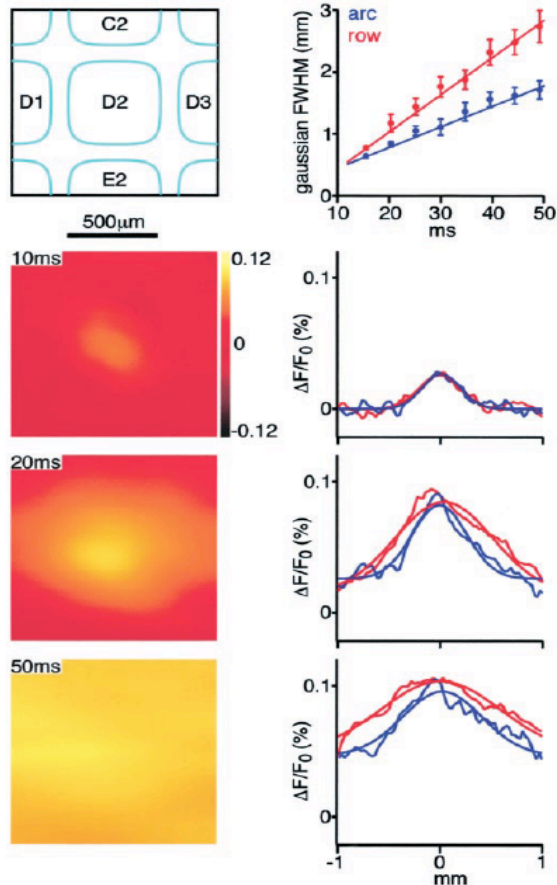
Figure 3.16: Direct visualization of superficicial layers spread of activity using *in vivo* voltage-sensitive dye recording in the rat barrel cortex. *Left:* Spatiotemporal dynamics of neocortical responses, evoked by a single brief whisker stimulation. The barrel map of layer 4 is shown on top. *Right:* The spatial extent of VSD signals are quantified by fitting Gaussian curves to the cross-section profile through the epicenter along the row (red curves) or arc (blue curves). From Petersen et al. (2003).

Thanks to its high spatial and temporal resolution, VSDI is the only technique allowing for a real-time visualization of a neuronal population activation at a sub-columnar resolution, in response to a sensory input.

3.5 SUMMARY

In this chapter, we have seen that many techniques aim at functionally recording or visualizing the activity of individual neurons or groups of neurons. Each technique has its own advantages and each provides different information about brain structure and function. However, the understanding of these brain structures is often limited by the spatial and temporal resolution of the techniques. Therefore, the combination of two or more of these techniques is an emergent solution to identify more precisely the brain activity. Figure 3.17 shows a 3D classification of all the techniques, according to their resolutions and the spatial scale (field of view) they can cover.
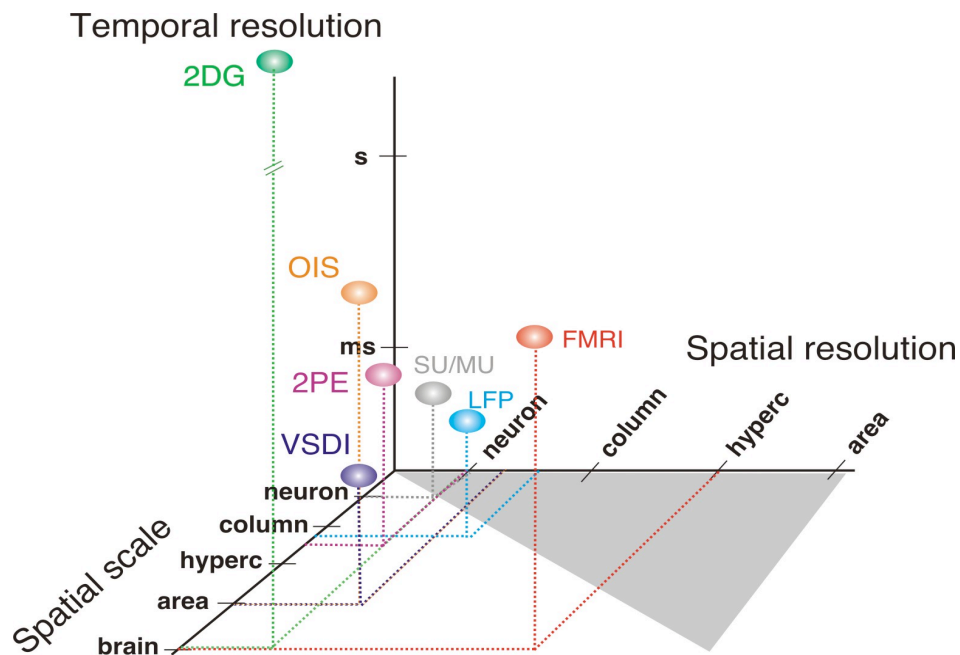
Figure 3.17: Imaging and non-imaging techniques are classified according to their resolutions, both spatial and temporal and their spatial scale.

The techniques mostly used for directly studying the neuronal activity consist in inserting one or several electrodes in the specific region of the brain, in order to measure the individual activity of one or several neurons (SU/MU), or a mean activity in the region (LFP). These techniques have thus a very high spatial and temporal resolution, but as disadvantage, they do not allowed to study the behavior of neurons as interconnected networks. Conversely, fMRI provides a non-invasive method to map the entire brain but with lower spatial resolution and especially very poor temporal resolution. In order to simultaneously record a large population of neurons, the choice goes to optical imaging techniques. OIS has a high spatial resolution and can cover a spatial scale of the cortical area but unfortunately it has a poor temporal resolution. Tsunoda et al. (2001) thus combine OIS and electrophysiology to understand the role of cortical columns in complex objects representation. 2PE microscopy presents an excellent spatial resolution. However, it measures slow signals (calcium signals) and only reaches the columnar spatial scale. With a high spatio-temporal resolution, VSDI seems to be the best compromise for studying large populations of neurons.

MODELING THE BRAIN STRUCTURES

OVERWIEW

We are now switching from the observation to the modelization of neurons and cortical microcircuits. In Chapter 1, we have seen that biological neurons are very complex systems, which send information via electrical and chemical signals. Here, we will see that mathematical modeling is a powerful tool for studying the inherent complexity of the brain. In Section 4.1, we provide an overview of the computational descriptions of a neuron. Artificial neurons are mainly used to reproduce the computational effectiveness of the brain while biological neuron models aim at accurately describe and predict biological processes. Cable theory (Rall, 1964) and Hodgkin-Huxley voltage-dependent conductance dynamics (Hodgkin and Huxley, 1952d) have proven to provide robust descriptions of single neuron synaptic integration and active responses. These systems of equations have been incorporated into the NEURON software which thus provides an efficient tool for simulating large populations of neurons. In this thesis, we are mainly interested in modeling the cortical column circuit previously described in Chapter 2. The set of techniques presented in Chapter 3 have made considerable advances in understanding the computational principles embedded into cortical circuitry. Recent models of mammalian cortical microcircuits based on experimental data are reported in Section 4.3. Further information in neuronal modeling can be found in several books (O'Reilly and Munakata, 2000; Scott, 2002; Dayan and Abbott, 2001).

Contents

4.1 NEURON MODELS

4.1.1 Artificial neurons: A bio-inspired computational tool

As presented in Chapter 1, neurons are the basic functional units of the brain. In order to understand how the brain could produce highly complex patterns by only using many basic units connected together, the field of artificial neural networks (ANN) have exploded. The key notions here are the notions of *parallelism* or *connectionism*, *adaptability* and *self-organization* which characterize a real brain and that ANN aims at reproduce. Here, we are going to present the main historically artificial neuron model: The McCulloch and Pitts model, followed by some elemental aspects of artificial neural networks. For more complete reviews on the subject, see (Bishop, 1994; Cheng and Titterington, 1994).

A simple artificial neuron model

Warren McCulloch and Walter Pitts first presented in 1943 the most simple model of one artificial neuron (see Fig. 4.1) derived from the analysis of the biological reality: Neurons work by processing information, i.e. they receive and provide information in form of spikes (Burnod, 1993), and the all-and-none property of biological neurons (as previously described) pushes them to do an analogy with the boolean logic where everything is true-or-false. In this model, the spike information is represented by spike rates x_j and synaptic strength are translated as synaptic weights w_j; these weights correspond to synaptic efficacy of synaptic connections in a biological neuron. Thus an inhibitory connection is indicated by a negative weight while a positive value indicates an excitatory connection. The McCulloch-Pitts neuron thus receives a weighted sum of inputs and provide a binary output, analogous to the firing rate of biological neurons

$$y = sgn(\sum_{j=1}^{p} w_j \, x_j + w_0) \tag{4.1}$$

where w_0 is a bias term (also viewed as a firing threshold) and $sgn(.)$ denotes the sign function. The neuron fires (y = +1) or not (y = -1) accordingly as

$$\sum_{j=1}^{p} w_j \, x_j + w_0 > 0 (\leq 0) \tag{4.2}$$

More generally,

$$y = f(\sum_{j=1}^{p} w_j \, x_j + w_0) \qquad (4.3)$$

where f denotes a non-linear function called the *activation function*. As in Equation 4.1, f is basically chosen as a unit step- of threshold function. A step further, the sigmoid function is also widely used as a continuous activation function of artificial neurons, making them suitable for analog in- and outputs. Indeed, sigmoidal functions allow to represent the gain function that transforms the average membrane potential of a neuron into an average firing rate (Gerstner and Kistler, 2002), thus a real-valued output.
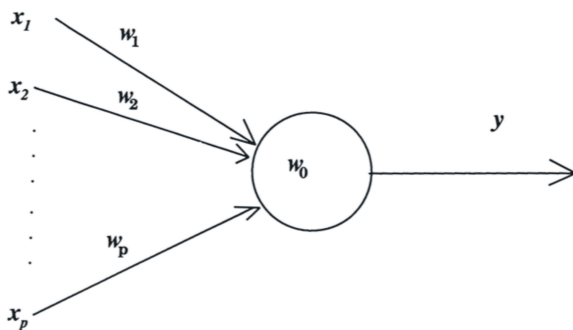
Figure 4.1: The McCulloch-Pitts neuron (McCulloch and Pitts, 1943).

These neurons, also called *perceptrons*, were presented as models of biological neurons but especially as conceptual components for circuits that could perform computational tasks. When connected together, an artificial network of binary neurons can encode any logical function (McCulloch and Pitts, 1943).

Artificial neural networks

Neural networks are sets of connected artificial neurons, e.g. McCulloch-Pitts neurons. Networks of such simple units can directly implement a large range of mathematical functions or "learn" more complex ones using learning algorithms and rules (Rumelhart et al., 1986). Its computational power is derived from clever choices for the network architecture (e.g. feed-forward, recurrent), and more precisely the values of the connection weights. Learning rules for neural networks prescribe how to adapt the weights to improve performance given some task. A classical example of neural networks is the *Multi-Layer Perceptron* (MLP). A two-layers perceptron with single output is for instance illustrated in Figure 4.2. Learning rules like error-backpropagation (Rumelhart et al., 1986) allow MLPs to perform many tasks, such as memory, pattern recognition and classification (Ripley, 1996; Bishop, 1995).
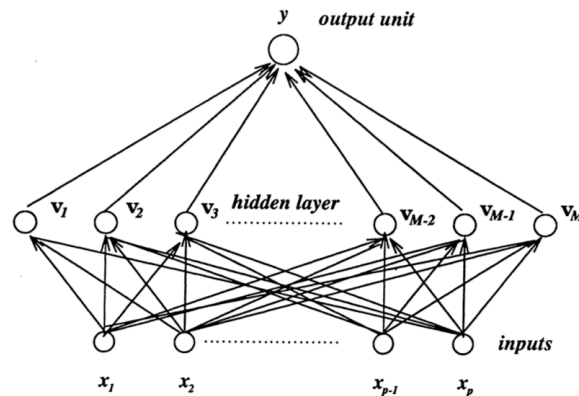
Figure 4.2: A single-output 2-layers perceptron (Cheng and Titterington, 1994)

A step further, spiking neural networks raises the level of biological realism by using individual spikes instead of rate coding (von der Malsburg, 1981). Theoretically, spiking neurons can perform very powerful computations with precisely timed spikes, as computational devices have been shown to be at least as computationally powerful as the sigmoidal neurons traditionally used in artificial neural networks (Maass, 1997). In the next section, we will present the integrate-and-fire neuron model, which is very commonly used in networks of spiking neurons. This model is simple to understand and implement. However, it captures generic properties of neural activity (Gerstner, 1999; Gerstner et al., 1999), and approximates very well the biophysical Hodgkin-Huxley neuron model, presented thereafter.

4.1.2 Biological neurons: from phenomenological to biophysical models

Many neuron models have been proposed by researchers, e.g. Hodgkin-Huxley (Hodgkin and Huxley, 1952e), Integrate-and-fire, FitzHugh-Nagumo (FitzHugh, 1969), Morris-Lecar (Morris and Lecar, 1981), Wilson (Wilson, 1999), Izhikevich (Izhikevich, 2004), to represent some of the characteristics of real neurons responses. In this section, we are not going to do an exhaustive review of these models. We will rather mainly present the Hodgkin-Huxley neuron model and compartmental modeling which are of primary interest for our future modelization of a biophysical cortical column (see part III).

Electrical circuits analogy

Previously described physiologically (see Chapter 1), the propagation of an action potential along the axon of a neuron can be modeled as the propagation of voltage in an equivalent electrical circuit. Indeed, the main idea of electrical circuit analogy is that the functional properties of a neuron, i.e. the movement of ions into and out of the cell

membrane, can be represented by an electrical circuit: The membrane of a neuron be-
haves like a capacitor, i.e. it accumulates ionic charges as the electrical potential across
the membrane changes, with the lipid bilayer as the dielectric material between the in-
side and outside of the membrane. The ionic permeabilities of the membrane are then
analogous to resistors and the electrochemical driving forces previously described are
analogous to batteries driving the ionic currents relative to each species of ion that is
able to pass through the membrane.
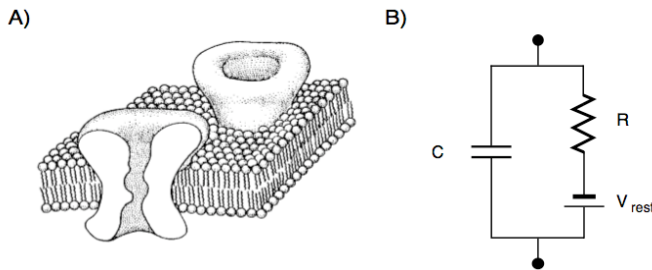
Figure 4.3: *A:* Schematic representation of a small patch of neuronal membrane. *B:* The equivalent electrical circuit for this patch of membrane. From Hille (1992).

Integrate-and-fire (IF) neuron model

The simplest biological neuron model was developed by Lapicque in 1907. At this time,
the mechanisms responsible for the generation of action potentials (see Section 1.1) were
still unknown, so the neuron model of Lapicque represented in Figure 4.4 is a very sim-
ple electric circuit consisting of a parallel capacitor and resistor, which respectively rep-
resent the capacitance and resistance of the cell membrane, driven by an input current
$I(t)$.

$$I(t) = I_R + I_C \tag{4.4}$$

with

$$I_R = \frac{u}{R} \tag{4.5}$$

where $u = V - V_{rest}$ and

$$I_C = C \frac{\mathrm{d}u}{\mathrm{d}t} \tag{4.6}$$

Thus, by multiplying by R and introducing the time constant $\tau_m = RC$ of the "leaky
integrator", this yields to the standard following form:

$$\tau_m \frac{\mathrm{d}u}{\mathrm{d}t} = -u(t) + R\,I(t) \tag{4.7}$$

It is basically a linear leaky integrator with a voltage threshold and a reset mechanism.
An action potential is generated when the membrane potential reaches a threshold.

   The IF model is relatively simple but nevertheless very useful. The main advantage
of this type of model compared to the following more biological Hodgkin-Huxley model is
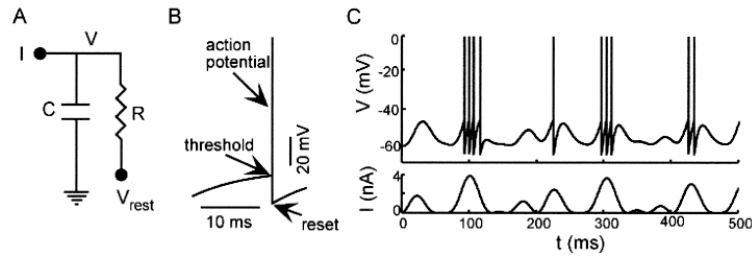
Figure 4.4: The integrate-and-fire model of Lapicque. (A) A neuron is modeled by an equivalent circuit consisting of a membrane capacitance C and membrane resistance R. I is an injected current, V is the membrane potential and V_{rest} is the resting membrane potential. (B) Action potential of an IAF model neuron. (C) Membrane potential of an IAF model neuron (upper trace) in response to a time-varying injected current (lower trace).

its simplicity. It has indeed only few parameters and allows to capture essential features of the neurons. It is thus easier to determine parameters from experimental data, and to simulate, analyze and understand networks of this type of neuron model. Examples of large IF network models can be found elsewhere (Mehring et al., 2003; Aviel et al., 2003; Morrison et al., 2007; Kumar et al., 2008). However, those models do not correctly reproduce neuronal dynamics close to the firing threshold. For our purpose, let us study conductance-based models.

The Hodgkin-Huxley (HH) neuron model

Using the biological basics presented in Chapter 1, we have now all the elements to present the most known model in computational neuroscience: the Hodgkin-Huxley model (Hodgkin and Huxley, 1952e). Compare to the phenomenological IF model, the HH model takes into account biophysical properties by including the dynamics of the voltage-dependent membrane conductances responsible for the generation of neuronal action potentials (conductance-based models). Indeed, Hodgkin and Huxley, in an extensive series of experiments on the giant axon of the squid, succeeded to measure the currents I_{Na}, I_K and I_L previously described in Section 1.1.3 and to describe their dynamics in terms of differential equations. Following the above electrical circuit analogy, Hodgkin and Huxley represented the electrical behaviour of a localized patch of squid axon membrane by the circuit shown in Figure 4.5.

The three ionic currents are indicated by resistances. The conductances of the Na^+ and K^+ currents are voltage-dependent, as indicated by the variable resistances. The conductances are in series with batteries, the values of which correpond to the respective reversal potentials of the ionic currents, E_{Na}, E_K and E_L. The outside is connected to ground assuming a negligible resistivity of the external medium. The equations describ-
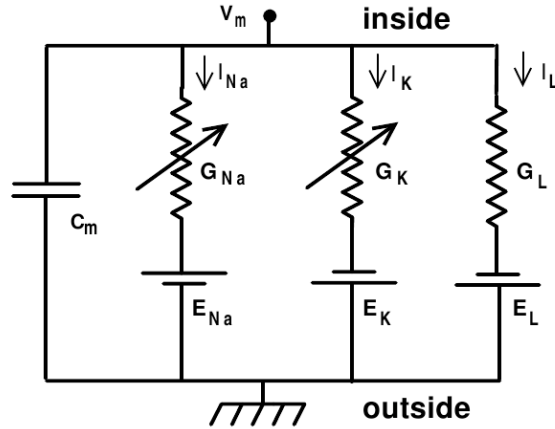
Figure 4.5: Electrical equivalent circuit proposed by Hodgkin and Huxley for a short segment of squid giant axon. The variable resistances represent voltage-dependent conductances (Hodgkin and Huxley, 1952e).

ing the circuit thus simply follow electrical laws:

$$I_{ext} = C_m \frac{dV}{dt} + I_i,$$ (4.8)

where

$$I_i = I_{Na} + I_K + I_L$$ (4.9)

Following Equation 1.3 of Section 1.1.3, individual ionic currents and conductances (or permeability) are linked by the relations:

$$\begin{cases} I_{Na} = g_{Na}(V - E_{Na}) \\ I_K = g_K(V - E_K) \\ I_L = g_L(V - E_L) \end{cases}$$ (4.10)

where E_{Na} and E_K are the equilibrium potentials for the sodium and the potassium ions. E_L is the potential at which the leakage current I_L mainly due to chloride is zero. g_L is constant, while g_{Na} and g_K are time- and voltage-dependent.

Equation 4.8 can then be rewritten as follows:

$$C_m \frac{dV}{dt} = I_{ext} - \sum_i g_i(V - E_i)$$ (4.11)

To complete the HH model, a description of the sodium and potassium channels behavior. These channels are modeled as voltage-dependent conductances controlled by

three types of activation particles, or *gating variables*:

$$\begin{cases} g_{Na}(V,t) = G_{Na}\, m(V,t)^3\, h(V,t) \\ g_K(V,t) = G_K\, n(V,t)^4 \end{cases} \tag{4.12}$$

where the constants G_{Na} and G_K are the maximal conductances. Time and voltage dependence reside in the so-called gating variables, described by the state variables m, h and n. m and n represent activation gates for sodium and potassium channels respectively, while h represents inactivation gate only for sodium channels (see the definition of voltage-gated ion channels in Chapter 1). These variables, associated to their power, allow to represent in a simplified manner the dynamics of the conductances (see Hodgkin and Huxley (1952e) for all the details). Their dynamic variation after a change of membrane potential follows a first-order differential equation, which represents the temporal evolution of the probability of the gate g to be in the open or closed state:

$$\tau_g(V)\, \frac{\mathrm{d}g}{\mathrm{d}t} = g_\infty(V) - g \tag{4.13}$$

where $g_\infty(V)$ is called the steady-state activation function and $\tau_g(V)$ the activation time constant. Their voltage-dependent relationship is illustrated by the plots in Fig. 4.6 for the three previous types of gating variables m, h, n and modeled through the following experimentally verified equation:

$$\tau_g = \frac{1}{\alpha_g + \beta_g},\, g_\infty = \alpha_g\, \tau_g \tag{4.14}$$

where α and β parameters are voltage-dependent rate constants which have been experimentally (for a temperature of $6.3°\text{C}$) derived to be equal to:

$$\begin{cases} \alpha_n = \frac{0.01\,(10-V)}{\mathrm{e}^{\frac{10-V}{10}} - 1}, \beta_n = 0.125\, \mathrm{e}^{\frac{-V}{80}} \\ \alpha_m = \frac{0.1\,(25-V)}{\mathrm{e}^{\frac{25-V}{10}} - 1}, \beta_m = 4\, \mathrm{e}^{\frac{-V}{18}} \\ \alpha_h = 0.07\, \mathrm{e}^{\frac{-V}{20}}, \beta_h = \frac{1}{\mathrm{e}^{\frac{30-V}{10}} + 1} \end{cases} \tag{4.15}$$

Four first-order differential equations (4.11 and 4.13 for each gating variable) together with the supporting algebraic equations for the potassium and the sodium conductances (4.12 and 4.15), form the complete Hodgkin-Huxley model:

$$\begin{cases} C_m\, \frac{\mathrm{d}V}{\mathrm{d}t} = I_{ext} - G_{Na}\, m^3\, h\, (V - E_{Na}) - G_K\, n^4\, (V - E_k) - g_L\, (V - E_L) \\ \frac{\mathrm{d}n}{\mathrm{d}t} = \alpha_n\, (1-n) - \beta_n\, n \\ \frac{\mathrm{d}m}{\mathrm{d}t} = \alpha_m\, (1-m) - \beta_m\, m \\ \frac{\mathrm{d}h}{\mathrm{d}t} = \alpha_h\, (1-h) - \beta_h\, h \end{cases} \tag{4.16}$$
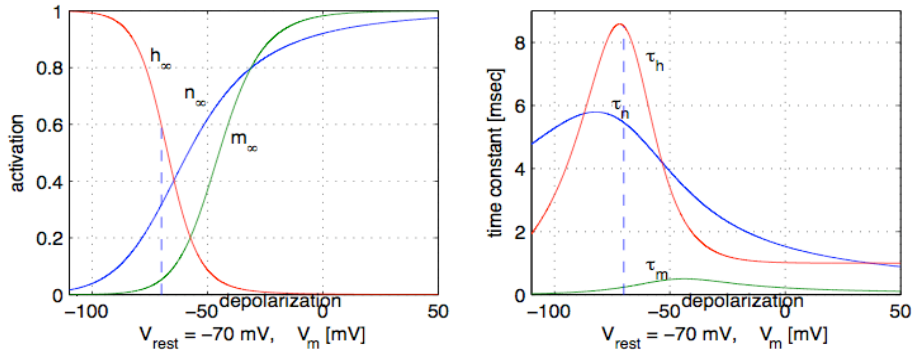
Figure 4.6: Hodgkin-Huxley model: Steady-state activation and inactivation functions (left) and time constants (right) are voltage-dependent.

Although the squid giant axon was an ideal simple model system, with only three different types of ionic currents, the Hodgkin-Huxley model is still nowadays THE standard of neuronal spiking models, with minor modifications and sometimes reductions (Fitzhugh-Nagumo and Morris-Lecar models), since 1952. The main reason is that the HH model does capture the essence of spiking through ionic currents (Na^+ and K^+), which enter and leave the cell through voltage-dependent channels. Moreover, the model is compact, and approximates well many of the features shared by different types of neurons (e.g. shape and duration of spiking, repetitive spiking in response to sustained inputs, refractoriness), while incorporating biophysical aspects of the neuron. It is then easy to add the appropriate currents for other channel types (usually using similar kinetic schemes). Accordingly, and since the model has been studied mathematically in great detail (Jack et al., 1975), it is the common choice of conductance based modeling for computational studies, as done in this thesis.

4.1.3 Biophysically detailed compartmental models

The cable theory

The application of cable theory to the study of electrical signaling in neurons has a long history, which is summarized by Rall (1989). When considering only passive electrical properties of neuronal membranes, it is possible to model them as an electrical cable, i.e. a cylinder composed of segments with capacitances C_m and resistances R_m combined in parallel (see Figure 4.7). For example, the simulation of dendrites that take into account only the passive membrane properties (as considered in the model presented in part III) shows that electrical currents decrement as they propagate along the neuronal projection. Such passive spread of electrical current is called electrotonic conductivity and the equation describing the decrement of the current in space and time is known in

the literature as the cable equation:

$$\tau_m \frac{\mathrm{d}V}{\mathrm{d}t} = E - V + \lambda^2 \frac{\mathrm{d}^2 V}{\mathrm{d}x^2} \tag{4.17}$$

where τ_m is the time constant $R_m C_m$ and λ is called the space constant of the cable and depends on its diameter. The cable equation describes the distribution of the membrane potential in space and time if a depolarizing or a hyperpolarizing impulse is applied (Stoilov et al., 1985).

Compartmental modeling

For our further modeling purpose (see Part III), we need to take into account the spatial structure of the neuron and especially the spatial structure of its dendrites. This can be done by using compartmental modeling techniques, where the dendrite is subdivided into sufficiently small compartments, also called segments in which the physical properties (e.g. diameter) are spatially uniform and the potential varies linearly between the centers of adjacent compartments. Two compartments are connected by resistors. Spatial discretization of the previous cable equation (4.17), produces a family of ordinary differential equations of the form:

$$C_j \frac{\mathrm{d}V_j}{\mathrm{d}t} + Iion_j = \sum_k \frac{V_k - V_j}{R_{jk}} \tag{4.18}$$

where V_j is the membrane potential in compartment j, $Iion_j$ is the net transmembrane ionic current in compartment j, C_j is the membrane capacitance of compartment j and R_{jk} is the axial resistance between the centers of compartment j and adjacent compartment k.
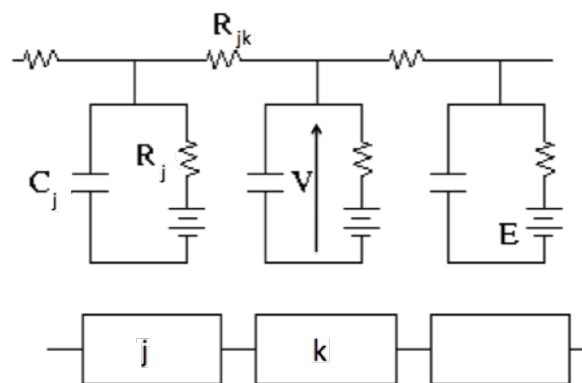
Figure 4.7: A simplified view of a neuronal fiber using the cable theory and compartmental modeling techniques. From Ermentrout (1998).

The sum of all the compartment areas is the total membrane area of the whole nerve. This compartmentalization method is the basic principle of the NEURON software used in this thesis. See Hines and Carnevale (1997) for further details on the integration methods used to solve the previous set of ordinary differential equations.

Reduced compartmental models of cortical cells

Using the compartmental modeling technique, detailed models containing hundreds of compartments (see reconstructed neurons in Fig. 4.8A) allowed to investigate many aspects of single neurons (Yamada et al., 1989; Bush and Sejnowski, 1991; Rall, 1967; Lytton and Sejnowski, 1991; Segev, 1992). However, these models involve thousands of coupled differential equations, hence requiring long computation time. When considering a network of neurons, simulations will require a higher order of magnitude of calculation and PC clusters and parallelization methods will be needed.

An alternative is to used simplified representations of single neurons with only few compartments. However, the geometry of such reduced model is important to accurately represent real cell properties, e.g. synaptic integration. Bush and Sejnowski (1993) built reduced compartmental models of layer II and layer V pyramidal cells of cat visual cortex. The neuron models are shown in Figure 4.8B and their respective dimensions are reported in Table 4.1. The authors then showed that these reduced models are good fits to the full models (Fig. 4.1) for a variety of stimuli and are suitable for network simulations involving multiple, spatially separated synaptic inputs to the neurons.
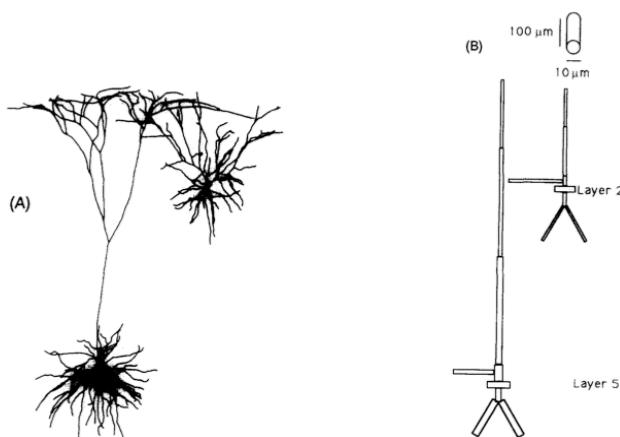
Figure 4.8: *A:* Detailed reconstruction of layer II and V pyramidal neurons. The full models have approximately 400 compartments. *B:* Geometries of reduced compartmental models of pyramidal cells (Bush and Sejnowski, 1993).

Similarly to pyramidal neurons, Bush and Sejnowski (1996) have also built a reduced

	Layer 5 pyramid		Layer 2 pyramid	
	Length (μm)	Diameters (μm)	Length (μm)	Diameters (μm)
Soma	23	17	21	15.3
Apical trunk	60	6	35	2.5
Obliques	150	3	200	2.3
Apical no. 1	400	4.4	180	2.4
Apical no. 2	400	2.9	–	–
Apical tuft	250	2	140	2
Basal trunk	50	4	50	2.5
Basals (2)	150	5	150	1.6

Table 4.1: Dimensions of reduced pyramidal neurons (Bush and Sejnowski, 1993).

compartmental model of interneurons. We will use the geometry of this model to built our excitatory (i.e. spiny stellate cells) and inhibitory interneurons models.

4.2 MODELING SYNAPTIC INTERACTIONS

The above Hodgkin-Huxley model thus allows to model intrinsic neuronal currents. For our further cortical column modelization, involving thousands of synapses, we need to model synaptic interactions. The general equation that describe transmitter-activated ion channels is:

$$I_{syn}(t) = g_{syn}(t)(V - E_{syn}), \tag{4.19}$$

where I_{syn} is the synaptic current, $g_{syn}(t)$ is a time-dependent conductance that will open at the arrival of a presynaptic spike, V is the postsynaptic membrane potential and E_{syn} is the reversal potential of the considered channel.

The parameter E_{syn} and the function $g_{syn}(t)$ can be used to characterize different types of synapse, e.g. $AMPA$ and $GABA$ for excitatory and inhibitory synapses respectively (see Chapter 1).

We only reviewed here the simplified kinetic models of $AMPA$ and $GABA_A$ synaptic receptors proposed by Destexhe et al. (1998). These models can be implemented with minimal computational expense using the NEURON simulator.

4.2.1 AMPA receptors

The kinetics of the AMPA receptor can be modeled by the following simplified two-state diagram:

$$C + T \underset{\beta}{\overset{\alpha}{\rightleftharpoons}} O, \tag{4.20}$$

where C and O represent respectively the closed and open states of the channel, T represents the concentration of neurotransmitter molecules, assuming to be released in a brief pulse at each arrival of a presynaptic spike Destexhe et al. (1994) and α and β are voltage-independent forward and backward rate constants. If r is defined as the fraction of the receptors in the open state, it is then described by the following first-order kinetic equation:

$$\frac{\mathrm{d}r}{\mathrm{d}t} = \alpha[T]\,(1 - r) - \beta\,r, \tag{4.21}$$

The postsynaptic current I_{AMPA} is then given by

$$I_{AMPA} = G_{AMPA}\,r\,(V - E_{AMPA}), \tag{4.22}$$

where G_{AMPA} is the maximal conductance, E_{AMPA} the reversal potential, and V the postsynaptic membrane potential (E_{AMPA} = 0 mV).

4.2.2 GABA receptors

Similarly, the postsynaptic current of $GABA$ receptors is given by:

$$I_{GABA} = G_{GABA}\,r\,(V - E_{GABA}), \tag{4.23}$$

where G_{GABA} is the maximal conductance of Cl^- channels and E_{GABA} its reversal potential (E_{GABA} = $E_{Cl} = -70mV$).

4.2.3 Synaptic integration

Using the previous kinetic models, the synaptic integration of multiple postsynaptic events is given by iterative expressions for successive postsynaptic currents, and is illustrated in Figure 4.9, for the two types of transmitter-gated receptor previously described. Both $AMPA$ and $GABA$ [1] receptors showed PSP amplitudes (lower panel) proportional to the number of presynaptic spikes (upper panel).

---

[1]Remember that here, $GABA$ refers to $GABA_A$.
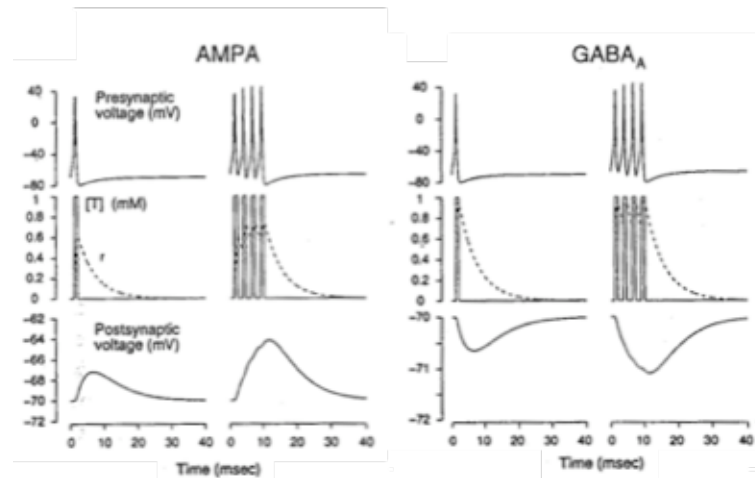
Figure 4.9: Summation of postsynaptic potentials in simplified kinetic models of $AMPA$ and $GABA$ receptors. From Destexhe et al. (1998).

4.3 CORTICAL MICROCIRCUIT MODELS

This section aims at reviewing the cortical microcircuit models we use in our context, in order to further develop a realistic model of a cortical column. There are many different models, so more than analyzing their computational performance or describing their purposes, we are rather interesting in the circuit connectivity template and parameters choice. More precisely we chose to present three models with a connectivity scheme based on experimental data.

4.3.1 Anatomical models of cortical function

Based on anatomical and electrophysiological studies, Douglas and Martin (1991) proposed a microcircuit model for cat visual cortex (Fig. 4.10), as already presented in Chapter 2. The model consists of two excitatory populations: Pyramidal cells in superficial layers (II/III), pyramidal cells in deep layers (V/VI), and one global inhibitory populations: Smooth cells in all layers. Layer IV spiny neurons (stellates and pyramidals) are grouped together with the superficial pyramidal neurons. These three populations interact with each other through excitatory and inhibitory (both $GABA_A$ and $GABA_B$ receptors) connections, and they all receive thalamic input (10-20% for spiny and smooth, 1-10% for deep spiny cells), though the deep layers receive only weak signals. Each population has also recurrent connections back to itself.

The majority of the excitatory input comes from local intracortical connections, which amplify the thalamic signals. The inhibitory control imposed by the fast $GABA_A$ and the slow $GABA_B$ connections prevents over-excitation in the superficial and deep layers
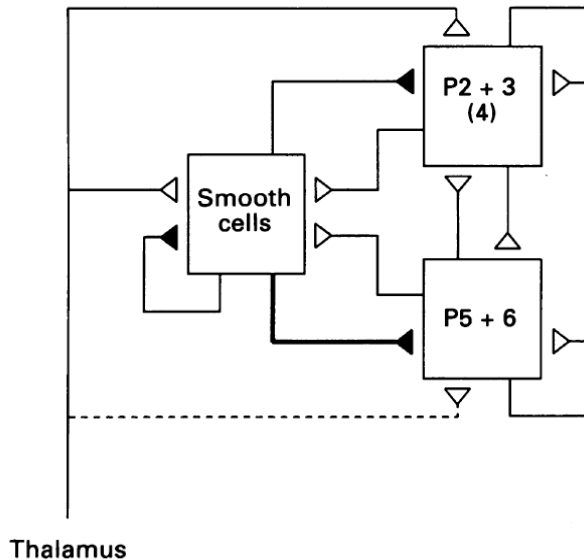
Figure 4.10:   Block diagram of the microcircuit model. The three boxes represent three different populations of neurons in the striate cortex: Layer II/III pyramidal cells, layer V/VI pyramidal cells and smooth inhibitory cells. Layer IV spiny stellate cells are incorporated with the superficial group of pyramidal cells. Excitatory (hollow triangles) and inhibitory (filled triangles) connections between the populations, and from the thalamus, are represented. From Douglas and Martin (1991).

neuronal populations. Excitatory feedback from pyramidal cells to smooth inhibitory cells stabilizes the network.

Later, these authors proposed another model based on anatomical data to functionally investigate more generic cortical circuitry (Douglas and Martin, 2004). The model diagram is shown in Figure 4.11. It consists in a patch of superficial pyramidal neurons (upper gray rectangles, layer II/III) and a patch of deep pyramidal neurons (lower-gray rectangles, layer V). Layer II/III pyramidal neurons receive feedforward excitatory input from subcortical, intra- and inter-areal sources. They also receive local recurrent feedback from deep pyramidal cells in the corresponding patch, from superficial cells in neighboring patches and from subcortical inter-areal connections. These inputs are processed by dendrites of the superficial neurons whose signal transfer properties are adjusted dynamically by the pattern of vertical inputs from smooth inhibitory cells in the same patch (represented by oblique dark arrows in the figure). Horizontal inhibitory inputs (upper horizontal dark gray line) then control the output of the superficial pyramidal neurons (i.e. soft winner-take-all (WTA) mechanism) (Maass, 2000; Yuille and Geiger, 2003). Hence, the superficial layer neurons within and between patches, and within and between areas, cooperate to make properties emerge. The deep layer neurons then process these signals and decide on the output to give to subcortical structures, like motor structures.
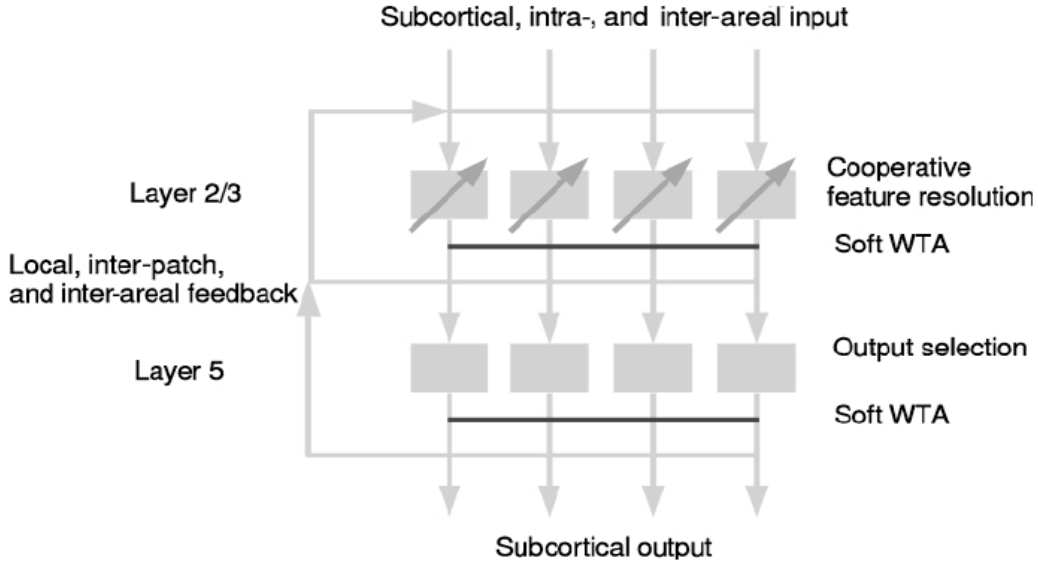
Figure 4.11: A simple model of cortical processing based on anatomical data. See text for details. From Douglas and Martin (2004).

4.3.2   A generic neural microcircuit model with IF neurons

In Maass et al. (2002), the authors proposed a model of cortical microcircuit consisting of randomly connected IF neurons, 20% of which were randomly chosen to be inhibitory (Fig. 4.12). Neurons and synapses parameters were chosen to fit biological data from microcircuits in rat somatosensory cortex, as quantified by Gupta et al. (2000); Markram et al. (1998b).

The synapses between these neurons are randomly created. The connectivity structure is defined by the following probability function:

$$P(a \rightarrow b) = C \, exp(-\frac{D^2(a, b)}{\lambda^2}) \tag{4.24}$$

where $P(a \rightarrow b)$ represents the probability of a synaptic connection from neuron a to neuron b, as well as that of a synaptic connection from neuron b to a, C is chosen depending on whether a and b are excitatory (E) or inhbitory (I) (EE: 0.3, EI: 0.2, IE: 0.4, II: 0.1), $D(a, b)$ is the euclidean distance between them in a three-dimensional grid of integer point and λ is a parameter which controls both the average number of connections and the average distance between neurons synaptically connected (here, λ =2). Dynamic synapses are also taken into account here, following Markram et al. (1998b).
The model thus exhibits a strong local connectivity. It can be considered as a single cortical column model. To connect several cortical columns between them, one can specify
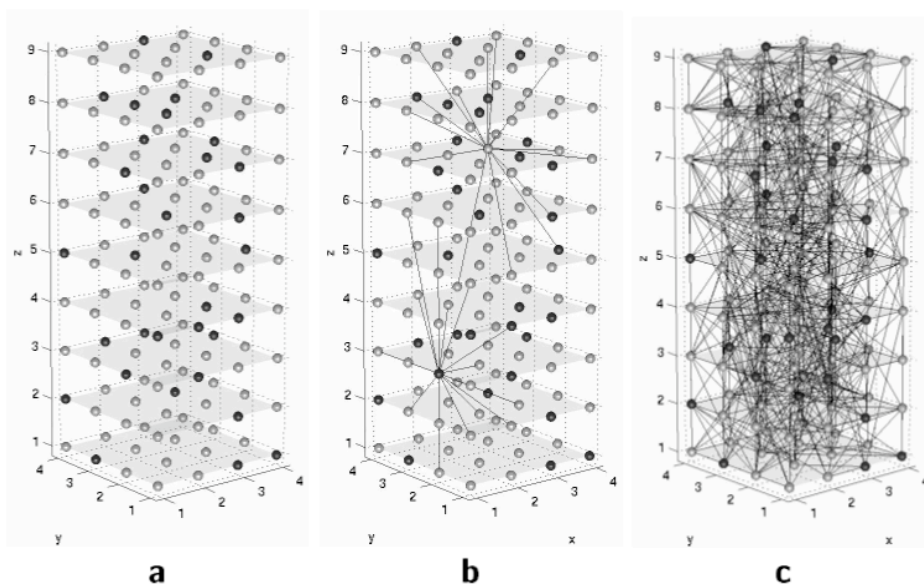
Figure 4.12: A generic neural microcircuit model with IAF neurons. *a:* 80% of excitatory neurons and 20% of inhibitory neurons are arranged on the nodes of a 3D gird. *b:* Neurons are randomly connected. *c:* Global connectivity of the model. From Maass et al. (2002).

separately for each pair of columns the probability of connections between neurons in these columns and the synaptic distribution for these connections, as done for the single column.

4.3.3 A biophysical cortical microcircuit model with HH neurons

In Haeusler and Maass (2007), the authors proposed a model of cortical microcircuit based on biological connectivity data from Thomson et al. (2002), while dynamic properties of synaptic connections are based, like the previous model, on data and models from Markram et al. (1998b); Gupta et al. (2000) (Fig. 4.13). The schematic diagram of connectivity data between neurons in different layers of the cortex has been studied in details in Chapter 2, Section 2.3.

The model consists of six main populations of neurons: One population of excitatory neurons and one population of inhibitory neurons in 3 main layers with 30%, 20% and 50% of the neurons assigned to layers 2/3, layer 4 and layer 5, respectively. The ratio between excitatory and inhibitory neurons is of 4:1. Neurons were models as conductance-based single compartment HH neurons with passive and active properties modeled according to Destexhe et al. (2001); Destexhe and Pare (1999). Furthermore, a background activity is simulated using fluctuating excitatory and inhibitory conductances from Destexhe et al. (2001) and thalamic afferents and feedforward cortical inputs are modeled
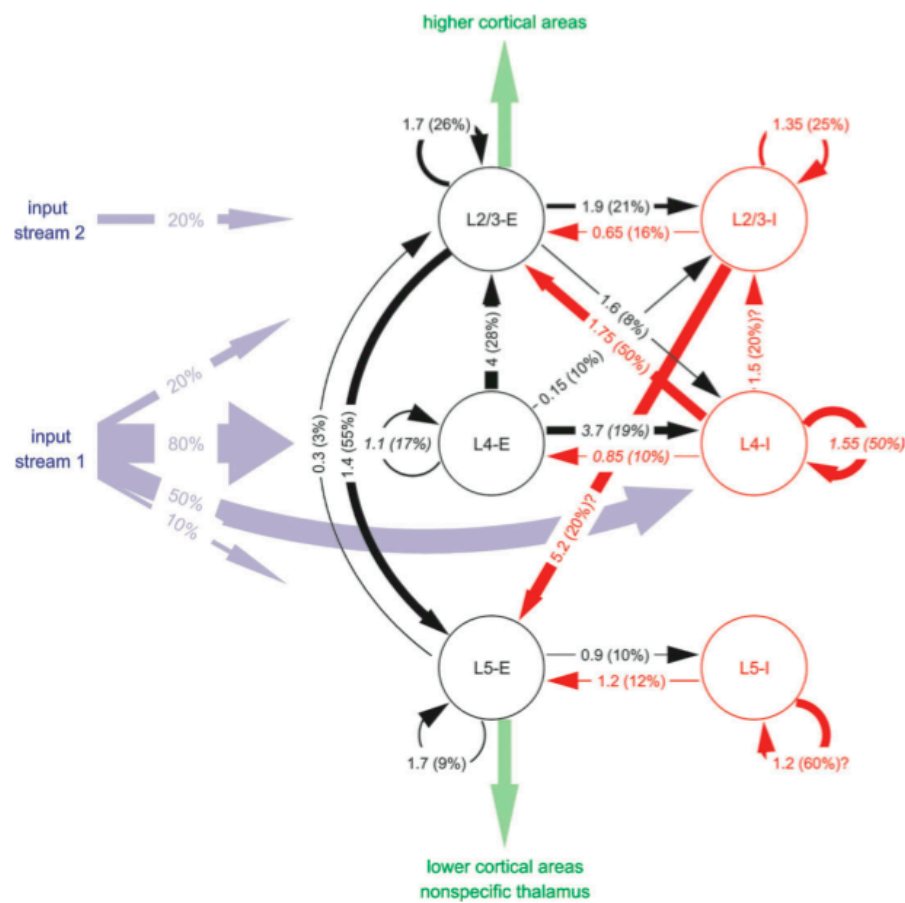
Figure 4.13: An example of biophysical cortical microcircuit model. Numbers at arrows indicate connection weights between two cell types, while connection probabilities are in parentheses (Thomson et al., 2002). From Haeusler and Maass (2007).

as multiple poisson spike trains (blue arrows in the figure).

We have seen in Chapter 2 that the common vertical intracortical microcircuit found in several areas can also be considered as the common connectivity pattern of a cortical column. Hence, these microcircuit models of cortical area can also be used as a biophysical cortical column model. For example, the model of Douglas and Martin (2004) can be easily interpreted as a cortical column model with laminar structure, when replacing in the text, in an adapted manner, "patch" by either "layer" or "column".
Others models of cortical microcircuits, such as mean field or neural field models, dedicated to a better understanding of the VSDI signal are reported in Chapter 6.

Part II

VSDI: Review and Models *

IMAGING THE BRAIN WITH VOLTAGE-SENSITIVE DYE

OVERWIEW

In the previous chapter 3, we have learnt that optical imaging comes within the scope of new imaging techniques that allow us to visualize the functioning brain at both high spatial and temporal resolutions. In this chapter, we focus on the Voltage-Sensitive Dye imaging technique, aiming at better understand the origin of the optical signal, essential to well understand the rest of this thesis, dealing with VSDI signals modeling. Indeed, although the underlying mechanism of this optical method is nowadays well understood, the recorded signal remains very complex and it seems difficult to isolate the contributions from its different components.

We start by giving a general introduction to VSDI (Section 5.1), followed by examples of applications to brain imaging (Section 5.2). We compare *in vitro* and *in vivo* recordings obtained with VSDI in several animal studies. Then we make the underlying limitations of this method explicit (Section 5.3): what does the VSD signal measure? A question that is not completely answered in the literature.

Contents

5.1 DETAILED PRINCIPLE

VSDI offers the possibility to visualize, in real time, the cortical activity of large neuronal populations with high spatial resolution (down to 20-50 μm) and high temporal resolution (down to the millisecond). With such resolutions, VSDI appears to be the best technique to study the dynamics of cortical processing at neuronal population level. Extensive reviews of VSDI have been published elsewhere (e.g. Grinvald and Hildesheim, 2004; Roland, 2002).

This invasive technique is also called "extrinsic optical imaging" because of the use of voltage sensitive dyes (Cohen et al., 1974; Ross et al., 1977; Waggoner and Grinvald, 1977; Gupta et al., 1981). After opening the skull and the dura mater of the animal, the dye molecules are applied on the surface of the cortex (Fig. 5.1A). They bind to the external surface of the membranes of all cells without interrupting their normal function and act as molecular transducers that transform changes in membrane potential into optical signals. More precisely, once excited with the appropriate wavelength (Fig. 5.1B), VSDs emit instantaneously an amount of fluorescent light that is function of changes in membrane potential, thus allowing for an excellent temporal resolution for neuronal activity imaging (Fig. 5.1C). The fluorescent signal is proportional to the membrane area of all stained elements under each measuring pixel.

"All elements" means all neuronal cells present in the cortex but also all non-neuronal cells, like glial cells (see Subsection 1.1.1 for more details). Moreover, neuronal cells include excitatory cells and inhibitory cells, whose morphology and intrinsic properties are quite different (see Salin and Bullier, 1995, for a review on the different type of neurons and connections in the visual cortex). Furthermore, each cell has various compartments, including dendrites, somata and axons. The measured signal thus combine all these components, which are all likely to be stained in the same manner.

The fluorescent signal is then recorded by the camera of the optical video imaging device and displayed as dynamic sequences on computer (see Figure 5.1). The submillisecond temporal resolution is reached by using ultra sensitive charge-coupled device (CCD) camera, whereas the spatial resolution is limited by optical scattering of the emitted fluorescence (Orbach and Cohen, 1983).
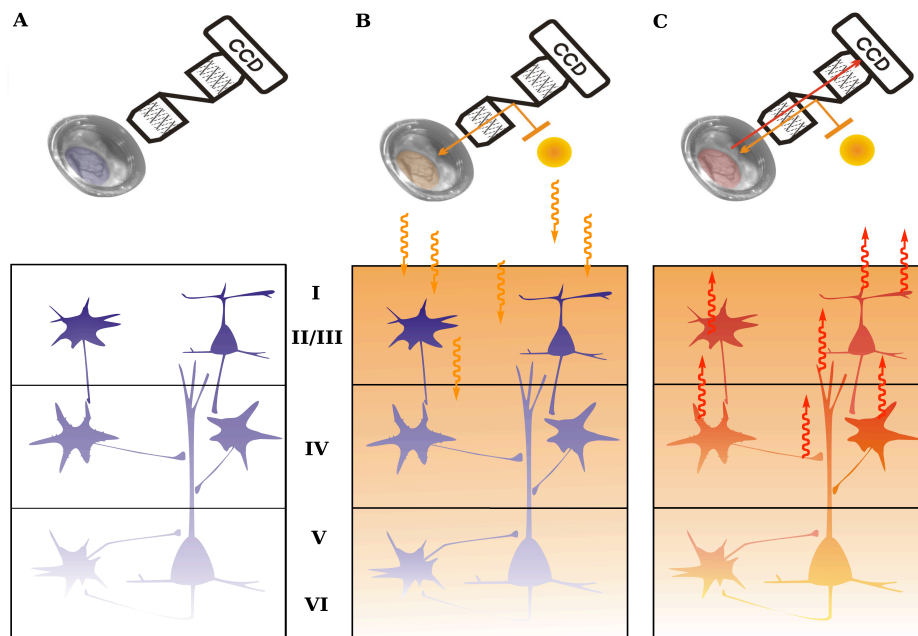
Figure 5.1: VSDI principle in three steps. The imaging chamber allows a direct access of the primary visual cortex V1 represented as a patch of cortex with its six layers. A) The dye, applied on the surface of the cortex, penetrates through the cortical layers of V1. B) All neuronal and non-neuronal cells are now stained with the dye and when the cortex is illuminated, the dye molecules act as molecular tranducers that transform changes in membrane potential into optical signals. C) The fluorescent signal (red arrow) is recorded by a CCD camera.

5.2 OPTICAL IMAGING OF NEURONAL POPULATION ACTIVITY

5.2.1 General history

The earliest optical recordings were made, at the single neuron level, both from cultured cells (Tasaki et al., 1968) and from various invertebrate preparations like ganglia of the leech (Salzberg et al., 1973), or the giant axon of the squid (Davila et al., 1973). For all other VSDI experiments, the VSD signal has a neuronal population resolution.

The VSDI method has then been used *in vitro* on brain slices, mainly in rodent and ferret. It allowed to optically record from the hippocampus (Grinvald et al., 1982), the visual cortex (Bolz et al., 1992; Albowitz and Kuhnt, 1993; Nelson and Katz, 1995; Yuste et al., 1997; Contreras and Llinas, 2001; Tucker and Katz, 2003a,b), the somatosensory cortex (Yuste et al., 1997; Antic et al., 1999; Contreras and Llinas, 2001; Petersen and Sakmann, 2001; Jin et al., 2002; Laaris and Keller, 2002; Berger et al., 2007) and from the auditory cortex (Jin et al., 2002; Kubota et al., 2006).

The salamander, largely used *in vitro* (Orbach and Cohen, 1983; Cinelli and Salzberg, 1992), was the first species also used *in vivo* for studying the olfactory system using VSDI (Orbach and Cohen, 1983), followed by the frog for the visual system (Grinvald et al., 1984), and the rodent for the somatosensory system. Indeed, initial *in vivo* studies of the somatosensory cortex have been made in anesthetized rodents, taking advantage of the thinness of the cortical dura (Orbach et al., 1985). More recently, VSDI in freely moving mice has also been performed with success (Ferezou et al., 2006).

Rodent and ferret were also used for studying the visual cortex *in vivo* (Roland et al., 2006; Lippert et al., 2007; Xu et al., 2007; Ahmed et al., 2008). However, the main VSDI experiments on visual modality were conducted on two other mammalian species: cat and monkey (Grinvald et al., 1994; Arieli et al., 1995; Shoham et al., 1999; Sharon and Grinvald, 2002; Slovin et al., 2002; Seidemann et al., 2002; Jancke et al., 2004; Sharon et al., 2007; Benucci et al., 2007; Reynaud et al., 2007; Yang et al., 2007). Experiments on anesthetized cats are very attractive for mapping and studying the primary visual cortex, whereas monkey experiments also associate behavioral measures.

Note that in order to move on to *in vivo* measurements, dye improvement has been a crucial step. Rina Hildesheim, from Amiram Grinvald's Laboratory, elaborated blue dye, that is absorbed away from the hemoglobin absorption peak (Shoham et al., 1999).

5.2.2   High spatial resolution for brain mapping

One domain of application of the VSDI, as other brain functional imaging, is brain mapping. Indeed, VSDI allows to build high-resolution functional maps, such as orientation or ocular-dominance maps (Shoham et al., 1999; Grinvald et al., 1999; Slovin et al., 2002; Sharon and Grinvald, 2002), as also obtained with optical imaging based on intrinsic signals (ISI) (Blasdel and Salama, 1986; Ts'o et al., 1990; Grinvald et al., 1991; Bonhoeffer and Grinvald, 1991; Hubener et al., 1997; Rubin and Katz, 1999). Comparaison between the two imaging techniques (Shoham et al., 1999; Grinvald et al., 1999; Slovin et al., 2002) confirms the high spatial resolution of VSDI methodology for mapping the functional architecture of the visual cortex. More generally, VSDI has been largely used for studying functional organization in the vertebrate central nervous system (CNS) (Olfactory bulb: Orbach and Cohen (1983); Cinelli and Salzberg (1990); Cinelli and Kauer (1992). Auditory cortex: Horikawa et al. (1996); Hosokawa et al. (1997); Taniguchi et al. (1992); Taniguchi and Nasu (1993). Visual cortex: Orbach et al. (1985); Yuste et al. (1997); Shoham et al. (1999); Slovin et al. (2002). Somatosensory cortex: Laaris and Keller (2002); Derdikman et al. (2003); Civillico and Contreras (2006)).

However, although it is possible to do such brain mapping using VSDI, it does not take advantage of the possibility to inspect neuronal activation dynamics.

5.2.3   High temporal resolution unveils the dynamics of cortical processing

The main benefit of the VSDI technique is the possibility for neuroscientists to go further electrophysiological studies and low resolution (either temporal or spatial) imaging techniques, since visualizing in real-time with high spatial resolution large populations of neurons, while supplying information about cortical networks temporal dynamics. Many neuroscientists are motivated to investigate how a sensory stimulus is represented dynamically on the cortical surface in space and time (Grinvald et al., 1984, 1994; Arieli et al., 1996; Petersen et al., 2003; Civillico and Contreras, 2006). More precisely, the spatiotemporal dynamics of the response to simple stimuli, e.g. local drifting-oriented gratings or single whisker stimulation, have been visualized using VSDI on *in vivo* preparations (Cat: Sharon et al. (2007); Rodent: Petersen et al. (2003)). Complex stimuli, e.g. the line motion or apparent motion illusions, have also been achieved using VSDI in the visual cortex of cats (Jancke et al., 2004) or ferrets (Ahmed et al., 2008), revealing fundamental principles of cortical processing *in vivo*. Nowadays, rapid and precise dynamic functional maps can even be obtained on behaving animals, as shown by Seidemann et al. (2002), Slovin et al. (2002) and Yang et al. (2007) on behaving monkeys, or by Ferezou et al. (2006) in freely moving mice.

These questions are now conceivable thanks to the persistent development of novel

dyes (Shoham et al., 1999; Grinvald and Hildesheim, 2004; Kee et al., 2008). Indeed, the developed dyes allowed to monitor in real time neuronal activation both in *in vivo* and *in vitro* Arieli et al. (1996); Grinvald et al. (1999); Petersen and Sakmann (2001); Petersen et al. (2003).

5.2.4 Functional connectivity reveals its dynamics

Combining the spatial and temporal advantages, an other direct application of VSDI is the possibility to study the functional connectivity of neuronal populations. Yuste et al. (1997) for example, investigated the connectivity diagram of rat visual cortex using VSDI. Vertical and horizontal connections have been detected. More generally, intracortical and intercortical interactions, occuring during sensory processing (especially visual), have been largely explored using VSDI, either *in vitro* or *in vivo*: Mapping functional connections using VSDI, has been done *in vitro* in the rat visual cortex (Bolz et al., 1992; Carlson and Coulter, 2008), in the guinea pig visual cortex (Albowitz and Kuhnt, 1993) and in the ferret visual cortex (Nelson and Katz, 1995; Tucker and Katz, 2003a,b), providing not only functional, but also anatomical and physiological information on the local network. For example, Tucker and Katz (2003a) investigated with VSDI how neurons in layer 2/3 of ferret visual cortex integrate convergent horizontal connections.

Authors in Orbach and Van Essen (1993) used VSDI in the visual system of the rat *in vivo* to map striate and extrastriate pathways. Feedforward propagating waves from V1 to other cortical areas, and feedback waves from V2 to V1 have been recently reported by Xu et al. (2007), thanks to VSDI. In addition, feedback depolarization waves (from areas 21 and 19 toward areas 18 and 17) were extensively studied by Roland et al. (2006) in ferrets after staining the visual cortex with VSD.

5.2.5 Conclusion

By adding a new dimension to existing brain functional imaging techniques, VSDI directly reports the spatiotemporal dynamics of neuronal populations activity. Many VSDI studies have then been conducted in order to investigate the spatio-temporal patterns of activity occuring in different parts of the CNS, *in vitro* or *in vivo*, on several preparations or animal species. The table 5.1 lists most articles presenting experimental results using VSDI techniques. The publications are first classified by the condition of the experiment, either *in vitro* or *in vivo*, and then by the experimental preparations or animal species. Additional information about dyes is available in the last columns (see Ebner and Chen, 1995, for a compilation of the commonly used dyes and their properties).

Conditions	Species	Related publications	Structure	Dye	$\lambda_{exc}(nm)$
In Vitro (Invertebrate preparations, cultured cells or brain slices)	Invertebrate (squid, skate, snail, leech)	Tasaki et al. (1968), Davila et al. (1973), Salzberg et al. (1973), Woolum and Strumwasser (1978), Gupta et al. (1981), Konnerth et al. (1987), Cinelli and Salzberg (1990), Antic and Zecevic (1995), Zochowski et al. (2000)	Giant neurons	styryl JPW1114 optimized for intracellular applications	540
			Axons	JPW1114 (fluorescence)	520
			Cerebellar parallel fibres	Pyrazo-oxonol RH482, RH155 (absorption)	
	Goldfish	Manis and Freeman (1988)	Optic tectum	Styryl RH414 (fluorescence)	540
	Salamander	Orbach and Cohen (1983), Cinelli and Salzberg (1992)	Olfactory bulb	Merocyanine XVII optimized for absorption measurements (Ross et al., 1977; Gupta et al., 1981), RH414, RH155	
	Rodent	Grinvald et al. (1982), Bolz et al. (1992), Albowitz and Kuhnt (1993), Yuste et al. (1997), Antic et al. (1999), Petersen and Sakmann (2001), Contreras and Llinas (2001), Laaris and Keller (2002), Jin et al. (2002), Kubota et al. (2006), Berger et al. (2007), Carlson and Coulter (2008), Kee et al. (2008)	Visual cortex	Fluorochrome Di-4-ANEPPS, RH414, Styryl RH795 (fluorescence)	500, 540
			Barrel cortex	JPW2038, RH155, RH482, NK3630, JPW1114, RH414, RH795	
			Auditory cortex	RH795 for fluorescence, Oxonol NK3630 for absorption	520, 705
			hippocampus	WW401	520
	Ferret	Nelson and Katz (1995), Tucker and Katz (2003a), Tucker and Katz (2003b)	Visual cortex	RH461 (fluorescence)	590
In Vivo (Anesthetized or awake)	Frog	Grinvald et al. (1984)	Visual cortex	Styryl RH414	520
	Salamander	Orbach and Cohen (1983), Kauer (1988)	Olfactory bulb	styryl RH160 and RH414 optimized for fluorescence measurements (Grinvald et al., 1982)	510, 540
	Rodent	Orbach et al. (1985), Orbach and Van Essen (1993), Petersen et al. (2003), Derdikman et al. (2003), Civillico and Contreras (2006), Ferezou et al. (2006), Berger et al. (2007), Lippert et al. (2007), Xu et al. (2007), Brown et al. (2009)	Barrel cortex	RH795, Oxonol RH1691, RH1692 and RH1838 optimized for in vivo fluorescent measurements (Shoham et al., 1999; Spors and Grinvald, 2002)	540, 630
			Visual cortex	RH1691, RH1838	630
	Ferret	Roland et al. (2006), Ahmed et al. (2008)	Visual cortex	RH795, RH1691	530, 630
	Cat	Arieli et al. (1995), Shoham et al. (1999), Sharon and Grinvald (2002), Jancke et al. (2004), Sharon et al. (2007), Benucci et al. (2007)	Visual cortex (area 17/18)	RH795, RH1692	530-40, 630
	Monkey	Grinvald et al. (1994), Shoham et al. (1999), Slovin et al. (2002), Seidemann et al. (2002), Reynaud et al. (2007), Yang et al. (2007)	Visual cortex (V1/V2)	RH1691, RH1692, RH1838	630
			Frontal Eye Field	RH1691	630

Table 5.1: Non-exhaustive list of publications related to VSDI, classified by experimental conditions (either *in vitro* or *in vivo*) and by species.

5.3 THE MULTI-COMPONENT ORIGIN OF THE OPTICAL SIGNAL

5.3.1 About the contribution from glial cells

In general, glial cells have been neglected by neuroscientists for a long time, especially because unlike neurons, they do not carry action potentials. However, glial cells have important functions (see Cameron and Rakic, 1991, for a review) and they may contribute to the VSD signal.

As already explained in Chapter 1, glial cells are known as the 'supporting cells" of the CNS and are estimated to outnumber neurons by as much as 50 to 1. However, their role in information representation or processing remains unresolved. Indeed, *in vitro* studies have shown increasing evidence for an active role of astrocytes in brain function(Schummers et al., 2008). Nevertheless, little is known about the behavior of astrocytes *in vivo*.

Authors in Schummers et al. (2008) used parallel two-photon calcium imaging and intrinsic optical imaging (see Chapter 3 for details about these techniques) in the ferret visual cortex *in vivo*, in order to show that astrocytes like neurons, respond to visual stimuli, share many of the receptive-field characteristics of neurons and strongly contribute to hemodynamic signals, thus to e.g. fMRI or ISI measurements.

When interpreting the VSD signal, we thus face two conflicting viewpoints.

Several studies (e.g. Konnerth and Orkand, 1986; Lev-Ram and Grinvald, 1986; Konnerth et al., 1987, 1988; Manis and Freeman, 1988) showed that the optical signal has two components: a "fast" followed by a "slow" signal. The latter has been revealed by doing successive staining with different dyes (e.g. RH482 and RH155), since each of them may preferentially stain different neuronal membranes. The authors then present evidence that this slow signal has a glial origin.

However, authors in Kelly and Van Essen (1974) showed that the glial responses are weak (depolarizations of only 1 to 7 mV in response to visual stimuli) and have a time scale of seconds. Recent paper of Schummers et al. (2008) confirms that the astrocyte response is delayed 3 to 4 s from stimulus onset, which is a very slow temporal response compared to neuron response. Generally, in VSDI, only the first 1000 ms are considered, since intrinsic activity may affect the signal after this time.

We understand here that the controversy about glial contribution is directly link to the used dye (Ebner and Chen, 1995), and the time course of the optical signal generated. Thus, glial activity is very unlikely to participate significantly to the VSD signal (when considering recent fast dyes), since the amplitude of glial response is weak and

its time-course is very slow.

5.3.2   About the contribution from excitatory versus inhibitory cells

We have seen in Chapter 1 that in the neocortex, neurons (despite their morphologic diversity) can be functionally classified in two groups: excitatory neurons, which represent about 80 percent of the cortical cells, and inhibitory neurons which represent about 20 percent of cortical cells (Douglas and Martin, 1990). Thus, it is tempting to say that the VSD signal mainly reflects the activity of excitatory neurons (Grinvald et al., 1999).
However, the VSD signal is proportional to changes in membrane potential. Thus, both excitatory and inhibitory neurons contribute positively to the VSD signal and it is hard to teaze apart contributions from excitatory or inhibitory cells. An additional level of complexity arises from the fact that inhibition operates generally in a shunting "silent" mode (Borg-Graham et al., 1998). In this mode, inhibition suppresses synaptic excitation without hyperpolarizing the membrane potential.
To conclude, the contribution of inhibitory cells to the VSD signal is unclear and would obviously benefit from modeling studies.

5.3.3   About the contribution from the various compartments

Neurons can be also decomposed into their main various compartments, whose surface and electrical activity are different (see Figure 5.2, green part):

- The soma, whose electrical activity can be either synaptic (SP for synaptic potential) or spiking (AP for action potential).

- The dendrites, that integrate presynaptic AP information from others cells. The electrical activity is mainly synaptic, however, back-propagating AP could be recorded in the dendrites (see Waters et al., 2005, for a review). Dendritic surface area of mammalian neurons have been estimated by Sholl (1955a); Aitken (1955) and Young (1958) to be ten to twenty times larger than cell bodies surface area, and to represents 90 percent of the total neuronal cell membrane (Eberwine, 2001).

- The axon, which carries spiking signals from the soma to the axon terminal. Spiking activity can be recorded on this part of neuron. In contrast with dendrites, the surface area of axons represents 1 percent of the total neuronal cell surface (Eberwine, 2001).

In the literature, regarding the difference in membrane areas of the various neuronal components and the nature of the signal, it is commonly accepted that the optical

signal, in a given pixel, mostly originates from the dendrites of cortical cells, and therefore, mainly reflects dendritic post-synaptic activity (Orbach et al., 1985; Grinvald and Hildesheim, 2004). Extensive comparaisons between intracellular recordings from a single neuron and VSDI also showed that the optical signal correlates closely with synaptic membrane potential changes (Petersen et al., 2003; Contreras and Llinas, 2001). However, no real quantitative analysis has been performed to date and it is more correct to state that the optical signal is multi-component since the VSD signal reflects the summed intracellular membrane potential changes of all neuronal compartments at a given cortical site. The aim then, is to determine the exact contribution of each component, which remains unknown. More precisely, what is quantitatively the contribution of dendritic activity? Can spiking activity be neglected?

5.3.4 About the contribution from cortical layers

The depth of the neocortex is about 2 mm. It is made up of six horizontal layers principally segregated by cell types and neuronal connections. The layer II mostly contains small pyramidal neurons that make strong connections with large pyramidal neurons of the layer V (Thomson and Morris, 2002).

Improved dyes, when put at the surface of the exposed cortex, can reach a depth of about 400 to 800 μm from the cortical surface, which mainly corresponds to superficial layers (Grinvald et al., 1999; Petersen et al., 2003). Furthermore, measures of the distribution of dye fluorescence intensity in rat visual and barrel cortex confirm that the optical signal mostly originates from superficial layers I-III (Ferezou et al., 2006; Lippert et al., 2007). Note that Lippert et al. (2007) used a special staining procedure, i.e. keeping the dura mater intact, but dried.

However, they did not take into account the fact that the activity in superficial layers could arise from neurons in deep layers, due to their dendritic arborization. Indeed, large pyramidal neurons in layer V have apical dendrites that reach superficial layers and may contribute to the signal. Therefore, the exact contribution of each cortical layer still has to be clarified.

5.3.5 About the contribution from thalamic versus horizontal connections

The origin of the signal can also be problematic when looking at the contribution from the different presynaptic activity origins, e.g. direct thalamic synaptic inputs, or horizontal inputs. Indeed, in response to a local stimulation, slow propagating waves can be recorded (Grinvald et al., 1994; Jancke et al., 2004; Roland et al., 2006; Xu et al., 2007;

Benucci et al., 2007). We can question what is the relative contribution of all the synaptic input sources of this phenomenon, i.e. feedforward, horizontal or feedback inputs. Dedicated models could help teazing apart those various contributions.

5.3.6 Conclusion

Figure 5.2 summarizes the four main questions not completely clarified to date:

- What are the contributions of the various neurons and neuronal components to the optical signal?

- What is the ratio between spiking and synaptic activity?

- What are the respective contributions of cells from deep versus superficial layers?

- What is the origin of the synaptic input? More precisely, what are the respective contributions of thalamic, local and long-range inputs?
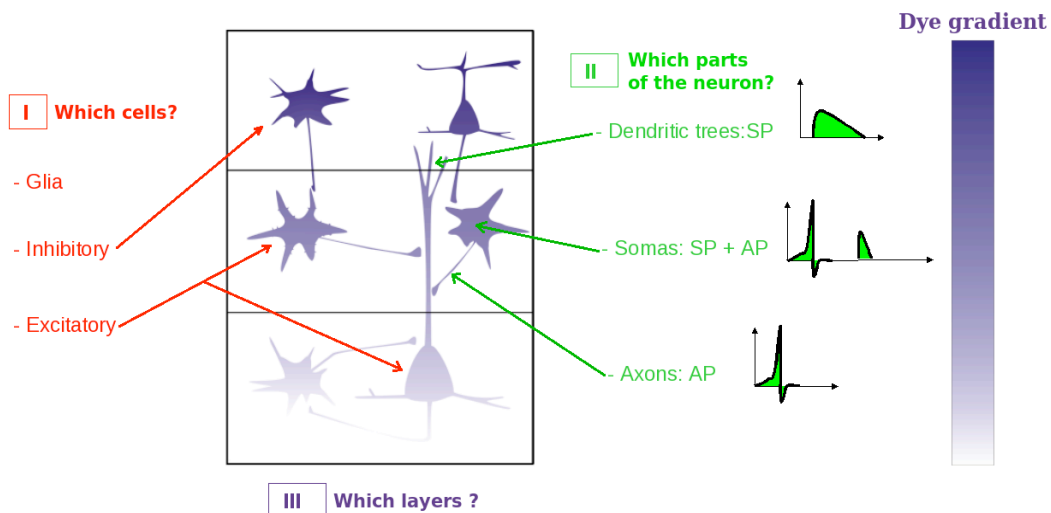
Figure 5.2: Contributions of the optical signal. Once neurons are stained by the VSD, every neuronal membrane contributes to the resulting fluorescent signal, but from where? and in which proportion? Answering these four questions could clarify the optical signal origins: 1) Which cells? 2) Which parts of the cell? 3) Which layers? 4) Which presynaptic origins?

To answer these questions, we propose in this thesis to develop a computational model in order to reproduce and analyse VSD signals. Existing models of VSD signals are reported in Chapter 6, while our proposed model is detailed in Part III.

BENEFITS OF MODELING FOR VSD SIGNAL ANALYSIS: VSDI MODELS INVENTORY

OVERWIEW

The goal of this chapter is to investigate the different models from the literature, used to reproduce and analyse the VSD signal. We quickly emphasize four of these models because of their scale of analysis, the mesoscopic scale. Unfortunately, none of those models can precisely answer the previous questions about the VSD signal sources, whose the scale is actually submesoscopic. Therefore, in the last section, we propose a list of specifications that an adapted model for this purpose, i.e. detailed analysis of the VSD signal origin, must satisfy. This model will be detailed in the next part of this thesis.

Contents

6.1 THE MESOSCOPIC SCALE

As previously described, the origin of the VSD signal is complex and remains to be estimated and explored. Therefore it could be interesting to see if the activity of a computational model could be related to this signal. However, the choice of the model's scale is very important and depends on what exactly the model is designed for. In the following paragraphs, several authors propose the *mesoscopic scale* as the best scale for analyzing the population VSD signal. In neuroscience, this scale lies between the microscopic scale of neurons and their chemical interactions and the macroscopic scale of brain activity. The mesoscopic scale is thus the scale at which the behavior of large assemblies of neurons is analyzable, without entering into microscopic considerations, mathematically unwieldy. Instead, it is a size which allows to manipulate average values, thus requiring only simple computations. Mean-field theory gives successful results in describing the activity interacting populations of neurons (Faugeras et al., 2009).

Following the concept previously defined in Chapter 2, a cortical column, i.e. the elementary processing unit in the brain, can be viewed as a mesoscopic unit, which is smaller than a macroscopic unit as a brain area and bigger than a microscopic unit as a neuron. It is thereby quite natural to use the mesoscopic scale to study the VSD signal since it is a population signal which reveals the columnar organization of the cortex (see Chapter 5). Several models have been built at this scale (Miikkulainen et al., 2005), Symes and Wennekers (2009),Grimbert et al. (2007), Rangan et al. (2005) and La Rota (2003), allowing to reproduce the dynamics of the VSD signal, i.e. time course and spatial extent. Those models are reviewed in the next section.

6.2 MODELING THE MESOSCOPIC VSD SIGNAL

6.2.1 Extended LISSOM model

The LISSOM (Laterally Interconnected Synergetically Self-Organizing Map) family of models was developed by Bednar, Choe, Miikkulainen and Sirosh, at the Universitey of Texas (Miikkulainen et al., 2005; Sirosh and Miikkulainen, 1994), as models of human visual cortex at a neural column level. It is based on the Self-Organizing Maps (SOM) algorithm (Kohonen, 2001) used to visualize and interpret large high-dimensional data sets. When extended, the LISSOM neural network models takes into account lateral interactions (excitatory and inhibitory connections), allowing to reproduce the pinwheel organization of the primary visual cortex map, such as orientation, motion direction se-

lectivity and ocular dominance maps.

Sit and Miikkulainen used such a LISSOM model to represent V1 and tried to show how the activity of such a computational model of V1 can be related to the VSD signal (Sit and Miikkulainen, 2007). Indeed, with an extented LISSOM model including propagation delays in the cortical connections, they showed that the orientation tuning curve and the response dynamics ot the model were similar to those measured with VSDI.

The model is a couple of two layers of neural units that represent the retina and V1. In V1, neural units account for a whole vertical column of cells. They receive input from the retina and also from neighbour columns (short-rang lateral excitatory and long-rang lateral inhibitory connections). Thus, the neuronal activity of unit $\mathbf{r}$ in V1 writes:

$$
\begin{aligned}
A(\mathbf{r}, t) &= \sigma\left(V(\mathbf{r}, t)\right), \\
V(\mathbf{r}, t) &= \sum_{\rho} \gamma_{\rho} \sum_{\mathbf{r}'} W_{\rho, \mathbf{r}, \mathbf{r}'} A(\mathbf{r}', t - d(\mathbf{r}, \mathbf{r}')) + \sum_{\mathbf{s}} \chi_{\mathbf{s}} R_{\mathbf{s}, \mathbf{r}},
\end{aligned}
\tag{6.1}
$$

where σ is a sigmoid activation function and the two terms are respectively the weighted sum of the lateral activations and the imput activation from the retina. $W_{\rho, \mathbf{r}, \mathbf{r}'}$ and $R_{\mathbf{s}, \mathbf{r}}$ are respectively the synaptic weights matrix of lateral and retinal connections, and $d(\mathbf{r}, \mathbf{r}')$ is the delay function between unit $\mathbf{r}$ and unit $\mathbf{r}'$. This is thus a scalar model of the neural activity.

Then, the computation of the VSD signal is done by looking only at the subthreshold activity $V(\mathbf{r}, t)$, given by the weighted sum of presynaptic activity. To simplify, the authors have extended the LISSOM model with delayed lateral connections to compute the VSD signal from subthreshold signal. This is thus a scalar linear model of the VSD signal built on convolutions.

This model, based on Hebbian self-organizing mechanisms, is simple and efficient to replicate the detailed development of the primary visual cortex. It is thus very useful to study VSDI functional maps. However, this model is not specific enough to answer the previous asked questions (see Subsection 5.3.6).

6.2.2 Mean field model of primary visual cortex layer 2/3

Symes and Wennekers (2009) have very recently developed a mean field computational model representing a patch of layer 2/3 visual cortex. The model represents a small patch of approximately 3 mm^2, using two arrays of cells (51x51 grids), one excitatory and one inhibitory. Each cell location is denoted by a spatial position $\mathbf{r} = (x, y)$ and the membrane potential at this location, representing the average local activity of a small

population of excitatory and inhibitory neurons, is governed by:

$$\tau \dot{V}(\mathbf{r}, t) = -(V(\mathbf{r}, t) - V_{rest}) - g_E (V(\mathbf{r}, t) - V_E) - g_I ((V(\mathbf{r}, t) - V_I) \tag{6.2}$$

where V_{rest} set to -70 mV is the resting potential of the cell, τ is its passive membrane time constant (10.4 ms and 7.6 ms for respectively excitatory and inhibitory cells), g_E and g_I represent respectively excitatory ($AMPA$) and inhibitory ($GABA_A$ synaptic inputs to the cell, and V_E, V_I their associated reversal potentials (0 mV and - 70 mV respectively).

The model includes both local and long-range lateral connectivity, from anatomical data presented in Chapter 2, Section 2.3. Connectivity strength within layer 2/3 is thus represented by a gaussian function:

$$\phi(d) = e^{-\frac{d^2}{2\sigma^2}} \tag{6.3}$$

where d represents the distance between cells. Different values of σ are used for excitatory (σ = 300 μm) and inhibitory (σ = 200 μm) connections, according to Kisvarday et al. (1997) data suggesting different extents of lateral excitatory and inhibitory connections.

The voltage-sensitive dye signal S generated by a model cell at location $\mathbf{r}$ is then computed by the following formula:

$$\tau \dot{S}(\mathbf{r}) = -S(\mathbf{r}) + K(\mathbf{r}) \tag{6.4}$$

where $K(\mathbf{r})$ is the sum of excitatory and inhibitory synaptic inputs (see Equation 6.2) to the model cell located at $\mathbf{r}$, whilst τ = 5 ms. Explicitly separating the relative contribution of both excitatory and inhibitory cells to the VSD signal, they obtained the final relation:

$$VSD(\mathbf{r}) = p\, S_E(\mathbf{r}) + (1 - p)\, S_I(\mathbf{r}) \tag{6.5}$$

where S^E and S^I are the excitatory and inhibitory VSD signals previously defined by equation 6.4, and p set to 0.8 represents the ratio between excitatory and inhibitory combined surface area of dendritic trees.

This model have been specifically built to investigate the mechanisms that underlie specific patterns of spatiotemporal activity observed *in vitro* in layer 2/3 of ferret primary visual cortex (Tucker and Katz, 2003b). However, the authors did only a qualitative comparison between the model and the experimental data, mainly because of the uncertainties related to the VSD signal origin.

6.2.3 Neural field model of a cortical area

Another approach, introduced by Grimbert et al. (2007, 2008), proposes neural fields as a suitable mesoscopic models of cortical areas, in link with VSD. Neural field are con-

tinuous networks of interacting neural masses, describing the dynamics of the cortical tissue at the population level (Wilson and Cowan, 1972, 1973). It could thus be applied to solve the direct problem of the VSD signal, providing the right parameters.

More precisely, the authors showed that neural fields can easily integrate the biological knowledge of cortical structure, especially horizontal and vertical connectivity patterns. Hence, they proposed a biophysical formula to compute the VSD signal in terms of the activity of a field.

The classical neural field model equation is used, either written in terms of membrane potential or in terms of activity of the different neural masses present in a cortical column. For example, if $\mathbf{r}$ represents one spatial position of the spatial domain defining the area, then the underlying cortical column is described, at time t, by either a vector $\mathbf{V}(\mathbf{r}, t)$ or $\mathbf{A}(\mathbf{r}, t)$:

$$\dot{\mathbf{V}}(\mathbf{r}, t) = -\mathbf{L}\,\mathbf{V}(\mathbf{r}, t) + \int_{\Omega} \mathbf{W}(\mathbf{r}, \mathbf{r}')\,\mathbf{S}(\mathbf{V}(\mathbf{r}', t))\,d\mathbf{r}' + \mathbf{I}_{ext}(\mathbf{r}, t), \tag{6.6}$$

and

$$\dot{\mathbf{A}}(\mathbf{r}, t) = -\mathbf{L}\,\mathbf{A}(\mathbf{r}, t) + \mathbf{S}\left(\int_{\Omega} \mathbf{W}(\mathbf{r}, \mathbf{r}')\,\mathbf{A}(\mathbf{r}', t))\,d\mathbf{r}' + \mathbf{I}_{ext}(\mathbf{r}, t)\right) \tag{6.7}$$

Here, $\mathbf{V}(\mathbf{r}, t)$ contains the average soma membrane potentials of the different neural masses present in the column (the vector's dimension then reprensents the number of neuronal types considered in every column). $\mathbf{A}(\mathbf{r}, t)$ contains the average activities of the masses. For example, A_i is the potential quantity of post-synaptic potential induced by mass i on the dendrites of all its postsynaptic partners. The actual quantity depends on the strength and sign (excitatory or inhibitory) of the projections (see Grimbert et al., 2007, 2008; Faugeras et al., 2008, for more details on the model's equations). The model include horizontal intercolumnar connections and also vertical intracolumnar connections between neural masses. The latter gives an advantage to this model compared to the previous one, since the vertical connectivity was not taken into account in the extended LISSOM model. Furthermore, extracortical connectivity is not made explicit here, though taken into account in Grimbert et al. (2007).

Hence, based on this biophysical formalism (and especially the activity-based model, which is more adapted than the voltage-based model), the authors propose a formula involving the variables and parameters of a neural field model to compute the VSD signal:

$$OI(\mathbf{r}, t) = \sum_{j=1}^{N} \int_{\Omega} \tilde{w}_j(\mathbf{r}, \mathbf{r}')\,A_j(\mathbf{r}', t)\,d\mathbf{r}', \tag{6.8}$$

where $\tilde{w}_j(\mathbf{r}, \mathbf{r}')$ contains all the biophysical parameters accounting for a cortical area

structure stained by a voltage-sensitive dye, i.e the different layers, the number of neurons, the number of dye molecules per membrane surface unit, the attenuation coefficient of light and also the horizontal and vertical distribution patterns of intra and inter-cortical connectivities.

This formula is the result of many decompositions of the total optical signal, from layer level to cellular membrane level, where the signal is simply proportional to the membrane potential.

Better than the Lissom model for our considerations, this large-scale model reproduces the spatiotemporal interactions of a cortical area in response to complex stimuli, e.g. line motion illusion, and allows, on average, to answer at the mesoscopic scale some previous questions (see Subsection 5.3.6). However, improvements on parameters tuning are still needed.

6.2.4   Conductance-based IAF neuronal network model

Another large-scale computational model of the primary visual cortex have been proposed by Rangan et al. (2005). The model is a two-dimensional patch of cortex, containing about 10^6 neurons with a preferred orientation, whose 80 percent are excitatory and 20 percent are inhibitory. The dynamics of single cell i is decribed by a single compartment, conductance-based, exponential integrate-and-fire equation (see Geisler et al., 2005, for more details on this neuron model). The derivation of this equation gives the membrane potential of neuron i of spatial position $\mathbf{r}_i$:

$$V(\mathbf{r}_i, t) = \frac{g_L \, V_L + (g_A^i(t) + g_N^i(t)) \, V_E + g_G^i(t) \, V_I}{g_L + g_A^i(t) + g_N^i(t) + g_G^i(t)} \qquad (6.9)$$

where g_L, g_A^i, g_N^i and g_G^i are respectively leak, AMPA, NMDA and GABA conductances, and V_L, V_E and V_I are respectively leak, excitatory and inhibitory reversal potentials. The authors then use $V(\mathbf{r}, t)$ to represent the VSD signal, i.e. the subthreshold dendritic activity in the superficial layers of the cortex. Poisson processes are used to simulate inputs from the thalamus and background noise.

This model allows, like the previous one (Grimbert et al., 2007), to reproduce the spatiotemporal activity patterns of V1, as revealed by VSDI, in response to complex stimuli, e.g. the line motion illusion. However, in comparison with Grimbert et al. (2007), no laminar structure is taken into account.

6.2.5   Linear model of the raw VSD signal

With the same scale of analysis, La Rota (2003) presented an interesting linear model in order to study the neural sources of the mesoscopic VSD signal. The author chose

a compromise between a detailed and a "black-box" model of the signal, by taking into account the important properties of the VSD signal and also the artefacts directly linked to its measure, in a mesoscopic, linear and additive model. The VSD signal of a cortical area can then be modeled by an intrinsic and an extrinsic components:

$$OI(t) = A(t) + \rho(t), \tag{6.10}$$

where A(t) represents the activity of the intrinsic component of the optical signal (i.e. the synaptic activity of the cortical area observed) and $\rho(t)$ represents all the noise and artefacts due to the measure (e.g. hemodynamic artefact, cardiovascular and respiratory movements, instrumental noise, etc.). In this model, inputs from the thalamus are considered as background noise and thus enter in the ρ component.

The model is interesting because it both takes into account the intrinsic and the extrinsic variability of the VSD signal. The latter being supposed already removed, when analyzing the signal in the three other presented models.

6.3 MODELING THE SUBMESOSCOPIC SOURCES OF THE VSD SIGNAL

Though able to reproduce the dynamics of the VSD signals, none of the previous mesoscopic models were specific enough to determine the different contributions of the optical signal. It is not surprising since they were not built for that purpose. As the sources of the VSD signal are actually submesoscopic, there is a need to develop a model at this spatial scale. The idea is thus to choose a scale adjusted to the methodological constraints of optical imaging. To quantify the contributions from excitatory vs. inhibitory neurons, such a model should take into account several types of neurons, or at least, one type of excitatory neurons and one type of inhibitory neurons, with realistic behaviors. To determine if the VSD signal mainly reflects postsynaptic activity, the modeled neurons must have at least three compartments, respectively for its soma, axon and dendrite. As we also want to know the layers participation to the signal, neurons in deep layers should have more than one dendrite, actually at least one per layer, in order to differentiate neurons whose dendrites reach superficial layers. Of course, this also implies several layers.

In optical imaging, one pixel size is about 50 μm. We thus decided to consider a cortical column of 50 μm diameter. Using the novel concept of cortical column proposed in Chapter 2, it is then easy to introduce a new distinction of cortical column into the previous table (see Table 6.1), whose the spatial scale is 50 μm, corresponding to one pixel of optical imaging. Therefore, this "optical" column lies between the anatomical and the

functional column. The scale being relatively small, compared to those used in the four presented models, we will call it an "intermediate mesoscopic scale". This cortical column must be embedded into a larger network, in order to be realistic.

Following all these requirements, we developed a detailed biophysically inspired model of a cortical column, embedded into an artificial hypercolumn (in the case of V1). This model is detailed in the next part of this thesis.

Type	Anatomical	Anatomo-functional	Functional		OI pixel
Name	Microcolumn Minicolumn	Macrocolumn	Ocular dominance, Orientation, Blobs, Barrels, Stripes	Hypercolumn	Optical column
Spatial scale (μm)	40	400-1000	200-400	600-1500	50
Number of neurons	80-100	10,000-60,000	2500-10,000	20,000-140,000	150-200

Table 6.1: The different types of cortical columns.

Part III

A biophysical cortical column model to study the multi-component origin of the VSD signal **

THE MODEL

OVERWIEW

Since none of the models presented in Chapter 6 were suitable for our purpose, we propose in this chapter a biophysical cortical column model, at a submesoscopic scale, in order to better understand and interpret biological sources of the signal recorded *in vivo* with VSDI. The model is composed of 180 neurons, each modeled with a multi-component neuronal model, as presented in Chapter 4, Section 4.1. These latter are connected following a cortical microcircuit as previously described in Chapter 4, Section 4.3. The generated model is used to solve the VSD direct problem, i.e. generate a VSD signal, given the neural substrate parameters and activities.

Section 7.2 presents in details all the specifications of this biophysically plausible cortical column model, as well as the linear formula allowing to compute the VSD signal. Section 7.3 presents the calibration of its behavior both at the individual neurons and the global network level.

Contents

7.1 INTRODUCTION

As explained in Chapter 5, voltage-sensitive dye imaging is based on voltage-sensitive dyes (VSDs), which binds to the membrane and transform variations in the membrane potential into optical fluorescence. The emitted fluorescence, recorded by a sensitive fast camera, is linearly correlated with changes in membrane potential per unit of membrane area of all the stained surfaces (Grinvald and Hildesheim, 2004), meaning all neuronal cells present in the cortex, but also all non-neuronal cells, such as glial cells. Neuronal cells include excitatory cells (e.g. pyramidal cells, spiny stellate cells) and inhibitory cells (e.g. basket cells, chandelier cells), whose morphology and intrinsic properties are quite different. Furthermore, each cell has various compartments, including dendrites, somata and axons. The measured signal is therefore a multiplexed signal that combines all these components. It is not straightforward to predict the result of the combination of such a large amount of intermingled components. Prediction of the origin of the VSD signal is also complicated by non-linearities in neuronal interaction. One important example of these non-linearities is coming from inhibition that mostly acts in a divisive manner through shunting of the postsynaptic recipient, without clear hyperpolarization of the membrane potential (Borg Graham et al 1998). In other terms, a strong inhibition will not obligatory induce a net decrease of the VSDI signal. Therefore, although the underlying mechanism of the VSDI is well understood (Grinvald and Hildesheim, 2004; Roland, 2002), the recorded signal remains very complex and it is difficult to isolate the relative contributions of its different components (see Chapter 5 for a detailed analysis of the VSD signal).

In this chapter, our aim is to better understand the origin of the VSD signal (see Fig. 5.2): What is the exact participation of the various neuronal components to this population signal? In particular, are excitatory and inhibitory cells participating equally for different levels of activity? What is the ratio between spiking and synaptic activity? Is this ratio the same when the network is at low versus high levels of activity? What are the respective participation of cells from deep versus superficial layers?

To answer those questions, our strategy has been to develop a biophysically inspired model to reproduce the optical imaging signal (see Fig. 7.1). We modeled in detail one cortical column of 50 μm, which is one optical imaging averaged pixel size (see Table 6.1). This scale also corresponds to the spatial scale of the biological experiments (Markram et al., 1998b; Gupta et al., 2000; Thomson et al., 2002; Thomson and Bannister, 2003), which were used to establish the precise local connectivity rules of columnar organization (Binzegger et al., 2004; Douglas and Martin, 2004; Haeusler and Maass, 2007) (see Chapter 2). To embed this isolated column into a larger, hence more realistic, cortical network, we simulated an additional synaptic bombardment according to Destexhe et al.

(2001). Four types of neurons were considered with only two distinct firing patterns, regular spiking and fast spiking, since they are known to be respectively the great majority of excitatory and inhibitory cells in the neocortex (Contreras and Palmer, 2003). To tease apart the different contributions of the various components of the signal, we dynamically explored functional parameters that are known to affect differentially those components. Among all parameters, we decided to manipulate the activity level (i.e. contrast) both at the single neuron and the global network level. These manipulations were applied within functional regimes that are known to affect differentially excitatory (RS cells) and inhibitory (FS cells) components of the network, but also the relative contribution of membrane depolarization and spiking output.
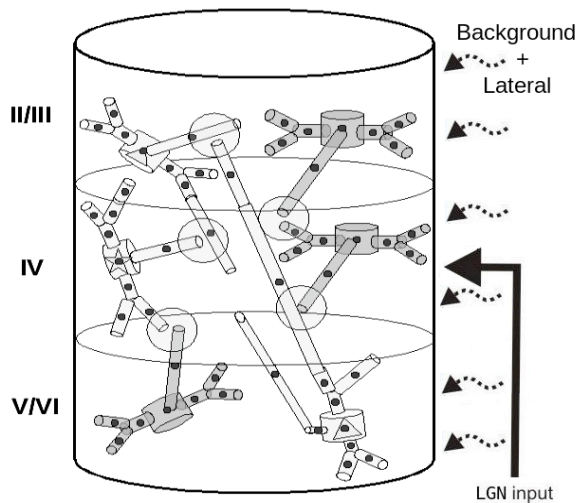
Figure 7.1: Schematic view of the cortical column model. Six specific populations of neurons: excitatory (light grey) and inhibitory (dark grey) populations in each of the three layers (2/3, 4, 5/6). Only few axo-dendritic synapses are represented (open circles), and the middle of each compartment are marked with a black dot.

In this following, we describe the proposed model of cortical column chosen to analyze biological sources of the optical signal. then we discuss its behavior and its application for VSD signal computation. Answers to the above questions are given in Chapter 8.

7.2 MATERIAL AND METHODS ⎯⎯⎯⎯⎯⎯⎯⎯⎯⎯⎯⎯⎯

7.2.1 Single neuron model

Each neuron is represented by a reduced compartmental description (see Bush and Sejnowski, 1993, and Section 4.1 for more details on the reduction method) with conductance-based Hodgkin-Huxley neuron model (see Hodgkin and Huxley, 1952d, and Section 4.1) in the soma and the axon. The dynamics of single cells are described by the following equation:

$$C_m \frac{dV}{dt} = I_{ext} - \sum_i g_i(V)(V - E_i) \tag{7.1}$$

where V is the membrane potential, I_{ext} is an external current injected into the neuron, C_m is the membrane capacitance, and where three types of current are represented: leak, potassium and sodium conductances or respectively g_L, g_K and g_{Na}. g_L is independent of V and determines the passive properties of the cells near resting potential. The sodium and potassium conductances are responsible for the spike generation.

A slow potassium conductance (called M-conductance) was also included in the dynamics of the excitatory population to reproduce the observed adaptation of the spike trains emitted by these neurons (Nowak et al., 2003). This feature seems to be absent in inhibitory neurons (Contreras and Palmer, 2003), as taken into account in this work.

Only passive dendrites were considered. Each neuron is represented with seven to nine compartments. As explained in Section 4.1, the link between two adjacent compartments j and k can be described by equation 7.2 (Hines and Carnevale, 1997).

$$C_j \frac{dV_j}{dt} + Iion_j = \sum_k \frac{V_k - V_j}{R_{jk}} \tag{7.2}$$

where V_j is the membrane potential in compartment j, $Iion_j$ is the net transmembrane ionic current in compartment j, C_j is the membrane capacitance of compartment j and R_{jk} is the axial resistance between the centers of compartment j and adjacent compartment k.

7.2.2 Network Architecture and Synaptic Interactions

We consider a class of models based on a cortical microcircuit (see Raizada and Grossberg, 2003; Douglas and Martin, 2004; Haeusler and Maass, 2007, and Section 4.3 for more details on this concept), whose simplified synaptic connections are made only between six specific populations of neurons: two populations (excitatory and inhibitory) for

three main layers (II/III, IV, V/VI). Thanks to the NEURON software[1] and its ModelDB database, providing an accessible location for storing and efficiently retrieving computational neuroscience models, we have been able to reconstruct four types of neurons (Bush et al., 1999): small pyramidal cells in layer II, spiny stellate cells in layer IV, large pyramidal cells in layer V and smooth stellate cells in all layers. More precisely, the chosen model is a model of 180 neurons, 143 excitatory neurons: 50 small pyramidal (SP) in layer II/III, 45 spiny stellate (SS) in layer IV, 48 large pyramidal (LP) in layer V/VI, and 37 inhibitory neurons of one unique type: respectively 14, 13, 10 smooth stellate in layers II/III, IV, V/VI (SmS2, SmS4, SmS5). The difference in morphology and membrane surface of these different neuronal types was then taken into account when computing the VSD signal (see Computation of the VSD signal).

Synaptic inputs were modeled as conductance changes (see Section 4.2). Excitatory $AMPA$ synapses are converging on dendrites of each neuron, whereas inhibitory $GABA$ synapses are converging on soma of each neuron (see Salin and Bullier, 1995, for a review on the subject). The number of synapses involved in the projections between these different neuronal types, including the afferent from the LGN (X/Y) (recalculated for 50 μm cortical column), were based on Binzegger et al. (2004) for the considered layers while latencies have been introduced for each connection, following Thomson and Lamy (2007). This network architecture was built using the neuroConstruct software[2] and run on the NEURON simulator. A schematic view of the model is given in Figure 7.1. Note that, as synaptic inputs are conductance-based and that the $GABA$ reversal potential was chosen equal to the resting potential (-70mV), our inhibitory interactions are mostly shunting and not hyperpolarizing (see Fig. 7.2). It has been indeed documented that inhibitory interactions are acting in a silent, shunting mode (Borg-Graham et al., 1998; Anderson et al., 2000; Fregnac et al., 2003). As VSDI signal reports changes of membrane potential, it was important to verify that the inhibition implemented in the model acts silently without net hyperpolarization.

7.2.3 Thalamic Afferents, Background Activity and Lateral Interactions

Inputs signals from the thalamus into the neocortex layer IV are simulated by applying 10 random spike trains to each neuron in layer IV (Alonso et al., 2001). Latencies were chosen randomly within a given temporal window (initially tested from 0 to 10 ms with a uniform distribution, and changed from 0 to 50 ms, see Results section) for each input connection, to reproduce the temporal properties of the geniculocortical pathway according to Reid and Alonso (1996). Rate of the thalamic input was manipulated to study the

---

[1]http://neuron.duke.edu
[2]http://www.neuroConstruct.org
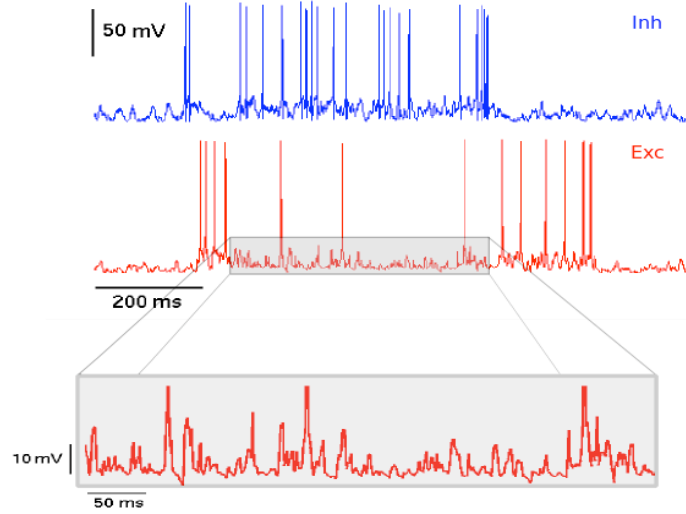
Figure 7.2: Inhibition operates in a shunting mode. The presynaptic inhibitory neuron (blue trace) shunts the activity of the postsynaptic excitatory neuron (red trace). When zooming (lower panel), we verify the divise effect of this inhibition since no net hyperpolarization is visible.

influence of cortical regime on the relative contributions of the different compartments (see details in Results section). At this point, the column is isolated.

The conditions relative to a larger network is simulated as follows. First, "background noise" was introduced in each neuron of the column. Typically, noise can be introduced in the form of stochastic fluctutation of a current or an ionic conductance. The stochastic model of Destexhe et al. (2001), containing two fluctuating conductances, is used here, allowing us to simulate synaptic backgroung activity similar to in vivo measurements for a large network.

Second, since background activity was not enough to reliably reproduce the experimental VSD signal (see Results), an entire hypercolumn of about 750 μm was simulated by introducing lateral interactions between neighboring columns. This is done by introducing an other set of random spike trains inputs whose frequency, synaptic delays and weights are given by the local network and biological data from Buzas et al. (2006) respectively (see Results).

7.2.4   Computation of the VSD signal

The VSD signal was simulated using a linear integration on the membrane surface of all neuronal components (Grinvald and Hildesheim (2004)). Here, the use of compartmental model has a real interest since the computation of the VSD signal, for a given layer L, is given by:

$$OI^L = \lambda^L \sum_{i=0}^{N^L} V_i(0.5)\, S_i \qquad (7.3)$$

where N^L is the number of compartments in layer L, S_i is the surface of the ith compartment, $V_i(0.5)$ is the membrane potential taken in the middle of the ith compartment, and λ^L represents the fluorescence's gradient or the illumination intensity of the dye in layer L.

We thus can take into account soma, axon and dendrites influences, introduce 2D geometrical properties (dendrites of large pyramidal neurons in layer V can reach superficial layers) and fluorescence's gradient depending on depth. According to Lippert et al. (2007) and Petersen et al. (2003), we chose to take $\lambda^2 = 0.95$, $\lambda^4 = 0.05$ and $\lambda^5 = 0$. This corresponds to dye diffusion in the rat without dura removal which might differ from data in higher mammal species. However, the only quantitative data on dye gradient unfortunately comes from this model (see Discussion section). Then, the total optical imaging signal is given by the following formula:

$$OI = \sum_{L \in \{Layers\}} OI^L \tag{7.4}$$

7.3 MODEL BEHAVIOR AND QUANTITATIVE ADJUSTMENTS

As mentioned in the introduction, our idea is to evaluate the contribution of the various components of the VSD signal as a function of activity level. It was therefore mandatory to develop a model that behaves realistically in response to different levels of activity, both at the single neuron and the global network level. We thus starting by fitting the model to intracellular recordings references providing information about subthreshold but also spiking activity as a function of the level of input activity.

7.3.1 Single neuron regimes

We adjusted the intrinsic properties of our isolated neurons to fit those shown in Nowak et al. (2003) from *in vivo* intracellular recordings. For each neuron, the optimized parameters were the channel conductances G_i, and the passive electrical properties of compartments: the specific axial resistance R_a and the specific capacitance C_m. The optimization algorithm used was the PRAXIS (principal axis) method described by Brent (1976) and embedded into the NEURON software. The parameters values are given in the table of Figure 7.3C. Excitatory and inhibitory neurons were modeled to have regular spiking (RS) and fast spiking (FS) intrinsic properties, since RS and FS cells are known to be respectively the great majority of excitatory and inhibitory cells in the neocortex (Contreras and Palmer, 2003) (see Chapter 1, Section 1.1). Figure 7.3 shows the action potential shapes of RS cells and FS cells of the model, showing that RS cells fired action potentials of 1 msec duration (Fig. 7.3A, Left) measured at threshold, whereas

FS cells (Fig. 7.3A, right) had short-duration action potential (0.5 msec at threshold), as documented in the literature (Contreras and Palmer, 2003). Examples of action potential responses to depolarizing current injection in these two populations are also plotted. Here, RS cells (Fig. 7.3B, left) produced adapting spike trains at about 60 Hz, whereas FS cells (Fig. 7.3B, right) generated high-frequency train of spikes at about 300 Hz with pronounced and brief spike after hyperpolarizations (AHPs), that fits properly the electrophysiological data from Nowak et al. (2003) and Contreras and Palmer (2003).

From these action potential reponses, we calculate the relationship between injected current intensity (in nA) and the total firing rate (in spikes per second). The slope (in Hz/nA) of the linear regression characterizes the current-frequency relationship of the neuron (Fig. 7.3D), which is one of the useful charateristics in distinguishing between different types of neurons, as explained by Nowak et al. (2003), especially RS and FS cells. This slope is considerably steeper in the FS cell (375 Hz/nA) compared with that for the RS cell (83.3 Hz/nA), in accordance with what is shown in Nowak et al. (2003) (519 Hz/nA for the FS cell and 85 Hz/nA for the RS cell).

7.3.2 Local network calibration

The next step in the validation of the model is to analyze the behavior of the whole connected local network of neurons. To calibrate this network at different working regimes, we chose to compare the input-output relationship predicted by the model to the contrast response function (CRF) of V1 neurons classically recorded electrophysiologically, as done in Contreras and Palmer (2003) (see Chapter 1, Section 1.2). The CRF describes the fact that cortical cells adjust non-linearly their response to an input with increasing strength (Albrecht and Hamilton, 1982). Nonlinearities in the CRF (compression and saturation) allow cortical cells to adjust the useful dynamic response to an operating range of contrast that can be modulated. This control is supposed to be adjusted by a dynamic balance between excitation and inhibition. Our manipulation of input strength was simply to increase the thalamic rate. The correspondence between input strength in contrast vs. spiking input rate is not straightforward. Therefore, we chose to adjust our model at saturation level for which the network regimes can be compared, and only made qualitative comparison for the rest of the response curve. The related parameters to be adjusted are then the weight values of synaptic connections, w_{EE}, w_{EI}, w_{IE} and w_{II} for connections between excitatory neurons, from excitatory neurons onto inhibitory neurons, from inhibitory onto excitatory neurons and between inhibitory neurons respectively. This is done using the PRAXIS optimization algorithm again. We obtain an interval for each of the four weight values by fitting both the spike rate and the membrane potential of the two populations, in response to contrast input, i.e. input rate. Then we generate uniformly distributed random numbers over this specific interval.

	SP2	LP5	SS4	SmS
G_{Na} $(mS/\mu m^2)$	0.3	1.5	0.4	0.34
G_K $(mS/\mu m^2)$	0.02	0.08	0.02	1.2
G_M $(mS/\mu m^2)$	0.004	0.003	0.004	not present
G_L $(mS/\mu m^2)$	9.10^{-5}	9.10^{-5}	3.10^{-4}	4.10^{-4}
C_m $(uF/\mu m^2)$	1.10^{-8}	1.10^{-8}	1.10^{-8}	2.10^{-8}(S,A) $2.21.10^{-8}$(D)
R_a $(kohm,\mu m)$	500(S,A) 2000(D)	500(S,A) 2000(D)	500(S,A) 2000(D)	500(S,A) 2000(D)
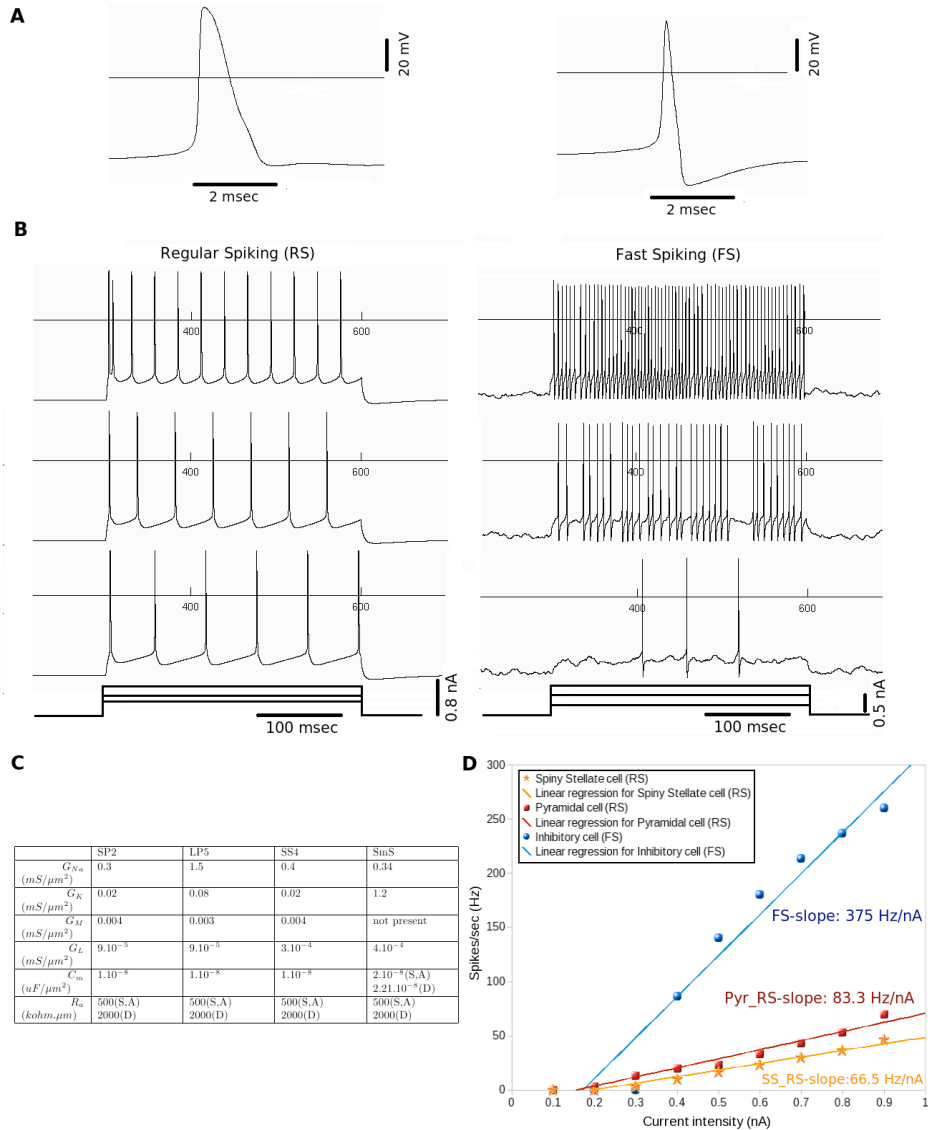
Figure 7.3: Adjustment of electrophysiology properties of isolated neurons. **A:** Action potential shape of regular and fast spiking cells. *Left*: regular spiking (RS) cell. *Right*: fast spiking (FS) cell. **B:** Examples of action potential responses to depolarizing current injection in the two main classes of cortical neuron of our model, fitted with intracellular recording from Nowak et al. (2003). *Left*: regular spiking (RS) cell. *Right*: fast spiking (FS) cell. **C:** Values of neurons parameters for the four types of neurons: small pyramidal cell in layer II (SP2), large pyramidal cell in layer V (LP5), spiny stellate in layer IV (SS4) and smooth stellate inhibitory cell (SmS). G_{Na}, G_K, G_M, G_L are respectively sodium, potassium, slow potassium and leak conductances. C_m is the specific membrane capacitance and R_a is the specific axial resistance (S, A, and D for respectively Somas, Axons and Dendrites compartments). **D:** Firing rate vs. current intensity (f-I curves) for the cells shown in Fig. 7.1B. Each point is the average of the mean firing rate for 5 repetitions of a given current intensity.

Input-output spiking rate functions of excitatory and inhibitory population of neurons, predicted by the model and obtained both with spike rate and membrane potential are reported in Figure 7.4A,C). We observe that this curves are very similar to the CRFs obtained electrophysiologically in Contreras and Palmer (2003) for the two main populations of neurons (RS and FS cells). As the authors suggested, the input-output spiking rate functions are best fitted by an hyperbolic ratio function (see black lines in Fig. 7.4 and Equation 1.9). We use the values of the three parameters, i.e. the exponent n, the semisaturation contrast C_{50} and the maximum value of the response R_{max}, of the hyperbolic ratio function, to quantify the quality of the fit. These three values are reported on each plot. As concluded by Contreras and Palmer (2003), there are no significant differences between the values of n and C_{50} obtained from spike responses and those obtained from membrane potential responses. To differentiate the two cells groups, the only important differences are in R_{max} obtained with spike rates, higher in FS cells (53.6 Hz) than in RS cells (11.7 Hz), as also obtained by the authors (59.4 Hz vs. 8 Hz respectively). Exponent n values are also very similar between our model and real neurons (1.6 vs. 2.03 for membrane potential and 2 vs. 2.15 for spike rate).

The resulting biophysical model is thus a balanced local network of detailed neurons (80% of RS cells and 20% of FS cells in the three main layers of the cortex), with thalamic inputs and background activity. We will now first verify the adequacy of the model by comparing our model dynamics with the same curves obtained experimentally. Thereafter, in Chapter 8, two different quantitative explorations of the origins of the VSD signal will be explored thanks to the neuronal compartmentalization of our model. A first correlation analysis will be devoted to dissect the neuronal elements that mostly influence the global signal dynamics. A second application will be to quantitatively predict the relative contributions of the various VSD signal sources for increasing level of thalamic input.

7.3.3 Temporal evolution of the modeled VSD signal

We simulated the VSD signal in response to known stimuli, and compared it to experimental results obtained by Reynaud et al. (2007). In this experiment, the visual stimuli, a small luminance gaussian is presented to a behaving monkey during 800 ms. Fig. 7.5A shows the temporal evolution of the modeled VSD signal (red line), which is compared to the experimental results obtained on monkey using VSDI (the mean curve is plotted in black while standard errors are represented by the gray area). Notice that we simulated the VSD signal in term of relative fluorescence by taking relative variations of fluorescence (ΔF) compared to the resting level (F) observed at rest.

The time course of the modeled signal in response to an abrupt change of the input

A

Hyperbolic ratio function:

$$R(C) = R_{max} * C^n / (C_{50}^n + C^n)$$

$R_{max} = 53.6$

$n = 2$
$C_{50} = 125$

$R_{max} = 11.7$

B

$R_{max} = 48$

$n = 1.6$
$C_{50} = 116$

$R_{max} = 14$

C

$R_{max} = 10.93$

$n = 1.6$
$C_{50} = 108$

$R_{max} = 7.32$

D

$R_{max} = 13$

$n = 1.5$
$C_{50} = 104$

$R_{max} = 8.26$
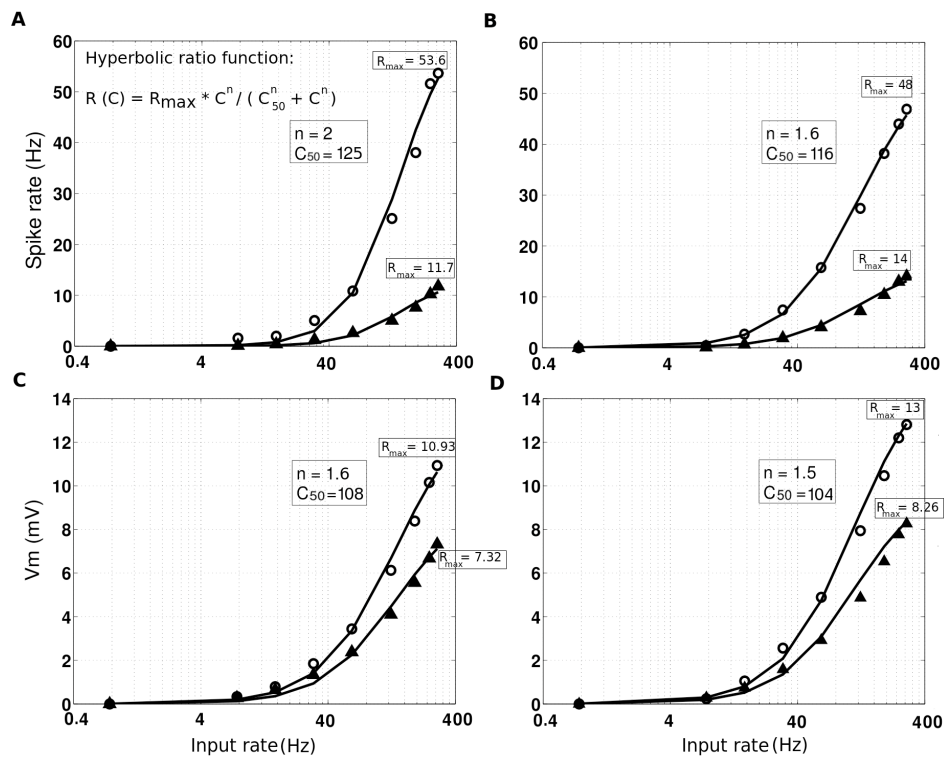
Figure 7.4: Input-output spiking rate function of excitatory (RS cells: filled triangles) and inhibitory (FS cells: open circles) population of neurons, obtained with spike rate and membrane potential, before (A,C) and after lateral interactions introduction (B,D). Each point is the average of the mean quantity for 10 repetitions of a given input rate. *A,B*: Spike rate. *C,D*: Membrane potential (Vm). Each input-output spiking rate function is fitted by an hyperbolic ratio function (black curves). The values of the parameters n, C_{50} and R_{max} are reported on the figure for each case.
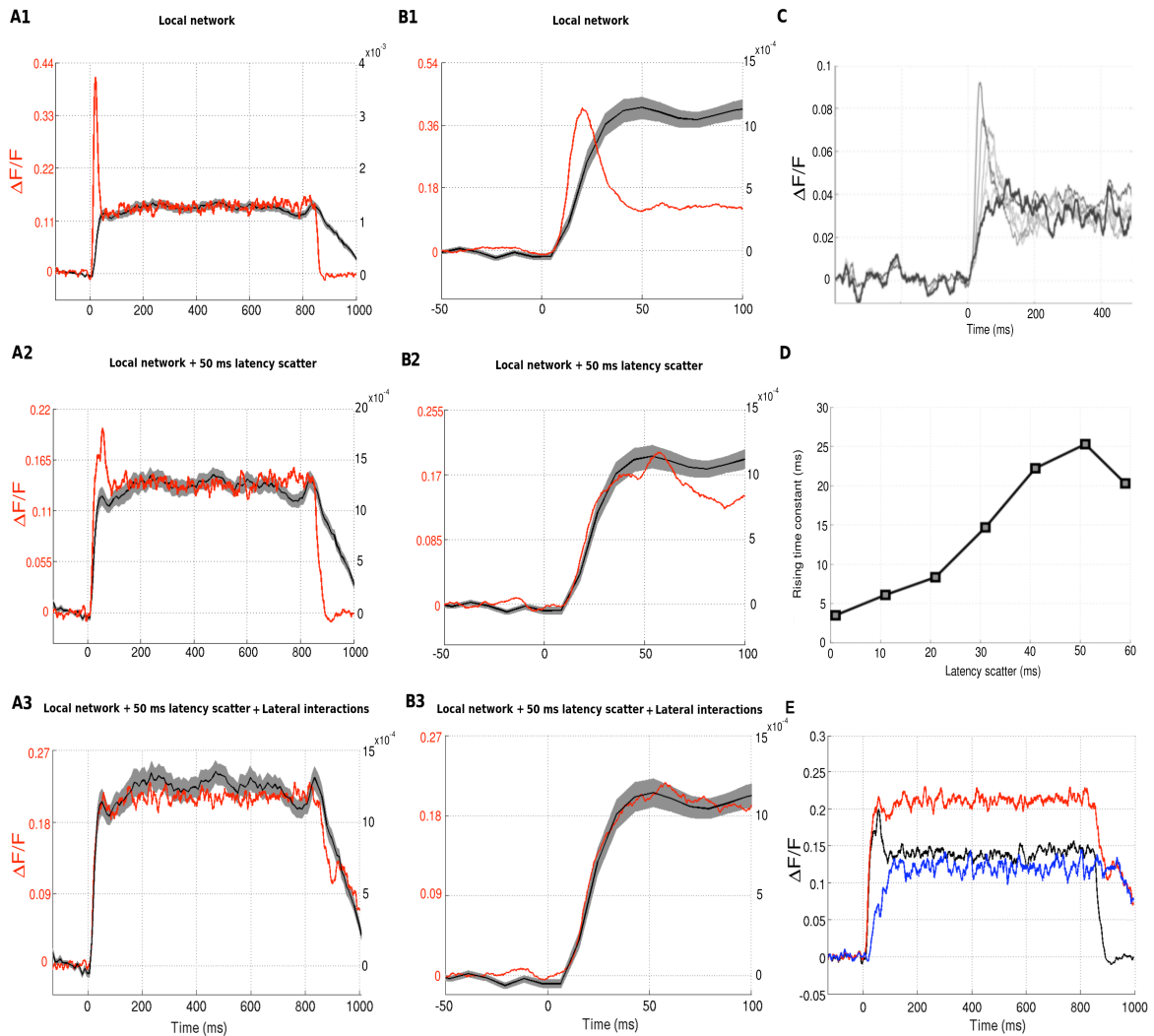
Figure 7.5: Temporal evolution of the VSD signal (red lines), from local to global network. Each curve is the average of the response for 50 repetitions. Mean responses obtained experimentally are superimposed to the modeled signal (black lines with standard error in gray), normalized to either fit the tonic (A1-A3) or the phasic (B1-B3) part of the signal. *A1:* The temporal evolution of the modeled VSD signal in response to an input of 800 ms is plotted as a function of time for a given input frequency (300 hz). *A2:* The temporal evolution of the modeled VSD signal is replotted after the introduction of 50 ms latency scatter on LGN inputs. *A3:* The temporal evolution of the modeled VSD signal is finally replotted after lateral interactions introduction. *B:* Zoom on the rising time course of the VSD responses: for the local network (B1), for the local network after introducing 50 ms latency scatter on LGN inputs (B2), and for the global network, i.e. after introducing the lateral connections (B3). *C:* Influence of the latency scatter (from 0 to 60 ms with a step of 10 ms) of LGN inputs on the VSD responses (input frequency of 64 Hz). *D:* Rising time constant plotted as a function of latency scatter. *E:* Superimposition of local plus latency scatter (black), lateral (blue) and global VSD responses (red), providing quantitative contributions of local and lateral inputs to the total VSD signal.

is faster than the experimental one: The onset of the response shows a large transient *peak* followed by a *plateau* and the transient offset is very sharp compared to the experimental one. Notice that in column A, the modeled signal is normalized to the sustained activity of the experimental signal, while in column B, it is normalized to its transient onset. What can be at the origin of such different dynamics? We first speculated that that the peak was due to a network synchronization at the response onset. We thus tested many parameters (membrane time constants of neurons, spontaneous activity, connections weights), but only the input latency scatter introduced was efficient at desynchronizing the network and slowing the rising time constant of the VSD signal. The analysis of this parameter to improve the rising time constant of VSD responses is described in Figs. 7.5C,D. The beginning of temporal responses is plotted for several values of the latency scatter (Fig. 7.5C, from 0 to 60 ms with a step of 10 ms). Then, in order to quantify the rising time constant of each response, we use an exponential fitting:

$$F(t) = a + k\left(1 - \frac{e^{-(t - offset)}}{\tau}\right) + k2\left(1 - \frac{e^{-(t - offset)}}{\tau 2}\right)(t >= offset) \qquad (7.5)$$

where a, k, $k2$, τ, $\tau 2$ and $offset$ are the fit parameters. By plotting the rising time constant, i.e. the mean of τ and $\tau 2$, as a function of the latency scatter (Fig. 7.5D), we obtain an optimal value of 50 ms, instead of the 10 ms first introduced (see the Methods section). This value is actually in accordance with several studies investigating the temporal latencies of lagged and non-lagged thalamic cells in response to retinal cells stimulation (Mastronarde, 1987; Harveit and Heggelund, 1992).

Increasing the latency scatter of the LGN inputs provides the expected effect, i.e. reducing the peak of the response onset (Fig. 7.5A2) and increasing the rising time constant (Fig. 7.5B2). The rising time constant of the modeled response (32.3 ms) is now much closer to the experimental one (35 ms). We have also notice that the latency depends on the input frequency of the stimulus (we will nevertheless keep a constant value of 50 ms for all the input frequencies). However, the transient onset and offset of the VSD signal are still faster than the experimental one (notice the response offset in A2 and the zoom of the response onset in B2). Furthermore, the model response still contains a prominent phasic component not present in experimental data.

Our next hypothesis was that the discrepancy in time constants could come from the fact that we modeled an isolated column representing only one pixel of VSDI, compared to the experimental conditions where a whole cortical network integrates the visual stimulation, representing interactions across many pixels. Therefore, in order to take into account an entire hypercolumn of about 750 μm, we reproduced lateral connections existing between our column and its neighbors columns. Each neuron of our column receives excitatory and inhibitory inputs. These lateral inputs were simulated by using

random spike trains whose frequencies were adjusted to the output frequencies of the local network. For example, one pyramidal cell in layer II receives spike trains from neighbors pyramidal and inhibitory cells also in layer II, and the frequency of these spike trains is given by the output mean frequency of pyramidal and inhibitory cells of our local column, for a given thalamic input. Synaptic weight of each lateral connection was adjusted proportionately to the cortical distance between neurons, also influencing the synaptic latency of the connection (Bringuier et al., 1999). Weight distributions for excitatory and inhibitory lateral connections were adjusted according to quantitative biological data taken from Buzas et al. (2006). The effect of adding lateral interactions is reported in Fig. 7.5A3. The global time course of the signal is largely improved thanks to lateral interactions introduction, resulting in a very close correlation between the model and the experimental signals. The transient onset and offset are very close to the experimental one (the rising time constant is 34ms for the model vs. 35ms for the experiment) and the model response was much less phasic, in accordance with the experimental data (Fig. 7.5B3). Interestingly, similar tiny phasic component at the beginning of the response is visible in the experimental and model responses. What happens in this condition is that the tonic component of the global response is boosted by the late lateral component that gradually feeds the modeled column (blue curve in Fig. 7.5E). The resulting dynamics (red curve in Fig. 7.5E) has therefore a residual phasic component that originates from the local integration (black curve in Fig. 7.5E).

Note that we verified that the lateral interactions introduction did not change the input-output functions for the spiking rate and the membrane potential of the neurons (see Figs. 7.4B,D).

7.3.4   Model stability

The model stability was tested by manipulating all the parameters previously quoted, regarding of their responsiveness. In order to prove the relevance of the model, it is important to verify that the model is stable to small variations of the parameters and sensitive to larger variations. For example, we studied in details two important parameters of the local network: the synaptic weights (w) and the number (Nc) of connections. Two main tests are reported in Fig. 7.6. The first one (left panel) shows the sensitivity of the model when removing one group of connections of the network. The second one (right panel) shows that manipulating the synaptic weight (w) and the connections number (Nc) parameters, while keeping the input efficiency constant, does not change the result, as expected. Several other numerical tests have been issued allowing to verify the numerical stability of the result with respect to small variations of parameters values. However, we have also checked that those parameters do change the response
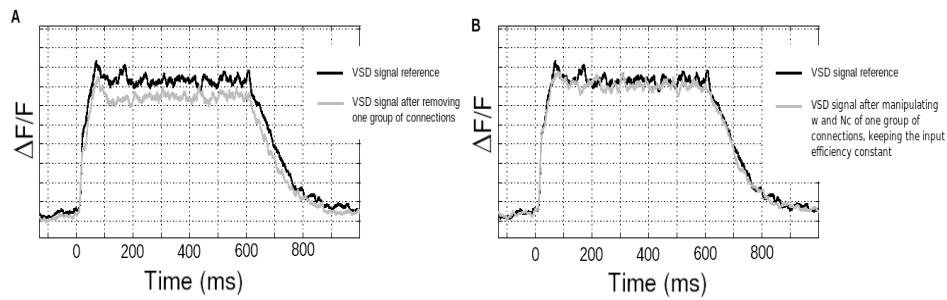
Figure 7.6: Model tolerance: Analysis of the synaptic weight (w) and the connections number (Nc) parameters. *A:* Temporal evolution of the VSD signal before (black curve) and after (gray curve) removing one group of connections ($W_{SP2-->LP5} = 0$). *B:* Temporal evolution of the VSD signal before (black curve) and after (gray curve) applying $W_{SP2-->LP5}/2$ and $Nc_{SP2-->LP5} * 2$. The input efficiency being kept constant, the two curves can be superposed.

for high variations, verifying that their order of magnitude is meaningfull, and their introduction not a redundance.

RESULTS

OVERWIEW

To perform a quantitative analysis of the relative contributions to the VSD signal, a detailed compartmental model was developed in Chapter 7 at a scale corresponding to one pixel of optical imaging.

In this chapter, we confirm and quantify the fact that the VSD signal is the result of an average from multiple components (Section 8.1). Not surprisingly, the compartments that mostly contribute to the signal are the upper layer dendrites of excitatory neurons. However, our model suggests that inhibitory cells, spiking activity and deep layers contributions are also significant and, more unexpected, are dynamically modulated with time and response strength. We discuss these results in Section 8.2.

Contents

8.1 QUANTITATIVE ANALYSIS OF THE VSD SIGNAL SOURCES

We simulated the VSD signal in term of relative fluorescence by taking relative variations of fluorescence (ΔF) compared to the resting level (F) observed at rest. A first important result that can be derived from our model is the actual computation of the fractional signal, comparing the variations of the fluorescence in response to an input with the overall amount of fluorescence emitted by the network at rest (amount of fluorescent emitted when the membrane is fluctuating spontaneously). In the model, evoked response are generally around 10 to 20% of fractional signal ($\frac{\Delta F}{F}$). However, in real experiments, the fractional signal is actually much smaller, usually around 1‰ (see Fig. 7.5). In other words, in our model condition, the fluorescence emitted by the global network at spontaneous level is 5 to 10 times larger than the evoked fluorescent response, whereas, in experimental conditions, the observed global fluorescence at rest is 1000 times larger. If we hypothesize that the amount of emitted fluorescent photons is the same in our model and in experimental conditions, this first result suggests that, in real experiment, the raw signal is mostly composed of experimental induced noise (optical and camera noise, bleaching, physiological noise, spurious staining of non neuronal tissue, etc...) at 99%, fluorescence coming from the network at rest contributes only around 1%, and the evoked signal 1‰.

8.1.1 Correlating the various compartments with the global population signal

Petersen et al. (2003) and Contreras and Palmer (2003) showed that the VSD signal and the membrane potential fluctuations of a single cell are strongly correlated. Here, we first verify that such a correlation is also observed on our model. We then systematically inspected which compartments and which activity type (subthreshold *vs.* spiking rate) are at the origin of the time-course fluctuations of the global VSD signal.

If we superimpose the dynamics of the model VSD signal to one local membrane potential response of one compartment of the model (Fig. 8.1A1), we observe that the VSD signal and the membrane potential changes of a single cell are correlated (Fig. 8.1A2). If we then plot the VSD signal as a function of the spike rate of a population of single cells (Fig. 8.2A1), the correlation is only apparent at the transient onset and offset (input-related signal), but high frequency modulation (noise on the plateau) is not correlated. This result qualitatively confirms that the VSD signal changes are principally arising from synaptic membrane potential fluctuations.

In order to quantify the relationship between the VSD population signal and both
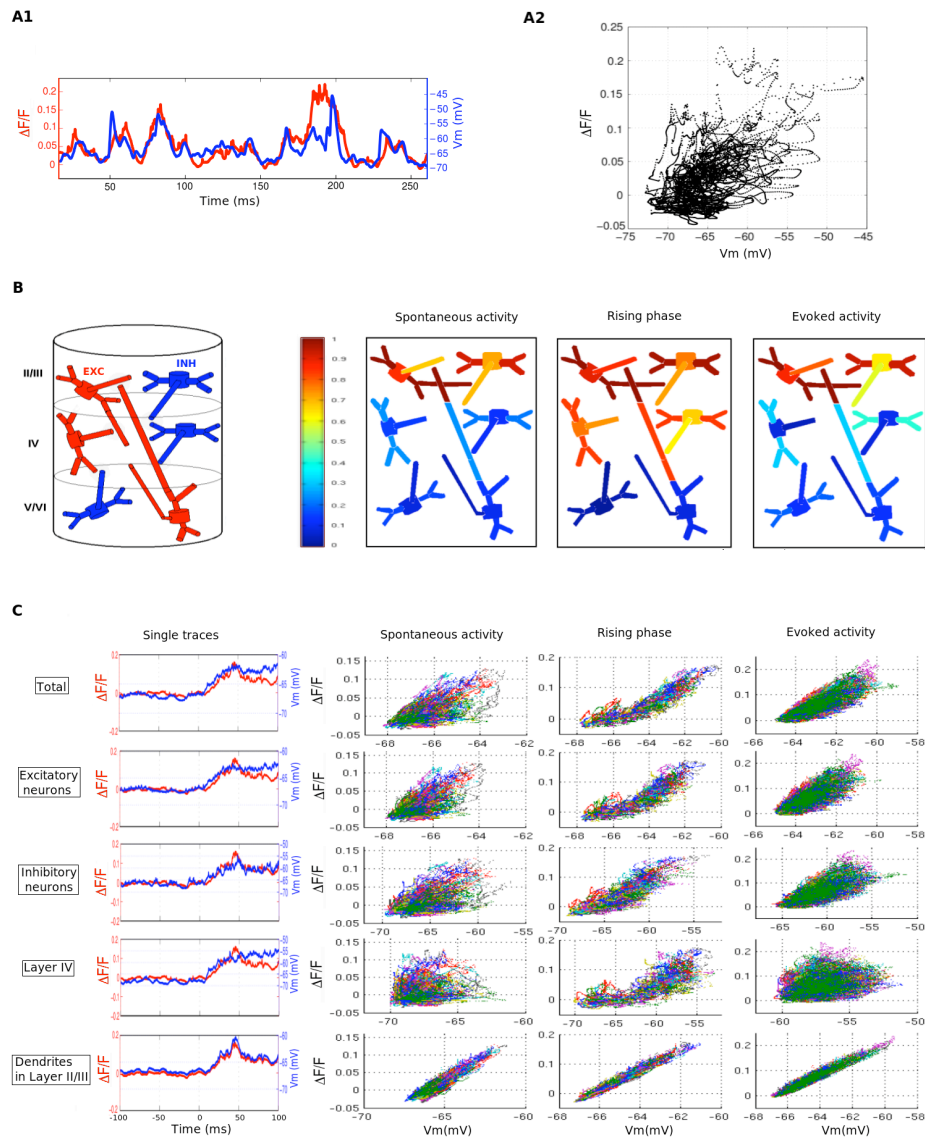
Figure 8.1: Correlating membrane potential fluctuations with VSDI global signal. *A1:* Individual membrane potential response (blue trace), superimposed to the modeled VSD signal (red trace, one trial). *A2:* From A1, the VSD signal is plotted as a function of changes in membrane potential of the individual neuron. *B:* Left: Spatial organization of excitatory (red) and inhibitory (blue) neurons in the column. Right: Graphical representation of the correlation coefficient between the VSD signal and the membrane potential of each compartments as a function of time for an input frequency of 130 Hz. Each frame represents a period of time (in milliseconds). [-200;-20]: Spontaneous activity. [0;50]: Rising phase (time 0 corresponds to the stimulation onset). [50;500]: Evoked activity. *C:* Trial to trial correlation analysis (30 trials) between the VSD signal and the membrane potential of five specific contributions (total, excitatory neurons, inhibitory neurons, layer IV and dendrites in layer V).
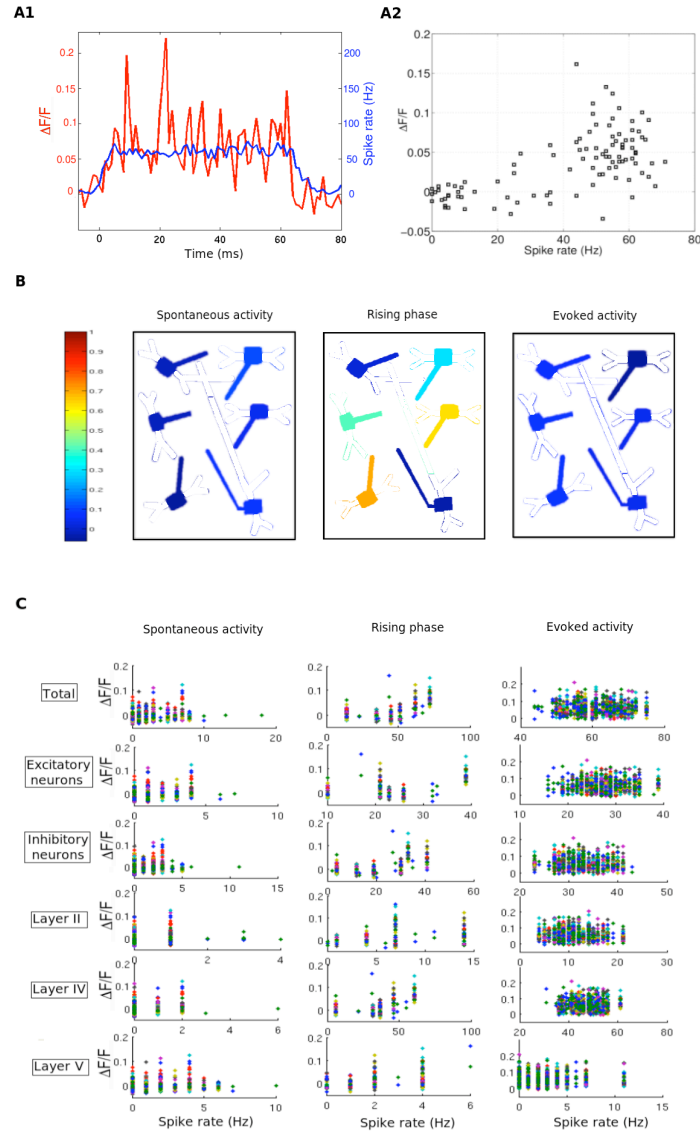
Figure 8.2: Correlating spiking rate with VSDI global signal. *A1:* Post stimulus time histogram constructed over the entire column (blue), giving spike counts per bin (10 ms), superimposed to the modeled VSD signal (red), which was binned at the same value. *A2:* The VSD signal plotted as a function of changes in spike rate of an individual neuron. *B:* Graphical representation of the correlation between the VSD signal and the spike rate of excitatory and inhibitory neurons (somas and axons only) in each layer. Same frames decomposition as previously used. *C:* Trial to trial correlation analysis (30 trials) between the VSD signal and the spike rate of six specific contributions (total, excitatory neurons, inhibitory neurons, layer II, layer IV and layer V).

the membrane potential and the spike rate of neuronal elements, we made a correlation study and quantitatively explored the question with our model by looking at each compartment independently. Figure 8.1B (resp. Fig. 8.2B) shows a frame sequence of our cortical column depicting the temporal evolution of the correlation coefficients (or r^2 coefficients) between the membrane potential (resp. the spike rate) of each single compartment and the total VSD signal. Each frame represents a different period of time (in milliseconds): The spontaneous activity (i.e. when no thalamic input is applied) corresponds to the interval [-200;-20]. The rising phase corresponds to the interval [0;50], time 0 is the time of the stimulation onset. Finally, the evoked or sustained activity (i.e. when the thalamic inputs are applied) corresponds to the interval [50;500]. During spontaneous and evoked activity, as the correlations were very stable over time, we averaged over the whole time period. Centered on the rising phase of the response, this representation provides a direct comparison of the correlations between on-going and evoked activity. The trial-to-trial analysis for five (resp. six) specific components is reported in Fig. 8.1C (resp. Fig. 8.2C).

Three main results emerge from this correlation study, either concerning input-related changes or high frequencies fluctuations of the signal: (1) The VSD signal is much more correlated with membrane potential than with spikes. The spiking activity of pyramidal neurons in layer II globally explains 2% of the VSD variance, whereas membrane potential of pyramidal neurons in layer II explains 78%. (2) Not surprisingly (see the signal computation part in Method), the VSD signal is mostly correlated with membrane potential of dendrites in superficial layers (last row in Fig. 8.1C). The maximal correlation coefficient that we obtained for all compartments, signal and time period was 0.96 for the rising phase of superficial layers depolarization. (3) At the stimulation onset, the correlation between the VSD signal and membrane potential of compartments in layer IV largely increases (from 0.13 to 0.72), the same being true for spiking activity (from 0.02 to 0.52). The latter result is clearly visible in the rising phase frame in Figs. 8.1B and 8.2B, and also in the trial to trial analysis of Fig. 8.1C (fourth row), where the best correlation between VSD signals and layer IV membrane potential is found at the rising phase, i.e. the phase occurring at the stimulation onset delineating spontaneous activity from evoked activity. This increase is due to the thalamic input providing a strong and local input in layer IV, thereby increasing temporarily the correlation with the VSD signal.

Three others results are also interesting to notice: (4) On-going and evoked activity present almost the same correlation coefficients (Fig. 8.1B, Fig. 8.2B). (5) Excitatory and inhibitory neurons show very similar correlation with the VSD signal. Lastly, (6) spiking activity of inhibitory neurons are more correlated to the VSD signal than excitatory neurons ($r^2 = 0.3$ for inhibitory neurons in layer II, in comparison to 0.015 for respective

excitatory neurons).

We therefore observe that there are dynamic changes of compartments correlations to the global VSD signal at a given thalamic input strength. However, as we previously mentioned, the balance between activity level in these various compartments will change when the input strength varies. We will now therefore inspect how the activity level affect the different contributions to the VSD global signal.

8.1.2   Contributions of the VSD signal when increasing the level of input activity

To investigate how changing the input frequency can affect the contribution of the various compartments to the population signal, we reproduced another VSDI experiment where the stimulus contrast was gradually increased (see Reynaud et al., 2007, seven contrasts presented) by computing the temporal evolution of the total VSD signal for seven different thalamic rates (Figs. 8.3A,B). The set of modeled VSD responses are very close to that of experimental signals at plateau values. The total VSD signal, averaged during 600 ms, is plotted as a function of input rate to be compared with the experimental contrast response function (Figs. 8.3C,D). This quantitative representation illustrates that the experimental and the model curves indeed have a very similar shape, both fitted by Naka Rushton function. Our global columnar activation is therefore behaving very closely to the biological column recorded experimentally.

However, note that there is a difference in the VSD time course. Experimentally, it is interesting to observe that, in response to a small drifting grating, the experimental VSD (Fig. 8.3A) is slower than the one measured in response to a static gaussian luminance stimulus (Fig. 7.5). We believe that this difference comes from the dynamic of the stimulus: Modulation of the contrast in time is differentially integrated in Simple and Complex cells and we believe that this slows down the VSDl time course. However, our current model was not designed for such a detailed columnar organization. Our assumption is that, when the response reaches a plateau, the contrast response function of the model and the experimental data can be compared based on the effect of contrast.

Following the previous formula (Eq. 7.4), we can now decompose the VSD signal in its different contributions: excitation, inhibition, somas, axons, dendrites, layer II, layer IV and layer V, and see how their participation to the global signal changes for different levels of input activity. Here we use our model to quantitatively predict the different contributions of the VSD signal, as a function of thalamic increasing input (Fig. 8.4). For all contributions, we computed the ratios as the amount of VSD signal from one compartment divided by the total VSD signal.

First, we looked at the relative contribution of excitation versus inhibition (Fig. 8.4A).
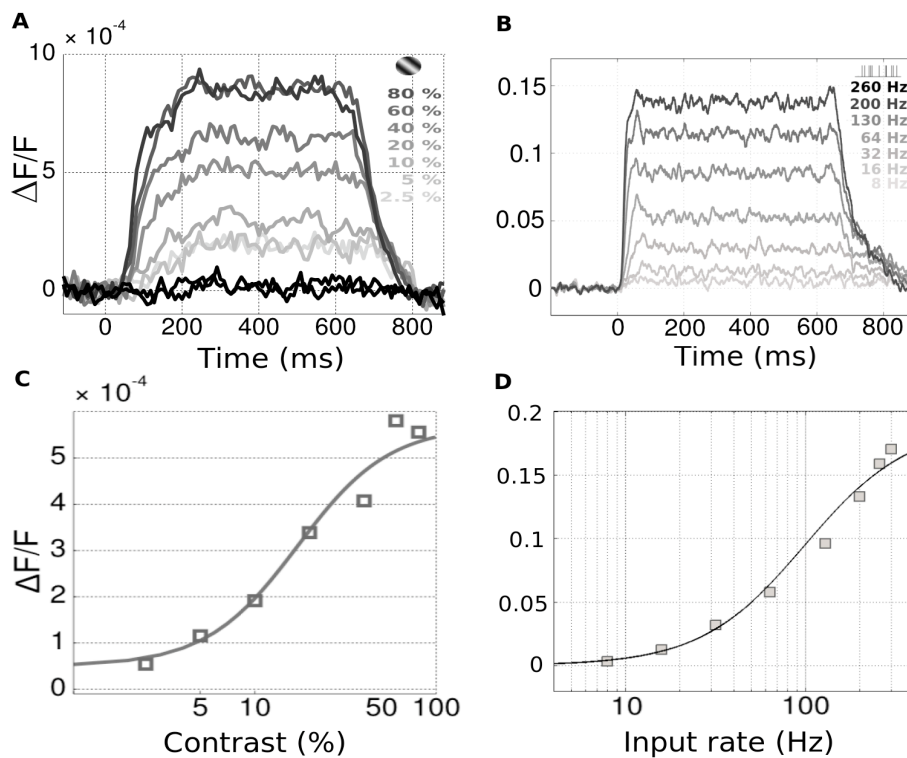
Figure 8.3: Total VSD signal computed from the entire network (local connectivity + lateral interactions) and plotted as a function of thalamic input rate. *Left*: VSDI experiment on monkey using VSDI (Reynaud et al., 2007). The experimental VSD signal is plotted as a function of time and in response to different input contrasts. *Right*: Model, each response is the average of the VSD signal for 100 repetitions of a given input rate.
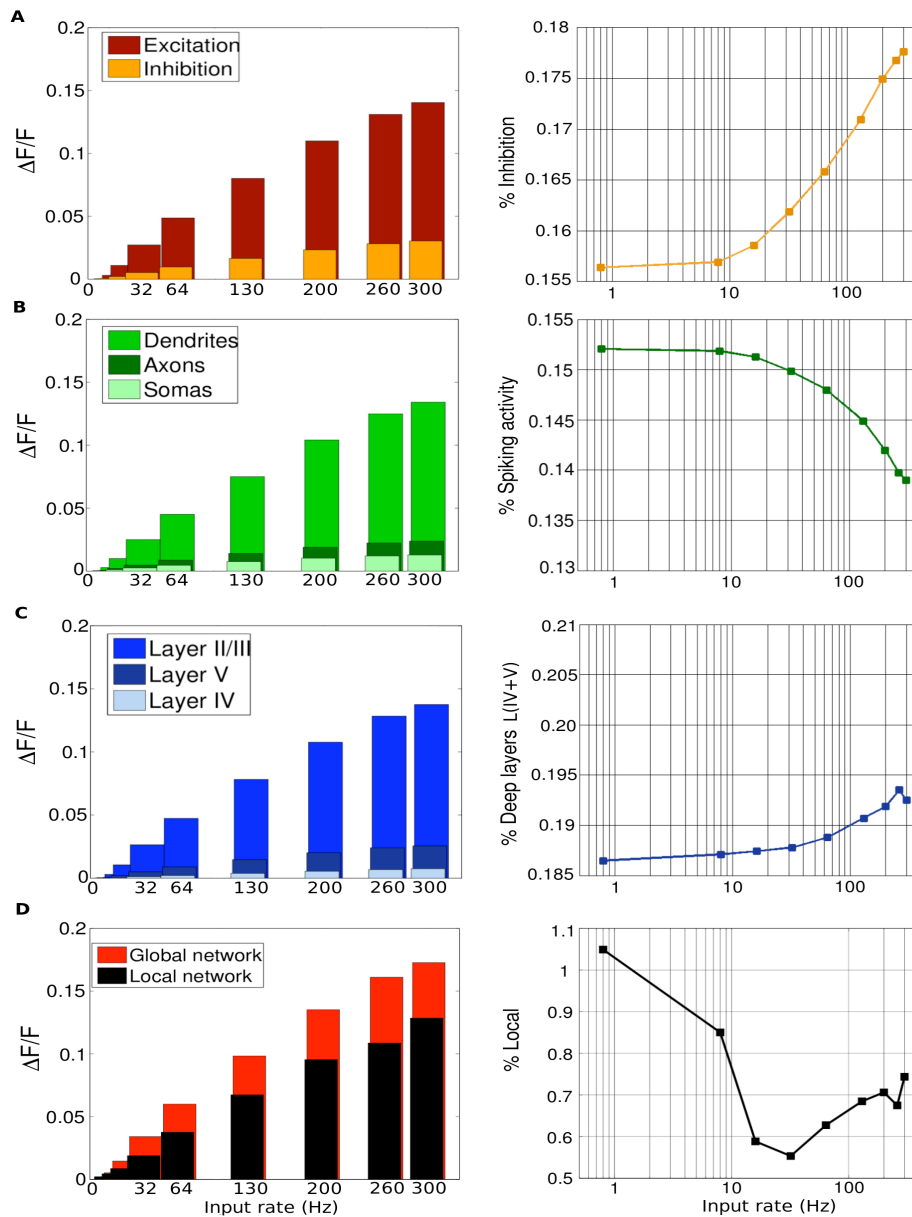
Figure 8.4: VSD responses in function of thalamic input rate showing quantitatively the different contributions of the VSD signal when increasing the level of input activity. The rationale between the different contributions are plotted in the right column. *A*: Excitation and inhibition contributions. The ratio inhibition/excitation shows that inhibition contribution lightly increases with input rate. *B*: Somas, axons and dendrites contributions. The ratio between axonic and dendritic activity is weakly decreasing with input rate. *C*: Layers contributions. Deep layers contribution weakly increases with input rate, as shown by the ratio in the right. *D*: Local vs. global contributions. The ratio between local and global activity shows that local activity contribution decreases when increasing the input activity.

Globally, excitatory cells are responsible of 83% of the total VSD response, and inhibitory cells participation represents 17% of the VSD signal. The ratio between inhibition and excitation (see right panel) shows that inhibition contribution increases with input rate, about 2.5% from low to high levels of activity. The proportion of inhibitory cell contribution is less than predicted on the sole basis of activity level and proportion of cellular types, demonstrating the utility of using such a model (see Discussion). Indeed, if one simply inspects what is the contribution of inhibition when decomposed at the level of dendrites soma and axons (Fig. 8.5A), we noticed that inhibitory dendrites contribute more than axons and somas. This might be caused by (i) spike thresholding that occurs at the soma, (ii) small spike width of inhibitory cells that minors the inhibitory spiking contribution, and (iii) inhibition that shunts membrane potential at the soma and not at the dendrites.

We then investigate whether the post-synaptic activity contributes differently than spiking activity (Fig. 8.4B). Globally, 77% of the optical signal comes from dendritic post-synaptic activity. The ratio between axonic and dendritic activity is decreasing with input rate, but weakly, suggesting that synaptic activity is even stronger at high level of activity. We attribute this increase in the fact that subthreshold PSPs at dendritic locations are not thresholded by spike generation, whereas spiking activity saturates at high level of activity. In other words, PSPs size continue to increase whereas spiking activity reaches a saturation plateau (see Fig. 8.5B for an illustration).
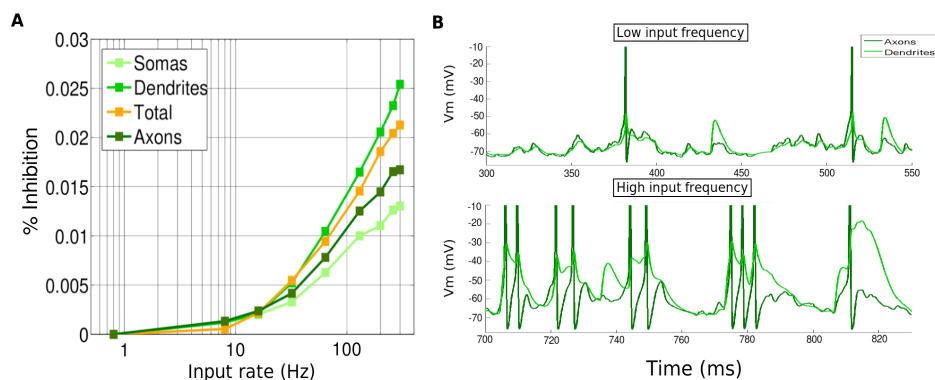
Figure 8.5: Decomposition of the inhibition contribution. *A*: Contributions of the different part of the neuron (somas, axons, dendrites) to the inhibition contribution. *B*: Dendritic and axonic activity of an individual neuron in layer II/III for low vs. high level of input activity.

What are the participation of cells belonging to deep layers in the global signal (Fig. 8.4C)? As expected, the optical signal mostly originates from layers II/III neurons (81%), but, the model shows that 19% of the signal in layer II/III comes from the superficial dendrites of deep layers neurons (layers IV and V). The ratio between deep and superficial neurons shows a tiny increase of deep layers contribution with input rate.

Finally, we quantified whether the proportion of activity arising from the local connectivity changes with input rate (Fig. 8.4D). The ratio is largely decreasing when increasing the input rate, showing that local activity contribution decreases with input rate. At low input, the signal is only coming from local recurrent activity (100%) and decreases to 50% for higher input frequency. The rest of the VSD global signal is coming from inputs from lateral connectivity that contribute more and more for increasing input rate.

Thereby, the model quantifies the fact that 80% of the VSD signal originates from dendritic activity of excitatory neurons in superficial layers. However, inhibitory cells, spiking activity and deep layers represent about 20% of the total that is non-negligible. The VSD signal should be considered as a dynamic signal whose constitution depends on time and activity levels.

8.2 DISCUSSION OF THE RESULTS

8.2.1 Summary and major results

The purpose of this work was to better understand what exactly the voltage-sensitive dye imaging signal measures. This question is indeed difficult to resolve at the physiological level since the signal is multi-component: The dye reflects the dynamics of the membrane potential of all membranes in the neuronal tissue, including all layers of the circuitry, all cell types (excitatory, inhibitory, glial) and all neuronal compartments (somas, axons, dendrites). However, no real quantitative analysis have been done in the literature and the origin of the VSD signal remain unresolved. Experimentally, this quantification is very difficult to realize *in vitro* and quasi impossible *in vivo*. Qualitatively, it is assumed that the VSD signal in a given pixel mostly originates from the dendrites of upper layers cortical cells, and therefore, mainly reflects dendritic activity (Grinvald and Hildesheim, 2004). In the same manner, authors in Lippert et al. (2007) looked at the distribution of fluorescence intensity to say that the VSD signal mostly originates from superficial layers (I-III) without taking into account the fact that activity in superficial layers could be provided by neurons in deep layers. It is the case if one considers the morphology of layer V and VI cortical neurons, whose apical dendrites do reach superficial layers (Thomson and Bannister, 2003).
To perform a quantitative analysis taking into account all these details, we used a realistic biophysical cortical column model, at a mesoscopic scale, with biological and electrical neural parameters of the laminar cortical structure. The model is based on a cortical mi-

crocircuit, whose synaptic connections are made between six specific populations of neurons, excitatory and inhibitory neurons in three main layers. Each neuron is represented by a reduced compartmental description with conductance-based Hodgkin-Huxley neuron model. The model is fed by a thalamic input with different levels of activity together with a continuous background activity and lateral connections, and offers the possibility to compute the VSD signal with a linear formula. We validated the model by comparing simulated and experimental VSD signals.

The model predicts the different contributions of this signal. As expected, the VSD signal mainly reflects dendritic activity (77%) of excitatory neurons (83%) in superficial layers (81%). However, inhibitory cells (17%), spiking activity (23%) and deep layers (19%) represent about 20% of the total signal that is non-negligible and should be taken into account in the interpretation of the VSD signal. Importantly, the contributions of these compartments change as a function of the general level of input activity, suggesting that the VSD signal has a dynamical multi-component origin. This result is reinforced by a correlation analysis that unveils a stronger involvement of layer IV neurons and inhibitory spiking activity during transient input (onset of the stimulus for example).

8.2.2 Dissecting the VSD signal

Excitatory vs. Inhibitory contribution

Our model's results suggest that the contribution of inhibitory cells to the global VSD signal increases with increasing input, from 15.6% to 17.8%. Could these results be predicted just on the basis of numbers the model was fed with?

To infer the overall inhibitory contribution to the VSD signal, one should take into account the fact that inhibitory cells are four times less numerous than excitatory cells, but also the cellular morphology difference between stellate vs. pyramidal neurons (larger membrane surface). In our model, following table 8.1, the membrane surface integrated over all inhibitory compartments represents only 12% of total membrane surface. This is lower than our observation and may be explained if now one takes into account activity level.

Neurons	Pyramidal L2	Pyramidal L5	Spiny Stellate L4	Smooth Stellate
Number	50	48	45	37
Total membrane surface (μm^2)	8218.4	21971.5	6694.7	6694.7

Table 8.1: Membrane surface of the modeled neuronal types.

Indeed, inhibitory cells are following the input with a higher spiking rate and subthreshold depolarization (see Fig. 7.4). Inhibitory spiking rate can indeed increase 3-4

times faster than excitatory spiking rate (Nowak et al., 2003). Therefore, as a first expectation, inhibitory cells should contribute more and more to the VSD signal for higher input rate. However, a deeper look at these values, tuned to fit experimental observations (Contreras and Palmer (2003)), actually shows that the ratio of inhibitory spiking activity over the sum of excitatory and inhibitory spiking rate does not change with increasing input rate (stays around 77%). At the level of membrane potential depolarization, the ratio is even decreasing from 75% to 62%.

This departs from our model prediction that inhibitory contribution actually increases with input rate. Deviation from such simple linear predictions originates from the multiple non-linearities that actually control the model behavior, and supposedly the actual biological network. For example, non-linearities exist in the conductance-based inhibition and spike generation that constraint membrane potential dynamics at the somatic level. When we decompose the contribution of inhibition at the level of dendrites, soma and axons (Fig. 8.5A), we indeed observe that the spike thresholding and spike width (smaller for inhibitory cells) strongly minor the inhibitory contribution. These observation demonstrates the need of this detailed biophysical model that takes into account all the details to make an exact estimation of the relative contribution of inhibition and excitation.

Synaptic vs. Spiking activity contribution

Similarly, the relative contribution of subthreshold vs. spiking activity is difficult to predict a priori. One would also have to take into account on one hand, linear parameters such as the smaller depolarization area under spiking activity, but also the smaller surface of axons compared to dendritic trees. On the other hand, non-linear interaction parameters as mentioned above are also present. Our model predicts that the overall contribution of pure spiking activity (on axons) to VSDI is of the order of 14%. Importantly, it also predicts that this contribution will decrease with input strength from 15.2% to 13.8%. We explain this decrease by the major contribution to VSD signal of synaptic activity in dendritic arborization of upper layers that is not constrained by membrane potential clamping occuring in the soma because of spikes or inhibitory conductances (Fig. 8.5B).

An important additional information is coming from the studies of temporal correlation between different compartments and the global VSD signal. The high frequency variation of the global VSD signal is mostly due to dendritic activity. Importantly, the global VSD signal variance is equally well explained for excitatory and inhibitory neurons, and for spontaneous and evoked activity. This correlation study also informed us that, during the response transient phase, the VSD signal becomes strongly correlated to activity of layer IV neurons (in accordance with Bush and Priebe, 1998) and also to spiking activity

of inhibitory neurons. This brings us to the conclusion that VSD transient and sustained phases have different origins. It may have important consequence when interpreting the signal, especially regarding to more complex natural visual stimuli, which contain many transients (Kremkow, 2009).

Thalamic vs. lateral inputs

The previous results suggest that the relative contribution of all compartments are not only a function of input strenght, but also of time, transient and sustained input having different impact on the recurrent cortical column (Douglas and Martin, 1991; Borg-Graham et al., 1998; Muller et al., 2001; Crowder et al., 2008; Stoelzel et al., 2008). More precisely, it is interesting to note that the synchrony of thalamic input generates a strong transient in the VSD signal that is attenuated by onset asynchronies and the presence of horizontal inputs (Fig. 7.5). However, a small phasic component is always present in the model and also in the observed response. This is strongly reminiscent of the so-called "notch" component introduced by Sharon and Grinvald (2002), identified by these authors as "a small transient drop in the rate at which the evoked response increased (...) which we term the evoked deceleration-acceleration (DA) notch". Our model suggests that this notch is the residual of a phasic response to stimulus onset, hidden under a large horizontal convergence of input from neighboring columns. One prediction of our model is therefore that the time constant of VSD signal is slowed down by horizontal converging input, that contributes more and more with time (Fig. 7.5E) and with increasing contrast (Fig. 8.4D). The VSD response is thus dynamic, from local to global activity with a time constant of about 100 ms (Fig. 7.5E).

Layers contribution

When we look at the contribution of lower layers, our result shows that, even if the dye gradient we chose is favoring dramatically upper layers (95%), cells in layer IV or layers V/VI contribute more than expected by the dye gradient. This is because activity in superficial layers is also provided by layers V and VI pyramidal neurons, whose apical dendrites do reach superficial layers (Thomson and Bannister, 2003). Because of the presence, in upper layers, of dendrites of lower layers, the contribution is four times more than what the gradient imposed (19% instead of 5%). In this model we used the distribution of fluorescence intensity estimated by Lippert et al. (2007) who concluded that the VSD signal mostly originates from superficial layers (I-III). One can question how much the dye gradient indeed interferes with our results. The only quantitative data on dye gradient comes from experiments on the rodent model by Kleinfeld and Delaney (1996); Petersen et al. (2003) and Lippert et al. (2007). Following the staining depth of the dye, the authors concluded that the VSD signals originate from superficial

cortical layers I-III. Their staining procedures on rat barrel and visual cortices however differ from that used on higher mammal species like monkey. We have therefore tested other ad-hoc values of dye gradient. When choosing striking different values ($\lambda^2 = 0.6$, $\lambda^4 = 0.3$ and $\lambda^5 = 0.1$), it appears that neither the relative contributions of the different components (excitation, inhibition, spiking activity, synaptic activity), nor their global evolution when increasing the level of input activity, have changed. As expected, the relative contribution of the different layers has obviously changed. For these values, 45% of the total signal comes from neurons in layer II/III, 20% from neurons in layer IV and 35% from neurons in layer V. The latter contribution can be decomposed into more precise quantities: 7% is from dendrites found in layer II/III, but belonging to layer V pyramidal cells, 20% is from dendrites found in layer IV but also belonging to layer V pyramidal cells and the last 8% is actually from neurons in layer V.

Part IV

Discussion

GENERAL DISCUSSION

OVERVIEW

In this final chapter, we will discuss the achievements and limitations of the present direct model of VSD signals. Possible improvements and future perspectives are also proposed. A general conclusion about this thesis is given at the end.

Contents

9.1   MODEL ACHIEVEMENTS AND PERSPECTIVES ⎯⎯⎯⎯⎯

9.1.1   A detailed biophysical model of layer II/III, IV and V neurons

This work investigates a problem of significant importance to neuroscience: The distribution of the voltage activity as measured by VSDI. It is known that the VSD signal stems from the membranes that are stained in the cortex, i.e. dendrites, axons and somata of the neurons as well as the glia cells (Grinvald and Hildesheim, 2004). However, it is not known to what extent this signal originates from inhibitory or excitatory neuron membrane potentials, or to what extent spiking activity influences the signal. These questions are important, as VSDI is becoming an increasingly used tool to study changes in population membrane potentials. We addresses this issue through a computational simulation of a biophysical cortical column comprised of 180 multi-comparments HH neurons in 3 main layers (II/III, IV, V). This column has a lateral area of 50x50 μm^2, corresponding to one pixel of optical imaging. We use the percentage dye of attenuation from the literature to calculate the contributions of our up to seven compartments neurons located in the supragranular, granular and infragranular layers and evaluate the different components of the VSD signal recorded *in vivo*. The main result is that the membrane compartment of supragranular layers contribute the most and especially the dendrites of the excitatory neurons. However, also dendrites of inhibitory cells and even spiking activity contribute significantly to the signal at high spiking rates.

Furthermore, we believe that these global observations will not be affected by improving the microscopic level or enlarging the mesoscopic aspect of the model. Rather, this study is the first attempt to better apprehend this complex signal and should help interpreting and designing VSDI experiments. We hope that further developments of such direct models will allow to help solving the inverse problem.

9.1.2   A model simple enough for answering the addressed questions

The present work shows that there were a need to develop a model at an intermediate scale between the so-called microscopic and mesoscopic scales. This simple compartmental model (only 7 compartments per neurons) is detailed enough in order to simulate and better understand which part of the neuron is involved in the generation of the dye signal, while it is simple enough to both derive tractable numerical simulations, and (more importantly) do not over-parametrize the problem.

A more detailed model of the neuron would have allow us to play with a larger number of parameters, may be allowing to encounter for "any" signal, so that the related interpretation would have been subject to caution. We would indeed have gain something

considering a more detailed model (for instance introducing some knowledge about the topography of the connection structure), but it is not clear that we would have learn more regarding the biophysical interpretation of the dye signal generation. It is anyway, thanks to the chosen method and the underlying software tools, very easy to enrich the present model of our pixelic column, as soon as a new interrogation regarding another aspect of the biological sources of this signal arises.

In fact, our position here was to use the *minimal* model which could integrate the data available in the literature, and which was relevant for the addressed questions.

9.1.3 Model reliability and software contribution

Although we modeled in details only a unique cortical column of 50 x 50 microns^2 lateral area, we reproduced the activity of an entire hypercolumn of about 750 μm by simulating continuous background activity and lateral connectivity between neighboring cortical columns. In order to calibrate neurons responses, we used optimization algorithms to select model parameters in accordance with experimental observations, both at single cell (Nowak et al., 2003) and fully connected network (Contreras and Palmer, 2003). By doing a stability analysis, we verified the reliability of the model with respect to small and large variations in parameters values.

The model was built step by step, i.e. single neurons, local network, background activity and then lateral interactions, in order to control precisely the action of each parameter and, as explained above, to find the minimal number of parameters required for reliably reproduce the VSD signal, as obtained experimentally using VSDI on monkey primary visual cortex.

The construction of such a realistic model has demanded a computational effort. However, thanks to the NEURON and neuroConstruct softwares, the implementation task was substantially reduced. The model code should be available soon in the ModelDB database, associated with a NeuroImage paper.

9.1.4 Reverse engineering

Once we have shown that the VSD signal is multi-composite and that the various contributions are a function of time and contrast, we may wonder whether reverse engineering is feasible? In other words, from the actual VSD signal, would it be possible to predict the contribution of the various components? This work showed that four unknown variables (contributions of the different compartments) are a function of two known variables (contrast and time here). Ideally, one would like to find two more known variables that would control the unknowns differentially. From there, theoretically at least, we could reconstruct the relative contributions of all these variables from the global VSD signal.

However, for that purpose, the model would need to be improved drastically to represent more functional parameters. Indeed, adding the notion of receptive field encoding orientation and position parameters could lead to a well-posed reverse problem (assuming linear equations), with four unknowns and four variable parameters (contrast, time, orientation and position). Therefore, for one given pixel, these four parameters could be varied in real VSDI, leading to a set of experimental recordings that could be used to adjust our model for reverse-engineering. This, ideally, could allow us to find back the origin of the signal.

Direct perspective: Modeling an orientation column

We thus wish to improve our model in the future to represent more functional parameter spaces in order to better constraint the various compartments participation to the global VSD signal.

A direct perspective is to increase the model size towards a larger network, accounting for columnar cortical architecture such as orientation maps. With such a model, new questions could be addressed, for example, trying to explain why VSDI signal has such a poor orientation selectivity (Sharon and Grinvald, 2002). Indeed, the response of any orientation column to a stimulus oriented orthogonal to the preferred direction is about 80% of the maximum response (Grinvald et al., 1999). In comparison, for the orthogonal stimulus, neurons have spiking response that is nearly null (5% of the maximum) and subthreshold activation a bit more than 20% of the maximum response (Monier et al., 2003). Therefore, a model at this stage would help understanding where the remaining 60% of activation in the global VSD signal is coming from. To enlarge the model with orientation selectivity, a large amount of improvements would be needed (see Ferster and Miller, 2000; Shapley et al., 2007, for reviews). For example, higher degree of specific lateral interactions among distant columns of varying orientation selectivity should be implemented.

9.1.5   Generalization of the cortical column model to other areas, species and signals

This model of cortical column was built based on anatomical and electrophysiological data from primary visual cortex of cats and monkeys. However, as reviewed in Chapter 2, the cortical column has a stereotypical neural microcircuit, which is repeated throughout the neocortex. Hence, when choosing appropriate values of parameters which depend on species and cortical areas (e.g. number of neurons, number of synapses per neuron), we believe that the proposed model could be used as a more general model of VSD activation, independently on cortical areas and species.

An other generalization, directly derives from this observation, can be made regarding to the model application. The model was specifically designed for studying the VSD signal sources. However, with minor modifications, our model should also be suitable for other measurements. For example, as briefly presented in Chapter 3, the LFP is the low-frequency part of extracellular recordings and is often attributed to synaptic activity of a large number of cells near the recording electrode. However, as VSDI, there is a lack in the exact origin of this signal, in particular with respect to the spatial arrangement of nearby neurons and the dynamics of the underlying spiking activity. Such a compartmental model could then possibly allow to compute the LFP signal as a weighted sum of each compartmental transmembrane currents (Pettersen et al., 2008). Although, to achieve this goal, we would need to increase the size of the cortical column ($> 200 \ \mu$m) and a model of extracellular flux would be necessary to integrate local current sources (Bedard et al., 2004; Bedard and Destexhe, 2009).

9.2 MODEL LIMITATIONS

9.2.1 Is the biophysical model detailed enough?

We only model in detail the pixelic column, even if we tried to increase the model size by simulating the neural substrate around this set of neurons through a reduce set of stochastic spiking sources as made explicit previously in the model specifications (see Section 7.2). This is clearly a weakness which potentially restricts the model's reliability, and an interesting perspective of the present work is to duplicate and to simulate several instances of the present model interacting as -up to our best present knowledge- in the *in vivo* context. At the implementation level, enlarging the model would require a higher order of magnitude of calculation, which is easily realizable on a cluster (though this is far beyond the present work), the underlying NEURON software having this parallelization capability. Another track is to make our model interact with a mesoscopic model of the V1 laminar network (i.e. a model considering a large network of punctual spiking neurons), in order the present pixelic column to be stimulated, but by more realistic inputs that pure stochastic inputs. At the implementation level, this requires the capability to have several neural simulators interoperable (i.e. a meta-simulator), which is realizable nowadays with the PyNN meta-simulation platform (Davison et al., 2009), though the present software tools are still at the development stage. In both cases, we hypothesize that the main improvements on the present biophysical model are towards the mesoscopic scale, looking for a better understanding of the interaction of the column

with the rest of the network, rather than looking for more details at the microscopic scale.

We also wonder whether a very detailed model like the Blue Brain Project developed by Markram (2006) could be adequate for our objectives. This impressive project recreates, down to the level of biologically accurate individual neurons, the neocortical column (0.5 by 2 mm containing 10,000 neurons) of a juvenile rat. It thus corresponds to the *macrocolumn* definition proposed in Chapter 2. As a direct consequence of this complexity, the simulation of this model requires a special calculator with a huge computational capacity. Such a model must then be able to compute and reproduce very accurately VSD signals. However, with its huge number of parameters, it would be difficult to make predictions on the links between model parameters and VSD observations. Although very reliable, this model could actually be too detailed to precisely answer the addressed questions concerning the VSD signal origin.

9.2.2   Inadequacies with experimental data

Although the model accurately reproduces the VSD signal, there are some experimental results, listed below, with which it is not consistent. However, these discrepancies are mainly due to the minimalism of the model.

More realistic thalamic input

The present model does not have a realistic representation of the LGN drive. Indeed, in the present study, inputs signals from the thalamus into neurons in layer IV are simulated by applying random spike trains of a given averaged discharge frequency. This solution was good enough to reproduce experiments with static stimuli or simply inspecting the impact of increasing contrast. However, as seen in Fig 7.5A when no latency adjustment is applied, the leading edge of the response is too early in time, as well as in Fig. 8.3 for more complex stimulus representation, i.e. drifting sinusoidal grating, within a larger network. It would thus be necessary to improve the thalamic input with a phasic-tonic representation as implement by (Gazeres et al., 1998). Actually, we may suppose that a more accurate model of the LGN drive would remove these discrepancies almost automatically.

Saturation at high contrasts

A potential perspective and improvement for the model would be the introduction of new non-linearities and test how much they affect our results. For example, we could introduce synaptic depression at thalamocortical synapses, suggested to play an important

role in contrast gain control mechanisms (Carandini et al., 2002). Indeed unlike contrast response function of V1 neurons presented in Chapter 1, Section 1.2, our modeled neurons do not completely saturate at high input rates (see Fig. 7.4). We thus think that our model could benefit from the introduction of the model proposed by Tsodyks et al. (1998). Moreover, the authors have proposed a NEURON implementation of a model of short-term synaptic plasticity, so it would be easy to implement it in our biophysical neurons model.

Detailed representation of long-range connections

The present model contains no detailed representation of the long-range lateral connections, nor does it contains any $NMDA$ channels. In comparison, the large scale cortical model of (Rangan et al., 2005) (see Chapter 6), although restricted to a single layer and to point neurons, does contain a realistic number of ion channels and extends laterally over several mm^2. Spiking neurons over large cortical distances are connected by long-range connections through $AMPA$ and $NMDA$ synapses. The authors claimed that these slow $NMDA$ conductances (see Fig. 1.4) allow to capture the behavior of *in vivo* spontaneous activity. Although they showed that only a very small ratio of $NMDA$ contribution (5%) provides the desired features, they also stated that without these $NMDA$ receptors, cells spontaneous activity is not consistent with *in vivo* experimental observations in the cat visual cortex anymore (Cai et al., 2005).

We thus wonder whether these observations on large scale point neurons models of a single cortical layer may propose some conjectures about possible origins of the discrepancies mentioned above. Perhaps our model, missing long-range connections arising from a large network with slow $NMDA$ conductances (and not just simulated lateral connections), operates too independent spatially, without the correlations in spiking activity induced by long-range correlations (Cai et al., 2005). The spontaneous activity produced by this "spatially independent" behavior of individual neurons within the model might thus be too small compared with experimental *in vivo* spontaneous activity. Moreover, $NMDA$, with its slow decay time, could also account for the experimental discrepancy associated with Figure 8.3A.

9.3 GENERAL CONCLUSION

In this thesis, we have emphasized the voltage-sensitive dyes imaging (VSDI) technique (Chapter 5), among the large panoply of techniques available to observe brain structures (Chapter 3). This optical method, thanks to its excellent spatial and tempo-

ral resolution, offers many possibilities for *in vitro* and more interestingly *in vivo* brain imaging. However, the recorded optical signal is multi-component and its origins are still unresolved. Indeed, no real quantitative analysis have been done in the literature since the contribution of each component, i.e. glial cells, excitatory cells, inhibitory cells, somas, axons, dendrites, layers, is very difficult to isolate from each others.

The main objective of this thesis was therefore to better understand what exactly the voltage-sensitive dye imaging signal measures and to raise awareness on its dynamical origin. To perform this quantitative analysis, this work suggested modeling as the appropriate solution. We started by looking in details at the columnar organization of the cerebral cortex, and more precisely of the primary visual cortex (Chapters 1 and 2), emphasizing the columnar structure as an appropriate model for our purpose (Chapter 4). We have then reviewed five existing models aiming at reproducing the VSD signal. The main advantage of those models was the ability to compare the same signal, i.e. the signal of an entire cortical area (Chapter 6). However, for our considerations, i.e. to find the different contributions of the VSD signal, none of those models was detailed enough.

We thus proposed a detailed biophysical cortical column model with compartmental neurons based on experimental data (Chapter 7), which allows to compute linearly the VSD signal taking into account the level of depolarization of each compartment, membrane surface and staining. On one hand, our model enables to have a realistic estimation of the relative contributions of the various components constituting the global signal (Chapter 8). On the other hand, it revealed that the composition of the signal is highly dynamic and depends on input strength and transience.

Finally, we discussed the advantages and limitations of our modeling approach, as well as further short- and medium-term perspectives, in order to improve the reliability of the model (Chapter 9).

Conclusion générale (en français)

Dans cette thèse, nous avons mis l'accent sur la technique d'imagerie optique basée sur l'utilisation de colorants sensibles au potentiel de membrane (VSDI, Chapitre 5), parmi la multitude de techniques disponibles aujourd'hui pour observer les structures du cerveau (Chapitre 3). Cette méthode optique offre de nombreuses possibilités en terme d'imagerie cérébrale *in vitro* et *in vivo*, grâce à son excellente résolution spatiale et temporelle. Cependant, le signal optique enregistré a plusieurs composantes et ses origines restent encore en grande partie inconnues. En effet, il est difficile de trouver dans la littérature une analyse quantitative de l'origine du signal VSD car les contributions de chaque composante, i.e. cellules gliales, excitatrices, inhibitrices, somas, axons, dendrites, couches, sont très difficiles à isoler les unes des autres par une mesure physiologique.

Le travail majeur de cette thèse a donc été de réaliser cette analyse quantitative pour mieux comprendre les origines du signal VSD, qui s'avéreront être dynamiques. La modélisation s'est alors présentée naturellement comme une solution appropriée. Nous avons commencé par regarder en détail l'organisation en colonnes du cortex cérébral et plus précisément du cortex visuel primaire (Chapitres 1 et 2), mettant l'accent sur la structure columnaire comme modèle adapté à notre objectif (Chapitre 4). Nous avons alors passé en revue cinq modèles de la littérature permettant de reproduire le signal VSD (Chapitre 6). Cependant, aucun de ses modéles n'a été construit dans le but de pouvoir déterminer les différentes contributions du signal.

Nous avons donc proposé un modèle biophysique de colonne corticale avec des neurones à compartiments basé sur des données expérimentales (Chapitre 7), qui nous a permis de calculer linéairement le signal VSD en prenant en considération le niveau de dépolarisation, la surface membranaire et la distribution de colorant de chaque compartiment. D'une part, ce modèle permet d'avoir une estimation réaliste des contributions relatives des différentes composantes du signal global (Chapitre 8). D'autre part, il a révélé que la composition du signal est hautement dynamique et dépend de la force de l'entrée et des états transitoires.

Enfin, nous avons discuté les opportunités et les limitations de cette approche, ainsi que les perspectives, à court et moyen terme, permettant d'améliorer la fiabilité du modèle (Chapitre 9).

Appendix
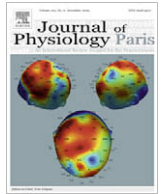
Voltage-sensitive dye imaging: Technique review and models

S. Chemla [a,*], F. Chavane [b]

[a] NeuroMathComp Team, INRIA Sophia-Antipolis, 2004 route des Lucioles, 06902 Sophia-Antipolis, France
[b] Institut de Neurosciences Cognitives de la Mediterranee, CNRS, Aix-Marseille University, UMR6193, 31 Chemin Joseph Aiguier, 13402 Marseille, France

ARTICLE INFO

ABSTRACT

In this review, we present the voltage-sensitive dye imaging (VSDI) method. The possibility offered for *in vivo* (and *in vitro*) brain imaging is unprecedented in terms of spatial and temporal resolution. However, the unresolved multi-component origin of the optical signal encourages us to perform a detailed analysis of the method limitation and the existing models. We propose a biophysical model at a mesoscopic scale in order to understand and interpret this signal.

© 2009 Elsevier Ltd. All rights reserved.

Contents

* Corresponding author.
  E-mail address: sandrine.chemla@sophia.inria.fr (S. Chemla).

Fig. 1. VSDI principle in three steps. The imaging chamber allows a direct access of the primary visual cortex V1 represented as a patch of cortex with its six layers. (A) The dye, applied on the surface of the cortex, penetrates through the cortical layers of V1. (B) All neuronal and non-neuronal cells are now stained with the dye and when the cortex is illuminated, the dye molecules act as molecular transducers that transform changes in membrane potential into optical signals. (C) The fluorescent signal (red arrow) is recorded by a CCD camera.

1. Introduction

Optical imaging comes within the scope of new imaging techniques that allow us to visualize the functioning brain at both high spatial and temporal resolutions. Specifically, there are two techniques mostly used *in vivo* (see Grinvald et al. (1999) for a detailed review); the first is based on intrinsic signals, and the second is based on voltage-sensitive dyes (VSDs). In this review, we focus on the second technique, aiming at better understand the origin of the optical signal. Extensive reviews of VSDI have been published elsewhere (e.g. Grinvald et al., 2004; Roland, 2002). Although the underlying mechanism of this optical method is nowadays well understood, the recorded signal remains very complex and it seems difficult to isolate the contributions from its different components. This review suggests modeling as the appropriate solution. Few models of the VSD signal exist that help to understand the optical signal in terms of functional organization and dynamics of a population neural network. A closer interaction between VSDI experimentalists and modelers is desirable.
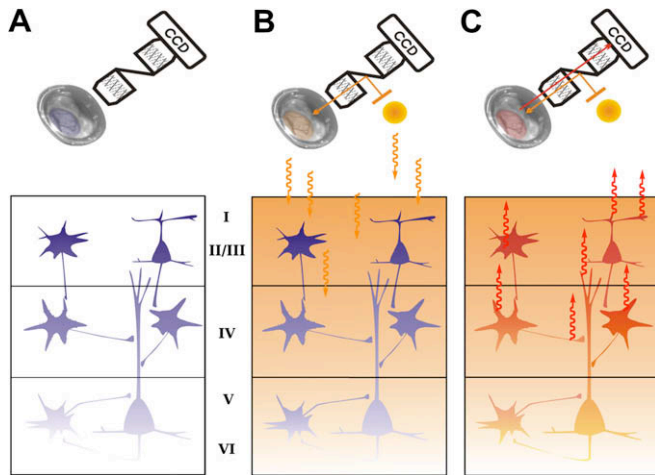
In the first part of this review, we give a general introduction to VSDI, followed by examples of applications to brain imaging. We compare *in vitro* and *in vivo* recordings obtained with VSDI in several animal studies. In a second part, we make the underlying limitations of this method explicit: what does the VSD signal measure? A question that is not completely answered in the literature. Finally, this review shows the benefit of brain activity modeling for optical signal analysis. Models of VSDI measures are reported. We both address what has already been done and what will be interesting to do in order to interpret the origins of the optical imaging signal.

2. VSDI for beginners

2.1. General principle

VSDI offers the possibility to visualize, in real time, the cortical activity of large neuronal populations with high spatial resolution (down to 20–50 µm) and high temporal resolution (down to the millisecond). With such resolutions, VSDI appears to be the best

technique to study the dynamics of cortical processing at neuronal population level.

This invasive technique is also called "extrinsic optical imaging" because of the use of voltage-sensitive dyes (Cohen et al., 1974; Ross et al., 1977; Waggoner and Grinvald, 1977; Gupta et al., 1981). After opening the skull and the dura mater of the animal, the dye molecules are applied on the surface of the cortex (Fig. 1A). They bind to the external surface of the membranes of all cells without interrupting their normal function and act as molecular transducers that transform changes in membrane potential into optical signals. More precisely, once excited with the appropriate wavelength (Fig. 1B), VSDs emit instantaneously an amount of fluorescent light that is function of changes in membrane potential, thus allowing for an excellent temporal resolution for neuronal activity imaging (Fig. 1C). The fluorescent signal is proportional to the membrane area of all stained elements under each measuring pixel.

"All elements" means all neuronal cells present in the cortex but also all non-neuronal cells, like glial cells (see Section 3.1 for more details). Moreover, neuronal cells include excitatory cells and inhibitory cells, whose morphology and intrinsic properties are quite different (see Salin and Bullier (1995) for a review on the different type of neurons and connections in the visual cortex). Furthermore, each cell has various compartments, including dendrites, somata and axons. The measured signal thus combine all these components, which are all likely to be stained in the same manner. The dye concentration is only depending on the depth of the cortex.

The fluorescent signal is then recorded by the camera of the optical video imaging device and displayed as dynamic sequences on computer (see Fig. 1). The submillisecond temporal resolution is reached by using ultra sensitive charge-coupled device (CCD) camera, whereas the spatial resolution is limited by optical scattering of the emitted fluorescence (Orbach and Cohen, 1983).

2.2. Optical imaging of neuronal population activity

2.2.1. General history

The earliest optical recordings were made, at the single neuron level, both from cultured cells (Tasaki et al., 1968) and from various invertebrate preparations like ganglia of the leech (Salzberg et al., 1973), or the giant axon of the squid (Davila et al., 1973). For all other VSDI experiments, the VSD signal has a neuronal population resolution.

The VSDI method has then been used *in vitro* on brain slices, mainly in rodent and ferret. It allowed to optically record from the hippocampus (Grinvald et al., 1982), the visual cortex (Bolz et al., 1992; Albowitz and Kuhnt, 1993; Nelson and Katz, 1995; Yuste et al., 1997; Contreras and Llinas, 2001; Tucker and Katz, 2003a; Tucker and Katz, 2003b), the somatosensory cortex (Yuste et al., 1997; Antic et al., 1999; Contreras and Llinas, 2001; Petersen et al., 2001; Jin et al., 2002; Laaris and Keller, 2002; Berger et al., 2007) and from the auditory cortex (Jin et al., 2002; Kubota et al., 2006).

The salamander, largely used *in vitro* (Orbach and Cohen, 1983; Cinelli and Salzberg, 1992), was the first species also used *in vivo* for studying the olfactory system using VSDI (Orbach and Cohen, 1983), followed by the frog for the visual system (Grinvald et al., 1984), and the rodent for the somatosensory system. Indeed, initial *in vivo* studies of the somatosensory cortex have been made in anesthetized rodents, taking advantage of the thinness of the cortical dura (Orbach et al., 1985). More recently, VSDI in freely moving mice has also been performed with success (Ferezou et al., 2006).

Rodent and ferret were also used for studying the visual cortex *in vivo* (Roland et al., 2006; Lippert et al., 2007; Xu et al., 2007;

Ahmed et al., 2008). However, the main VSDI experiments on visual modality were conducted on two other mammalian species: cat and monkey (Grinvald et al., 1994; Arieli et al., 1995; Sterkin et al., 1998; Shoham et al., 1999; Sharon and Grinvald, 2002; Slovin et al., 2002; Seidemann et al., 2002; Jancke et al., 2004; Sharon et al., 2007; Benucci et al., 2007; Reynaud et al., 2007; Yang et al., 2007). Experiments on anesthetized cats are very attractive for mapping and studying the primary visual cortex, whereas monkey experiments also associate behavioral measures.

2.2.2. High spatial resolution for brain mapping

One domain of application of the VSDI, as other brain functional imaging, is brain mapping. Indeed, VSDI allows to build high-resolution functional maps, such as orientation or ocular-dominance maps (Shoham et al., 1999; Grinvald et al., 1999; Slovin et al., 2002; Sharon and Grinvald, 2002), as also obtained with optical imaging based on intrinsic signals (ISI) (Blasdel and Salama, 1986; Ts'o et al., 1990; Grinvald et al., 1991; Bonhoeffer and Grinvald, 1991; Hubener et al., 1997; Rubin and Katz, 1999). Comparison between the two imaging techniques (Shoham et al., 1999; Grinvald et al., 1999; Slovin et al., 2002) confirms the high spatial resolution of VSDI methodology for mapping the functional architecture of the visual cortex. However, although it is possible to do such brain mapping using VSDI, it does not take advantage of the possibility to inspect neuronal activation dynamics.

2.2.3. High temporal resolution unveils the dynamics of cortical processing

The main benefit of the VSDI technique is the possibility for neuroscientists to go further electrophysiological studies and low

resolution (either temporal or spatial) imaging techniques, since visualizing in real time with high spatial resolution large populations of neurons, while supplying information about cortical networks temporal dynamics. Many neuroscientists are motivated to investigate how a sensory stimulus is represented dynamically on the cortical surface in space and time (Grinvald et al., 1984; Grinvald et al., 1994; Arieli et al., 1996; Petersen et al., 2003; Civillico and Contreras, 2006). More precisely, the spatiotemporal dynamics of the response to simple stimuli, e.g. local drifting-oriented gratings or single whisker stimulation, have been visualized using VSDI on *in vivo* preparations (Cat: Sharon et al., 2007; Rodent: Petersen et al., 2003). Complex stimuli, e.g. the line motion or apparent motion illusions, have also been achieved using VSDI in the visual cortex of cats (Jancke et al., 2004) or ferrets (Ahmed et al., 2008), revealing fundamental principles of cortical processing *in vivo*. Nowadays, rapid and precise dynamic functional maps can even be obtained on behaving animals, as shown by Seidemann et al. (2002), Slovin et al. (2002) and Yang et al. (2007) on behaving monkeys, or by Ferezou et al. (2006) in freely moving mice.

There questions are conceivable thanks to the persistent development of novel dyes (Shoham et al., 1999; Grinvald et al., 2004; Kee et al., 2009). Indeed, the developed dyes allowed to monitor in real time neuronal activation both in *in vivo* and *in vitro* preparations (Arieli et al., 1996; Grinvald et al., 1999; Petersen et al., 2001; Petersen et al., 2003).

2.2.4. Functional connectivity reveals its dynamics

Combining the spatial and temporal advantages, an other direct application of VSDI is the possibility to study the functional con-

Table 1
Non-exhaustive list of publications related to VSDI, classified by experimental conditions (either *in vitro* or *in vivo*) and by species.

Conditions	Species	Related publications	Structure	Dye	λ_{exc} (nm)
In vitro (invertebrate preparations, cultured cells or brain slices)	Invertebrate (squid, skate, snail, leech)	Tasaki et al. (1968), Davila et al. (1973), Salzberg et al. (1973), Woolum and Strumwasser (1978), Gupta et al. (1981), Konnerth et al. (1987), Cinelli and Salzberg (1990), Antic and Zecevic (1995), and Zochowski et al. (2000)	Giant neurons / Axons / Cerebellar parallel fibres	Styryl JPW1114 optimized for intracellular applications / JPW1114 (fluorescence) / Pyrazo-oxonol RH482, RH155 (absorption)	540 / 520
	Goldfish Salamander	Manis and Freeman (1988) / Orbach and Cohen (1983) and Cinelli and Salzberg (1992)	Optic tectum / Olfactory bulb	Styryl RH414 (fluorescence) / Merocyanine XVII optimized for absorption measurements (Ross et al., 1977; Gupta et al., 1981), RH414, RH155	540
	Rodent	Grinvald et al. (1982), Bolz et al. (1992), Albowitz and Kuhnt (1993), Yuste et al. (1997), Antic et al. (1999), Petersen et al. (2001), Contreras and Llinas (2001), Laaris and Keller (2002), Jin et al. (2002), Kubota et al. (2006), Berger et al. (2007), Carlson and Coulter (2008), and Kee et al. (2009)	Visual cortex / Barrel cortex / Auditory cortex hippocampus	Fluorochrome Di-4-ANEPPS, RH414, Styryl RH795 (fluorescence) / JPW2038, RH155, RH482, NK3630, JPW1114, RH414, RH795 / RH795 for fluorescence, Oxonol NK3630 for absorption / WW401	500, 540 / 520, 705 / 520
	Ferret	Nelson and Katz (1995) and Tucker and Katz (2003a,b)	Visual cortex	RH461 (fluorescence)	590
In vivo (anesthetized or awake)	Frog Salamander	Grinvald et al. (1984) / Orbach and Cohen (1983) and Kauer (1988)	Visual cortex / Olfactory bulb	Styryl RH414 / Styryl RH160 and RH414 optimized for fluorescence measurements (Grinvald et al., 1982)	520 / 510, 540
	Rodent	Orbach et al. (1985), Orbach and Van Essen (1993), Petersen et al. (2003), Derdikman et al. (2003), Civillico and Contreras (2006), Ferezou et al. (2006), Berger et al. (2007), Lippert et al. (2007), Xu et al. (2007), and Brown et al. (2009)	Barrel cortex / Visual cortex	RH795, Oxonol RH1691, RH1692 and RH1838 optimized for in vivo fluorescent measurements (Shoham et al., 1999; Spors et al., 2002) / RH1691, RH1838	540, 630 / 630
	Ferret	Roland et al. (2006) and Ahmed et al. (2008)	Visual cortex	RH795, RH1691	530, 630
	Cat	Arieli et al. (1995), Sterkin et al. (1998), Shoham et al. (1999), Sharon and Grinvald (2002), Jancke et al. (2004), Sharon et al. (2007), and Benucci et al. (2007)	Visual cortex (area 17/18)	RH795, RH1692	530-40, 630
	Monkey	Grinvald et al. (1994), Shoham et al. (1999), Slovin et al. (2002), Seidemann et al. (2002), Reynaud et al. (2007), and Yang et al. (2007)	Visual cortex (V1/V2) / FEF	RH1691, RH1692, RH1838 / RH1691	630 / 630

nectivity of neuronal populations. Yuste et al. (1997) for example, investigated the connectivity diagram of rat visual cortex using VSDI. Vertical and horizontal connections have been detected. More generally, intracortical and intercortical interactions, occurring during sensory processing (especially visual), have been largely explored using VSDI, either *in vitro* or *in vivo*: Mapping functional connections using VSDI, has been done *in vitro* in the rat visual cortex (Bolz et al., 1992; Carlson and Coulter, 2008), in the guinea pig visual cortex (Albowitz and Kuhnt, 1993) and in the ferret visual cortex (Nelson and Katz, 1995; Tucker and Katz, 2003a; Tucker and Katz, 2003b), providing not only functional, but also anatomical and physiological information on the local network. For example, Tucker and Katz (2003a) investigated with VSDI how neurons in layer 2/3 of ferret visual cortex integrate convergent horizontal connections.

Orbach and Van Essen (1993) used VSDI in the visual system of the rat *in vivo* to map striate and extrastriate pathways. Feedforward propagating waves from V1 to other cortical areas, and feedback waves from V2 to V1 have been recently reported by Xu et al. (2007), thanks to VSDI. In addition, feedback depolarization waves (from areas 21 and 19 toward areas 18 and 17) were extensively studied by Roland et al. (2006) in ferrets after staining the visual cortex with VSD.

2.3. Conclusion

By adding a new dimension to existing brain functional imaging techniques, VSDI directly reports the spatiotemporal dynamics of neuronal populations activity. Many VSDI studies have then been conducted in order to investigate the spatiotemporal patterns of activity occurring in different parts of the CNS, *in vitro* or *in vivo*, on several preparations or animal species. The Table 1 lists most articles presenting experimental results using VSDI techniques. The publications are first classified by the condition of the experiment, either *in vitro* or *in vivo*, and then by the experimental preparations or animal species. Additional information about dyes is available in the last columns (see Ebner and Chen (1995) for a compilation of the commonly used dyes and their properties).

3. The multi-component origin of the optical signal

3.1. About the contribution from glial cells

In general, glial cells have been neglected by neuroscientists for a long time, especially because unlike neurons, they do not carry action potentials. However, glial cells have important functions (see Cameron and Rakic (1991) for a review) and they may contribute to the VSD signal.

Glial cells are known as the "supporting cells" of the CNS and are estimated to outnumber neurons by as much as 50–1. However, their role in information representation or processing remains unresolved. Indeed, *in vitro* studies have shown increasing evidence for an active role of astrocytes in brain function. However, little is known about the behavior of astrocytes *in vivo*.

When interpreting the VSD signal, we face two conflicting viewpoints. Konnerth and Orkand (1986), Lev-Ram and Grinvald (1986), Konnerth et al. (1987), Konnerth et al. (1988) and Manis and Freeman (1988) showed that the optical signal has two components: a "fast" followed by a "slow" signal. The latter has been revealed by doing successive staining with different dyes (e.g. RH482 and RH155), since each of them may preferentially stain different neuronal membranes. The authors then present evidence that this slow signal has a glial origin.

However, Kelly and Van Essen (1974) showed that the glial responses are weak (depolarizations of only 1–7 mV in response to visual stimuli) and have a time scale of seconds. Recent paper of Schummers et al. (2008) confirms that the astrocyte response is delayed 3–4 s from stimulus onset, which is a very slow temporal response compared to neuron response. Generally, in VSDI, only the first 1000 ms are considered, since intrinsic activity may affect the signal after this time.

We understand here that the controversy about glial contribution is directly link to the used dye (Ebner and Chen, 1995), and the time course of the optical signal generated. Thus, glial activity is very unlikely to participate significantly to the VSD signal (when considering recent fast dyes), since the amplitude of glial response is weak and its time course is very slow.

3.2. About the contribution from excitatory versus inhibitory cells

In the neocortex, neurons (despite their morphologic diversity) can be functionally classified in two groups: excitatory neurons, which represent about 80% of the cortical cells, and inhibitory neurons which represent about 20% of cortical cells (Douglas and Martin, 1990). Thus, it is tempting to say that the VSD signal mainly reflects the activity of excitatory neurons (Grinvald et al., 1999).

However, the VSD signal is proportional to changes in membrane potential. Thus, both excitatory and inhibitory neurons contribute positively to the VSD signal and it is hard to teaze apart contributions from excitatory or inhibitory cells. An additional level of complexity arises from the fact that inhibition operates generally in a shunting "silent" mode (Borg-Graham et al., 1998). In this mode, inhibition suppresses synaptic excitation without hyperpolarizing the membrane potential.

To conclude, the contribution of inhibitory cells to the VSD signal is unclear and would obviously benefit from modeling studies.

3.3. About the contribution from the various compartments

Neurons can be also decomposed into their main various compartments, whose surface and electrical activity are different (see Fig. 2, green part):

(a) The soma, whose electrical activity can be either synaptic (SP for synaptic potential) or spiking (AP for action potential).
(b) The dendrites, that integrate presynaptic AP information from others cells. The electrical activity is mainly synaptic, however, back-propagating AP could be recorded in the dendrites (see Waters et al. (2005) for a review). Dendritic surface area of mammalian neurons have been estimated by Sholl (1955a), Aitken (1955), and Young (1958) to be 10–12 times larger than cell bodies surface area, and to represents 90% of the total neuronal cell membrane (Eberwine, 2001).
(c) The axon, which carries spiking signals from the soma to the axon terminal. Spiking activity can be recorded on this part of neuron. In contrast with dendrites, the surface area of axons represents 1% of the total neuronal cell surface (Eberwine, 2001).

In the literature, regarding the difference in membrane areas of the various neuronal components and the nature of the signal, it is commonly accepted that the optical signal, in a given pixel, mostly originates from the dendrites of cortical cells, and therefore, mainly reflects dendritic post-synaptic activity (Orbach et al., 1985; Grinvald et al., 2004). Extensive comparisons between intracellular recordings from a single neuron and VSDI also showed that the optical signal correlates closely with synaptic membrane potential changes (Petersen et al., 2003; Contreras and Llinas, 2001). However, no real quantitative analysis has been performed to date
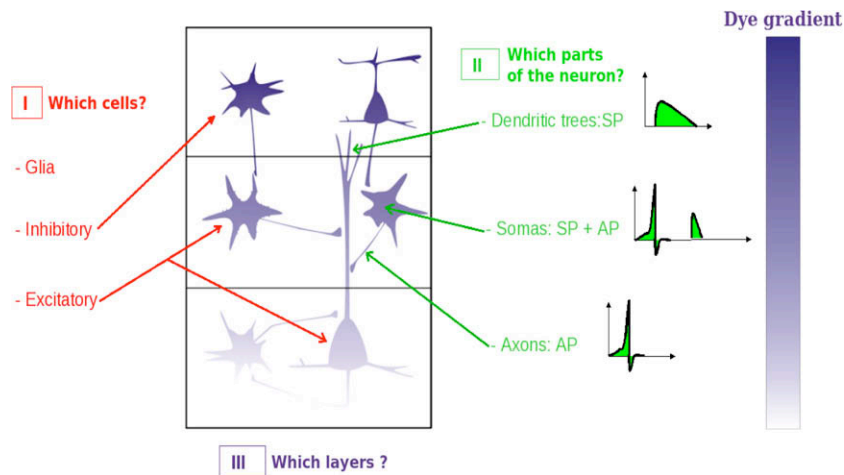
Fig. 2. Contributions of the optical signal. Once neurons are stained by the VSD, every neuronal membrane contributes to the resulting fluorescent signal, but from where? and in which proportion? Answering these four questions could clarify the optical signal origins: (1) Which cells? (2) Which parts of the cell? (3) Which layers? (4) Which presynaptic origins?

and it is more correct to state that the optical signal is multi-component since the VSD signal reflects the summed intracellular membrane potential changes of all neuronal compartments at a given cortical site. The aim then, is to determine the exact contribution of each component, which remains unknown. More precisely, what is quantitatively the contribution of dendritic activity? Can spiking activity be neglected?

3.4. About the contribution from cortical layers

The depth of the neocortex is about 2 mm. It is made up of six horizontal layers principally segregated by cell types and neuronal connections. The layer II mostly contains small pyramidal neurons that make strong connections with large pyramidal neurons of the layer V (Thomson and Morris, 2002).

Improved dyes, when put at the surface of the exposed cortex, can reach a depth of about 400–800 μm from the cortical surface, which mainly corresponds to superficial layers (Grinvald et al., 1999; Petersen et al., 2003). Furthermore, measures of the distribution of dye fluorescence intensity in rat visual and barrel cortex confirm that the optical signal mostly originates from superficial layers I–III (Ferezou et al., 2006; Lippert et al., 2007). Note that Lippert et al. (2007) used a special staining procedure, i.e. keeping the dura mater intact, but dried.

However, they did not take into account the fact that the activity in superficial layers could arise from neurons in deep layers, due to their dendritic arborization. Indeed, large pyramidal neurons in layer V have apical dendrites that reach superficial layers and may contribute to the signal. Therefore, the exact contribution of each cortical layer still has to be clarified.

3.5. About the contribution from thalamic versus horizontal connections

The origin of the signal can also be problematic when looking at the contribution from the different presynaptic activity origins, e.g. direct thalamic synaptic inputs, or horizontal inputs. Indeed, in response to a local stimulation, slow propagating waves can be recorded (Grinvald et al., 1994; Jancke et al., 2004; Roland et al., 2006; Xu et al., 2007; Benucci et al., 2007). We can question what is the relative contribution of all the synaptic input sources of this phenomenon, i.e. feedforward, horizontal or feedback inputs. Dedicated models could help teazing apart those various contributions.

3.6. Conclusion

Fig. 2 summarizes the four main questions not completely clarified to date:

(a) What are the contributions of the various neurons and neuronal components to the optical signal?
(b) What is the ratio between spiking and synaptic activity?
(c) What are the respective contributions of cells from deep versus superficial layers?
(d) What is the origin of the synaptic input? More precisely, what are the respective contributions of thalamic, local and long-range inputs?

To answer these questions, a possibility is to develop computational models in order to reproduce and analyse VSD signals. Models of VSD signals are reported in the next and last part of this review.

4. Benefits of modeling for optical signal analysis

The goal of this section is to investigate the different models from the literature, used to reproduce and analyse the VSD signal. We quickly emphasize three of these models because of their scale of analysis. In the last subsection, we present, in detail, an intermediate model that would allow to answer the previous questions about the VSD signal contributions.

4.1. Which scale for which model?

As previously described, the origin of the VSD signal is complex and remains to be estimated and explored. Therefore, it could be interesting to see if the activity of a computational model could be related to this signal. However, the choice of the model's scale is very important and depends on what exactly the model is designed for. We propose in the following paragraphs that the mesoscopic scale seems would be the best scale for analyzing the population VSD signal. In neuroscience, this scale is generally used to define the elementary processing unit in the brain, the cortical column. We start by defining our concept of cortical columns.

Since the 1950s, thanks to the work of Mountcastle (1957), we know that the cerebral cortex has a columnar organization. In 1960s and 1970s, Hubel and Wiesel (1962, 1965, 1977) followed

Mountcastle's discoveries by showing that ocular dominance and orientations are organized in a columnar manner in cat and monkey visual cortex. Today, the notion of cortical column becomes a large controversy since the original concept is expanding, year after year, discovery after discovery, to embrace a variety of different structures, principles and names. A 'column' now refers to cells in any vertical cluster that share the same tuning for any given receptive field attribute (see Horton and Adams (2005) for a detailed review on the cortical column concept). A novel and useful concept is to propose that each definition of cortical column depends on its type (anatomical, functional, physico-functional) and its spatial scale, as detailed in Table 2. A minicolumn or a microcolumn is an anatomical column of about 100 neurons, since its spatial scale is about 40 µm. Next, orientation or ocular dominance columns are classified as functional columns whose the spatial scale is between 200 and 300 µm, containing several minicolumns. An hypercolumn in V1 or a macrocolumn in the general case, then represents a physico-functional unit containing a full set of values for any given functional parameter. Its spatial scale can be up to 600 µm and contains about 10^4 neurons. Finally, neural mass is a mesoscopic concept which depends on the spatial scale. When looking at a cortical area, it can be used to represent, for example, all the pyramidal neurons contained in it (about 10^5 neurons).

Into these definitions and in order to reproduce exactly the same signal, i.e. time course and spatial extent, it seems appropriate to construct models at a large mesoscopic scale which could represent an entire cortical area. Models from Miikkulainen et al. (2005), Grimbert et al. (2007), Rangan et al. (2005) and La Rota (2003) consider this scale, that can be view as the neurons population scale.

An other point of view is to choose a much finer scale allowing to construct a more detailed biophysical model in order to quantitatively estimate the exact contribution of the VSD signal (excitation vs. inhibition, parts of the neuron, layers participation, etc.). In optical imaging, the visual scale studied, which is about 50 µm, corresponds to one pixel. It is still a population activity since it represents about 200 neurons, but the scale being relatively small, we will call it "intermediate mesoscopic scale". This model is detailed in the last section.

4.2. Mesoscopic scale: models of a cortical area

4.2.1. Extended LISSOM model

The Laterally Interconnected Synergetically Self-Organizing Map (LISSOM) family of models was developed by Bednar, Choe, Miikkulainen and Sirosh, at the University of Texas (Miikkulainen et al., 2005; Sirosh and Miikkulainen, 1994), as models of human visual cortex at a neural column level. It is based on the Self-Organizing Maps (SOM) algorithm (from Kohonen, 2001) used to visualize and interpret large high-dimensional data sets. When extended, the LISSOM neural network models takes into account lateral interactions (excitatory and inhibitory connections), allowing to reproduce the pinwheel organization of the primary visual cortex map, such as orientation, motion direction selectivity and ocular-dominance maps.

Sit and Miikkulainen used such a LISSOM model to represent V1 and tried to show how the activity of such a computational model of V1 can be related to the VSD signal (Sit and Miikkulainen, 2007). Indeed, with an extended LISSOM model including propagation delays in the cortical connections, they showed that the orientation tuning curve and the response dynamics of the model were similar to those measured with VSDI.

The model is a couple of two layers of neural units that represent the retina and V1. In V1, neural units account for a whole vertical column of cells. They receive input from the retina and also from neighbour columns (short-rang lateral excitatory and long-rang lateral inhibitory connections). Thus, the neuronal activity of unit $\mathbf{r}$ in V1 writes:

$$A(\mathbf{r}, t) = \sigma(V(\mathbf{r}, t)),$$
$$V(\mathbf{r}, t) = \sum_{\rho} \gamma_{\rho} \sum_{\mathbf{r}'} W_{\rho, \mathbf{r}, \mathbf{r}'} A(\mathbf{r}', t - d(\mathbf{r}, \mathbf{r}')) + \sum_{\mathbf{s}} \chi_{\mathbf{s}} R_{\mathbf{s}, \mathbf{r}}, \quad (1)$$

where σ is a sigmoid activation function and the two terms are respectively the weighted sum of the lateral activations and the input activation from the retina. $W_{\rho, \mathbf{r}, \mathbf{r}'}$ and $R_{\mathbf{s}, \mathbf{r}}$ are respectively the synaptic weights matrix of lateral and retinal connections, and $d(\mathbf{r}, \mathbf{r}')$ is the delay function between unit $\mathbf{r}$ and unit $\mathbf{r}'$. This is thus a scalar model of the neural activity.

Then, the computation of the VSD signal is done by looking only at the subthreshold activity $V(\mathbf{r}, t)$, given by the weighted sum of presynaptic activity. To simplify, the authors have extended the LISSOM model with delayed lateral connections to compute the VSD signal from subthreshold signal. This is thus a scalar linear model of the VSD signal built on convolutions.

This model, based on Hebbian self-organizing mechanisms, is simple and efficient to replicate the detailed development of the primary visual cortex. It is thus very useful to study VSDI functional maps. However, this model is not specific enough to answer the previous asked questions (see Section 3.6).

4.2.2. Neural field model of a cortical area

Another approach, introduced by Grimbert et al. (2007) and Grimbert et al. (2008), proposes neural fields as a suitable mesoscopic models of cortical areas, in link with VSD. Neural field are continuous networks of interacting neural masses, describing the dynamics of the cortical tissue at the population level (Wilson and Cowan, 1972; Wilson et al., 1973). It could thus be applied to solve the direct problem of the VSD signal, providing the right parameters. More precisely, the authors showed that neural fields can easily integrate the biological knowledge of cortical structure, especially horizontal and vertical connectivity patterns. Hence, they proposed a biophysical formula to compute the VSD signal in terms of the activity of a field.

The classical neural field model equation is used, either written in terms of membrane potential or in terms of activity of the different neural masses present in a cortical column. For example, if $\mathbf{r}$ represents one spatial position of the spatial domain defining the area, then the underlying cortical column is described, at time t, by either a vector $\mathbf{V}(\mathbf{r}, t)$ or $\mathbf{A}(\mathbf{r}, t)$:

Table 2
The different types of cortical columns.

	Anatomical	Ol pixel	Functional	Physico-functional	Cortical area
Type of cortical column	Microcolumn or minicolumn	*Our column*	Orientation, ocular dominance column	Macrocolumn or hypercolumn (V1)	Neural mass
Spatial scale	40–50 µm	50–100 µm	200–300 µm	600 µm (and more)	10 mm
Number of neurons	80–100 neurons	200 neurons	Several minicolumns	60–100 minicolumns or 10,000 neurons	100X Thousand neurons of the same type (pyr, stellate, etc.)

$$\dot{\mathbf{V}}(\mathbf{r}, t) = -\mathbf{LV}(\mathbf{r}, t) + \int_{\Omega} \mathbf{W}(\mathbf{r}, \mathbf{r}')\mathbf{S}(\mathbf{V}(\mathbf{r}', t))d\mathbf{r}' + \mathbf{I}_{ext}(\mathbf{r}, t), \qquad (2)$$

and

$$\dot{\mathbf{A}}(\mathbf{r}, t) = -\mathbf{LA}(\mathbf{r}, t) + \mathbf{S}\left(\int_{\Omega} \mathbf{W}(\mathbf{r}, \mathbf{r}')\mathbf{A}(\mathbf{r}', t)d\mathbf{r}' + \mathbf{I}_{ext}(\mathbf{r}, t) \right) \qquad (3)$$

Here, $\mathbf{V}(\mathbf{r}, t)$ contains the average soma membrane potentials of the different neural masses present in the column (the vector's dimension then represents the number of neuronal types considered in every column). $\mathbf{A}(\mathbf{r}, t)$ contains the average activities of the masses. For example, A_i is the potential quantity of post-synaptic potential induced by mass i on the dendrites of all its post-synaptic partners. The actual quantity depends on the strength and sign (excitatory or inhibitory) of the projections (see Grimbert et al. (2007, 2008) and Faugeras et al. (2008) for more details on the model's equations). The model include horizontal intercolumnar connections and also vertical intracolumnar connections between neural masses. The latter gives an advantage to this model compared to the previous one, since the vertical connectivity was not taken into account in the extended LISSOM model. Furthermore, extracortical connectivity is not made explicit here, though taken into account in Grimbert et al. (2007).

Hence, based on this biophysical formalism (and especially the activity-based model, which is more adapted than the voltage-based model), the authors propose a formula involving the variables and parameters of a neural field model to compute the VSD signal:

$$OI(\mathbf{r}, t) = \sum_{j=1}^{N} \int_{\Omega} \tilde{w}_j(\mathbf{r}, \mathbf{r}')A_j(\mathbf{r}', t)d\mathbf{r}', \qquad (4)$$

where $\tilde{w}_j(\mathbf{r}, \mathbf{r}')$ contains all the biophysical parameters accounting for a cortical area structure stained by a voltage-sensitive dye, i.e. the different layers, the number of neurons, the number of dye molecules per membrane surface unit, the attenuation coefficient of light and also the horizontal and vertical distribution patterns of intra and intercortical connectivities.

This formula is the result of many decompositions of the total optical signal, from layer level to cellular membrane level, where the signal is simply proportional to the membrane potential.

Better than the Lissom model for our considerations, this large-scale model reproduces the spatiotemporal interactions of a cortical area in response to complex stimuli, e.g. line motion illusion, and allows, on average, to answer at the mesoscopic scale some previous questions (see Section 3.6). However, improvements on parameters tuning are still needed.

4.2.3. Conductance-based IAF neuronal network model

Another large-scale computational model of the primary visual cortex have been proposed by Rangan et al. (2005). The model is a two-dimensional patch of cortex, containing about 10^6 neurons with a preferred orientation, whose 80% are excitatory and 20% are inhibitory. The dynamics of single cell i is described by a single compartment, conductance-based, exponential integrate-and-fire equation (see Geisler et al. (2005) for more details on this neuron model). The derivation of this equation gives the membrane potential of neuron i of spatial position $\mathbf{r}_i$:

$$V(\mathbf{r}_i, t) = \frac{g^L V^L + (g_i^A(t) + g_i^N(t))V^E + g_i^G(t)V^I}{g^L + g_i^A(t) + g_i^N(t) + g_i^G(t)} \qquad (5)$$

where g^L, g_i^A, g_i^N and g_i^G are respectively leak, AMPA, NMDA and GABA conductances, and V^L, V^E and V^I are respectively leak, excitatory and inhibitory reversal potentials.

The authors then use $V(\mathbf{r}, t)$ to represent the VSD signal, i.e. the subthreshold dendritic activity in the superficial layers of the cor-

tex. Poisson processes are used to simulate inputs from the thalamus and background noise.

This model allows, like the previous one Grimbert et al. (2007), to reproduce the spatiotemporal activity patterns of V1, as revealed by VSDI, in response to complex stimuli, e.g. the line motion illusion. However, in comparison with Grimbert et al. (2007), no laminar structure is taken into account.

4.2.4. Linear model of the raw VSD signal

With the same scale of analysis, La Rota (2003) presented an interesting linear model in order to study the neural sources of the mesoscopic VSD signal. The author chose a compromise between a detailed and a "black-box" model of the signal, by taking into account the important properties of the VSD signal and also the artefacts directly linked to its measure, in a mesoscopic, linear and additive model. The VSD signal of a cortical area can then be modeled by an intrinsic and an extrinsic components:

$$OI(t) = A(t) + \rho(t), \qquad (6)$$

where $A(t)$ represents the activity of the intrinsic component of the optical signal (i.e. the synaptic activity of the cortical area observed) and $\rho(t)$ represents all the noise and artefacts due to the measure (e.g. hemodynamic artefact, cardiovascular and respiratory movements, instrumental noise, etc.). In this model, inputs from the thalamus are considered as background noise and thus enter in the ρ component.

The model is interesting because it both takes into account the intrinsic and the extrinsic variability of the VSD signal. The latter being supposed already removed, when analyzing the signal in the three other presented models.

4.3. Biophysical model at the intermediate mesoscopic scale

Since none of the previous models was specific enough to determine the different contributions of the optical signal, a biological cortical column model, at an intermediate mesoscopic scale, has also been proposed in order to better understand and interpret biological sources of VSD signals (Chemla et al., 2007). This scale corresponds to one pixel of optical imaging: about 50 μm and the related model solves the direct VSD problem, i.e. generates a VSD signal, given the neural substrate parameters and activities. Using a detailed compartmental model allows to push the state of the art at this level. This model confirms and quantifies the fact that the VSD signal is the result of an average from multiple components.

4.3.1. Model specifications

Into the above cortical columns paradigm and for our specific model, we introduced a new distinction of a cortical column (see Fig. 2, second column). The spatial scale is about 50 μm, corresponding to one pixel of optical imaging. Given this spatial scale, the number of neurons, that has been evaluated from Binzegger et al. (2004), is about 200.

We then consider a class of models based on a cortical microcircuit (see Raizada and Grossberg (2003), Douglas and Martin (2004), and Haeusler et al. (2007) for more details on this concept), whose synaptic connections are made only between six specific populations of neurons: two populations (excitatory and inhibitory) for three main layers (2/3, 4, 5/6).

Each neuron is represented by a reduced compartmental description (see Bush and Sejnowski (1993) for more details on the reduction method) with conductance-based Hodgkin–Huxley neuron model (see Hodgkin and Huxley, 1952) in the soma and the axon. Thus, the dynamics of single cells are described by the following equation:

$$C_m \frac{dV}{dt} = I_{ext} - \sum_i g^i(V)(V - V^i) \qquad (7)$$

where V is the membrane potential, I_{ext} is an external current injected into the neuron, C_m is the membrane capacitance, and where three types of current are represented: leak, potassium and sodium conductances or respectively G_L, G_K and G_{Na}. G_L is independent of V and determines the passive properties of the cells near resting potential. The sodium and potassium conductances are responsible for the spike generation. Furthermore, a slow potassium conductance was included in the dynamics of the excitatory population to reproduce the observed adaptation of the spike trains emitted by these neurons (see Nowak et al., 2003). This feature seems to be absent in inhibitory neurons, as taken into account in this model.

Only passive dendrites were considered. Each neuron represented with seven to nine compartments. The link between compartments can then be described by Eq. (8) (Hines and Carnevale, 1997).

$$C_j \frac{dV_j}{dt} + Iion_j = \sum_k \frac{V_k - V_j}{R_j k} \qquad (8)$$

where V_j is the membrane potential in compartment j, $Iion_j$ is the net transmembrane ionic current in compartment j, C_j is the membrane capacitance of compartment j and R_{jk} is the axial resistance between the centers of compartment j and adjacent compartment k.

Synaptic inputs are modeled as conductance changes. Excitatory AMPA synapses are converging on soma and dendrites of each neuron, whereas inhibitory GABA synapses are only converging on soma of each neuron (Salin and Bullier, 1995). The number of synapses involved in the projections between these different neuronal types, including the afferent from the LGN, were recalculated for a 50 µm cortical column, based on Binzegger et al. (2004) for the considered layers, while latencies have been introduced for each connection following Thomson et al. (2007).

Input signals from the thalamus into the neocortex layer IV was simulated by applying random spike trains to each neuron in layer IV and random latency have been introduced for each input connection to simulate the temporal properties of geniculocortical pathway. Then we increased the frequency of the spike trains in order to represent stimulus contrast and see how the model transforms an increasing input, i.e. the contrast response function (see Albrecht et al., 1982). At this point, the column is isolated. A step further, the conditions relative to a larger network are reproduced as follows: First, "background noise" was introduced in each neuron of the column. Typically, noise can be introduced in the form of stochastic fluctuation of a current or an ionic conductance. The stochastic model of Destexhe et al. (2001), containing two fluctuating conductances, is used here, allowing us to simulate synaptic background activity similar to in vivo measurements, for a large network. Second, lateral connections between two neighboring columns are reproduced by introducing an other set of random spike trains inputs whose frequency, synaptic delays and synaptic weights are adapted for fitting experimental data. Fig. 3 shows a schematic of the model, with thalamic input, background activity and lateral interactions. Examples of neuronal response have been plotted in function of increasing input or contrast.

4.3.2. Computation of the VSD signal

The VSD signal is simulated using a linear integration on the membrane surface of neuronal components. Here, the use of compartmental model has a real interest. Indeed, the computation of the VSD signal, for a given layer L, is given by:

$$OI^L = \lambda^L \sum_{i \in \{Compartments\}} V_i S_i \qquad (9)$$

where S_i and V_i are respectively the surface and the membrane potential of the ith compartment and λ^L represents the fluorescence's gradient or the illumination intensity of the dye in layer L.
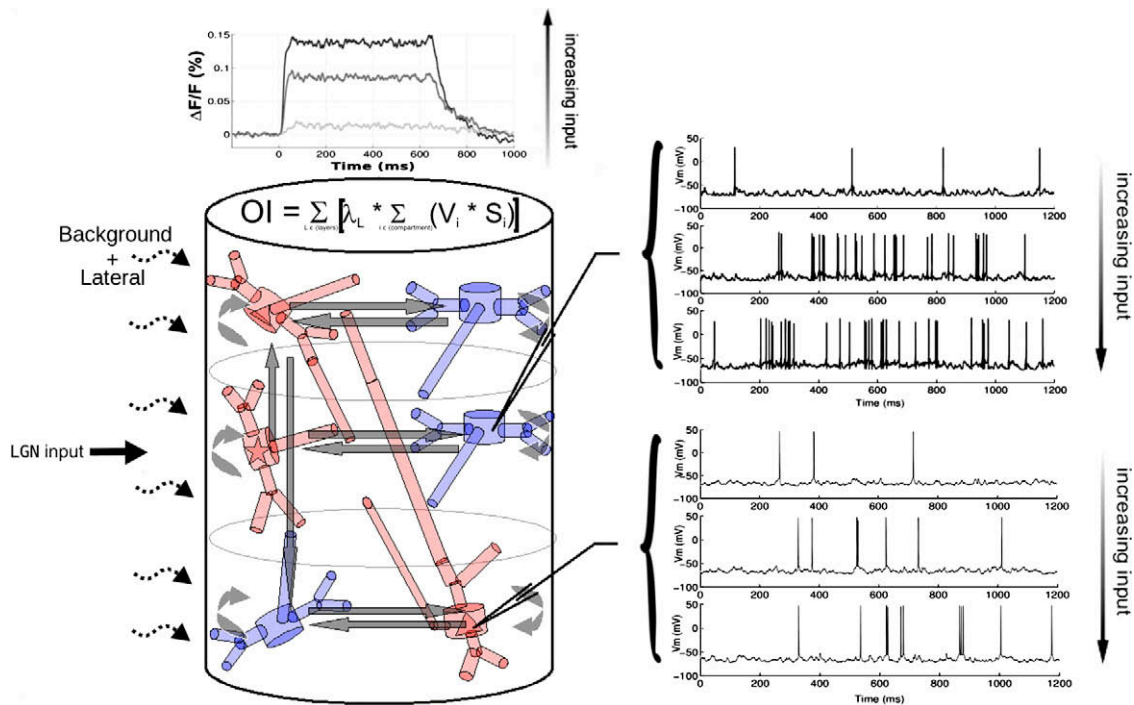
Fig. 3. Model representation taking into account thalamic input contrast, background activity and lateral connections and offering the possibility to compute the VSD signal with a linear formula. In output, inhibitory and excitatory neuronal responses are plotted in function of increasing input or contrast (right inset). The temporal evolution of the VSD signal in response to 600 ms stimuli and in function of increasing input is also emphasized.

Thus, this model takes into account soma, axon and dendrites influences, introduces 3D geometrical properties (dendrites of large pyramidal neurons in layer 5 can reach superficial layers) and fluorescence gradient depending on depth. According to Lippert et al. (2007) and Petersen et al. (2003), $\lambda^2 = 0.95$, $\lambda^4 = 0.05$ and $\lambda^5 = 0$. Then, the total optical imaging signal is given by the following formula:

$$OI = \sum_{L \in \{Layers\}} OI^L \qquad (10)$$

Following this framework, the VSD signal is simulated in response to known stimuli (Fig. 3, bottom right inset) and compared to experimental results (Chemla et al., 2008).

Thanks to its compartmental construction, this model can predict the different contributions of the VSD signal. It thus gives the possibility to quantitatively answer the previous asked questions: excitation vs. inhibition, spiking vs. synaptic activity and superficial vs. deep layers: The model confirms that the VSD signal mainly reflects dendritic activity (75%) of excitatory neurons (80%) in superficial layers (80%). However, these numbers are changing when increasing the level of input activity. At high level of activity, inhibitory cells, spiking activity and deep layers become non-negligible, and should be taken into account in the computation of the VSD signal. These results will be the subject of a future publication.

5. Conclusion

In this review, we have presented the voltage-sensitive dyes imaging (VSDI) technique in a general and elementary manner. This optical technique, thanks to its excellent spatial and temporal resolution, offers many possibilities for *in vitro* and more interestingly *in vivo* brain imaging.

However, the recorded optical signal is multi-component and its origins are still unresolved. Indeed, the contribution of each component, i.e. glial cells, excitatory cells, inhibitory cells, somas, axons, dendrites, layers, is very difficult to isolate from the others.

This review suggests modeling as the appropriate solution. We reported four existing models that try to reproduce and analyse the VSD signal. The main advantage of these models, all built at a mesoscopic scale, is the ability to compare the same signal, i.e. the signal of an entire cortical area. However, for our considerations, i.e. find the different contributions of the VSD signal, those models have not the right scale. Thus, we proposed a biophysical cortical column model, at an intermediate mesoscopic scale, in order to find the biological sources of the VSD signal. Using a such compartmental model should be of great value for doing a quantitative analysis of the different contributions of the optical signal.

References

Ahmed, B., Hanazawa, A., Undeman, C., Eriksson, D., Valentiniene, S., Roland, P.E., 2008. Cortical dynamics subserving visual apparent motion. Cereb. Cortex 18 (12), 2796–2810.

Aitken, J.T., 1955. Observations on the larger anterior horn cells in the lumbar region of the cat's spinal cord. J. Anat. 89, 571.

Albowitz, B., Kuhnt, U., 1993. The contribution of intracortical connections to horizontal spread of activity in the neocortex as revealed by voltage sensitive dyes and a fast optical recording method. Eur. J. Neurosci. 5 (10), 1349–1359.

Albrecht, D., Hamilton, D., 1982. Striate cortex of monkey and cat: contrast response function. J. Neurophysiol. 48 (1), 217–233.

Antic, S., Zecevic, D., 1995. Optical signals from neurons with internally applied voltage-sensitive dyes. J. Neurosci. 15 (2), 1392–1405.

Antic, S., Major, G., Zecevic, D., 1999. Fast optical recordings of membrane potential changes from dendrites of pyramidal neurons. J. Neurophysiol. 82 (3), 1615–1621.

Arieli, A., Shoham, D., Hildesheim, R., Grinvald, A., 1995. Coherent spatiotemporal patterns of ongoing activity revealed by real-time optical imaging coupled with single-unit recording in the cat visual cortex. J. Neurophysiol. 73 (5), 2072–2093.

Arieli, A., Sterkin, A., Grinvald, A., Aerster, A., 1996. Dynamics of ongoing activity: explanation of the large variability in evoked cortical responses. Science 273 (5283), 1868–1871.

Benucci, A., Robert, A.F., Carandini, M., 2007. Standing waves and traveling waves distinguish two circuits in visual cortex. Neuron 55 (1), 103–117.

Berger, T., Borgdorff, A., Crochet, S., Neubauer, F.B., Lefort, S., Fauvet, B., Ferezou, I., Carleton, A., Luscher, H.R., Petersen, C.C., 2007. Combined voltage and calcium epifluorescence imaging in vitro and in vivo reveals subthreshold and suprathreshold dynamics of mouse barrel cortex. J. Neurophysiol. 97 (5), 3751–3762.

Binzegger, T., Douglas, R., Martin, K., 2004. A quantitative map of the circuit of cat primary visual cortex. J. Neurosci. 24 (39), 8441–8453.

Blasdel, G.G., Salama, G., 1986. Voltage-sensitive dyes reveal a modular organization in monkey striate cortex. Nature 321 (6070), 579–585.

Bolz, J., Novak, N., Staiger, V., 1992. Formation of specific afferent connections in organotypic slice cultures from rat visual cortex cocultured with lateral geniculate nucleus. J. Neurosci. 12 (8), 3054–3070.

Bonhoeffer, T., Grinvald, A., 1991. Iso-orientation domains in cat visual cortex are arranged in pinwheel-like patterns. Nature 353 (6343), 429–431.

Borg-Graham, L., Monier, C., Fregnac, Y., 1998. Visual input evokes transient and strong shunting inhibition in visual cortical neurons. Nature 393, 369–373.

Brown, C.E., Aminoltejari, K., Erb, H., Winship, I.R., Murphy, T.H., 2009. In vivo voltage-sensitive dye imaging in adult mice reveals that somatosensory maps lost to stroke are replaced over weeks by new structural and functional circuits with prolonged modes of activation within both the peri-infarct zone and distant sites. J. Neurosci. 29 (6), 1719–1734.

Bush, P., Sejnowski, T., 1993. Reduced compartmental models of neocortical pyramidal cells. J. Neurosci. Methods 46, 159–166.

Cameron, R.S., Rakic, P., 1991. Glial cell lineage in the cerebral cortex: a review and synthesis. Glia 4, 124–137.

Carlson, G.C., Coulter, D.A., 2008. In vitro functional imaging in brain slices using fast voltage-sensitive dye imaging combined with whole-cell patch recording. Nat. Protocols 3 (2), 249–255.

Chemla, S., Chavane, F., Vieville, T., Kornprobst, P., 2007. Biophysical cortical column model for optical signal analysis. In: Cns07. <http://www.cnsorg.org>.

Chemla, S., Vieville, T., Chavane, F., 2008. Biophysical cortical column model for optical signal analysis. In: Areadne08. <http://www.areadne.org/>.

Cinelli, A.R., Salzberg, B.M., 1990. Multiple site optical recording of transmembrane voltage (msortv), single-unit recordings, and evoked field potentials from the olfactory bulb of skate (raja erinacea). J. Neurophysiol. 64 (6), 1767–1790.

Cinelli, A.R., Salzberg, B.M., 1992. Dendritic origin of late events in optical recordings from salamander olfactory bulb. J. Neurophysiol. 68 (3), 786–806.

Civillico, E.F., Contreras, D., 2006. Integration of evoked responses in supragranular cortex studied with optical recordings in vivo. J. Membr. Biol. 96 (1), 336–351.

Cohen, L., Salzberg, B.M., Davila, H.V., Ross, W.N., Landowne, D., Waggoner, A.S., Wang, C.H., 1974. Changes in axon fluorescence during activity: molecular probes of membrane potential. J. Membr. Biol. 19 (1), 1–36.

Contreras, D., Llinas, R., 2001. Voltage-sensitive dye imaging of neocortical spatiotemporal dynamics to afferent activation frequency. J. Neurosci. 21 (23), 9403–9413.

Davila, H.V., Salzberg, B.M., Cohen, L.B., Waggoner, A.S., 1973. A large change in axon fluorescence that provides a promising method for measuring membrane potential. Nat. New Biol. 241 (109), 159–160.

Derdikman, D., Hildesheim, R., Ahissar, E., Arieli, A., Grinvald, A., 2003. Imaging spatiotemporal dynamics of surround inhibition in the barrels somatosensory cortex. J. Neurosci. 23 (9), 3100–3105.

Destexhe, A., Rudolph, M., Fellous, J., Sejnowski, T., 2001. Fluctuating synaptic conductances recreate in-vivo-like activity in neocortical neurons. Neuroscience 107, 13–24.

Douglas, R.J., Martin, K.A.C., 1990. Neocortex. In: shepeherd, G. (Ed.), Synaptic Organization of the Brain. Oxford University Press, New York, pp. 220–248.

Douglas, R., Martin, K.A.C., 2004. Neuronal circuit of the neocortex. Ann. Rev. Neurosci. 27, 419.

Eberwine, J., 2001. Molecular biological of axons: a turning point. Neuron 32 (6), 959–960.

Ebner, T.J., Chen, G., 1995. Use of voltage-sensitive dyes and optical recordings in the central nervous system. Prog. Neurobiol. 46 (5), 463–506.

Faugeras, O., Grimbert, F., Slotine, J.-J., 2008. Absolute stability and complete synchronization in a class of neural fields models. SIAM J. Appl. Math. 61 (1), 205–250.

Ferezou, I., Bolea, S., Petersen, C.C.H., 2006. Visualizing the cortical representation of whisker touch: voltage-sensitive dye imaging in freely moving mice. Neuron 50, 617–629.

Geisler, C., Brunel, N., Wang, X.-J., 2005. Contributions of intrinsic membrane dynamics to fast network oscillations with irregular neuronal discharges. J. Neurophysiol. 94, 4344–4361.

Grimbert, F., Faugeras, O., Chavane, F., 2007. From neural fields to VSD optical imaging. In: Cns07. <http://www.cnsorg.org>.

Grimbert, F., Faugeras, O., Chavane, F., 2008. Neural field model of vsd optical imaging signals. In: Areadne08. <http://www.areadne.org/>.

Grinvald, A., Manker, A., Segal, M., 1982. Visualization of the spread of electrical activity in rat hippocampal slices by voltage-sensitive optical probes. J. Physiol. 333, 269–291.

Grinvald, A., Anglister, L., Freeman, J.A., Hildesheim, R., Manker, A., 1984. Real time optical imaging of naturally evoked electrical activity in the intact frog brain. Nature 308 (5962), 848–850.

Grinvald, A., Frostig, R.D., Siegel, R.M., Bartfeld, E., 1991. High-resolution optical imaging of functional brain architecture in the awake monkey. Proc. Natl. Acad. Sci. USA 88 (24), 11559–11563.

Grinvald, A., Lieke, E., Frostig, R.D., Hildesheim, R., 1994. Cortical point-spread function and long-range lateral interactions revealed by real-time optical imaging of macaque monkey primary visual cortex. J. Neurosci. 14, 2545–2568.

Grinvald, A., Shoham, D., Shmuel, A., Glaser, D., Vanzetta, I., Shtoyerman, E., Slovin, H., Arieli, A., 1999. In-vivo optical imaging of cortical architecture and dynamics. In: Windhorst, U., Johansson, H. (Eds.), Modern Techniques in Neuroscience Research. Springer Verlag, pp. 893–969.

Grinvald, A., Hildesheim, R., 2004. Vsdi: a new era in functional imaging of cortical dynamics. Nature 5, 874–885. <www.nature.com/reviews/neuro>.

Gupta, R.G., Salzberg, B.M., Grinvald, A., Cohen, L., Kamino, K., Boyle, M.B., Waggoner, S., Wang, C.H., 1981. Improvements in optical methods for measuring rapid changes in membrane potential. J. Membr. Biol. 58 (2), 123–137.

Haeusler, S., Maass, W., 2007. A statistical analysis of information-processing properties of lamina-specific cortical microcircuits models. Cereb. Cortex 17 (January), 149–162.

Hines, M., Carnevale, N., 1997. The neuron simulation environment. Neural Comput. 9, 1179–1209.

Hodgkin, A., Huxley, A., 1952. A quantitative description of membrane current and its application to conduction and excitation in nerve. J. Physiol. 117, 500–544.

Horton, J., Adams, D.L., 2005. The cortical column: a structure without a function. Philos. Trans. R. Soc. Lond. B. Biol. Sci. 360 (1456), 837–862.

Hubel, D., Wiesel, T., 1962. Receptive fields, binocular interaction and functional architecture in the cat visual cortex. J. Physiol. 160, 106–154.

Hubel, D., Wiesel, T., 1965. Receptive fields and functional architecture in two nonstriate visual areas (18 and 19) of the cat. J. Neurophysiol. 28, 229–289.

Hubel, D., Wiesel, T., 1977. Functional architecture of macaque monkey. Proc. Roy. Soc., Lond. [B], 1–59.

Hubener, M., Shoham, D., Grinvald, A., Bonhoeffer, T., 1997. Spatial relationships among three columnar systems in cat area 17. J. Neurosci. 17 (23), 9270–9284.

Jancke, D., Chavane, F., Naaman, S., Grinvald, A., 2004. Imaging cortical correlates of illusion in early visual cortex. Nature 428, 423–426.

Jin, W., Zhang, R., Wu, J., 2002. Voltage-sensitive dye imaging of population neuronal activity in cortical tissue. J. Neurosci. Methods 115, 13–27.

Kauer, J.S., 1988. Real-time imaging of evoked activity in local circuits of the salamander olfactory bulb. Nature 331 (6152), 166–168.

Kee, M.Z., Wuskell, J.P., Loew, L.M., Augustine, G.J., Sekino, Y., 2009. Imaging activity of neuronal populations with new long-wavelength voltage-sensitive dyes. Brain Cell Biol. 36 (5–6), 157–172.

Kelly, J.P., Van Essen, D.C., 1974. Cell structure and function in the visual cortex of the cat. J. Physiol. 238, 515–547.

Kohonen, T., 2001. Self-Organizing Maps, third extended ed. Springer.

Konnerth, A., Orkand, R.K., 1986. Voltage-sensitive dyes measure potential changes in axons and glia of the frog optic nerve. Neurosci. Lett. 66 (1), 49–54.

Konnerth, A., Obaid, A.L., Salzberg, B.M., 1987. Optical recording of electrical activity from parallel fibres and other cell types in skate cerebellar slices in vitro. J. Physiol. 393, 681–702.

Konnerth, A., Orkand, P.M., Orkand, R.K., 1988. Optical recording of electrical activity from axons and glia of frog optic nerve: potentiometric dye responses and morphometrics. Glia 1 (3), 225–232.

Kubota, M., Hosokawa, Y., Horikawa, J., 2006. Layer-specific short-term dynamics in network activity in the cerebral cortex. Neuroreport 17 (11), 1107–1110.

Laaris, N., Keller, A., 2002. Functional independence of layer iv barrels. J. Neurophysiol. 87 (2), 1028–1034.

La Rota, C., 2003. Analyse de l'activité électrique multi-ties du cortex auditif chez le cobaye. Ph.D. Thesis, Université Joseph Fourier, Grenoble I.

Lev-Ram, V., Grinvald, A., 1986. Ca^{2+}- and K$^+$-dependent communication between central nervous system myelinated axons and oligodendrocytes revealed by voltage-sensitive dyes. Proc. Natl. Acad. Sci. USA 83 (17), 6651–6655.

Lippert, M.T., Takagaki, K., Xu, W., Huang, X., Wu, J.Y., 2007. Methods for voltage-sensitive dye imaging of rat cortical activity with high signal-to-noise ratio. J. Neurophysiol. 98, 502–512.

Manis, P.B., Freeman, J.A., 1988. Fluorescence recordings of electrical activity in goldfish optic tectum in vitro. J. Neurosci. 8 (2), 383–394.

Miikkulainen, R., Bednar, J.A., Choe, Y., Sirosh, J., 2005. Computational Maps in the Visual Cortex. Springer, Berlin.

Mountcastle, V., 1957. Modality and topographic properties of single neurons of cat's somatosensory cortex. J. Neurophysiol. 20, 408–434.

Nelson, D.A., Katz, L.C., 1995. Emergence of functional circuits in ferret visual cortex visualized by optical imaging. Neuron 15 (1), 23–34.

Nowak, L.G., Azouz, R., Sanchez-Vives, M.V., Gray, C., McCormick, D., 2003. Electrophysiological classes of cat primary visual cortical neurons in vivo as revealed by quantitative analyses. J. Neurophysiol. 89, 1541–1566. <http://jn.physiology.org/cgi/content/abstract/89/3/1541>.

Orbach, H.S., Cohen, L.B., 1983. Optical monitoring of activity from many areas of the in vitro and in vivo salamander olfactory bulb: a new method for studying functional organization in the vertebrate central nervous system. J. Neurosci. 3, 2251–2262.

Orbach, H.S., Van Essen, D.C., 1993. In vivo tracing of pathways and spatio-temporal activity patterns in rat visual cortex using voltage sensitive dyes. Exp. Brain Res. 94 (3), 371–392.

Orbach, H.S., Cohen, L.B., Grinvald, A., 1985. Optical mapping of electrical activity in rat somatosensory and visual cortex. J. Neurosci. 5, 1886–1895.

Petersen, C., Sakmann, B., 2001. Functional independent columns of rat somatosensory barrel cortex revealed with voltage-sensitive dye imaging. J. Neurosci. 21 (21), 8435–8446.

Petersen, C., Grinvald, A., Sakmann, B., 2003. Spatiotemporal dynamics of sensory responses in layer 2/3 of rat barrel cortex measured in vivo by voltage-sensitive dye imaging combined with whole-cell voltage recordings and neuron reconstructions. J. Neurosci. 23 (3), 1298–1309.

Raizada, R., Grossberg, S., 2003. Towards a theory of the laminar architecture of the cerebral cortex: computational clues from the visual system. Cereb. Cortex 13, 100–113.

Rangan, A.V., Cai, D., McLaughlin, D.W., 2005. Modeling the spatiotemporal cortical activity associated with the line-motion illusion in primary visual cortex. Proc. Natl. Acad. Sci. USA 102 (52), 18793–18800.

Reynaud, A., Barthelemy, F., Masson, G., Chavane, F., 2007. Input–output transformation in the visuo-oculomotor network. Arch. Ital. Biol., 145.

Roland, P.E., 2002. Dynamic depolarization fields in the cerebral cortex. Trends Neurosci. 25.

Roland, P.E., Hanazawa, A., Undeman, C., Eriksson, D., Tompa, T., Nakamura, H., Valentiniene, S., Ahmed, B., 2006. Cortical feedback depolarization waves: a mechanism of top-down influence on early visual areas. Proc. Natl. Acad. Sci. USA 103 (33), 12586–12591.

Ross, W.N., Salzberg, B.M., Cohen, L.B., Grinvald, A., Davila, H.V., Waggoner, A.S., Wang, C.H., 1977. Changes in absorption, fluorescence, dichroism, and birefringence in stained giant axons: optical measurements of membrane potential. J. Membr. Biol. 33 (1–2), 141–183.

Rubin, B.D., Katz, L.C., 1999. Optical imaging of odorant representations in the mammalian olfactory bulb. Neuron 23 (3), 499–511.

Salin, P., Bullier, J., 1995. Corticocortical connections in the visual system: structure and function. Psychol. Bull. 75, 107–154.

Salzberg, B.M., Davila, H.V., Cohen, L.B., 1973. Optical recording of impulses in individual neurons of an invertebrate central nervous system. Nature 246, 508–509.

Schummers, J., Yu, H., Sur, M., 2008. Tuned responses of astrocytes and their influence on hemodynamic signals in the visual cortex. Science 320, 1638–1643.

Seidemann, E., Arieli, A., Grinvald, A., Slovin, H., 2002. Dynamics of depolarization and hyperpolarization in the frontal cortex and saccade goal. Science 295 (5556), 862–865.

Sharon, D., Grinvald, A., 2002. Dynamics and constancy in cortical spatiotemporal patterns of orientation processing. Science 295 (5554), 512–515.

Sharon, D., Jancke, D., Chavane, F., Na'aman, S., Grinvald, A., 2007. Cortical response field dynamics in cat visual cortex. Cereb. Cortex 17 (12), 2866–2877.

Shoham, D., Glaser, D., Arieli, A., Kenet, T., Wijnbergeb, C., Toledo, Y., Hildesheim, R., Grinvald, A., 1999. Imaging cortical dynamics at high spatial and temporal resolution with novel blue voltage-sensitive dyes. Neuron 24 (4), 791–802.

Sholl, D.A., 1955a. The organization of the visual cortex in the cat. J. Anat. 89, 33–46.

Sirosh, J., Miikkulainen, R., 1994. Cooperative self-organization of afferent and lateral connections in cortical maps. Biol. Cybern. 71, 66–78.

Sit, Y.F., Miikkulainen, R., 2007. A computational model of the signals in optical imaging with voltage-sensitive dyes. Neurocomputing 70 (10–12), 1853–1857.

Slovin, H., Arieli, A., Hildesheim, R., Grinvald, A., 2002. Long-term voltage-sensitive dye imaging reveals cortical dynamics in behaving monkeys. J. Neurophysiol. 88 (6), 3421–3438.

Spors, H., Grinvald, A., 2002. Spatio-temporal dynamics of odor representations in the mammalian olfactory bulb. Neuron 34 (2), 301–315.

Sterkin, A., Lampl, I., Ferster, D., Grinvald, A., Arieli, A., 1998. Realtime optical imaging in cat visual cortex exhibits high similarity to intracellular activity. Neurosci. Lett. 51.

Tasaki, I., Watanabe, A., Carnay, L., 1968. Changes in fluorescence, turbidity, and bireference associated with nerve excitation. Proc. Natl. Acad. Sci. USA 61, 883–888.

Thomson, A., Lamy, C., 2007. Functional maps of neocortical local circuitry. Front. Neurosci. 1 (1), 19–42.

Thomson, A., Morris, O., 2002. Selectivity in the inter-laminar connections made by neocortical neurones. J. Neurocytol. 31 (3–5), 239–246.

Ts'o, D.Y., Frostig, R.D., Lieke, E.E., Grinvald, A., 1990. functional organization of primate visual cortex revealed by high resolution optical imaging. Science 249 (4967), 417–420.

Tucker, T.R., Katz, L.C., 2003a. Recruitment of local inhibitory networks by horizontal connections in layer 2/3 of ferret visual cortex. J. Neurophysiol. 89 (1), 501–512.

Tucker, T.R., Katz, L.C., 2003b. Spatiotemporal patterns of excitation and inhibition evoked by the horizontal network in layer 2/3 of ferret visual cortex. J. Neurophysiol. 89 (1), 488–500.

Waggoner, A.S., Grinvald, A., 1977. Mechanisms of rapid optical changes of potential sensitive dyes. Ann. NY Acad. Sci. 30 (303), 217–241.

Waters, J., Schaefer, A., Sakmann, B., 2005. Backpropagating action potentials in neurones: measurement, mechanisms and potential functions. Prog. Biophys. Mol. Biol. 87 (1), 145–170.

Wilson, H., Cowan, J., 1972. Excitatory and inhibitory interactions in localized populations of model neurons. Biophys. J. 12, 1–24.

Wilson, H., Cowan, J., 1973. A mathematical theory of the functional dynamics of cortical and thalamic nervous tissue. Biol. Cybern. 13 (2), 55–80.

Woolum, J.C., Strumwasser, F., 1978. Membrane-potential-sensitive dyes for optical monitoring of activity in aplysia neurons. J. Neurobiol. 9 (3), 185–193.

Xu, W., Huang, X., Takgaki, K., Wu, J., 2007. Compression and reflection of visually evoked cortical waves. Neuron 55 (1), 119–129.

Yang, Z., Heeger, D.J., Seidemann, E., 2007. Rapid and precise retinotopic mapping of the visual cortex obtained by voltage-sensitive dye imaging in the behaving monkey. J. Neurophysiol. 98 (2), 1002–1014.

Young, J.Z., 1958. Anatomical considerations. EEG Clin. Neurophysiol. 10, 9–11.

Yuste, R., Tank, D.K., Kleinfeld, D., 1997. Functional study of the rat cortical microcircuitry with voltage-sensitive dye imaging of neocortical slices. Cereb. Cortex 7 (6), 546–558.

Zochowski, M., Wachowiak, M., Falk, C.X., Cohen, L.B., Lam, Y.W., Antic, S., Zecevic, D., 2000. Imaging membrane potential with voltage-sensitive dyes. Biol. Bull. 198 (1), 749–762.

Bibliography

Abbott, L., Regehr, W., 2004. Synaptic computation. Nature 431, 796–803.

Abeles, M., 1991. Neural circuits of the cerebral cortex. Cambridge University Press.

Adrian, E., 1914. The all-or-none principle in nerve. J. Physiol. 47 (6), 460–474.

Ahmed, B., Allison, J., Douglas, R., Martin, K., 1997. An intracellular study of the contrast-dependence of neuronal activity in cat visual cortex. Cereb. Cortex 7, 559–570.

Ahmed, B., Hanazawa, A., Undeman, C., Eriksson, D., Valentiniene, S., Roland, P. E., 2008. Cortical dynamics subserving visual apparent motion. Cereb. Cortex 18 (12), 2796–2810.

Aitken, J. T., 1955. Observations on the larger anterior horn cells in the lumbar region of the cat's spinal cord. J. Anat., Lond. 89, 571.

Albowitz, B., Kuhnt, U., 1993. The contribution of intracortical connections to horizontal spread of activity in the neocortex as revealed by voltage sensitive dyes and a fast optical recording method. Eur. J. Neurosci. 5 (10), 1349–1359.

Albrecht, D., 1995. Visual cortex neurons in monkey and cat: Effect of contrast on the spatial and temporal phase transfer functions. Vis. Neurosci., 1191–1210.

Albrecht, D., Farrar, S., Hamilton, D., 1984. Spatial contrast adaptation characteristics of neurones recorded in the cat's visual cortex. J. Physiol. (Lond) 347, 713–739.

Albrecht, D., Geisler, W., 1991. Motion selectivity and the contrast-response function of simple cells in the visual cortex. Vis. Neurosci. 7, 531–546.

Albrecht, D., Hamilton, D., 1982. Striate cortex of monkey and cat: Contrast response function. J. Neurophysiol. 48 (1), 217–233.

Alonso, J., Usrey, W., Reid, R., 2001. Rules of connectivity between geniculate cells and simple cells in cat primary visual cortex. J. Neurosci. 21 (11), 4002–4015.

165

Anderson, J., Carandini, M., Ferster, D., 2000. Orientation tuning of input conductance, excitation, and inhibition in cat primary visual cortex. J. Neurophysiol. 84 (2), 909–926.

Antic, S., Major, G., Zecevic, D., 1999. Fast optical recordings of membrane potential changes from dendrites of pyramidal neurons. J. Neurophysiol. 82 (3), 1615–1621.

Antic, S., Zecevic, D., 1995. Optical signals from neurons with internally applied voltage-sensitive dyes. J. Neurosci. 15 (2), 1392–1405.

Arbib, M., 2002. Handbook of brain theory and neural netw. The MIT Press.

Arieli, A., Shoham, D., Hildesheim, R., Grinvald, A., 1995. Coherent spatiotemporal patterns of ongoing activity revealed by real-time optical imaging coupled with single-unit recording in the cat visual cortex. J. Neurophysiol. 73 (5), 2072–2093.

Arieli, A., Sterkin, A., Grinvald, A., Aerster, A., 1996. Dynamics of ongoing activity: explanation of the large variability in evoked cortical responses. Science 273 (5283), 1868–1871.

Aviel, Y., Mehring, C., Abeles, M., Horn, D., 2003. On embedding synfire chains in a balanced network. Neural Comput. 15 (6), 1321–1340.

Baccus, S., Meister, M., 2002. Fast and slow contrast adaptation in retinal circuitry. Neuron 36 (5), 909–919.

Bargas, J., Galarraga, E., 1998. Ion channels: Keys to neuronal specialization. The handbook of brain theory and Neural Netw., 496–501.

Bedard, C., Destexhe, A., 2009. Macroscopic models of local field potentials and the apparent 1/f noise in brain activity. Biophysical Journal 96 (7), 2589–2603.

Bedard, C., Kroger, H., Destexhe, A., 2004. Modeling extracellular field potentials and the frequency-filtering properties of extracellular space. Biophysical Journal 86, 1829–1842.

Belliveau, J., Kennedy, D., McKinstry, R., Buchbinder, B., Weisskoff, R., Cohen, M., Vevea, J., Brady, T., Rosen, B., 1991. Functional mapping of the human visual cortex by magnetic resonance imaging. Science 254 (5032), 716–719.

Ben-Yishai, R., Bar-Or, R., Sompolinsky, H., 1995. Theory of orientation tuning in visual cortex. Proc. Natl. Acad. Sci. U. S. A. 92, 3844–3848.

Benucci, A., Robert, A. F., Carandini, M., 2007. Standing waves and traveling waves distinguish two circuits in visual cortex. Neuron 55 (1), 103–117.

Berger, H., 1929. Uber das elektroencephalogramm des menschen. Arch. Psychiat. Nervenkr. 87, 527–570.

Berger, T., Borgdorff, A., Crochet, S., Neubauer, F. B., Lefort, S., Fauvet, B., Ferezou, I., Carleton, A., Luscher, H. R., Petersen, C. C., 2007. Combined voltage and calcium epifluorescence imaging in vitro and in vivo reveals subthreshold and suprathreshold dynamics of mouse barrel cortex. J. Neurophysiol. 97 (5), 3751–3762.

Binzegger, T., Douglas, R., Martin, K., Sep. 2004. A quantitative map of the circuit of cat primary visual cortex. J. Neurosci. 24 (39), 8441–8453.

Bishop, C., 1994. Neural networks and their applications. Rev. Sci. Instrum. 65 (6), 1803.

Bishop, C., 1995. Neural Netw. for pattern recognition. Clarendon Press, Oxford.

Blakemore, C., Campbell, F., 1969. On the existence of neurones in the human visual system selectively sensitive to the orientation and size of retinal images. J. Physiol. 203 (1), 237–260.

Blasdel, G., 1992. Orientation selectivity, preference, and continuity in monkey striate cortex. J. Neurosci. 12 (8), 3139–3161.

Blasdel, G., Campbell, D., 2001. Functional retinotopy of monkey visual cortex. J. Neurosci. 21 (20), 8286–8301.

Blasdel, G. G., Salama, G., 1986. Voltage-sensitive dyes reveal a modular organization in monkey striate cortex. Nature 321 (6070), 579–585.

Bolz, J., Gilbert, C., Wiesel, T., 1989. Pharmacological analysis of cortical circuitry. TINS 12 (8), 292–296.

Bolz, J., Novak, N., Staiger, V., 1992. Formation of specific afferent connections in organotypic slice cultures from rat visual cortex cocultured with lateral geniculate nucleus. J. Neurosci. 12 (8), 3054–3070.

Bonds, A., 1989. Role of inhibition in he specification of orientation selectivity of cells in the cat striate cortex. Vis. Neurosci. 2, 41–55.

Bonds, A., 1991. Temporal dynamics of contrast gain in single cells of the cat striate corte. Vis. Neurosci. 6, 239–255.

Bonhoeffer, T., Grinvald, A., 1991. Iso-orientation domains in cat visual cortex are arranged in pinwheel-like patterns. Nature 353 (6343), 429–431.

Bonhoeffer, T., Grinvald, A., 1996. Optical imaging based on intrinsic signals. the methodology. In: Toga A, Mazziota J, editors. Brain mapping: the methods. London Academic Press, 55–97.

Bonin, V., Mante, V., Carandini, M., Nov. 2005. The suppressive field of neurons in Lateral Geniculate Nucleus. J. Neurosci. 25 (47), 10844–10856.

Borg-Graham, L., Monier, C., Fregnac, Y., 1998. Visual input evokes transient and strong shunting inhibition in visual cortical neurons. Nature 393, 369–373.

Bosking, W. H., Crowley, J., Fitzpatrick, D., 2002. Spatial coding of position and orientation in primary visual cortex. Nat. Neurosci. 5 (9), 874–882.

Bosking, W. H., Zhang, Y., Schofield, B., Fitzpatrick, D., 1997. Orientation selectivity and the arrangement of horizontal connections in tree shrew striate cortex. J. Neurosci. 17 (6), 2112–2127.

Boyden, E., Zhang, F., Bamberg, E., Nagel, G., Deisseroth, K., 2005. Millisecond-timescale, genetically-targeted optical control of neural activity. Nat. Neurosci. 8 (9), 1263–1268.

Boynton, G., 2005. Contrast gain in the brain. Neuron 47, 476–477.

Brent, R., 1976. A new algorithm for minimizing a function of several variables without calculating derivatives. Englewood Cliffs, NJ : Prentice Hall, pp. 200–248.

Bringuier, V., Chavane, F., Glaeser, L., Fregnac, Y., 1999. Horizontal propagation of visual activity in the synaptic integration field of area 17 neurons. Science 283 (5402), 695–699.

Brown, C. E., Aminoltejari, K., Erb, H., Winship, I. R., Murphy, T. H., 2009. In vivo voltage-sensitive dye imaging in adult mice reveals that somatosensory maps lost to stroke are replaced over weeks by new structural and functional circuits with prolonged modes of activation within both the peri-infarct zone and distant sites. J. Neurosci. 29 (6), 1719–1734.

Bullock, T., 1979. New attempts to assess specialization of function in the nervous system. Zh. Evol. Biokhim. Fiziol. 15 (5), 449–458.

Burnod, Y., 1993. An adaptive neural network: the cerebral cortex. Masson, Paris, 2nd edition.

Bush, P., Priebe, N., 1998. Gabaergic inhibitory control of the transient and sustained components of orientation selectivity in a model microcolumn in layer 4 of cat visual cortex. Neural Comput. 10 (4), 855–867.

Bush, P., Prince, D., Miller, K., 1999. Increased pyramidal excitability and nmda conductance can explain posttraumatic epileptogenesis without disinhibition: A model. J. Neurophysiol. 82, 1748–1758.

Bush, P., Sejnowski, T., 1991. Simulations of a reconstructed cerebellar purkinje cell based on simplified channel kinetics. Neural Comp. 3, 299–309.

Bush, P., Sejnowski, T., 1993. Reduced compartmental models of neocortical pyramidal cells. J. Neurosci. Methods 46, 159–166.

Bush, P., Sejnowski, T., 1996. Inhibition synchronizes sparsely connected cortical neurons within and between columns in realistic network models. J. Comput. Neurosci. 3 (2), 91–110.

Buxhoeveden, D., Casanova, M., 2002. The minicolumn hypothesis in neuroscience. Brain 125, 935–951.

Buzas, P., Eysel, U. T., Adorjan, P., Kisvarday, Z. F., 2001. Axonal topography of cortical basket cells in relation to orientation, direction and ocular dominance maps. J. Comp. Neurol. 437, 259–285.

Buzas, P., Kovacs, K., Ferecsko, A. S., Budd, J. M., Eysel, U. T., Kisvarday, Z. F., 2006. Model-based analysis of excitatory lateral connections in the visual cortex. J. Comp. Neurol. 499, 861–881.

Cai, D., Rangan, A. V., McLaughlin, D. W., 2005. Architectural and synaptic mechanisms underlying coherent spontaneous activity in v1. Proc Natl Acad Sci 102 (16), 5868–5873.

Callaghan, P., 1991. Principles of nuclear magnetic resonance microscopy. Oxford University Press.

Callaway, E., 1998. Local circuits in primary visual cortex of the macaque monkey. Annu. Rev. Neurosci. 21, 47–74.

Callaway, E., 2004. Feedforward, feedback and inhibitory connections in primate visual cortex. Neural Netw. 17, 625–632.

Cameron, R. S., Rakic, P., 1991. Glial cell lineage in the cerebral cortex: a review and synthesis. Glia 4, 124–137.

Carandini, M., Heeger, D., 1994. Summation and division by neurons in primate visual cortex. Science 264, 1333–1336.

Carandini, M., Heeger, D., Movshon, J., nov 1997. Linearity and normalization in simple cells of the macaque primary visual cortex. Jounal of Neuroscience 17 (21), 8621–8644.

Carandini, M., Heeger, D., Senn, W., 2002. A synaptic explanation of suppression in visual cortex. J. Neurosci. 22 (22), 10053–10065.

Cardin, J.A. amd Carlen, M., Meletis, K. amd Knoblich, U., Zhang, F., Deisseroth, K., Tsai, L., Moore, C., 2009. Driving fast-spiking cells induces gamma rhythm and controls sensory responses. Nature 459, 663–668.

Carlson, G. C., Coulter, D. A., 2008. In vitro functional imaging in brain slices using fast voltage-sensitive dye imaging combined with whole-cell patch recording. Nature Protocols 3 (2), 249–255.

Caton, R., 1785. Electrical currents of the brain. The Journal of Nervous and Mental Disease 2 (4), 610.

Chander, D., Chichilnisky, E., 2001. Adaptation to temporal contrast in primate and salamander retina. J. Neurosci. 21 (24), 9904–9916.

Chapman, B., Zahs, K., Stryker, M., 1991. Relation of cortical cell orientation selectivity to alignment of receptive fields of the geniculocortical afferents that arborize within a single orientation column in ferret visual cortex. J. Neurosci. 11 (5), 1347–1458.

Chemla, S., Chavane, F., 2009. Voltage-sensitive dye imaging: Technique review and models. J. Physiol., Paris, doi: 10.1016/j.jphysparis.2009.11.009.

Cheng, B., Titterington, D., 1994. Neural networks: A review from a statistical perspective. Statistical Science 9, 2–54.

Cheng, H., Chino, Y., Smith, E. r., Hamamoto, J., Yoshida, K., 1995. Transfer characteristics of lateral geniculate nucleus x neurons in the cat: effects of spatial frequency and contrast. J. Neurophysiol. 74 (6), 2548–2557.

Cinelli, A. R., Kauer, J. S., 1992. Voltage-sensitive dyes and functional activity in the olfactory pathway. Annu. Rev. Neurosci. 15, 321–351.

Cinelli, A. R., Salzberg, B. M., 1990. Multiple site optical recording of transmembrane voltage (msortv), single-unti recordings, and evoked field potentials from the olfactory bulb of skate (raja erinacea). J. Neurophysiol. 64 (6), 1767–1790.

Cinelli, A. R., Salzberg, B. M., 1992. Dendritic origin of late events in optical recordings from salamander olfactory bulb. J. Neurophysiol. 68 (3), 786–806.

Civillico, E. F., Contreras, D., 2006. Integration of evoked responses in supragranular cortex studied with optical recordings in vivo. J. Membr. Biol. 96 (1), 336–351.

Cohen, L., Salzberg, B. M., Davila, H. V., Ross, W. N., Landowne, D., Waggoner, A. S., Wang, C. H., 1974. Changes in axon fluorescence during activity: molecular probes of membrane potential. J. Membr. Biol. 19 (1), 1–36.

Cole, K., 1949. Some physical aspects of bioelectric phenomena. Proc. Natl. Acad. Sci. 35, 558–565.

Connors, B., Gutnick, M., 1990. Intrinsic firing patterns of diverse neocortical neurons. Trends Neurosci. 13 (3), 99–104.

Contreras, D., Llinas, R., 2001. Voltage-sensitive dye imaging of neocortical spatiotemporal dynamics to afferent activation frequency. J. Neurosci. 21 (23), 9403–9413.

Contreras, D., Palmer, L., 2003. Response to contrast of electrophysiologically defined cell classes in primary visual cortex. J. Neurosci. 23 (17), 6936–6945.

Cooper, G., Robson, J., 1968. Successive transformations of visual information in the visual system. In: Pattern Recognition, I.E.E.E. N.P.L. Conf. Publ. 42, 134–143.

Crair, M., Ruthazer, E., Gillespie, D., Stryker, M., 1997. Ocular dominance peaks at pinwheel center singularities of the orientation map in cat visual cortex. J. Neurophysiol. 77 (6), 3381–3385.

Crook, J., Engelmann, R., Lowel, S., 2002. Gaba-inactivation attenuates colinear facilitation in cat primary visual cortex. Exp. Brain Res. 143, 295–302.

Crook, J., Eysel, U., 1992. Gaba-induced inactivation of functional characterized sites in cat visual cortex (area 18): Effects on orientation tuning. J. Neurosci. 12, 1816–1825.

Crook, J., Kisvarday, Z., Eysel, U., 1996. Gaba-induced inactivation of functionally characterized sites in cat visual cortex (area 18): Effects on direction selectivity. J. Neurophysiol. 75, 2071–2088.

Crook, J., Kisvarday, Z., Eysel, U., 1998. Evidence for a contribution of lateral inhibition to orientation tuning and direction selectivity in cat visual cortex: Reversible inactivation of functionally characterized sites combined with neuroanatomical tracing techniques. Eur. J. Neurosci. 10, 2056–2075.

Crowder, N., Hietanen, M., Price, N., Clifford, C., Ibbotson, M., 2008. Dynamic contrast change produces rapid gain control in visual cortex. J. Physiol. 586 (Pt 17), 4107–4119.

Das, A., Gilbert, C., 1999. Topography of contextual modulations mediated by short-range interactions in primary visual cortex. Nature 399, 655–661.

Davila, H. V., Salzberg, B. M., Cohen, L. B., Waggoner, A. S., 1973. A large change in axon fluorescence that provides a promising method for measuring membrane potential. Nat. New. Biol. 241 (109), 159–160.

Davison, A., Bruderle, D., Eppler, J., Kremkow, J., Muller, E., Pecevski, D., Perrinet, L., Yger, P., 2009. Pynn: a common interface for neuronal network simulators. Frontiers in Neuroinformatics 2.

Dayan, P., Abbott, L. F., 2001. Theoretical Neuroscience : Computational and Mathematical Modeling of Neural Systems. MIT Press.

de Graaf, R., 1998. In vivo nmr spectroscopy: principle and techniques. Chichester: Wiley.

De Valois, R., Cottaris, N., Mahon, L., Elfar, S., Wilson, J., 2000. Spatial and temporal receptive fields of geniculate and cortical cells and directional selectivity. Vision Res. 40, 3685–3702.

Dean, A., 1981. The relationship between response amplitude and contrast for cat striate cortical neurones. J. Physiol. 318, 413–427.

Dean, A., 1983. Adaptation-induced alteration of the relation between response amplitude and contrast in cat striate cortical neurones. Vision Res. 23, 249–256.

DeAngelis, G., Ghose, G., Ohzawa, I., Freeman, R., 1999. Functional micro-organization of primary visual cortex: Receptive field analysis of nearby neurons. J. Neurosci. 19 (9), 4046–4064.

DeAngelis, G., Ohzawa, I., Freeman, R., 1993. Spatiotemporal organization of simple-cell receptive fields in the cat's striate cortex. ii. linearity of temporal and spatial summation. J. Neurophysiol. 69, 1118–1135.

DeAngelis, G., Ohzawa, I., Freeman, R., 1995. Receptive-field dynamics in the central visual pathways. TINS 18 (10), 451–458.

DeFelipe, J., 1993. Neocortical neuronal diversity: chemical heterogeneity revealed by colocalization studies of classic neurotransmitters, neuropeptides, calcium-binding proteins and cell surface molecules. Cereb. Cortex. 3 (4), 273–289.

DeFelipe, J., Jones, E., 1985. Vertical organization of gamma-aminobutyric acid-accumulating intrinsic neuronal systems in monkey cerebral cortex. J. Neurosci. 5 (12), 3246–3260.

Demb, J., 2008. Functional circuitry of visual adaptation in the retina. J. Physiol. 586 (18), 4377–4384.

Denk, W., Delaney, K., Gelperin, A., Kleinfeld, D., Strowbridge, B., Tank, D., Yuste, R., 1994. Anatomical and functional imaging of neurons using 2-photon laser scanning microscopy. J. Neurosci. 54 (2), 151–162.

Denk, W., Strickler, J., Webb, W., 1990. Two-photon laser scanning microscopy. Science 248, 73–76.

Denk, W., Svoboda, K., 1997. Photon upmanship: why multiphoton imaging is more than a gimmick. Neuron 18 (3), 351–357.

Derdikman, D., Hildesheim, R., Ahissar, E., Arieli, A., Grinvald, A., 2003. Imaging spatiotemporal dynamics of surround inhibition in the barrels somatosensory cortex. J. Neurosci. 23 (8), 3100–3105.

Derrington, A., Lennie, P., 1984. Spatial and temporal contrast sensitivities of neurones in lateral geniculate nucleus of macaque. J. Physiol. 357, 219–240.

Destexhe, A., Mainen, Z., Sejnowski, T., 1994. Synthesis of models for excitable membranes, synaptic transmission and neuromodulation using a common kinetic formalism. J. Comput. Neurosci. 1 (3), 195–230.

Destexhe, A., Mainen, Z., Sejnowski, T., 1998. Kinetic models of synaptic transmission. MIT Press, Cambridge.

Destexhe, A., Pare, D., 1999. Impact of network activity on the integrative properties of neocortical pyramidal neurons in vivo. J. Neurophysiol. 81 (4), 1531–1547.

Destexhe, A., Rudolph, M., Fellous, J., Sejnowski, T., 2001. Fluctuating synaptic conductances recreate in-vivo-like activity in neocortical neurons. Neuroscience 107, 13–24.

Destexhe, A., Rudolph, M., Pare, D., 2003. The high-conductance state of neocortical neurons in vivo. Nat. Rev. Neurosci. 4 (9), 739–751.

DeYoe, E., Bandettini, P., Neitz, J., Miller, D., Winans, P., Oct. 1994. Functional Magnetic Resonance Imaging (fMRI) of the human brain. Journal Neuroscience Methods 54 (2), 171–187.

Douglas, R., Martin, K. A. C., 2004. Neuronal circuit of the neocortex. Annu. Rev. Neurosci. 27, 419.

Douglas, R. J., Martin, K. A. C., 1990. Neocortex. in: G shepeherd, ed. synaptic organization of the brain. Oxford University Press, New York, 220–248.

Douglas, R. J., Martin, K. A. C., 1991. A functional microcircuit for cat visual cortex. J. Physiol. 440, 735–769.

Douglas, R. J., Martin, K. A. C., Whitteridge, D., 1989. A canonical microcircuit for neocortex. Neural Comput. 1 (4), 480–488.

Duong, T., Freeman, R., 2007. Contrast sensitivity is enhanced by expansive nonlinear processing in the lateral geniculate nucleus. J. Neurophysiol. 99, 367–372.

Duong, T., Kim, D., Ugurbil, K., Kim, S., 2000. Spatiotemporal dynamics of the bold fmri signals: toward mapping submillimeter cortical columns using the early negative response. Magn. Reson. Med. 44 (2), 231–242.

Eberwine, J., 2001. Molecular biological of axons: a turning point... Neuron 32 (6), 959–960.

Ebner, T. J., Chen, G., 1995. Use of voltage-sensitive dyes and optical recordings in the central nervous system. Progress in Neurobiology 46 (5), 463–506.

Eilers, J., Konnerth, A., 1997. Dendritic signal integration. Curr. Opin. Neurobiol. 7 (3), 385–390.

Engel, S., Glover, G., Wandell, B., 1997. Retinotopic organization in human visual cortex and the spatial precision of functional MRI. Cereb. Cortex 7, 181–192.

Enroth-Cugell, C., Robson, J. G., 1966. The contrast sensitivity of retinal ganglion cells of the cat. J Physiol 187, 517–552.

Ermentrout, B., 1998. Neural networks as spatio-temporal pattern-forming systems. Reports on Progress in Physics 61, 353–430.

Ernst, U., Pawelzik, K., Sahar-pikielny, C., Tsodyks, M., 2001. Intracortical origin of visual maps. Nat. Neurosci. 4 (4), 431–436.

Faugeras, O., Grimbert, F., Slotine, J.-J., 2008. Absolute stability and complete synchronization in a class of neural fields models. SIAM Journal of Applied Mathematics 69, 205–250.

Faugeras, O., Touboul, J., Cessac, B., 2009. A constructive mean-field analysis of multi-population neural netw. with random synaptic weights and stochastic inputs. Front. Comput. Neurosci. 3 (1), doi:10.3389/neuro.10.001.2009.

Felleman, D., Van Essen, D., 1991. Distributed hierarchical processing in the primate cerebral cortex. Cereb Cortex 1, 1–47.

Ferezou, I., Bolea, S., Petersen, C. C. H., 2006. Visualizing the cortical representation of whisker touch: Voltage-sensitive dye imaging in freely moving mice. Neuron 50, 617–629.

Ferster, Lindstrom, 1983. An intracellular analysis of geniculo-cortical connectivity in area 17 of the cat. J. Physiol. 342, 181–215.

Ferster, Lindstrom, 1985a. Augmenting responses evoked in area 17 of the cat by intra-cortical axon collaterals of cortico-geniculate cells. J. Physiol. 367, 217–232.

Ferster, Lindstrom, 1985b. Synaptic excitation of neurones in area 17 of the cat by in-tracortical axon collaterals of cortico-geniculate cells. J. Physiol. 367, 233–252.

Ferster, D., Miller, K. D., Mar. 2000. Neural mechanisms of orientation selectivity in the visual cortex. Annual Review of Neuroscience 23, 441–471.

FitzHugh, R., 1969. Mathematical models for excitation and propagation in nerve. Biological Engineering. H.P. Schawn (Ed.), New York: McGraw-Hill.

Fregnac, Y., Monier, C., Chavane, F., Bandot, P., Graham, L., 2003. Shunting inhibition, a silent step in visual cortical computation. J. Physiol., Paris 97, 441–451.

Friedman, H., Bruce, C., Goldman-Rakic, P., 1989. Resolution of metabolic columns by a double-label 2-dg technique: Interdigitation and coincidence in visual cortical areas of the same monkey. J. Neurosci. 9, 4111–4121.

Frostig, R. D., 2009. In Vivo Optical Imaging of Brain Function (Second Edition). Taylor & Francis Group LLC.

Fuhrmann, G., Segev, I., Markram, H., Tsodyks, M., 2002. Coding of temporal information by activity-dependent synapses. J. Neurophysiol. 87, 140–148.

Gauck, V., Jaeger, D., 2003. The contribution of nmda and ampa conductances to the control of spiking in neurons of the deep cerebellar nuclei. J. Neurosci. 23 (22), 8109–8118.

Gazeres, N., Borg-Graham, L., Fregnac, Y., 1998. A model of non-lagged X responses to flashed stimuli in the cat lateral geniculate nucleus. Vis. Neurosci. 15, 1157–1174.

Geisler, C., Brunel, N., Wang, X.-J., 2005. Contributions of intrinsic membrane dynamics to fast network oscillations with irregular neuronal discharges. J. Neurophysiol. 94, 4344–4361.

Geisler, W., Albrecht, D., 1992. Cortical neurons: isolation of contrast gain control. Vision Res. 32 (8), 1409–1410.

Geisler, W., Albrecht, D., Salvi, R., Sanders, S., 1991. Discrimination performance of single neurons: Rate and temporal-pattern information. J. Neurophysiol. 66, 334–362.

Gerstner, W., 1999. Spiking Neurons. MIT-press.

Gerstner, W., Kempter, R., Leo van Hemmen, J., Wagner, H., 1999. Hebbian Learning of Pulse Timing in the Barn Owl Auditory System. MIT-press.

Gerstner, W., Kistler, W. M., 2002. Mathematical formulations of hebbian learning. Biological Cybernetics 87, 404–415.

Gilbert, C., 1983. Microcircuitry of the visual cortex. Annu. Rev. Neurosci. 6, 217–247.

Gilbert, C., Wiesel, T. N., 1979. Morphology and intracortical projections of functionally characterized neurones in the cat visual cortex. Nature 280 (5718), 120–125.

Gilbert, C., Wiesel, T. N., 1983. Clustered intrinsic connection in cat visual cortex. J. Neurosci. 3 (5), 1116–1133.

Gilbert, C., Wiesel, T. N., 1989. Columnar specificity of intrinsic horizontal and cortico-cortical connections in cat visual cortex. J. Neurosci. 9 (4), 1389–1399.

Grimbert, F., Faugeras, O., Chavane, F., 2007. From neural fields to VSD optical imaging. in: Cns07.
URL http://www.cnsorg.org

Grimbert, F., Faugeras, O., Chavane, F., 2008. Neural field model of vsd optical imaging signals. in: Areadne08.
URL http://www.areadne.org/

Grinvald, A., Anglister, L., Freeman, J. A., Hildesheim, R., Manker, A., 1984. Real time optical imaging of naturally evoked electrical activity in the intact frog brain. Nature 308 (5962), 848–850.

Grinvald, A., Frostig, R. D., Siegel, R. M., Bartfeld, E., 1991. High-resolution optical imaging of functional brain architecture in the awake monkey. Proc Natl Acad Sci U S A 88 (24), 11559–11563.

Grinvald, A., Hildesheim, R., 2004. Vsdi: A new era in functional imaging of cortical dynamics. Nature 5 (11), 874–885.

Grinvald, A., Lieke, E., Frostig, R. D., Gilbert, C. D., Wiesel, T. N., 1986. Functional architecture of cortex revealed by optical imaging of intrinsic signals. Nature 324 (6095), 361–364.

Grinvald, A., Lieke, E., Frostig, R. D., Hildesheim, R., 1994. Cortical point-spread function and long-range lateral interactions revealed by real-time optical imaging of macaque monkey primary visual cortex. J. Neurosci. 14, 2545–2568.

Grinvald, A., Manker, A., Segal, M., 1982. Visualization of the spread of electrical activity in rat hippocampal slices by voltage-sensitive optical probes. J. Physiol. 333, 269–291.

Grinvald, A., Shoham, D., Shmuel, A., Glaser, D., Vanzetta, I., Shtoyerman, E., Slovin, H., Arieli, A., 1999. In-vivo optical imaging of cortical architecture and dynamics. Modern Techniques in Neuroscience Research (Windhorst U., Johansson H. Springer Verlag), 893–969.

Grinvald, A., Slovin, H., Vanzetta, I., 2000. Non-invasive visualization of cortical columns by fmri. Nat. Neurosci. 3 (2), 105–107.

Gupta, A., Wang, Y., Markram, H., 2000. Organizing principles for a diversity of gabaergic interneurons and synapses in the neocortex. Science 287 (5451), 273–278.

Gupta, R. G., Salzberg, B. M., Grinvald, A., Cohen, L., Kamino, K., Boyle, M. B., Waggoner, S., Wang, C. H., 1981. Improvements in optical methods for measuring rapid changes in membrane potential. J. Mem. Biol. 58 (2), 123–137.

Haeusler, S., Maass, W., jan 2007. A statistical analysis of information-processing properties of lamina-specific cortical microcircuits models. Cereb. Cortex 17, 149–162.

Halasy, K., Somogyi, P., 1993. Distribution of gabaergic synapses and their targets in the dentate gyrus of rat: a quantitative immunoelectron microscopic analysis. J. Hirnforsch. 34 (3), 299–308.

Hartline, H., 1940. The receptive fields of optic nerve fibers. Am. J. Physiol. 130, 690–699.

Harveit, E., Heggelund, P., 1992. The effect of contrast on the visual response of lagged and nonlagged cells in the cat lateral geniculate nucleus. Vis. Neurosci. 9, 515–525.

Hausser, M., 2001. Synaptic function: Dendritic democracy. Curr. Biol. 11, R10–R12.

Hellwig, B., 2000. A quantitative analysis of the local connectivity between pyramidal neurons in layers 2/3 of the rat visual cortex. Biol. Cybern. 82 (2), 111–121.

Helmchen, F., Denk, W., 2002. New developments in multiphoton microscopy. Curr. Opin. Neurobiol. 12 (5), 593–601.

Helmchen, F., Denk, W., 2005. Deep tissue two-photon microscopy. Nat. methods 2 (12), 932–940.

Hestrin, S., 1992. Activation and desensitization of glutamate-activated channels mediating fast excitatory synaptic currents in the visual cortex. Neuron 9 (5), 991–999.

Hille, B., 1992. Ionic Channels of Excitable Membranes (2nd ed.). Sunderland. MA: Sinauer.

Hines, M., Carnevale, N., 1997. The neuron simulation environment. Neural Comput. 9, 1179–1209.

Hirsch, J., Gilbert, C., 1991. Synaptic physiology of horziontal connections in the cat's visual cortex. J. Neurosci. 11, 1800–1809.

Hodgkin, A., Huxley, A., 1939. Action potentials recorded from inside a nerve fiber. Nature 144, 710–711.

Hodgkin, A., Huxley, A., 1952a. The components of membrane conductance in the giant axon of loligo. J. Physiol. 116 (4), 473–496.

Hodgkin, A., Huxley, A., 1952b. Currents carried by sodium and potassium ions through the membrane of the giant axon of loligo. J. Physiol. 116 (4), 449–472.

Hodgkin, A., Huxley, A., 1952c. The dual effect of membrane potential on sodium conductance in the giant axon of loligo. J. Physiol. 116 (4), 497–506.

Hodgkin, A., Huxley, A., 1952d. Movement of sodium and potassium ions during nervous activity. Cold Spring Harb. Symp. Quant. Biol. 17, 43–52.

Hodgkin, A., Huxley, A., 1952e. A quantitative description of membrane current and its application to conduction and excitation in nerve. J. Physiol. 117 (4), 500–544.

Hodgkin, A., Huxley, A., Katz, B., 1952. Measurement of current-voltage relations in the membrane of the giant axon of loligo. J. Physiol. 116 (4), 424–448.

Holmes, W., 1990. Is the function of dendritic spines to concentrate calcium. Brain Research 519, 338–342.

Horikawa, J., Hosokawa, Y., Kubota, M., Nasu, M., Taniguchi, I., 1996. Optical imaging of spatiotemporal patterns of glutamatergis excitation and gabaergic inhibition in the guinea-pig auditory cortex in vivo. J. Physiol 497 (3), 629–638.

Horton, J., Adams, D., April 2005. The cortical column: a structure without a function. Philos. Trans. R. Soc. Lond. B. Biol. Sci. 360 (1456), 837–862.

Hosokawa, Y., Horikawa, J., Nasu, M., Taniguchi, I., 1997. Real-time imaging of neural activity during binaural interaction in the guinea pig auditory cortex. J. Comp. Physiol [A] 181 (6), 607–614.

Hu, X., Le, T., Ugurbil, K., 1997. Evaluation of the early response in fmri in individual subjects using short stimulus duration. Magn. Reson. Med 37, 877–884.

Hubel, D., Wiesel, T., 1965. Receptive fields and functional architecture in two nonstriate visual areas (18 and 19) of the cat. J. Neurophysiol. 28, 229–289.

Hubel, D., Wiesel, T., 1974. Sequence regularity and geometry of orientation columns in the monkey striate cortex. J. Comp. Neurol. 158 (3), 267–293.

Hubel, D., Wiesel, T., 1977. Functional architecture of macaque monkey. Proceedings of the Royal Society, London [B], 1–59.

Hubel, D. H., Wiesel, T. N., 1959. Receptive fileds of single neurones in the cat's striate cortex. J. Physiol. 148, 574–591.

Hubel, D. H., Wiesel, T. N., 1962. Receptive fields, binocular interaction and functional architecture in the cat's visual cortex. J. Physiol. 160, 160–154.

Hubel, D. H., Wiesel, T. N., 1963. Shape and arrangement of columns in cat's striate cortex. J. Physiol. 165, 559–568.

Hubel, D. H., Wiesel, T. N., 1969. Anatomical demonstration of columns in the monkey striate cortex. Nature 221 (5182), 747–750.

Hubel, D. H., Wiesel, T. N., Stryker, M. P., 1978. Anatomical demonstration of orientation columns in macaque monkey. J. Comp. Neur. 177, 361–380.

Hubener, M., Shoham, D., Grinvald, A., Bonhoeffer, T., 1997. Spatial relationships among three columnar systems in cat area 17. J. Neurosci. 17 (23), 9270–9284.

Huguenard, J., Hamill, O., Prince, D., 1989. Sodium channels in dendrites of rat cortical pyramidal neurons. Proc. Natl. Acad. Sci. USA 86 (7), 2473–2477.

Ikeda, H., M.J., W., 1974. Sensitivity of neurones in visual cortex (area 17) under different levels of anesthesia. Exp. Brain. Res. 20, 471–484.

Izhikevich, E., 2003. Simple model of spiking neurons. IEEE Transactions on Neural Networks 14 (6), 1569–1572.

Izhikevich, E., 2004. Which model to use for cortical spiking neurons? IEEE Transactions on Neural Networks 15, 1063–1070.

Izhikevich, E. M., 2006. Dynamical Systems in Neuroscience: The Geometry of Excitability and Bursting. The MIT Press.

Jack, J., Noble, D., Tsien, R., 1975. Electric current flow in excitable cells. Clarendon Press, Oxford.

Jancke, D., Chavane, F., Naaman, S., Grinvald, A., 2004. Imaging cortical correlates of illusion in early visual cortex. Nature 428, 423–426.

Jin, W., Zhang, R., Wu, J., 2002. Voltage-sensitive dye imaging of population neuronal activity in cortical tissue. Journal of Neuroscience Methods 115, 13–27.

Kandel, E., Schwartz, J., Jessel, T., 2000. Principles of Neural Science, 4th Edition. McGraw-Hill.

Kaplan, E., Purpura, K., Shapley, R., 1987. Contrast affects the transmission of visual information through the mammalian lateral geniculate nucleus. J. Physiol.. 391, 267–288.

Kaplan, E., Shapley, R., 1986. The primate retina contains two types of ganglion cells, with high and low contrast sensitivity. Proc. Natl. Acad. Sci. USA 83, 2755–2757.

Katz, L., Callaway, E., 1992. Development of local circuits in mammalian visual cortex. Annu. Rev. Neurosci. 15, 31–56.

Kauer, J. S., 1988. Real-time imaging of evoked activity in local circuits of the salamander olfactory bulb. Nature 331 (6152), 166–168.

Kee, M. Z., Wuskell, J. P., Loew, L. M., Augustine, G. J., Sekino, Y., 2008. Imaging activity of neuronal populations with new long-wavelength voltage-sensitive dyes. Brain Cell. Biol. 36 (5-6), 157–172.

Kelly, J. P., Van Essen, D. C., 1974. Cell structure and function in the visual cortex of the cat. J. Physiol. 238, 515–547.

Kennedy, C., Des Rosiers, M., Jehle, J., Reivich, M., Sharpe, F., Sokoloff, L., 1975. Mapping of functional neural pathways by autoradiographic survey of local metabolic rate with (14c)deoxyglucose. Science 187 (4179), 850–853.

Kim, D., Duong, T., Kim, S., 2000. High-resolution mapping of iso-orientation columns by fmri. Nat. Neurosci. 3 (2), 164–169.

Kim, S., Ashe, J., A.P., G., Merkle, H., Ellermann, J., Menon, R., Ogawa, S., Ugurbil, K., 1993a. Functional imaging of human motor cortex at high magnetic field. J. Neurophysiology 69 (1), 297–302.

Kim, S., Ashe, J., Hendrich, K., Ellermann, J., Merkle, H., Menon, R., Ogawa, S., Ugurbil, K., 1993b. Functional magnetic resonance imaging of motor cortex: hemispheric asymmetry and handedness. Science 261, 615–617.

Kim, S., Fukuda, M., 2008. Lessons from fmri about mapping cortical columns. Neuroscientist 14 (3), 287–299.

Kisvarday, Z., Eysel, U., 1993. Functional and structural topography of horizontal inhibitory connections in cat visual cortex. Eur. J. Neurosci. 5, 1558–1572.

Kisvarday, Z., Kim, D., Eysel, U., Bonhoeffer, T., 1994. Relationship between lateral inhibitory connections and the topography of the orientation map in cat visual cortex. Eur. J. Neurosci. 6, 1619–1632.

Kisvarday, Z., Martin, K., Freund, T., Magloczky, Z., Whitteridge, D., Somogyi, P., 1986. Synaptic targets of hrp-filled layer iii pyramidal cells in the cat striate cortex. Exp. Brain Res. 64, 541–552.

Kisvarday, Z., Toth, E., Rausch, M., Eysel, U., 1997. Orientation-specific relationship between populations of excitatory and inhibitory lateral connections in the visual cortex of the cat. Cereb. Cortex 7, 605–618.

Kleinfeld, D., Delaney, K., 1996. Distributed representation of vibrissa movement in the upper layers of somatosensory cortex revealed with voltage-sensitive dyes. J. Comp. Neurol. 375, 89–108.

Kohonen, T., 2001. Self-Organizing Maps. Springer, third, extended edition.

Komatsu, Y., Nakajima, S., Toyama, K., Fetz, E., 1988. Intracortical connectivity revealed by spike-triggered averaging in slice preparations of cat visual cortex. Brain Res. 442, 359–362.

Konnerth, A., Obaid, A. L., Salzberg, B. M., 1987. Optical recording of electrical activity from parallel fibres and other cell types in skate cerebellar slices in vitro. J. Physiol. 393, 681–702.

Konnerth, A., Orkand, P. M., Orkand, R. K., 1988. Optical recording of electrical activity from axons and glia of frog optic nerve: potentiometric dye responses and morphometrics. Glia 1 (3), 225–232.

Konnerth, A., Orkand, R. K., 1986. Voltage-sensitive dyes measure potential changes in axons and glia of the frog optic nerve. Neurosci. Lett. 66 (1), 49–54.

Kremkow, J., jul 2009. Correlating excitation and inhibition in visual cortical circuits: Functional consequences and biological feasibility. Ph.D. thesis, Université de Aix-Marseille II.

Kritzer, M., Cowey, A., Somogyi, P., 1992. Patterns of inter- and intralaminar gabaergic connections distinguish striate (v1) and extrastriate (v2, v4) visual cortices and their functionally specialized subdivisions in the rhesus monkey. J. Neurosci. 12 (11), 4545–4564.

Kubota, M., Hosokawa, Y., Horikawa, J., 2006. Layer-specific short-term dynamics in network activity in the cerebral cortex. Neuroreport 17 (11), 1107–1110.

Kuffler, S. W., 1953. Discharge patterns and functional organization of mammalian retina. J. Neurophysiol. 16, 37–68.

Kumar, A., Schrader, S., Aerster, A., Rotter, S., 2008. The high-conductance state of cortical networks. Neural Comput. 20 (1), 1–43.

La Rota, C., Jan. 2003. Analyse de l'activité électrique multi-ties du cortex auditif chez le cobaye. Ph.D. thesis, Université Joseph Fourier, Grenoble I.

Laaris, N., Keller, A., 2002. Functional independence of layer iv barrels. J. Neurophysiol. 87 (2), 1028–1034.

Lancet, D., Greer, C., Kauer, J., Shepherd, G., 1982. Mapping of odor-related neuronal activity in the olfactory bulb by high-resolution 2-deoxyglucose autoradiography. Proc. Natl. Acad. Sci. USA 79, 670–674.

Lev-Ram, V., Grinvald, A., 1986. Ca2+- and k+- dependend communication between central nervous system myelinated axons and oligodendrocytes revealed by voltage-sensitive dyes. Proc. Natl. Acad. Sci. USA 83 (17), 6651–6655.

LeVay, S., 1988. The patchy intrinsic projections of visual cortex. Prog. Brain. res. 75, 147–161.

LeVay, S., Connolly, M., Houde, J., Van Essen, D., 1985. The complete pattern of ocular dominance stripes in the striate cortex and visual field of the macaque monkey. J. Neurosci. 5, 486–501.

LeVay, S., Nelson, S., 1991. Columnar organization of the visual cortex. CRC Press, pp. 266–315.

Levitt, J., Schumer, R., Sherman, S., Spear, P., Movshon, J., 2001. Visual response properties of neurons in the lgn of normally reared and visually deprived macaque monkeys. J. Neurophysiol. 85 (5), 2111–2129.

Li, B., Thompson, J., Duong, T., Peterson, M., Freeman, R., 2006. Origins of cross-orientation suppression in the visual cortex. J. Neurophysiol. 96, 1755–1764.

Li, C., Creutzfeldt, O., 1984. The representation of contrast and other stimulus parameters by single neurons in area 17 of the cat. Pflugers Arch. 401 (3), 304–314.

Lippert, M. T., Takagaki, K., Xu, W., Huang, X., Wu, J. Y., 2007. Methods for voltage-sensitive dye imaging of rat cortical activity with high signal-to-noise ratio. J. Neurophysiol. 98, 502–512.

Logothetis, N., 2003. Mr imaging in the non-human primate: studies of function and of dynamic connectivity. Curr. Opin. neurobiol. 13 (5), 630–642.

Lund, J., 1988. Anatomical organization of macaque monkey striate visual cortex. Annu. Rev. Neurosci. 11, 253–288.

Lund, J., Wu, C., 1997. Local circuit neurons of macaque monkey striate cortex: Iv. neurons of laminae 1-3a. J. Comp. Neurol. 384, 109–126.

Lund, J., Yoshioka, T., 1991. Local circuit neurons of macaque monkey striate cortex: Iii. neurons of laminae 4b, 4a, and 3b. J. Comp. Neurol. 311 (2), 234–258.

Lytton, W., Sejnowski, T., 1991. Simulations of cortical pyramidal neurons synchronized by inhibitory interneurons. J. Neurophysiol. 66, 1059–1079.

Maass, W., 1997. Fast sigmoidal networks via spiking neurons. Neural Comput. 9, 279–304.

Maass, W., 2000. On the computational power of winner-take-all. Neural Comput. 12, 2519–2535.

Maass, W., Natschlager, T., Markram, H., 2002. Computational models for generic cortical microcircuits. In: J. Feng, editor, Computational Neuroscience: A comprehensive approach. CRC-Press.

Maffei, L., Fiorentini, A., 1973. The visual cortex as a spatial frequency analyser. Vision Res. 13, 1255–1267.

Maffei, L., Fiorentini, A., Bisti, S., 1973. Neural correlate of perceptual adaptation to gratings. Science. 182, 1036–1038.

Magee, J., Johnston, D., 1995. Synaptic activation of voltage-gated channels in the dendrites of hippocampal pyramidal neurons. Science 268 (5208), 301–304.

Malach, R., Amir, Y., Harel, M., Grinvald, A., 1993. Relationship between intrinsic connections and functional architecture revealed by optical imaging and in vivo targeted biocytin injections in primate striate cortex. Proc. Natl. Acad. Sci. USA 90 (22), 10469–10473.

Malonek, D., Spitzer, H., 1989. Response histogram shapes and tuning curves: The predicted responses of several cortical cell types to drifting gratings stimuli. Bio. Cybern. 60 (6), 469–475.

Manis, P. B., Freeman, J. A., 1988. Fluorescence recordings of electrical activity in goldfish optic tectum in vitro. J. Neurosci. 8 (2), 383–394.

Mante, V., Frazor, R. A., Bonin, V., S., W., Carandini, M., 2005. Independence of luminance and contrast in natural scenes and in the early visual system. Nat. Neurosci. 8 (12), 1690–1697.

Markram, H., 2006. The blue brain project. Nat Rev Neurosci 7 (2), 153–60.

Markram, H., Gupta, A., Uziel, A., Wang, T., Tsodyks, M., 1998a. Information processing withfrequency-dependent synaptic connections. Neurobiol. Lern. Mem. 70 (1-2), 101–112.

Markram, H., Helm, P., Sakmann, B., 1995. Dendritic calcium transients evoked by single back-propagating action potentials in rat neocortical pyramidal neurons. J. Physiol. 485 (Pt 1), 1–20.

Markram, H., Lubke, J., Frotscher, M., Roth, A., Sakmann, B., 1997. Physiology and anatomy of synaptic connections between thick tufted pyramidal neurones in the developing rat neocortex. J. Physiol. 500 (Pt 2), 409–440.

Markram, H., Toledo-Rodriguez, M., Wang, Y., Gupta, A., Silberberg, G., Wu, C., 2004. Interneurons of the neocortical inhibitory system. Nature Reviews Neuroscience 5, 793–804.

Markram, H., Wang, Y., Tsodyks, M., 1998b. Differential signaling via the same axon of neocortical pyramidal neurons. Proc. Natl. Acad. Sci. USA 95 (9), 5323–5328.

Martin, K., Whitteridge, D., 1984. Form, function and intracortical projections of spiny neurones in the striate visual cortex of the cat. J. Physiol. 6353, 463–504.

Mason, A., Nicoll, A., Stratford, K., 1991. Synaptic transmission between individual pyramidal neurons of the rat visual cortex in vitro. J. Neurosci. 11 (1), 72–84.

Mastronarde, D., 1987. Two classes of single-input x-cells in cat lateral geniculate nucleus. i. receptive-field properties and classification of cells. J. Neurophysiol. 57 (2), 357–380.

Matsubara, J., 1988. Local, horizontal connections within area 18 of the cat. Prog. Brain Res. 75, 163–172.

McCormick, D., Connors, B., Lighthall, J., Prince, D., 1985. Comparative electrophysiology of pyramidal and sparsely spiny stellate neurons of the neocortex. J. Neurophysiol. 54 (4), 782–806.

McCulloch, W., Pitts, W., 1943. A logical calculus of the ideas immanent in nervous activity. Bull. Math. Biophys. 5, 115–133.

McDonald, C., Burkhalter, A., 1993. Organization of long-range inhibitory connections with rat visual cortex. J. Neurosci. 13 (2), 768–781.

McGuire, B., Gilbert, C., Rivlin, P., Wiesel, T., 1991. Targets of horizontal connections in macaque primary visual cortex. J. Comp. Neurol. 305, 370–392.

Mehring, C., Hehl, U., Kubo, M., Diesmann, M., Aersten, A., 2003. Activity dynamics and propagation of synchronous spiking in locally connected random networks. Biol. Cybern. 88 (5), 395–408.

Miikkulainen, R., Bednar, J. A., Choe, Y., Sirosh, J., 2005. Computational Maps in the Visual Cortex. Springer, Berlin.

Mitchison, G., Crick, F., 1982. Long axons within the striate cortex: their distribution, orientation, and patterns of connection. Proc. Natl. Acad. Sci. USA 79 (11), 3661–3665.

Mitzdorf, U., 1985. Current source-density method and application in cat cerebral cortex: Investigation of evoked potentials and eeg phenomena. Physiological reviews 65 (1), 37–100.

Monier, C., Chavane, F., Baudot, P., Graham, L., Fregnac, Y., 2003. Orientation and direction selectivity of synaptic inputs in visual cortical neurons: A diversity of combinations produces spike tuning. Neuron 37 (4), 663–680.

Morris, C., Lecar, H., 1981. Voltage oscillations in the barnacle giant muscle fiber. Biophysics J. 35, 193–213.

Morrison, A., Straube, S., Plesser, H., Diesmann, M., 2007. Exact subthreshold integration with continuous spike times in discrete-time neural network simulations. Neural Comput. 19 (1), 47–79.

Mountcastle, V., 1957. Modality and topographic properties of single neurons of cat's somatosensory cortex. J. Neurophysiol. 20, 408–434.

Mountcastle, V., 1997. The columnar organization of the neocortex. Brain 120, 701–722.

Movshon, J., Thompson, I., Tolhurst, D., 1978a. Receptive field organization of complex cells in the cat's striate cortex. J. Physiol. (Lond) 283, 79–99.

Movshon, J., Thompson, I., Tolhurst, D., 1978b. Spatial summation in the receptive fields of simple cells in the cat's striate cortex. J. Physiol. (Lond) 283, 53–77.

Movshon, J., Tolhurst, D., 1975. On the response linearity of cells in the cat visual cortex. J. Physiol. 249, 56–57.

Muller, J., Metha, A., Krauskopf, J., Lennie, P., 2001. Information conveyed by onset transients in responses of striate cortical neurons. J. Neurosc. 21 (17), 6978–6990.

Nagel, G., Ollig, D., Fuhrmann, M., 2002. Channelrhodopsin-1: a light-gated proton channel in green algae. Science 296 (5577), 2395–2398.

Nauhaus, I., Busse, L., Carandini, M., Ringach, D., 2009. Stimulus contrast modulates functional connectivity in visual cortex. Nat. Neurosci. 12, 70–76.

Nelson, D. A., Katz, L. C., 1995. Emergence of functional circuits in ferret visual cortex visualized by optical imaging. Neuron 15 (1), 23–34.

Nettleton, J., Spain, W., 2000. Linear to supralinear summation of ampa-mediated epsps in neocortical pyramidal neurons. J. Neurophysiol. 83 (6), 3310–3322.

Nowak, L., Barone, P., 2009. Contrast adaptation contributes of contrast-invariance of orientation tuning of primate v1 cells. PLoS ONE 4 (3), e4781.

Nowak, L., Bullier, J., 1998a. Axons, but not cell bodies, are activated by electrical stimulation in cortical gray matter. i. evidence from chronaxie measurements. Exp. Brain Res. 118 (4), 477–488.

Nowak, L., Bullier, J., 1998b. Axons, but not cell bodies, are activated by electrical stimulation in cortical gray matter. ii. evidence from selective inactivation of cell bodies and axon initial segments. Exp. Brain Res. 118 (4), 489–500.

Nowak, L., James, A., Bullier, J., 1997. Corticocortical connections between visual areas 17 and 18a of the rat studied in vitro: spatial and temporal organization of functional synaptic responses. Exp. Brain Res. 117 (2), 219–241.

Nowak, L. G., Azouz, R., Sanchez-Vives, M. V., Gray, C., McCormick, D., 2003. Electrophysiological classes of cat primary visual cortical neurons in vivo as revealed by quantitative analyses. J. Neurophysiol. 89 (3), 1541–1566.

Ogawa, S., Lee, T., Kay, A., Tank, D., 1990. Brain magnetic resonance imaging with contrast dependent on blood oxygenation. Proc. Natl. Acad. Sci. USA 87, 9868–9872.

Ogawa, S., Tank, D., Menon, R., Ellermann, J., Kim, S.-G., Merkle, H., Ugurbil, K., 1992. Intrinsic signal changes accompanying sensory stimulation: Functional brain mapping with magnetic resonance imaging. Proc. Natl. Acad. Sci. USA 89, 5951–5955.

Ohki, K., Chung, S., Ch'ng, Y., Kara, P., Reid, R., 2005. Functional imaging with cellular resolution reveals precise micro-architecture in visual cortex. Nature 433, 597–603.

Ohki, K., Chung, S., Kara, P., Hubener, M., Bonhoeffer, T., Reid, R., 2006. Highly ordered arrangement of single neurons in orientation pinwheels. Nature 442, 925–928.

Ohzawa, I., Sclar, G., Freeman, D., 1985. Contrast gain control in the cat's visual cortex. J. Neurophysiol. 54, 651–667.

Ohzawa, I., Sclar, G., Freeman, R., 1982. Contrast gain control in the cat visual cortex. Nature 298 (5871), 266–268.

Opie, L. H., 2004. Heart physiology: from cell to circulation. Lippincott williams and wilkins.

Orbach, H. S., Cohen, L. B., 1983. Optical monitoring of activity from many areas of the in vitro and in vivo salamander olfactory bulb: a new method for studying functional organization in the vertebrate central nervous system. J. Neurosci. 3, 2251–2262.

Orbach, H. S., Cohen, L. B., Grinvald, A., 1985. Optical mapping of electrical activity in rat somatosensory and visual cortex. J. Neurosci. 5, 1886–1895.

Orbach, H. S., Van Essen, D. C., 1993. In vivo tracing of pathways and spatio-temporal activity patterns in rat visual cortex using voltage sensitive dyes. Exp. Brain Res. 94 (3), 371–392.

O'Reilly, R. C., Munakata, Y., 2000. Computational Explorations in Cognitive Neuroscience. A Bradford Book. The MIT Press.

Perea, G., Araque, A., 2009. Glia modulates synaptic transmission. Brain Research Reviews. doi: 10.1016/j.brainresrev.2009.10.005.

Peters, A., Jones, E. (Eds.), 1984. Cerebral cortex, cellular components of the cerebral cortex. Vol. 1. Plenum, New York.

Peters, A., Yilmaz, E., 1993. Neuronal organization in area 17 of cat visual cortex. Cereb. Cortex 3, 49–68.

Petersen, C., Grinvald, A., Sakmann, B., feb 2003. Spatiotemporal dynamics of sensory responses in layer 2/3 of rat barrel cortex measured in vivo by voltage-sensitive dye imaging combined with whole-cell voltage recordings and neuron reconstructions. J. Neurosci. 23 (3), 1298–1309.

Petersen, C., Sakmann, B., nov 2001. Functional independent columns of rat somatosensory barrel cortex revealed with voltage-sensitive dye imaging. J. Neurosci. 21 (21), 8435–8446.

Pettersen, K., Hagen, E., Einevoll, G., 2008. Estimation of population firing rated and current source densities from laminar electrode recordings. J. Comput. Neurosci. 24 (3), 291–313.

Powell, T., Mountcastle, V., 1959a. The cytoarchitexture of the postcentral gyrus of the monkey macaca mulatta. Bull Johns Hopkins Hosp. 105, 108–131.

Powell, T., Mountcastle, V., 1959b. Some aspects of the functional organization of the cortex of the postcentral gyrus of the monkey: a correlation of findings obtained in a single unit analysis with cytoarchitecture. Bull Johns Hopkins Hosp. 105, 133–162.

Priebe, N., Ferster, D., 2006. Mechanisms underlying cross-orientation suppression in cat visual cortex. Nat. Neurosci. 9, 552–561.

Purve, D., Augustine, G., Fitzpatrick, D., Hall, W., LaMantia, A.-S., McNamara, J., Williams, S., 2004. Neuroscience (third edition). Sinauer Associates, Inc.

Raizada, R., Grossberg, S., 2003. Towards a theory of the laminar architecture of the cerebral cortex: Computational clues from the visual system. Cereb. Cortex 13, 100–113.

Rakic, P., 1995. Radial versus tangential migration of neuronal clones in the developing cerebral cortex. Proc. Natl. Acad. Sci. USA 92 (25), 11323–11327.

Rakic, P., 2003. Developmental and evolutionary adaptations of cortical radial glia. Cereb. Cortex 13 (6), 541–549.

Rall, W., 1964. Theoretical significance of dendritic trees for neuronal input-output relations. In: R. Reiss (Ed.), Neural theory and modeling, Stanford University Press. Stanford, CA, 73–97.

Rall, W., 1967. Distinguishing theoretical synaptic potentials computed for different soma-dendritic distributions of synaptic input. J. Neurophysiol. 30, 1138–1168.

Rall, W., 1989. Cable theory for dendritic neurons. In: Methods in neuronal modeling: From synapses to networks. MIT Press, Cambridge, MA, USA, 9–92.

Rangan, A. V., Cai, D., McLaughlin, D. W., 2005. Modeling the spatiotemporal cortical activity associated with the line-motion illusion in primary visual cortex. Proc Natl Acad Sci 102 (52), 18793–18800.

Reid, R., Alonso, J., 1996. The processing and encoding of information in the visual cortex. Curr. Opin. Neurobiol. 6 (4), 475–480.

Reynaud, A., Barthelemy, F., Masson, G., Chavane, F., 2007. Input-ouput transformation in the visuo-oculomotor network. Arch. Ital. Biol. 145.

Ripley, B., 1996. Pattern recognition and Neural Netw. Clarendon Press, Oxford.

Robson, J., 1966. Linear and nonlinear operations in the visual system. Investigative Ophthalmology and Visual Science (Suppl.) 29, 117.

Rockland, K., Lund, J., 1982. Iwidespread periodic intrinsic connections in the tree shrew visal cortex. Science 215, 1532–1534.

Roland, P. E., 2002. Dynamic depolarization fields in the cerebral cortex. Trends Neurosci. 25 (4), 183–190.

Roland, P. E., Hanazawa, A., Undeman, C., Eriksson, D., Tompa, T., Nakamura, H., Valentiniene, S., Ahmed, B., 2006. Cortical feedback depolarization waves: a mechanism of top-down influence on early visual areas. Proc Natl Acad Sci 103 (33), 12586–12591.

Ross, W. N., Salzberg, B. M., Cohen, L. B., Grinvald, A., Davila, H. V., Waggoner, A. S., Wang, C. H., 1977. Changes in absorption, fluorescence, dichroism, and birefringence in stained giant axons: optical measurements of membrane potential. J. Membr. Biol. 33 (1-2), 141–183.

Roy, C., Sherrington, C., 1890. On the regulation of the blood supply of the brain. J. Physiol. (London) 11, 85–108.

Rubin, B. D., Katz, L. C., 1999. Optical imaging of odorant representations in the mammalian olfactory bulb. Neuron 23 (3), 499–511.

Rumelhart, D., Hinton, G., Williams, R., 1986. Learning internal representation by backpropagating errors. Nature 323, 533–536.

Salin, P., Bullier, J., 1995. Corticocortical connections in the visual system: structure and function. Psychol. Bull. 75, 107–154.

Salzberg, B. M., Davila, H. V., Cohen, L. B., 1973. Optical recording of impulses in individual neurons of an invertebrate central nervous system. Nature 246, 508–509.

Sanchez-Vives, M., Nowak, L., McCormick, D., 2000a. Cellular mechanisms of long-lasting adaptation in visual cortical neurons in vitro. J. Neurosci. 20 (11), 4286–4299.

Sanchez-Vives, M., Nowak, L., McCormick, D., 2000b. Membrane mechanisms underling contrast adaptation in cat area 17 in vivo. J. Neurosci. 20 (11), 4267–4285.

Schneider, M., Gradinaru, V., Zhang, F., Deisseroth, K., 2008. Controlling neuronal activity. Am. J. Psychiatry 165 (5), 562.

Schummers, J., Yu, H., Sur, M., 2008. Tuned responses of astrocytes and their influence on hemodynamic signals in the visual cortex. science 320, 1638–1643.

Sclar, G., May 1987. Expression of retinal contrast gain control by neurons of the cat's lateral geniculate nucleus. Experimental Brain Research 66 (3), 589–596.

Sclar, G., Freeman, D., 1982. Orientation selectivity in the cat's striate cortex is invariant with stimulus contrast. Exp. Brain Res. 46 (3), 457–461.

Sclar, G., Lennie, P., DePriest, D., 1890. Contrast adaptation in striate cortex of macaque. Vision Res. 29, 747–755.

Sclar, G., Maunsell, J., Lennie, P., 1990. Coding of image contrast in central visual pathways of the macaque monkey. Vision Res. 30 (1), 1–10.

Scott, A., 2002. Neuroscience: A mathematical primer. Springer-Verlag.

Segev, I., 1992. Single neurone models: oversimple, complex and reduced. TINS 15 (11), 414–421.

Seidemann, E., Arieli, A., Grinvald, A., Slovin, H., 2002. Dynamics of depolarization and hyperpolarization in the frontal cortex and saccade goal. Science 295 (5556), 862–865.

Shapley, R., Enroth-Cugell, C., 1984. Visual adaptation and retinal gain controls. Progress in retinal research 3, 263–346.

Shapley, R., Hawken, M., Xing, D., 2007. The dynamics of visual responses in the primary visual cortex. Prog. Brain Res. 165, 21–32.

Shapley, R., Kaplan, E., Soodak, R., 1981. Spatial summation and contrast sensitivity of x and y cells in the lateral geniculate nucleus of the macaque. Nature 292 (5823), 543–545.

Shapley, R. M., Victor, J. D., 1978. The effect of contrast on the transfer properties of cat retinal ganglion cells. J. Physiol. 285 (1), 275–298.

Sharon, D., Grinvald, A., 2002. Dynamics and constancy in cortical spatiotemporal patterns of orientation processing. Science 295 (5554), 512–515.

Sharon, D., Jancke, D., Chavane, F., Na'aman, S., Grinvald, A., 2007. Cortical response field dynamics in cat visual cortex. Cereb. Cortex 17 (12), 2866–2877.

Shaw, G., Harth, E., Schelbel, A., 1982. Cooperativity in brain functionl assemblies of approximately 30 neurons. Experimental Neurology 77 (2), 324–358.

Sherman, S., Guillery, R., 1996. The functional organization of thalamocortical relays. J. Neurophysiol., 76, 1367–1395.

Shoham, D., Glaser, D., Arieli, A., Kenet, T., Wijnbergeb, C., Toledo, Y., Hildesheim, R., Grinvald, A., 1999. Imaging cortical dynamics at high spatial and temporal resolution with novel blue voltage-sensitive dyes. Neuron 24 (4), 791–802.

Sholl, D. A., 1955a. The organization of the visual cortex in the cat. J. Anat. 89, 33–46.

Shou, T., Li, X., Zhou, Y., Hu, B., 1996. Adaptation of visually evoked responses of relay cells in the dorsal lateral geniculate nucleus of the cat following prolonged exposure to drifting gratings. Vis. Neurosci. 13, 605–613.

Shouval, H., Goldberg, D., Jones, J., Beckerman, M., Cooper, L., 2000. Structured long-range connections can provide a scaffold for orientation maps. J. Neurosci. 20 (3), 1119–1128.

Sillito, A., 1975a. The contribution of inhibitory mechanisms to the receptive field properties of neurones in the striate cortex of the cat. J. Physiol. 250 (2), 305–329.

Sillito, A., 1975b. The effectiveness of bicuculline as an antagonist of gaba and visually evoked inhibition in the cat's striate cortex. J. Physiol. 250 (2), 287–304.

Sillito, A., 1977. Inhibitory processes underlying the directional specificity of simple, complex and hypercomplex cells in the cat's visual cortex. J. Physiol. (London) 271, 699–720.

Sillito, A., 1979. Inhibitory mechanisms influencing complex cell orientation selectivity and their modification at high resting discharge levels. J. Physiol. (London) 289, 33–53.

Sillito, A., Kemp, J., Milson, J., Beradi, N., 1980. A re-evaluation of the mechanisms underlying simple cell orientation selectivity. Brain Res. 194, 517–520.

Sincich, L., Blasdel, G., 2001. Oriented axon projections in primary visual cortex of the monkey. J. Neurosci. 21 (12), 4416–4426.

Sirosh, J., Miikkulainen, R., 1994. Cooperative self-organization of afferent and lateral connections in cortical maps. Biological Cybernetics 71, 66–78.

Sit, Y. F., Miikkulainen, R., 2007. A computational model of the signals in optical imaging with voltage-sensitive dyes. Neurocomputing 70 (10-12), 1853–1857.

Skottun, B., De Valois, R., Grosof, D., Movshon, J., Albrecht, D., Bonds, A., 1991. Classifying simple and complex cells on the basis of response modulation. Vision Res. 31, 1079–1086.

Slovin, H., Arieli, A., Hildesheim, R., Grinvald, A., 2002. Long-term voltage-sensitive dye imaging reveals cortical dynamics in behaving monkeys. J. Neurophysiol. 88 (6), 3421–3438.

So, P., Dong, C., Masters, B., Berland, K., 2000. Two-photon excitation fluorescence microscopy. Annu. Rev. Biomed. Eng. 2, 399–429.

Sohal, V., Zhang, F., Yizhar, O., Deisseroth, K., 2009. Parvalbumin neurons and gamma rhythms enhance cortical circuit performance. Nature 459, 698–702.

Solomon, S. G., Peirce, J. W., Dhruv, N. T., Lennie, P., apr 2004. Profound contrast adaptation early in the visual pathway. Neuron 42, 155–162.

Somers, D., Nelson, S., Sur, M., 1995. An emergent model of orientation selectivity in cat visual cortical simple cells. J. Neurosci. 15 (8), 5448–5465.

Somogyi, P., 1989. Synaptic organization of gabaergic neurons and gaba-a receptors in the lateral geniculate nucleus and visual cortex. Neural Mechanisms of Visual Perception, 35–63.

Somogyi, P., Kisvarday, Z., Martin, K., Whitteridge, D., 1983. Synaptic connections of morphologically identified and physiologically characterized large basket cells in the striate cortex of cat. Neuroscience 10 (2), 261–294.

Spors, H., Grinvald, A., Apr 2002. Spatio-temporal dynamics of odor representations in the mammalian olfacgtory bulb. Neuron 34 (2), 301–315.

Stark, D., Bradley, W., 1999. Magnetic resonance imaging. St Louis, MO: Mosby.

Stepanyants, A., Hirsch, J., Martinez, L., Kisvarday, Z., Ferecsko, A., Chklovskii, D., 2002. Local potential connectivity in cat primary visual cortex. Cereb. Cortex 18 (1), 13–28.

Stepanyants, A., Hirsch, J., Martinez, L., Kisvarday, Z., Ferecsko, A., Chklovskii, D., 2008. Local potential connectivity in cat primary visual cortex. Cereb. Cortex 18 (1), 13–28.

Stepanyants, A., Martinez, L., Ferecsko, A., Kisvarday, Z., 2009. The factions of short- and long-range connections in the visual cortex. Proc. Natl. Acad. Sci. USA 106 (9), 3555–3560.

Stewart, W., Kauer, J., Shepherd, G., 2004. Functional organization of rat olfactory bulb analysed by the 2-deoxyglucose method. J. Comp. Neurol. 185 (4), 4111–4121.

Stoelzel, C., Bereshpolova, Y., Gusev, A., Swadlow, H., 2008. The impact of an lgnd impulse on the awake visual cortex: synaptic dynamics and the sustained/transient distinction. J. Neurosci. 28 (19), 5018–5028.

Stoilov, S., Rusanov, E., Mitex, D., Genkov, D., 1985. Biophysics. Publishing house Medicine and Physical Culture, Sofia.

Stuart, G., Sakmann, B., 1994. Active propagation of somatic action potentials into neocortical pyramidal cell dendrites. Nature 367 (6458), 69–72.

Stuart, G., Spruston, N., Sakmann, B., Hausser, M., 1997. Action potential initiation and backpropagation in neurons of the mammalian cns. Trends Neurosci. 20 (3), 125–131.

Svoboda, K., Denk, W., Kleinfeld, D., Tank, D., 1997. In vivo dendritic calcium dynamics in neocortical pyramidal neurons. Nature 385 (6612), 161–165.

Swindale, N., 1990. Is the cerebral cortex modular? Trends Neurosci. 13 (12), 487–492.

Symes, A., Wennekers, T., 2009. Spatiotemporal dynamics in the cortical microcircuit: A modelling study of primary visual cortex layer 2/3. Neural Netw. 22 (8), 1079–1092.

Tamas, G., Buhl, E., Somogyi, P., 1997. Fast ipsps elicited via multiple synaptic release sites by different types of gabaergic neurone in the cat visual cortex. J. Physiol. 500, 715–738.

Taniguchi, I., Horikawa, J., Moriyama, T., Nasu, M., 1992. Spatio-temporal pattern of frequency representation in the auditory cortex of guinea pigs. Neurosci. Lett. 146 (1), 37–40.

Taniguchi, I., Nasu, M., 1993. Spatio-temporal representation of sound intensity in the guinea pig auditory cortex observed by optical recording. Neurosci. Lett. 151 (2), 178–181.

Tank, D., Ogawa, S., Ugurbil, K., 1992. Mapping the brain with mri. Curr. Biol. 2 (10), 525–528.

Tasaki, I., Watanabe, A., Carnay, L., 1968. Changes in fluorescence, turbidity, and bireference associated with nerve excitation. Proc. Natl. Acad. Sci. USA 61, 883–888.

Thomson, A., Deuchars, J., 1994. Temporal and spatial properties of local circuits in neocortex. Trends Neurosci. 17 (3), 119–126.

Thomson, A., Deuchars, J., 1997. Synaptic interactions in neocortical local circuits: dual intracellular recordings in vitro. Cereb. Cortex 7 (6), 510–522.

Thomson, A., Deuchars, J., West, D., 1993. Single axon excitatory postsynaptic potentials in neocortical interneurons exhibit pronounced paired pulse facilitation. Neuroscience 54 (2), 347–360.

Thomson, A., Lamy, C., nov 2007. Functional maps of neocortical local circuitry. Frontiers in Neuroscience 1 (1), 19–42.

Thomson, A., Morris, O., 2002. Selectivity in the inter-laminar connections made by neocortical neurones. Journal of Neurocytology 31 (3-5), 239–246.

Thomson, A., West, D., 1993. Fluctuations in pyramid-pyramid excitatory postsynaptic potentials modified by presynaptic firing pattern and postsynaptic membrane potential using paired intracellular recordings in rat neocortex. Neuroscience 54 (2), 329–346.

Thomson, A. M., Bannister, A. P., Jan. 2003. Interlaminar connections in the neocortex. Cereb. Cortex 13, 5–14.

Thomson, A. M., Bannister, A. P., Mercer, A., Morris, O. T., 2002. Target and temporal pattern selection at neocortical synapses. The Royal Society 357, 1781–1791.

Toledo-Rodriguez, M., Gupta, A., Wang, Y., Wu, C., Markram, H., 2003. Neocortex: Basic neuron types. The handbook of brain theory and Neural Netw., 719–725.

Tootell, R., Hadjikhani, N., Mendola, J., Marrett, S., Dale, A., May 1998. From retinotopy to recognition: fMRI in human visual cortex. Trends in Cognitive Sciences 2 (5), 174–183.

Tootell, R., Silverman, M., Switked, E., De Valois, R., 1982. Deoxyglucose analysis of retinotopic organization in primate striate cortex. Science 218 (4575), 902–904.

Ts'o, D., Gilbert, C., 1988. The organization of chromatic and spatial interactions in the primate striate cortex. J. Neurosci. 8 (5), 1712–1727.

Ts'o, D., Gilbert, C., Wiesel, T., 1986. Relationships between horizontal interactions and functional architecture in cat striate cortex as revealed by cross-correlation analysis. J. Neurosci. 6 (4), 1160–1170.

Ts'o, D. Y., Frostig, R. D., Lieke, E. E., Grinvald, A., 1990. Functional organization of primate visual cortex revealed by high resolution optical imaging. Science 249 (4967), 417–420.

Tsodyks, M., Pawelzik, K., Markram, H., 1998. Neural networks with dynamic synapses. Neural Comput. 10 (4), 821–835.

Tsumoto, T., Eckart, W., Creutzfeldt, O., 1979. Modification of orientation sensitivity of cat visual cortex neurones by removal of gaba-mediated inhibition. Exp. Brain Res. 34, 351–363.

Tsunoda, K., Yamane, Y., Nishizaki, M., Tanifuji, M., 2001. Complex objects are represented in macaque inferotemporal cortex by the combination of feature columns. Nat. Neurosci. 4 (8), 832–838.

Tucker, T. R., Katz, L. C., 2003a. Recruitment of local inhibitory networks by horizontal connections in layer 2/3 of ferret visual cortex. J. Neurophysiol. 89 (1), 501–512.

Tucker, T. R., Katz, L. C., 2003b. Spatiotemporal patterns of excitation and inhibition evoked by the horizontal network in layer 2/3 of ferret visual cortex. J. Neurophysiol. 89 (1), 488–500.

Turner, R., Le Bihan, D. anf Moonen, C., Despres, D., Frank, J., 1991. Echo-planar time course mri of cat brain oxygenation changes. Magn. Reson. Med. 22 (1), 159–166.

Vanzetta, I., Grinvald, A., 2008. Coupling between neuronal activity and microcirculation: Implications for functional brain imaging. HFSP Journal 2 (2), 79–98.

von der Malsburg, C., 1981. The correlation theory of brain function. Internal Report 81-2, Max-Planck-Institute for Biophysical Chemistry, Gottingen, Germany.

Waggoner, A. S., Grinvald, A., 1977. Mechanisms of rapid optical changes of potential sensitive dyes. Ann. N. Y. Acad. Sci. 30 (303), 217–241.

Warnking, J., Dojat, M., Guerin-Dugue, A., Delon-Martin, C., Olympieff, S., Richard, N., Chehikian, A., Segebarth, C., 2002. fMRI retinotopic mapping - step by step. NeuroImage 17, 1665–1683.

Waters, J., Schaefer, A., Sakmann, B., 2005. Backpropagating action potentials in neurones: measurement, mechanisms and potential functions. Prog. Biophys. Mol. Biol. 87 (1), 145–170.

Watts, J., Thomson, A. M., 2005. Excitatory and inhibitory connections show selectivity in the neocortex. J. Physiol. 562.1, 89–97.

Weliky, M., Kandler, K., Fitzpatrick, D., Katz, L., 1995. Patterns of excitation and inhibition evoked by horizontal connections in visual cortex share a common relationship to orientation columns. Neuron 15 (3), 541–552.

Wells, R., 2005. Cortical neurons and circuits: a tutorial introduction. Unpublished paper, www.mrc.uidaho.edu.

White, E., 1989. Cortical circuits: synaptic organization of the cerbral cortex: structure, function and theory. Berlin: Birkhauser Verlag.

Wilson, H., 1999. Simplified dynamics of human and mammalian neocortical neurons. Journal of Theoretical Biology 200, 375–388.

Wilson, H., Cowan, J., 1972. Excitatory and inhibitory interactions in localized populations of model neurons. Biophys. J. 12, 1–24.

Wilson, H., Cowan, J., sep 1973. A mathematical theory of the functional dynamics of cortical and thalamic nervous tissue. Biological Cybernetics 13 (2), 55–80.

Wohrer, A., 2008. Model and large-scale simulator of a biological retina with contrast gain control. Ph.D. thesis, University of Nice Sophia-Antipolis.

Woolum, J. C., Strumwasser, F., 1978. Membrane-potential-sensitive dyes for optical monitoring of activity in aplysia neurons. J. Neurobiol. 9 (3), 185–193.

Xing, J., Gerstein, G., 1996. Networks with lateral connectivity. ii. development of neuronal grouping and corresponding receptive field changes. J. Neurophysiol. 75 (1), 200–216.

Xu, W., Huang, X., Takgaki, K., Wu, J., 2007. Compression and reflection of visually evoked cortical waves. Neuron 55 (1), 119–129.

Yamada, W., Koch, C., Adams, P., 1989. Multiple channels and calcium dynamics. In: Methods in Neuronal Modeling. MIT Press, Cambridge, MA, 97–134.

Yang, Z., Heeger, D. J., Seidemann, E., 2007. Rapid and precise retinotopic mapping of the visual cortex obtained by voltage-sensitive dye imaging in the behaving monkey. J. Neurophysiol. 98 (2), 1002–1014.

Young, J. Z., 1958. Anatomical considerations. EEG Clin. Neurophysiol. 10, 9–11.

Yuille, A., Geiger, D., 2003. Winner-take-all networks. In: The Handbook of Brain Theory and Neural Networks, ed. M. Arbib. Cambridge, MA. MIT Press, 1228–1231.

Yuste, R., Denk, W., 1995. Dendritic spines as basic functional units of neuronal integration. Nature 375 (6533), 682–684.

Yuste, R., Majewska, A., 1991. On the function of dendritic spines. Neuroscientist 7 (5), 387–395.

Yuste, R., Tank, D. K., Kleinfeld, D., 1997. Functional study of the rat cortical microcircuitry with voltage-sensitive dye imaging of neocortical slices. Cereb. Cortex 7 (6), 546–558.

Zaghloul, K., Boahen, K., Demb, J., 2005. Contrast adaptation in subthreshold and spiking responses of mammalian y-type retinal ganglion cells. J. Neurosci. 25 (4), 860–868.

Zipfel, W., Williams, R., Webb, W., 2003. Nonlinear magic: multiphoton microscopy in the biosciences. Nat. Biotechnol. 21 (11), 1369–1377.

Zochowski, M., Wachowiak, M., Falk, C. X., Cohen, L. B., Lam, Y. W., Antic, S., Zecevic, D., 2000. Imaging membrane potential with voltage-sensitive dyes. Biol. Bull. 198 (1), 749–762.